

UCLA

UCLA Electronic Theses and Dissertations

Title

Utilizing Small Molecules to Study Mitochondrial Presequence-Degrading Protease

Permalink

<https://escholarship.org/uc/item/8nm1z5z8>

Author

Wijaya, Juwina

Publication Date

2015

Peer reviewed|Thesis/dissertation

UNIVERSITY OF CALIFORNIA

Los Angeles

Utilizing Small Molecules to Study Mitochondrial Presequence-Degrading Protease

A dissertation submitted in partial satisfaction of the
requirements for the degree Doctor of Philosophy
in Biochemistry and Molecular Biology

by

Juwina Wijaya

2015

© Copyright by

Juwina Wijaya

2015

ABSTRACT OF THE DISSERTATION

Utilizing Small Molecules to Study Mitochondrial Presequence-Degrading Protease

by

Juwina Wijaya

Doctor of Philosophy in Biochemistry and Molecular Biology

University of California, Los Angeles, 2015

Professor Carla Marie Koehler, Chair

Proper mitochondrial function contributes to cell's health and integrity. Perturbations in mitochondrial homeostasis have been linked to diseases, specifically neurodegenerative diseases. Understanding the players of mitochondrial homeostasis will be beneficial for identification of potential therapeutic pathways. The mitochondrion is equipped with proteases that together serve as a quality control system to maintain homeostasis. While knockout using yeast genetics and RNAi approaches are powerful, new tools that are more rapid and specific are needed to elucidate the role of mitochondrial proteases. In this study, I utilize a high-throughput screening approach to discover and utilize small molecule modulators to characterize presequence-degrading protease (PreP).

PreP degrades N-terminal mitochondrial-targeting sequences and other small bioactive peptides, including amyloid-beta peptide, implicating it in Alzheimer's Diseases. Nonetheless,

not much is known about this protease. An in vitro fluorescence donor-quencher based assay was adapted for high-throughput screening of PreP modulators. From a collection of over 100,000 drug-like small molecules, we discovered numerous modulators of PreP.

MitoBloCK-60 was identified as a specific inhibitor of PreP. This piperazine-derivative does not uncouple mitochondria and affect viability of cells. Crystal structure of small molecule-bound protein at 2.3 Å revealed key bindings and specificity determinants. MitoBloCK-60 binds within the catalytic chamber of PreP, specifically at the substrate recognition exosite, inducing a conformational change in PreP that limits substrate binding. MitoBloCK-60 treatment in cultured cells suggests the role of PreP in mitochondrial quality control pathways. By being able to modulate PreP activity rapidly and selectively, we will provide insight into the involvement of PreP in mitochondria in general and how dysfunction of PreP could lead to diseases.

The dissertation of Juwina Wijaya is approved.

Catherine F. Clarke

Alexander M. Van der Blik

Carla Marie Koehler, Committee Chair

University of California, Los Angeles

2015

DEDICATION

Buat Papi dan Mami, for your making everything a possibility

TABLE OF CONTENTS

List of Figures

Acknowledgements

Vita

Chapter 1.	Introduction – High-throughput screening methods to develop small molecule probes targeting mitochondria.....	1
Chapter 2.	Discovery and characterization of small molecules modulators of presequence-degrading protease.....	41
Chapter 3.	Small molecule modulator reveals the role of presequence protease in mitochondrial quality control pathways.....	130

LIST OF FIGURES

Chapter 1.		
Figure 1.	Pathways of protein import into mitochondria	28
Figure 2.	Mitochondrial proteases maintain homeostasis.....	29
Chapter 2		
Figure 1-1.	The mitochondrion is a site for various cellular processes.....	70
Figure 1-2.	Import of matrix-targeted precursor to mitochondria.....	71
Figure 2-1.	Workflow of PreP high-throughput screening project	72
Figure 2-2.	Plasmid map of PreP construct for HTS.....	73
Figure 2-3.	Robust expression and successful purification of recombinant 6X-His-PreP.....	74
Figure 2-4.	Western blot confirmed successful PreP purification.....	75
Figure 3-1.	HTS assay development and optimization.....	76
Figure 3-2.	General protease inhibitors do not inhibit PreP activity.....	78
Figure 4-1.	Pilot screen result.....	79
Figure 4-2.	Dichlorobenzamil does not inhibit PreP.....	80
Figure 4-3.	Data processing sample.....	81
Figure 4-4.	Data analyses to mark compounds that inhibited and enhanced PreP activity.....	83
Figure 4-5.	IDE expression and purification.....	84
Figure 4-6.	Representative data for IDE counterscreen.....	85
Figure 5-1.	T057 attenuates activity of PreP <i>in vitro</i>	86
Figure 5-2.	T057 does not permeabilize mitochondria.....	87
Figure 5-3.	T057 does not impair respiration and uncouple mitochondria.....	88
Figure 5-4.	T057 inhibits import of mitochondrial proteins.....	89
Figure 5-5.	T057 protects PreP, but not IDE, from degradation by thermolysin.....	90
Figure 5-6.	T057 is an uncompetitive or a mixed inhibitor.....	91
Figure 5-7.	Structure-Activity Relationship (SAR) study of T057.....	92

Figure 5-8.	T057 treatment in cultured cells does not affect viability and impair mitochondrial morphology.....	93
Chapter 3.		
Figure 1.	MitoBloCK-60 inhibits PreP activity.....	164
Figure 2.	MB-60 inhibits PreP activity <i>in vitro</i>	165
Figure 3.	Structural analysis of MB-60-bound human PreP.....	166
Figure 4.	HDX-MS confirms MB-60 binding site within PreP and explains the mechanism by which MB-60 enhances the interaction between PreP-N and PreP-C.....	167
Figure 5.	PreP activity is redox-regulated.....	168
Figure 6.	MB-60 is synergistic with CCCP to induce mitophagy.....	170
Figure S1.	Schematic of PreP high-throughput screen.....	179
Figure S2.	Compounds in the chemical library that did not inhibit PreP.....	180
Figure S3.	Representative regions of hPreP in complex with MB-60 in stereoview.....	181
Figure S4.	SAXS data analysis of hPreP	182
Figure S5.	Summary of hydrogen/deuterium exchange rates of hPreP.....	183
Figure S6.	Comparison of hydrogen/deuterium exchange rates of hPreP induced by MB-60.....	185
Figure S7.	MB-60 does not impair general mitochondrial function.....	186
Figure S8.	MB-60 does not impair import of precursors into isolated mitochondria.....	188
Figure S9.	MB-60 is not toxic to mammalian and yeast cells.....	189
Figure S10.	Examples of images that were quantified for Fig 6c.....	191
Figure S11.	Examples of images that were quantified for Fig 6c.....	192
Figure S12.	MB-60 accelerates PINK1 recruitment in a dose-dependent manner...	194
Figure S13.	Validation of PreP's role in stress pathways using knockdown and knockout approaches.....	195
Figure S14.	MB-60 reveals the role of PreP in mitochondrial stress pathways.....	197

LIST OF TABLES

Chapter 2		
Table 1-1.	Chemical libraries screened at UCLA MSSR.....	94
Table 2-1.	Summary of screened compounds (1 st round of screening).....	94
Table 2-2.	Summary of screened compounds (2 nd round of screening).....	94
Table 3.	Summary of hits from LS library.....	95
Table 4.	Yeast strains used in this study.....	113
Chapter 3		
Table S1A.	Small molecule screening data.....	172
Table S1B.	HTS assay protocol.....	173
Table S2.	Summary of screened compounds.....	174
Table S3.	Data collection and structure refinement statistics.....	175

Table S4	SAXS data collection and scattering-derived parameters.....	177
Table S5	Yeast strains used in this study.....	178

APPENDICES

Chapter 2.		
Appendix A	Compounds repository: small molecules that inhibit MPP and PreP....	114
Appendix B.	Compounds repository: Overlap hits from LS library.....	115
Appendix C.	Compounds repository: scaffolds of hits from LS library.....	116

ACKNOWLEDGEMENTS

I am truly humbled by this journey. It is a dream come true to finally write these words. First, I would like to thank my advisor, Dr. Carla Koehler, for the opportunity to work in a lab and pursue my dream of becoming a scientist. Carla saw more potential in me than I did myself and I could not be more grateful for her love (sometimes tough) and support. I hope that my work will make her proud because she paved the way for me to continue growing as a scientist. I would also like to extend my gratitude to my committee members, Dr. Alex van der Blik, Dr. Michael A Teitell, Dr. Jorge Z Torres, and Dr. Catherine Clarke for challenging me to think critically and for their advice and guidance over the years. I am also grateful for Dr. Robert Damoiseaux's expertise and support throughout my graduate career.

I am forever indebted to Samuel Hasson for his mentorship and friendship. From day one where he kindly spent two hours out of his graduate research time to explain cloning and showed me how to use clone manager; week one where he taught me high-throughput screening methodologies, and to the forty five minutes he carved out of his hectic day as an investigator at Pfizer to talk to me about the next step in my career. Sam is always there supporting, advocating, and providing me with the best opportunities. I am grateful to have such an exemplary role model and to be able to call him a friend.

My time in graduate school would not be as rewarding if it were not for the colleagues and friends that I have met over the years. Dr. Martin Phillips at the UCLA-DOE shared instrument facility have taught me numerous methods and in many occasions provided me with hands-on technical assistance. Thank you past and present members of the Koehler lab. Yavuz Oktay, Heather Tienson, Non Miyata, Esther Neubel, Cennyana Boon, Tanya Hioe, Meghan

Johnson, Colin Douglas, Eric Torres, Eriko Shimada, Jesmine Cheung, Michael Conti, Matthew Maland and Janos Steffen. To Sonya Neal (aka Soney Sone) for her ability to bring so much positivity into anything and everything. Your enthusiasm on science and life is incredibly uplifting. To Deepa Dabir for our friendship; thank you for making my unlimited texting plan worth it! There are way too many text exchanges between us, both good and bad, but I would not have it any other way. Thank you for your (and David and K's) kindness and support. I am also thankful for the opportunity to mentor two outstanding undergraduate students. I have no doubt that Julia Mayer and Jisoo Han will both be very successful in their careers. Cheers, Koehler lab, for the jar, fantasy football, potlucks, birthday cakes, and happy hours: thank you for the camaraderie. To my entire biochemistry and molecular biology cohort, I could not have found better group of friends to embark on this journey with. I wish them all the best in their future endeavors.

This acknowledgement bit would not be complete without expressing my gratitude to the rock of my life, my family. No words can describe how indebted and thankful I am to my parents and my sisters. Dad, for your tough and endless love. Mom, for your love, patience and relentlessness. Thank you for giving me the privilege to go on this journey. Wisiani, Jufilin, and Fiwany, I am so thankful to have all of you in my life. Finally, I would like to extend my gratitude to Dan McNamara for being the best BB. In the words of E.E. Cummings, "I carry [their] heart[s] with me (I carry [them] in my heart)."

Chapter 1 is an introduction to targeting the mitochondrion as a drug target using high-throughput chemical biology. Different approaches and challenges are highlighted.

Chapter 2 highlights the assay development, screening, and initial characterization of the screening hits. PreP expression construct was generated by Colin Douglas. Sam Hasson assisted in the assay development and pilot screen. IDE was cloned, expressed, and purified with the assistance of Julia Mayer. Hit generation algorithm was created by Sam Hasson. I would like to thank Winnie Hwong and Jong Lee for their technical assistance at the screening center, Jisoo Han for technical assistance, and Vanessa Breslin for help with small molecule chemistry.

Chapter 3 is a version of a manuscript in preparation to be authored by myself, Liang WG, Mo S, Saunders JM, Damoiseaux R, Lee D, Li S, Wiseman RL, Tang WJ, and Koehler CM. Small molecule modulator reveals the role of presequence protease in mitochondrial quality control pathway. Colin Douglas generated PreP expression construct. IDE counterscreen was conducted with the help of Julia Mayer. Sam Hasson wrote the macro for data analysis. The Tang group contributed to the structural data. The Wiseman group performed qPCR and RNAseq analyses for proteostasis data. I would also like to thank Jong Lee and Winnie Hwong for assistance during small molecule screen, and to Deepa Dabir and Janos Steffen for helpful discussions.

VITA

2005-2007	Foothill College Los Altos Hills, California
2010	B.S in Biochemistry University of California, Los Angeles
2010-2015	Graduate Student Researcher Department of Chemistry and Biochemistry University of California, Los Angeles
2010-2015	Teaching Assistant Department of Chemistry and Biochemistry University of California, Los Angeles

PRESENTATIONS AND PUBLICATIONS

Wijaya. J, Damoiseaux R.D, and Koehler C.M (2012). A high-throughput screen to identify small molecule modulators of mitochondrial proteases. Presented at David S. Sigman Memorial Symposium and Lectureship, University of California, Los Angeles.

Wijaya. J, Damoiseaux R.D, and Koehler C.M (2012). Utilizing small molecules to characterize presequence-degrading protease . Presented at Gordon Research Conference: Protein Translocation Across Membranes, Galveston, Texas.

Wijaya. J, Damoiseaux R.D, and Koehler CM (2013). Characterization of small molecule modulators of presequence-degrading protease. Presented at David S. Sigman Memorial Symposium and Lectureship, University of California, Los Angeles.

Wijaya. J, Damoiseaux R.D, and Koehler C.M (2014).). Utilizing small molecules to study mitochondrial presequence-degrading protease: possible role of PreP in quality control. Presented at David S. Sigman Memorial Symposium and Lectureship, University of California, Los Angeles.

Wijaya. J, Damoiseaux R.D, and Koehler C.M (2014). Utilizing small molecules to study mitochondrial presequence-degrading protease: possible role of PreP in quality control. Presented at Society of Laboratory Automation and Screening 3rd Annual Conference, San Diego, California.

Wijaya. J, Liang W.G, Mo S, Lee D, Lee S, Damoiseaux R.D, Tang W.J, and Koehler C.M (2015). Utilizing small molecules to study mitochondrial presequence-degrading protease. Presented at Society of Laboratory Automation and Screening 4th Annual Conference, Washington DC, District of Columbia.

HONORS AND AWARDS

- 2007 English Certificate in Written Communication
Foothill College
Los Altos Hills, California
- 2007 Honors Scholar
Foothill College
Los Altos Hills, California
- 2007-2010 Honors Program, Dean's Honors List
University of California, Los Angeles
- 2010 Dolores Cannon Southam Award for Excellence in
Research
Department of Chemistry and Biochemistry
University of California, Los Angeles
- 2015 Excellence in Research Fellowship
Department of Chemistry and Biochemistry
University of California, Los Angeles
- 2015 Tony B. Academic Travel and Poster Award
Society of Laboratory Automation and Screening
4th Annual Conference, Washington DC

Chapter 1: Introduction – High-throughput screening methods to develop small molecule probes targeting mitochondria

Introduction

As scientists, we seek to understand how things work by either breaking or fixing them. In the cellular context, this is typically achieved by the classic genetic knockout approach, eliminating specific proteins and then observing the molecular and phenotypic outcomes. While this approach has been widely successful in organisms such as *S. cerevisiae* and *D. melanogaster*, genetic knockout approach is not as straightforward in mammalian systems with larger genomes and slower reproductive rates¹⁻³. Another approach to dissect molecular mechanisms of proteins is by using small, synthetic organic molecules. These molecules can either attenuate or increase activity of a specific protein, and prevent protein-protein interactions. This chemical biology approach is particularly useful to study essential proteins where knockout approach is not an option. Additionally, small molecule studies do not involve ablation of target proteins, which allows for discovery of protein functions that would not be possible with genetic approach. Small molecules also provide a rapid and often, a reversible way to modulate target proteins. They can exert their effects on proteins as soon as binding occurs and can, most of the time, be washed away to allow proteins to return to their native states, allowing for additional temporal control that is not afforded by genetic perturbations⁴. Finally, these small molecules could also be designed and synthesized for therapeutics.

Studies on small molecules as probes and drugs have been on the rise in the past decade, targeting a wide range of cellular processes from signaling, metabolism, oxidative

phosphorylation, and many more, studying proteins such as kinases, oxidoreductases, proteases, transferases, ion channels, G protein-coupled receptors, and others^{1,4-7}. These small molecules that modulate a particular protein or a specific function are discovered by performing high-throughput screens (HTS), utilizing a subset of chemical libraries⁶. Of a particular interest is utilizing chemical biology approach to study mitochondria, specifically by developing small molecules that target mitochondrial proteins and functions. In this review, we will discuss why the mitochondrion is an attractive target for small molecules development, specifically highlighting mitochondrial import machineries and proteases and their implications in diseases. We will also outline different ways in which small molecule modulators are discovered, developed, and validated. Finally, we will include examples of screens, and discuss successes and challenges of using chemical biology to study this complex organelle.

Mitochondrial dysfunctions underlie and contribute to diseases pathologies.

Evolutionary derived from endosymbiotic bacteria, the mitochondrion functions extend beyond the boundaries of the cells and influence organism's health and physiology. While the most studied function of mitochondria is its energy-producing ability, numerous studies are actively being conducted to gain insight into mitochondrial metabolism, dynamics, translation, protein import, quality control, and biogenesis, highlighting the complexity of mitochondrial functions⁸⁻¹³. Dysfunctions in these processes underlie diseases and contribute to diseases' pathologies. As such, drug discovery and probe development targeting mitochondria is especially beneficial to understand diseases mechanisms and remedies.

The mitochondrion is a membrane-bound organelle comprised of the outer membrane (OM), the inner membrane (IM), the intermembrane space (IMS), and the matrix. Various

proteins reside in these sub-compartments and while the mitochondrion has its own genome (mtDNA), only 13 proteins are encoded by the mtDNA¹⁴. The remaining mitochondrial proteins are nuclearly-encoded and synthesized in the cytosol. The human mitochondrial is approximately 16.6 kilobases circular DNA found in the matrix. It encodes about 13 proteins, 22 tRNAs, and two rRNAs¹⁴. Proteins encoded by the mtDNA are mostly respiratory chain proteins that must assemble with other proteins encoded by nuclear DNA (nDNA) to form the respiratory chain complexes¹⁵. The respiratory chain complexes are vital for ATP production via oxidative phosphorylation (OXPHOS). The mtDNA is particularly susceptible to oxidative damage, especially from reactive oxygen species (ROS) generated by complex I and III during OXPHOS^{13,16}. As such, mutations in the mtDNA and nDNA that encode for respiratory chain subunits and assembly factors are found to be causative of mitochondrial encephalomyopathies^{14,17}. These include Pearson's syndrome, leber hereditary optic neuropathy (LHON), mitochondrial encephalomyopathies, lactic acidosis, stroke-like syndrome (MELAS), myoclonus epilepsy with ragged-red fibers (MERRF), neuropathy ataxia and retinas pigmentosa (NARP), and leigh syndrome, and many others¹⁷⁻¹⁹. The results of mutations or deletions in the mtDNA are clinically heterogeneous. Large deletion in the mtDNA cause disease such as Pearson's syndrome and Kearns-Sayre syndrome (KSS)²⁰. Mutations in gene encoding tRNAs, m.A3243>G and m.8344A>G, which globally affect translation, cause MELAS and MERRF respectively. These mutations affect the tRNA leucine and lysine, respectively¹⁴. Mutation in the protein coding gene of ATPase6 (m.8993T>G) results in NARP¹⁹. One of the most challenging aspects in studying these diseases is that the diseases present themselves differently, depending on the degree of heteroplasmy (the co-existence of normal and mutated mtDNA) within the organism²¹. While the specific mutations-causing genes have been mapped, studying

mitochondrial disorders related to mtDNA mutations is still challenging due to the lack of animal models. Cybrid cells in which cells' mtDNA are removed and replaced with a mixture of wild-type and mutated mtDNA have been successful in confirming how mutations lead to defect in respiration, protein synthesis, and ATP production¹⁶. Nonetheless, better tools are needed to model these diseases with the ultimate goal of developing therapeutics.

Mitochondrial proteins encoded by nDNA are synthesized in the cytosol and imported to mitochondria with the aid of mitochondrial import machineries²². Mitochondrial proteins are synthesized as preproteins in the cytosol. These proteins typically carry N-terminal presequence/mitochondrial-targeting sequences (MTS) that allow for their recognition and import to mitochondria^{9,23}. MTS are typically amphipathic and α -helical in nature. For matrix-targeted protein, translocase of the outer membrane (TOM) recognizes MTS and drives translocation of preproteins across the membrane to the translocase of inner membrane complex (TIM)²⁴. There are two TIM complexes, each recognizing different proteins. For matrix proteins, preproteins pass through the TIM23 complex to enter the matrix where it can fold and function following removal of MTS by matrix peptidases (Figure 1C)²⁵. For membrane proteins, in addition to N-terminal MTS, they also carry additional targeting information within the membrane-spanning domain termed the stop-transfer sequence, allowing them to be inserted into the inner membrane²⁶ (Figure 1C). The other TIM complex, TIM22 recognizes targeting information of mitochondrial carrier proteins such as ADP/ATP transporter, and aids in their insertion in the inner membrane. Small TIM proteins act as chaperones in the IMS²⁷ (Figure 1D). Import of IMS proteins such as the small TIMs utilizes the MIA import pathway(Figure 1B)²⁸. IMS proteins carry cysteine-rich CX₃C motif that is recognized by oxidoreductase Mia40 once they enter IMS^{29,30}. Mia40 oxidizes and folds IMS cysteine-rich proteins. To recycle Mia40 for

successive round of protein folding, sulfhydryl oxidase Erv1/ALR reduces Mia40 and passes electrons along to cytochrome c. Electrons are ultimately passed on to molecular oxygen³⁰⁻³². Import of OM precursor proteins are not as well characterized as the others. β -barrel proteins on OM inserted to the membrane by SAM complex^{32,33} (Figure 1A). β -barrel proteins carry signals that allow them to first enter the IMS and recognition of their OM localization signal by the SAM complex allowed them to be inserted to the OM^{26,34}.

A number of mitochondrial import machineries are found to be essential⁹. As such, defects in translocation machineries could impair mitochondrial functions and contribute to disease pathologies. TIMM8a/DDP1 forms complex TIMM13 to aid in protein import into the intermembrane space²⁹. Point mutation in yeast homolog, Tim8 protein (C66W) leads Mohr-Tranebjaerg/deafness-dystonia syndrome, an x-linked neurodegenerative disorder characterized deafness, cortical blindness and dystonia²⁹. Biochemical studies led to the discovery in which the point mutation leads to an unstable protein that fails to form complex with Tim13²⁹. The defect in complex assembly reduces import of Tim23, an integral component of mitochondrial import machineries²⁹. Similarly, defect in import of pyruvate dehydrogenase (PDH) results in PDH deficiency, with symptoms such as microcephaly and cerebral atrophy⁹. Studies later showed Arg to Pro mutation within MTS results in reduced import to mitochondria. Mutation in the motor proteins essential to drive translocation of matrix proteins, DNAJC19 is associated with dilated cardiomyopathy with ataxia (DCMA)³⁵. Specifically, mutation within the splice acceptor of DNAJC19 results in a loss of exon 4, leading to a motor protein lacking DNAJ domain³⁶.

Currently, not a lot of tools are available to study mitochondrial protein machineries and import process. A number of proteins are essential; hence genetic knockout approach is not the most suitable way to understand the molecular mechanisms of protein import. Temperature-

sensitive mutants have often been employed to study essential proteins, nonetheless, this method does not allow for temporal and precise modulation that chemical biology approach provides. As such, development of small molecule tools will be advantageous not tease out specific import mechanisms and provide basis to understand how defects in mitochondrial protein import lead to diseases.

Following import, precursor proteins are processed in order for it to fold and function properly. Presequences/MTS are removed by numerous processing peptidase such as matrix-processing peptidase (MPP), inner membrane peptidase (IMP), Oct1, and Icp55³⁷⁻³⁹ (Figure 2). Upon translocation MTS on the preprotein is cleaved MPP in the matrix and IMP the inner membrane⁴⁰. Additional processing might occur in the matrix where MPP performs a second cleavage, Oct1 removes an additional octapeptide, or Icp55 removes a single amino acid from the protein^{37,41,42}. Icp55 cleavage is particularly important to stabilize proteins. Discovery of Icp55 establishes the N-end rule of mitochondrial proteins where it was found that certain amino acids on the N-terminus render proteins to be more susceptible to degradation than others⁴¹. Another membrane-embedded protease in the inner membrane is the rhomboid protease. In yeast, rhomboid protease Pcp 1 is involved in processing of cytochrome c peroxidase 1 (Ccp1) and mitochondrial genome maintenance 1 (Mgm1)⁴³. Pcp1 knockout yeast loses its mtDNA and exhibits growth defect in non-fermentable carbon source⁴⁴. In human, rhomboid protease PARL is involved in OPA1 and PINK1 processing, thereby regulating mitochondrial dynamics and quality control^{45,46}.

As with the translocation machineries, mutations in processing proteases are linked to various diseases. Mutation in α -subunit of the MPP heterodimer leads to non-progressive cerebellar ataxia (SCAR2)⁴⁷. Specifically, Ala 377 Thr mutation impairs activity of MPP,

leading to accumulation of preproteins including frataxin, and increase in hydrogen peroxide level⁴⁷. Frataxin is a matrix protein involved in iron-sulfur biogenesis and has been shown to underlie a neurodegenerative disease, Friedreich Ataxia (FRDA)^{48,49}. The aforementioned mutation from SCAR2 patients also leads to reduction of MPP in patients' lymphoblastoid cells and fibroblasts^{47,50}. MPP is an essential protein, as such, reduction in MPP level likely contribute to disease pathology. Downstream of MPP, another member of M16 family of proteases degrades the MPP-cleaved MTS. Presequence protease/peptidase (PreP) degrades MTS to smaller peptides such that they can be exported to cytosol by mitochondrial ABC transporters⁵¹. In vitro, these peptides can bind to membrane and perturb in membrane integrity and mitochondrial electrochemical gradient^{52,53}. Interestingly, PreP is able to degrade amyloid-beta (A β) peptide in vitro⁵⁴. Whether A β is imported and localized to mitochondria warrants further investigation.

With the complexity of processes occurring inside the mitochondrion, the mitochondrion is equipped with quality control systems in order to ensure homeostasis. There are numerous proteases residing in different mitochondrial sub-compartments whose functions are to degrade misfolded or damaged proteins (Figure 2). In the matrix, membrane-bound m-AAA (ATPase Associated with diverse cellular Activities) proteases such as AFG3L2 (AFG ATP-ase family gene 3-like 2) and SPG7 (spastic paraplegia 7) not only degrade misfolded proteins, but also important for respiratory complex assembly⁵⁵. Yeast devoid of the m-AAA proteases exhibit decreased respiration and ATP synthesis⁵⁶. Ribosomal protein MrpL32 is processed on the N-terminus by yeast m-AAA, resulting in mature protein. Dominant negative variant of AFG3L2 increases processing of OPA1, a mitochondrial fission protein via OMA1 and results in

mitochondrial fragmentation⁵⁷. Furthermore, AFG3L2 ablation results neuropathies in mice⁵⁸. Mutation in SPG7 has been mapped in hereditary spastic paraplegia⁵⁹.

In addition to the membrane-bound proteases, there are other oligomeric proteases in the matrix. Lon is an ATP-dependent protease with a serine protease domain containing catalytic serine-lysine dyad⁶⁰. Lon is a part of mitochondrial quality control system as it is able to degrade misfolded and damaged proteins. Substrates of Lon have been mostly studied *in vitro*, in *E. coli* and in yeast, however, substrates of human Lon have not been very well characterized. Lon is responsible for degrading aconitase, a TCA cycle enzyme susceptible to damage by reactive oxygen species (ROS)⁵⁵. *In vitro*, Lon degrades MPP- α subunit and murine steroidogenic acute regulatory protein (StAR).⁶¹ Lon has also been shown to associate with mtDNA and contributes to the regulation of complex IV assembly⁶². Thus, Lon has a role in regulating respiration in response to cellular and environmental stress. Interestingly, Lon gene expression is upregulated in hypoxic condition, in lymphoma cell lines, non-small-cell lung cancer carcinomas, and other tumor cell lines⁶³. Knockdown of Lon results in aberrant mitochondria and cell death. Since the mechanisms and regulations of human Lon are not very well understood, this particular protease is an attractive target for small molecules study given the crucial role of Lon in mitochondrial function and its implication in disease such as cancer.

Another oligomeric protease in the matrix is the ClpXP. ClpXP is a complex formed by CLPP (ClpP, caseinolytic peptidase P and ClpX, caseinolytic peptidase X)⁵⁵. It is a serine protease has been shown to degrade numerous model peptides⁶⁴. Nonetheless, the endogenous substrates of ClpXP have not been very well characterized. In *C. elegans*, ClpXP plays a major role in the mitochondrial unfolded protein response (UPR^{mt})^{10,65,66}. Peptides degraded by ClpXP are exported to the cytosol by transporter HAF1. These peptides serve as a signal for

transcription factor ATFS1 to induce transcription of mitochondrial chaperones and protective genes such as CHOP, mtHSP70, HSP60, and Lon⁶⁷. While the UPR^{mt} pathways have been characterized the most in *C. elegans*, most recent ClpXP studies in mammalian cells showed overexpression of ClpX results in increased expression of the mitochondrial proteostasis genes expressed in *C. elegans*, suggesting a conservation between model organisms⁶⁸. Small molecule probes of ClpXP could provide additional insights into mitochondrial quality control system.

In the intermembrane space, HtrA/Omi protease is reported to degrade misfolded proteins in the IMS and to interact with apoptotic proteins⁶⁹. Most recent study reveals the role of HtrA in UPR^{mt}. ROS triggers a signaling cascade involving phosphorylation of estrogen receptor α (ER α), resulting in the upregulation of HtrA/Omi to degrade proteins damaged by ROS^{69,70}. Inner membrane i-AAA proteases, YME1L and OMA1 are involved in both processing and quality control⁷¹. YME1L not only degrades misfolded proteins, it also has been shown to cleave OPA1, regulating mitochondrial fission and Atg32, regulating selective removal of damaged mitochondria (mitophagy)^{72,73}.

As highlighted above, our understanding of mitochondrial proteases are growing rapidly, but a lot of the biology remains unknown. The major shortcoming in studying mitochondrial proteases in vivo is that very few tools are available to modulate activity of these proteases in model organisms such as yeast, zebrafish, and cultured cells. Chemical biology approach pro could shed light into the functions and the disease implications of these proteases in vivo.

High-throughput screening approaches to discover and develop small molecules probes

There are two ways in which one can discover and develop small molecules probes: a target-based and a phenotypic-based approach. Below we will discuss examples of target-based

and phenotypic-based screens targeting mitochondrial proteases and protein translocation machineries.

Target-based small molecule screens

In the post-genomic era, a target-based screen is the main approach for drug and probe discovery. In this approach, a protein of interest is identified and validated, typically for its role in pathways or diseases. Biochemical, biophysical, and bioinformatics methods could be employed to validate the target of interest. A functional *in vitro* assay is then designed and miniaturized for HTS. A screen is further conducted to identify small molecules that modulate the protein of interest. Most target-based small molecule screens measure fluorescence as a function of the target protein. Target-based screens typically use recombinant proteins and it the most straightforward approach since all the parameters are known and controlled. Target-based screens also enable for structure-activity relationship (SAR) optimization of hits from the primary screen. Limitations of this type of drug and probe discovery include specificity and the need to validate the cellular activities of the molecules *in vivo*.

Design of mitochondrial target-based screens/Assay development

The goal of target-based HTS is to measure the function of an enzyme in the presence of thousands and even millions of compounds in a timely and highly reproducible manner. The central player of an enzyme assay is the protein of interest. In a cellular context, proteins can be modified by post-translational modifications, proteins can have interacting partners and co-factors, and they can also have various length and forms (splice variants). In HTS assay, it is best that the target closely resemble its physiologic state to ensure that the hits identified will be relevant *in vivo*. While the ideal scenario is to have the most biologically relevant form of target protein, it is not always plausible to express and purify the enzyme in the native state. For

instance, membrane proteins are technically challenging to purify and retained in their native states. As such, it is important to create multiple constructs and test the purity, activity, and stability of the target protein.

Choice of expression system will also impact the quality of target proteins. While *E. coli* is the most widely-used expression system, it might not express human proteins well⁷⁴. Yeast, Sf9 cells/baculovirus, and mammalian cells are alternative expression systems⁷⁵⁻⁷⁷. For proteins that are not soluble, inclusion of tags such as glutathione-s-transferase (GST), and maltose-binding protein (MBP) and expression with co-chaperones could enhance solubility and expression, while ensuring that the tag does not interfere with function⁷⁸. Upon successful expression, protein extraction methods should carefully be considered to ensure proper protein folding thus activity. Purification from inclusion body (*E. coli system*) requires proteins to be denatured and then re-folded, which might not result in the native protein conformation⁷⁴. Furthermore, purity of the target must be monitored as impurities might affect HTS result. Ideally, enough proteins should be produced for an entire screen using of large-scale protein production to reduce batch-to-batch variability. The effect of freeze-thaw cycle on the activity and stability of the enzyme should also be taken into account.

Once the target protein is expressed, purified, and tested for activity, one must consider the HTS parameters as they might interfere with the assay. For instance, proteins will be incubated in the presence of compounds' solvent, typically dimethylsulfoxide (DMSO) and the presence of such organic compound might affect protein stability or activity. A DMSO-tolerance test, titrating different amount of DMSO must be conducted to rule out the effect of DMSO. Furthermore, one must consider the effect of the HTS "hardware," namely the liquid dispenser. Some proteins can bind irreversibly to the tubing, resulting in a reduced amount of enzymes on

the actual screening plates. Low amount bovine serum albumin (BSA), and detergents such as NP-40, CHAPS, TWEEN, and Triton present in the buffer could alleviate such problem (<0.01%). Additionally, the stability of the protein within the bottle container or the liquid dispensing tubing over time must be tested. Environmental factors such as light and temperature should also be considered.

Choice of buffer is extremely important to ensure the optimum environment for the enzyme. Buffers should closely mimic physiological condition for the enzyme and these include salt concentration, metal ions/co-factors, and pH. Buffers such as TRIS, HEPES, and MOPS are commonly used for enzyme assays since they are best at maintaining physiological pH. For proteins requiring co-factors such as metal ions, these ions could be added to the buffer and tested to ensure the optimal concentration that gives the best signal to noise ratio. Excess zinc has been shown to inhibit zinc metalloproteases⁷⁹. Tris has been shown to chelate metal ions, which could affect the activity of enzymes requiring metal ions⁸⁰.

The other player in an enzyme assay is the substrate. Choice of substrate, similar, to enzyme construct can significantly affect the quality of the assay. The best substrate should be stable and biologically relevant. Substrate should also be added at the ideal concentration⁸¹. While increasing substrate concentration can result in a high signal to noise ratio, this might not allow for identification of hits with specific modality⁸². Ideal substrate concentration should be around the K_m (measure of substrate turnover to product) of the enzyme^{83,84}. This allows investigators to capture small molecule hits that are competitive, uncompetitive, and noncompetitive in nature. If the substrate concentration used is above the K_m of the enzyme, the majority of the substrate will occupy the active site of the enzyme, making it harder for competitive inhibitors to bind and be identified as hits⁸⁵. If the substrate is much lower relative to

the K_m , there is very little of enzyme-substrate complex in the solution, making it harder to identify uncompetitive inhibitors. Non-competitive inhibitors are not affected by the substrate amount because they bind at an allosteric site that is not influenced by presence of substrate⁸⁴.

In measuring the functionality of the target protein, one can decide on a direct or indirect detection method. In a direct detection mode, either substrate disappearance or product appearance is directly measured, typically through fluorescence. In an indirect method, the assay is coupled to another reaction that measures the progress or completion of the assay. For instance, ATP hydrolysis results in ADP and inorganic phosphate. This can be coupled by addition of reagents that can bind to inorganic phosphate and results in increase in signal. Malachite green is commonly used to measure ATP hydrolysis. Free inorganic phosphate react with malachite green molybdate, resulting in the formation of green molybdophosphoric acid complex that can be measured on a plate reader at 620-640 nm⁸⁶. We will discuss a few *in vitro* biochemical assays that have been used to screen for modulators of mitochondrial proteins below.

Applications

To report activities of proteases, fluorogenic substrates are often used⁸⁷. This type of substrate carries fluorophore on one end and a quencher on the other end. Intact substrate gives no or very little fluorescence whereas cleaved substrate results in an increase in fluorescence^{88,89}. The enzymatic cleavage of substrate can be monitored over time. An analogous assay is using fluorescence resonance energy transfer (FRET) substrates¹⁵. A donor and acceptor molecules attached to the end of the substrate will transfer energy when the substrate is intact whereas when it is cleaved, the fluorescence dissipate because the donor-acceptor molecules are no longer close to each other to allow for FRET to occur⁹⁰.

An example of using fluorogenic peptide as a substrate is when we synthesized a peptide that is made up of part of leuromorphin sequence, attached an methoxycoumarin (MCA) fluorophore and a proprietary quencher (JPT) and use this as substrate to screen for inhibitors of mitochondrial presequence-degrading protease (PreP). A similar screen conducted for small molecules inhibitors of mitochondrial matrix-processing peptidase (MPP) use an intramolecular-quenched presequence of yeast alcohol dehydrogenase as the substrate. In both of these cases, we used a direct method of detection by measuring increase of fluorescence as a function of peptide cleavage, which corresponds to protein activity. We learned from the screen that it is important to measure basal fluorescence level prior to substrate addition, as many small molecules are intrinsically fluorescent and could contribute to the end point reading. Our PreP screen led us to the discovery of MitoBloCK-60, which when used as a probe, revealed an unexpected role of PreP in activation of mitochondrial stress pathways. A successful screen using indirect method of detection is when Dabir et al used amplex red coupled assay to identify inhibitors of a mitochondrial sulfhydryl oxidase, Erv1⁹¹. The redox activity of Erv1 was measured by oxidation of dithiothreitol (DTT), which produces hydrogen peroxide (H₂O₂). H₂O₂ oxidizes amplex red in the presence of horseradish peroxidase (HRP) to fluorescence resofurin⁹². The screen identified MitoBloCK-6 as an inhibitor of erv1 and MitoBloCK-6 probed the role of erv1 in stem cell development⁹¹. A similar assay in which the function of protein is indirectly detected is an ATPase assay. The malachite green assay described earlier indirectly detects the level of organic phosphate in the solution, as a function of ATP hydrolysis. This type of assay can be applied to recombinant mitochondrial ATPases such as LON, AF3GL2, SPG7, and others.

Finally, a more recently developed method is to use activity-based probes (ABP) to measure protease activity⁹³. ABPs are small molecules that covalently bind to the active form of

an enzyme. ABPs typically consist of a tag, a spacer, and an electrophilic group that traps within an active site of a nucleophile⁹⁴. When the tag is fluorescence, the binding of ABPs to their targets can be monitored by fluorescence polarization and/or fluorescence microscopy. Binding of fluorescence ABP on an active site of a protein results in slower tumbling of the ABP molecule, thus giving a high fluorescence polarization. In contrast, free ABP tumbles freely in the solution and fluorescence polarization is reduced^{88,93}. Utilizing ABP, one can identify small molecules that inhibit binding of ABP to protease active site. Wolf et al uses fluorescence-ABP and discovered β -lactones as novel class of inhibitors targeting bacterial rhomboid protease GlpG⁹⁵. More recently, the same group extended their study where they used ABP to obtain an inhibitor fingerprint of 13 rhomboid proteases⁹⁶. Furthermore, the inhibitors discovered were utilized as probes where they identified an unexpected auto-processing ability of rhomboid proteases⁹⁶. There is currently no known inhibitor of mitochondrial rhomboid proteases, nonetheless, given the tools available to measure activity of rhomboid proteases, specific ABP can be designed to target mitochondrial rhomboid protease as PARL, which play role in quality control and homeostasis. In addition to rhomboid protease, ABP has also been utilized to create a peptide reporter substrate and peptide inhibitor of the Lon protease with the goal of enhancing our understanding of Lon's functions in normal and disease state⁹⁷. Additionally, since the substrates of many mitochondrial proteases are not very well characterized, the advent of ABP could be a way to characterize these proteases.

Characterization of hits obtained from target-based screens

One of the main concerns in target-based approach is the specificity of the hits toward the target. While the *in vitro* system is simple and easy to set up, a battery of secondary assays or

counterscreens must be in place to tackle the specificity concern. For instance, to determine specific hits of PreP, we performed counterscreens of the initial hits with two other proteins, MPP and IDE, both belonging in the same family of M16 protease as PreP. We found there were molecules that both inhibit PreP and MPP. Non-specific hits could also be problematic as they can lead to unexpected toxicity and interpretation in the biological system. While it simple and easy to synthesize, the drawback of using fluorogenic substrates is that they might not be necessary relevant in a cellular context. Fluorogenic peptides are typically short, only containing the sequences that are necessary for reaction to occur. Small molecules can also react with these peptides and result in false positive or negative. As such, it is important to design complimentary assays to ensure that the hits are not specific to just the substrate used.

In addition to exhibiting specificity, the characterization of small molecule probes must also include mechanism of action studies. Structure-activity relationship (SAR) study is extremely crucial to understand the mechanism of action and to optimize the lead compound. Traditionally, SAR studies have been focused on the specific compound groups in collaboration with chemists. Today, the traditional approach can be complemented with bioinformatics, which results in a better and more comprehensive large-scale SAR. Data mining has emerged as a powerful tool of SAR study⁹⁸. Review on large-scale SAR analysis can be found here⁹⁹ and also briefly discussed later. Following lead optimization through SAR, another important aspect of small molecules development is understanding how and where the molecules bind within the target. Fluorescence polarization and anisotropy could be used to show that the molecules indeed bind to the target⁵. Further characterization includes IC₅₀ analysis and classic enzyme kinetics to determine inhibition modality. Copeland et al has extensively reviewed the characterization of small molecule inhibitors by classic enzyme kinetics approach here⁸¹⁻⁸⁴. Biophysical methods

such as fluorescence spectroscopy, differential scanning calorimetry (DSC), surface plasmon resonance (SPR) and isothermal titration calorimetry (iTC) are increasingly being used to understand small molecule binding parameters^{100,101}.

Another powerful approach to understand mechanism of action is by structural biology approach. X-ray crystallography structure of small molecule bound to target provides a molecular insight into the mechanism of inhibition. X-ray structure also aids in compound optimization. Complementary to structural approach, proteomics approach has emerged to be powerful in small molecule validation and characterization. Hydrogen/deuterium exchange coupled with mass spectrometry (HDX-MS) can also highlight the regions within the target protein that are most influenced by small molecule binding¹⁰². Once the small molecule has been characterized and declared as lead compound, the long-term goal is to use the compound as probe to understand mechanisms of proteins *in vivo*. A checklist of what constitute a good probe can be found here¹⁰³.

Phenotypic-based small molecule screens

In a phenotypic-based approach, a pathway or phenotype of interest is identified then a screen is performed to identify small molecules that perturb the pathway or result in change in phenotype. Phenotypic screens afford the possibility of discovering therapeutics targets, as the screens are more biologically relevant than screens with recombinant proteins. While phenotypic screen is extremely powerful, one of the biggest challenges is identifying the specific target of the molecule that gives rise to the observed phenotype. Secondary assays to identify the exact target of the small molecules must also be in the works simultaneously. Below we highlight a few important considerations for setting up phenotypic-based screens targeting mitochondria.

Design of mitochondrial phenotypic screens

Model system

Budding yeast, *Saccharomyces cerevisiae* is commonly used for phenotypic screen, owing to the ease of manipulation and high level of conservation of mitochondrial genes and functions. For a more complex model system, immortalized cell lines are easily obtainable, can be grown in high quantities and convenient. However, one must take into consideration the metabolic states of these cells. Some of these cell lines are highly glycolytic, which might not be suitable to study mitochondrial functions. On the other hand, primary cells lines are more biologically relevant and can be specifically derived from patients. Other model organisms such as worms (*C. elegans*) and zebrafish (*D. rerio*) can be genetically manipulated to tag mitochondrial protein or processes and have since been extensively used in phenotypic screens especially since they allow for physiological observations at the multi-organ level.

Assay Development

Measurement of ATP level is often used to measure compound toxicity. Assays measuring ATP level are well established and they typically involve a reporter-based assay¹⁰⁴. ROS level can be used to measure toxicity and the level of mitochondrial homeostasis. Mitochondria-targeted redox sensitive proteins can be oxidized by ROS and their intensity can be used to indirectly measure ROS level^{105,106}. Alternatively, ethidium-based dyes such as DCFDA and MitoSox are commonly used to measure hydrogen peroxide and superoxide level respectively¹⁰⁷. Woolley et al wrote a great comprehensive analyses of different ROS probes and their applicability in different systems¹⁰⁸. Measurement of membrane potential ($\Delta\Psi$) is particularly useful to monitor functional state of mitochondria. Respiring mitochondria would have an established level of $\Delta\Psi$ whereas damaged or stressed mitochondria would show a

reduced $\Delta\Psi$. To measure membrane potential, multiple dyes can be used. For instance, mitoTracker and tetramethylrhodamine (TMRM) accumulate in mitochondria in the presence of $\Delta\Psi$. These dyes, along with fluorescently-tagged mitochondrial proteins can also be utilized to monitor mitochondrial morphology. Cell growth conditions as such as medium, incubation, seeding, temperature, and pH can affect the analysis. For instance, mitochondria undergo less fission upon nutrient starvation, thereby showing long, fused mitochondrial morphology. It is important that cells are seeded at optimal density that represents an optimal, non-stressed condition. Reviews on probe selections have been described^{104,109–111}. In addition to probes, reporter genes are great tools to monitor mitochondria. Luciferase-based gene reporter assay has been extensively used in high-throughput screens to measure promoter activity any protein of interest¹¹². For instance, gene expression of COX2, encoded by mtDNA can be used to measure mitochondrial biogenesis; activation of mitochondrial stress pathways can be measured by monitoring LON promoter reporter activity. The ability to monitor these various parameters by assay multiplexing makes HCS extremely powerful and informative.

Applications

Many of the assays described above can be set up in different organisms from yeast, cultured cells, and whole organism such as zebrafish. Montague et al used yeast to screen for small molecules that increases mitochondrial membrane potential. Using a $\Delta\Psi$ membrane sensitive dye, DiOC₃6, the authors discovered a subset of molecules that not only increase $\Delta\Psi$, but also ATP level first in yeast then confirmed in cultured cells¹¹³, further validating that findings in yeast can be extended to mammalian cells and possibly other model systems.

Import of nuclearly-encoded mitochondrial proteins utilizes various mitochondrial translation machineries. Genetic knockout approach is often not suitable to study protein import

because a lot of the import machinery proteins are essential. To facilitate mechanistic studies, small molecules are developed to measure import efficiency and how defect in import contribute to diseases. Hasson et al utilizes yeast as a model organism to probe the mechanism of protein import through the TIM22 complex¹¹⁴. Specifically, the authors used temperature-sensitive mutant of Tim10, a protein involved in chaperoning precursor proteins to the TIM22 complex, and conducted a growth-based phenotypic screen to discover compounds that induce synthetic lethality. Yeast is a great platform for drug discovery due to its homology to human, ease in genetic manipulations, and simple readouts¹. More than 30% of human proteins have yeast homolog. In fact, the majority of mitochondrial translocation machineries were first discovered and characterized in yeast¹¹⁵. The ease of genetic manipulation in yeast allowed the authors to generate and use a temperature-sensitive strain that grow at permissive temperature (25°C) but not at non-permissive temperature (37°C). The authors identified compounds that are synthetic lethal at permissive temperature by measuring optical density of yeast at 600 nm. The lead compound, MitoBloCK-1 inhibits import of preproteins that utilize TIM22 complex. Although MitoBloCK-1 might have multiple targets in yeast, the authors designed secondary assays to determine specific inhibition site of the small molecule, which is critical for phenotypic-based screens. MitoBloCK-1 was found to inhibit import by preventing binding of substrate to tim9/10 complex to the substrate, thus the substrate failed to be reach the TIM22 translocon, highlighting the importance of the assembly and chaperoning of tim9/10 complex in import of TIM22 substrates, all of which will not be possible with classical genetic approach.

Miyata et al also used yeast as a model system and designed an assay to screen for inhibitors of that block import of proteins that utilize the TIM23 complex. Mitochondria-targeting signal of subunit 9 of ATP synthase from *N. crassa* was fused with URA3 gene (Su9-

Ura3)¹¹⁶. Presence of Su9 drives translocation of Ura3 to mitochondrial matrix through the TIM23 complex and render yeast unable to grow on media lacking uracil. If Su9-Ura3 does not enter mitochondria, however, Ura3 is present in the cytosol and yeast can grow on media lacking uracil. By measuring yeast growth in the presence of small molecules, the authors identified MitoBloCK-12/DECA (Dequalinium chloride) as an FDA-approved small molecule inhibitor of protein import through the TIM23 complex. The discovery of DECA as mitochondrial import inhibitor is not only useful to study the mechanics of TIM23 substrate proteins import, but also for possible therapeutics since numerous proteins are found to be mislocalized to mitochondria. The authors utilized MitoBloCK-12/DECA to pharmacologically rescue of a mislocalized mutant of peroxisomal enzyme, alanine:glyoxylate aminotransferase^{P11LG170R} (AGT^{P11LG170R}). This mutation is the underlying cause of primary hyperoxaluria (PH1). AGT usually traffics to the peroxisome to detoxify glyoxylate and prevent oxalate accumulation, however, mutations in the N-terminal end of AGT generate a mitochondrial targeting sequence that allows for AGT import to mitochondria. Treatment of cells overexpressing AGT^{P11LG170R} with DECA blocks import of mutant protein to mitochondria and restores trafficking of AGT to peroxisome where it can prevent oxalate accumulation. This study is another great example on how discoveries in model organism such as yeast can be directly translated to mammalian systems¹.

While phenotypic screening measuring growth or fluorescence is a useful readout, an emerging and powerful method to set up a screen is by using microscopy (high content screening/HCS). HCS allows for measurement of multiple parameters thus gaining much more information from a single image. For instance, an assay using microscopy to monitor localization of mutant AGT in mammalian system has been developed¹¹⁷. In addition to the protein of interest, cells can also be labeled with dyes to mark different cellular compartments such as

nucleus, peroxisome, lysosome, and mitochondria. An image acquired in HCS is the extremely powerful as not only will it show the location of AGT within the cell, it will also show the status of other compartments in the presence of small molecules.

In contrast correcting mislocalized proteins, another strategy is to use small molecules to purposely mislocalize proteins. For instance, preventing oncoproteins to localize to certain cellular compartments can help treat cancer. Ras is overexpressed in cancer. Palmostatin B, which inhibits depalmitoylation of acyl protein thioesterase 1 (APT1) can inhibit localization of palmitoylated Ras on the cell surface and reduce cancer cells survival^{118,119}. For mitochondria, HCS can be powerful to identify modulators that influence fumarate hydratase/fumarase localization. Fumarase underlies a tumor susceptibility syndrome, hereditary leiomyomatosis and renal cancer cell (HRLCC)^{120,121}. Inactivation of fumarase in HRLCC stabilize hypoxia-induced factor (HIF) and enhance tumorigenesis¹²⁰⁻¹²². Fumarase is dually localized to mitochondrial matrix and cytosol¹²³. Under stress, a subset of fumarase residing in the cytosol is imported to the nucleus to aid in DNA damage repair, specifically double DNA breaks¹²⁴. HCS can be applied in this case to identify modulators that can regulate fumarase localization for both mechanistic and therapeutics applications. In a whole organism screen such as zebrafish screens, HCS can be used to monitor multiple organs. Transgenic zebrafish lines expressing fluorescent mitochondria can be used to monitor mitochondria in neuron and hearts^{91,116,125}.

Characterization of hits obtained from phenotypic screens

While phenotypic screens enables researcher to observe the direct effects of small molecules in a more biologically relevant setting, identifying the molecular target of the molecule remains a hurdle, not to mention that a single molecule could target multiple proteins or pathways (off-target effects). Orthogonal approach utilizing biochemical, genetic, and

bioinformatics methods can complement each other in target identification. Affinity purification method enables for targets to be pulled down with immobilized small molecules. Target can then be identified via mass spectrometry (MS)^{126,127}. This approach emerged as the most popular strategy for target identification as it is unbiased and it probes the entire proteome. Combination of SILAC-based quantitative proteomics with affinity chromatography have greatly improve target identification within these past few years¹²⁸. Nonetheless, this method comes with its own challenges. Identifying binding of small molecules to low abundance proteins can be challenging in a mixture of millions of proteins. On the other hand, high abundance proteins can bind non-specifically to immobilized small molecules beads. Other parameters such as compound solubility and choice of buffers should also be noted to ensure successful chemical proteomics.

More recent methods have emerged that does not require immobilization of small molecules to beads. One method relies on the idea that small molecule binding changes the conformation of the target protein and results in increased resistance to proteolysis. Drug affinity responsive target stability (DARTS) has shown binding of FKBP12 to rapamycin, celecoxib to COX2, and many others decreased target's sensitivity to proteolytic degradation¹²⁹. While DARTS have been quite successful, one cannot rule out the fact that protease sensitivity might not be decreased upon small molecule binding. Another biochemical method, target identification by chromatographic co-elution (TICC), relies on the principle that small molecule binding leads to increase in the retention time of target protein. TICC has been successfully used to identify binding of molecules to low abundance targets¹³⁰. Another biochemical method, cellular thermal shift assay (CETSA) relies on the principle of increased target's thermodynamic as a result of small molecule binding¹³¹. The proof-of principle study of CETSA was highlighted by an increase in melting temperature and stabilization of p38 α and ERK1/2 in the presence of

their respective inhibitors¹³². Furthermore, CETSA has been nicely adapted for high-throughput screens. The success of CETSA is demonstrated by growing number of publications utilizing CETSA to identify target of small molecules^{133,134}.

In addition to biochemical approaches, genetic screening has been widely successful in identifying drug targets. The ease of genetic manipulation in yeast such as *S. cerevisiae* has provided the best proof-of concept in utilizing genetic screening for target identification. Integration of chemical-genetic and genetic interaction can aid in identifying cellular targets. Drug-induced haploinsufficient profiling (HIP) leverages the fact that decreased level of the target gene in a heterozygous population results in increased drug sensitivity¹³⁵. An analogous approach, homozygous profiling (HOP) utilizes fully deleted yeast strains to identify a pathway that small molecules act on. Single-deletion mutant that interact with small molecules can show synthetic lethality². The readily available yeast single deletion mutants can be treated with small molecules and chemical-genetic profile can be generated and provide insight into the molecular targets or pathways affected by the small molecules^{137,138}. By screening yeast deletion library, the genome-wide profile can be generated and analyzed to infer the drug's target. Complementary to the HIP/HOP approach, multicopy suppression profiling (MSP) uses overexpression yeast strains with the idea that increasing the copy number of genes will decrease sensitivity to small molecules¹³⁶. Together, these yeast genetics assays provide distinct information that can be integrated to reveal the molecular target and mechanisms of small molecules.

Extending upon genetic-based approach in yeast, genome-wide RNAi and cDNA libraries can be employed in mammalian system to identify drug targets. RNAi screen can be performed to find genes that phenocopy the effect of small molecules. Alternatively, if some

mechanistic clues are available, a more focused RNAi library could be used. While this approach is powerful, genetic knockdown does not always phenocopy small molecules effect. Numerous small molecules targeting kinases do not give the same effect as RNAi knockdown¹³⁹. Nonetheless, RNAi knockdown can still validate the target of small molecules. Similar to the idea of a HIP assay, reducing the copy number of target gene with RNAi can render cells more sensitive to small molecules. For example, Sato et al showed knockdown of prohibitin leads to increased sensitivity of cells to aurilide¹⁴⁰, Castoreno et al discovered small molecule inhibitors that target rho signaling in cytokinesis by partially reducing the amount of Rho GTPase available using RNAi¹⁴¹. The authors further showed the specificity of the targets when overexpression renders cells resistant to the small molecule. Analogous to MSP in yeast, overexpression of target genes using cDNA library could aid in validating small molecule target.

Rounding up the orthogonal approach to identify drug targets, it would be remiss to exclude the powerful tools of bioinformatics. Connectivity map project is a database that stores gene expression profiles from cultured human cells treated with small molecules¹⁴². Transcriptional profiles derived from molecules perturbing the same pathway is likely to be similar. Another bioinformatics approach, CSNAP (Chemical Similarity Network Analysis Pulldown), utilizes chemical similarity network to infer drug target¹⁴³. List of databases, methods, and applications can be found in here¹⁴⁴.

***In silico* probe development and drug design**

Over the last decade, there has been an increasing growth in computational (*in silico*) approach to drug and probe discovery. *In silico* approach uses algorithms and softwares to store biological data and then create simulations and predictions to advance drug discovery. Computational drug discovery relies on the availability of structures of the target proteins. The

structure serves as the reference point for virtual drug screenings using various algorithms¹⁴⁵. If the structure is not available, a homology model can be created from closely related homologs. Some of the specific methods currently being used to design and discover probe include databases of previously characterized drugs, quantitative-structure activity relationship (QSAR), molecular modeling/docking, machine learning, data mining, and network analysis^{144,146,147}. While a lot of improvements have been made towards a better *in silico* drug design and discovery, these improvements are often not enough to replace the experimental approaches. Nonetheless, *in silico* methods could serve as alternative and complementary approaches to experimental drug discovery. The tremendous ongoing development in the field could only add to the sophisticated toolbox for scientists to develop chemical tools to study protein functions.

Concluding remarks

Looking forward, we anticipate mitochondria to grow as an attractive drug target. There are still a lot of unknowns within the mitochondria and the HTS approach, developing probes to study mitochondrial functions will lead to many great biological discoveries. Here, we outlined the different methods to set up and follow up on hits for both target-based and phenotypic-based screens, and highlighted a number of successful screens. In the near future, recently developed genome editing technologies (TALEN, ZFN, CRISPR) provide an exciting avenue to advance HTS technologies. While increasing assay system and complexity increased biological relevance, it also comes with decreased throughput and mechanism of action improvements. Nonetheless, at the end, multifaceted approaches will complement each other to ultimately increase our understanding of the fundamental biology and provide basis to develop therapeutics.

Figures

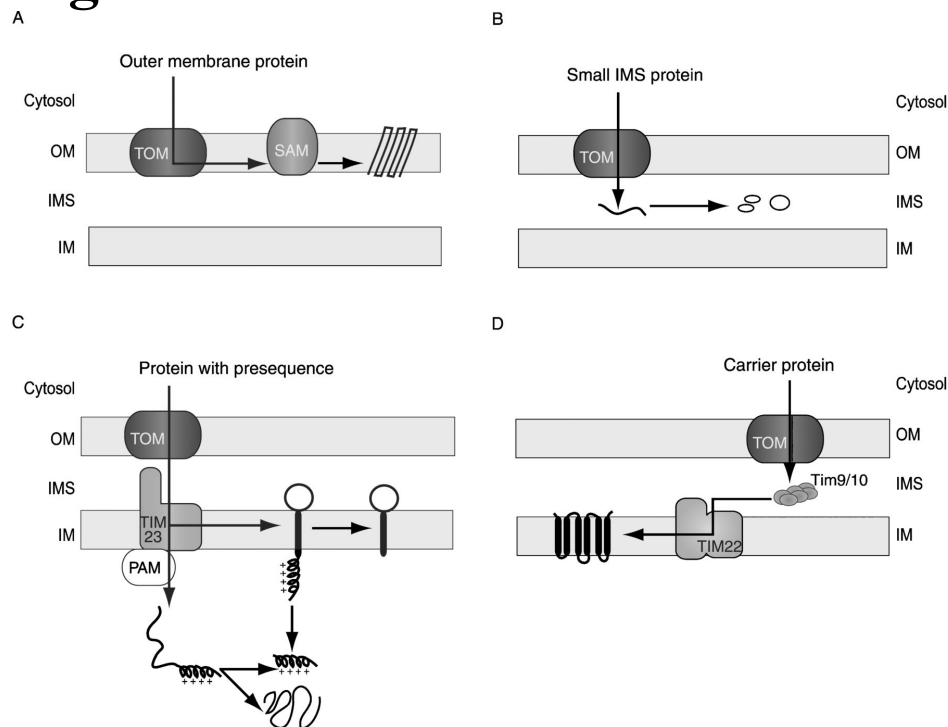


Figure 1¹⁴⁸. Pathways of protein import into mitochondria. (A) Outer membrane, β -barrel proteins are imported and inserted to the OM by the SAM complex. (B) IMS-targeted proteins are typically cysteine-rich proteins that import through the MIA pathway. In the IMS, the redox-relay system involving mia40 and erv1 folds proteins to their native conformations. (C) Matrix-targeted proteins carry N-terminal presequences that are recognized by the TOM complex. Once they are imported across the membrane, they are passed on to the TIM23 complex. Preproteins enter the matrix and immediately processed by MPP to produce mature proteins. IM-targeted proteins carry both N-terminal presequences and top-transfer signals that allow for their insertion on to the IM via the TIM23 translocon. (D) Carrier proteins are chaperoned by small TIM proteins and delivered to the TIM22 translocon upon entry to mitochondria. TIM22 complex inserts carrier proteins to the inner membrane.

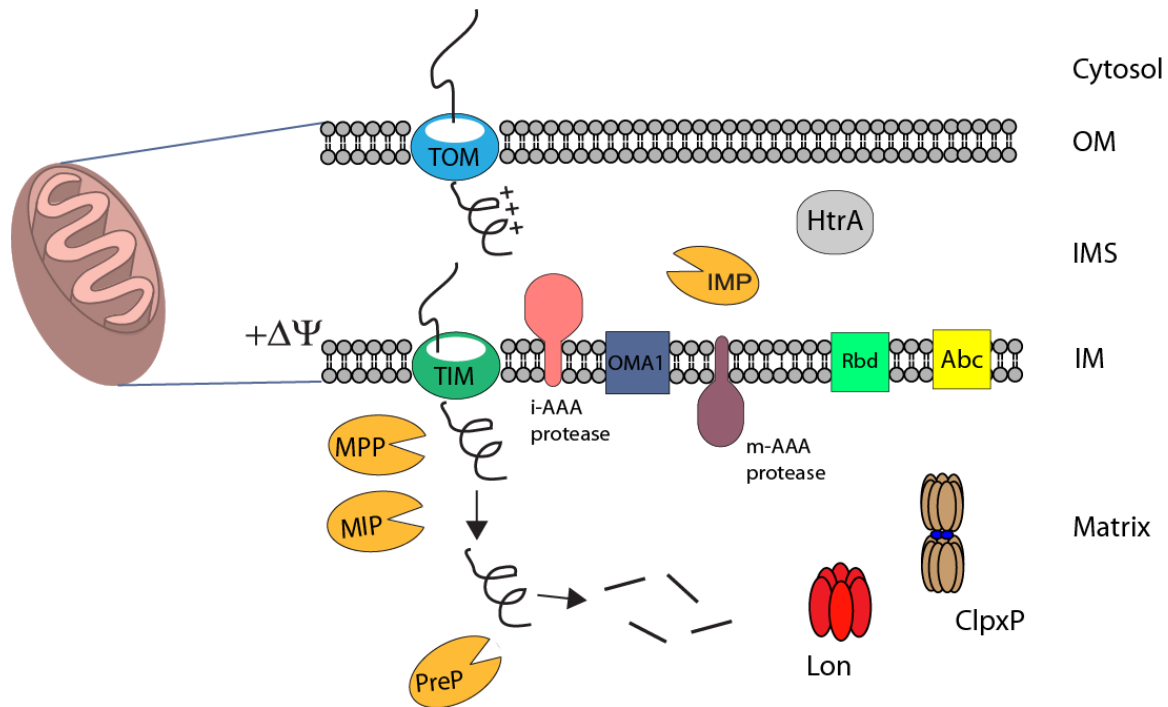


Figure 2. Mitochondrial proteases maintain homeostasis. Processing peptidases (yellow) are involved in protein maturation. In the matrix, MPP and MIP cleave mitochondrial targeting sequence (MTS) and PreP degrades MTS upon MPP cleavage. IMP functions like MPP in the intermembrane space (IMS). AAA proteases facing the IMS and matrix degrade misfolded and damaged proteins. HtrA/Omi protease in the IMS is upregulated in the presence of ROS. Oligomeric proteases such as Lon and ClpXP are also involved in quality control by degrading misfolded and damaged proteins. ClpXP has been shown to be directly involved in activation of UPR^{mt} in *C. elegans*.

References

1. Lasserre, J.-P. *et al.* Yeast as a system for modeling mitochondrial disease mechanisms and discovering therapies. *Dis. Model. Mech.* **8**, 509–526 (2015).
2. Boone, C., Bussey, H. & Andrews, B. J. Exploring genetic interactions and networks with yeast. *Nat. Rev. Genet.* **8**, 437–49 (2007).
3. Khurana, V., Tardiff, D. F., Chung, C. Y. & Lindquist, S. Toward stem cell-based phenotypic screens for neurodegenerative diseases. *Nat. Rev. Neurol.* **11**, 339–350 (2015).
4. Schreiber, S. L. Small molecules: the missing link in the central dogma. *Nat. Chem. Biol.* **1**, 64–6 (2005).
5. Stockwell, B. R. Exploring biology with small organic molecules. *Nature* **432**, 846–854 (2004).
6. Swinney, D. C. & Anthony, J. How were new medicines discovered? *Nat. Rev. Drug Discov.* **10**, 507–19 (2011).
7. Stockwell, B. R. Chemical Genetic Screening Approaches to Neurobiology. *Neuron* **36**, 559–562 (2002).
8. Tait, S. W. G. & Green, D. R. Mitochondria and cell death: outer membrane permeabilization and beyond. *Nat. Rev. Mol. Cell Biol.* **11**, 621–632 (2010).
9. MacKenzie, J. A. & Payne, R. M. Mitochondrial protein import and human health and disease. *Biochim. Biophys. Acta* **1772**, 509–23 (2007).
10. Baker, B. M. & Haynes, C. M. Mitochondrial protein quality control during biogenesis and aging. *Trends Biochem. Sci.* **36**, 254–61 (2011).
11. Kompore, M. & Rizzo, W. B. Mitochondrial fatty-acid oxidation disorders. *Semin. Pediatr. Neurol.* **15**, 140–9 (2008).
12. Pirinen, E., Lo Sasso, G. & Auwerx, J. Mitochondrial sirtuins and metabolic homeostasis. *Best Pract. Res. Clin. Endocrinol. Metab.* **26**, 759–70 (2012).
13. Suomalainen, A. Mitochondrial roles in disease: a box full of surprises. *EMBO Mol. Med.* e201505350 (2015). doi:10.15252/emmm.201505350
14. Lott, M. T. *et al.* mtDNA Variation and Analysis Using MITOMAP and MITOMASTER. *Curr. Protoc. Bioinformatics* **1**, 1.23.1–1.23.26 (2013).

15. Hüttemann, M., Kadenbach, B. & Grossman, L. I. Mammalian subunit IV isoforms of cytochrome c oxidase. *Gene* **267**, 111–123 (2001).
16. Swerdlow, R. H. Mitochondria and cell bioenergetics: increasingly recognized components and a possible etiologic cause of Alzheimer's disease. *Antioxid. Redox Signal.* **16**, 1434–55 (2012).
17. Dimauro, S. A history of mitochondrial diseases. *J. Inherit. Metab. Dis.* **34**, 261–76 (2011).
18. Scheibye-Knudsen, M., Fang, E. F., Croteau, D. L., Wilson, D. M. & Bohr, V. A. Protecting the mitochondrial powerhouse. *Trends Cell Biol.* (2014). doi:10.1016/j.tcb.2014.11.002
19. Wallace, D. C. A mitochondrial paradigm of metabolic and degenerative diseases, aging, and cancer: a dawn for evolutionary medicine. *Annu. Rev. Genet.* **39**, 359–407 (2005).
20. DiMauro, S., Schon, E. a, Carelli, V. & Hirano, M. The clinical maze of mitochondrial neurology. *Nat. Rev. Neurol.* **9**, 429–44 (2013).
21. Milane, L., Trivedi, M., Singh, A., Talekar, M. & Amiji, M. Mitochondrial biology, targets, and drug delivery. *J. Control. Release* **207**, 40–58 (2015).
22. Neupert, W. *et al.* [17] Analysis of Mitochondrial Protein Import Pathway in *Saccharomyces cerevisiae* with Translocation Intermediates By. **8432**, 241–252 (1995).
23. Kmiec, B., Teixeira, P. F. & Glaser, E. Shredding the signal: targeting peptide degradation in mitochondria and chloroplasts. *Trends Plant Sci.* (2014). doi:10.1016/j.tplants.2014.09.004
24. Horst, M. & Kronidou, N. G. Protein import into mitochondria. *Membr. Protein Transp.* **1**, 109–143 (1995).
25. Neupert, W. Protein import into mitochondria. *Annu. Rev. Biochem.* **66**, 863–917 (1997).
26. Neupert, W. & Herrmann, J. M. Translocation of proteins into mitochondria. *Annu. Rev. Biochem.* **76**, 723–749 (2007).
27. Bohnert, M., Pfanner, N. & van der Laan, M. A dynamic machinery for import of mitochondrial precursor proteins. *FEBS Lett.* **581**, 2802–10 (2007).
28. Gabriel, K. *et al.* Novel mitochondrial intermembrane space proteins as substrates of the MIA import pathway. *J. Mol. Biol.* **365**, 612–20 (2007).
29. Roesch, K. Human deafness dystonia syndrome is caused by a defect in assembly of the DDP1/TIMM8a-TIMM13 complex. *Hum. Mol. Genet.* **11**, 477–486 (2002).

30. Tienson, H. L. *et al.* Reconstitution of the mia40-erv1 oxidative folding pathway for the small tim proteins. *Mol. Biol. Cell* **20**, 3481–90 (2009).
31. Longen, S. *et al.* Systematic analysis of the twin cx(9)c protein family. *J. Mol. Biol.* **393**, 356–68 (2009).
32. Wenz, L.-S., Opaliński, Ł., Wiedemann, N. & Becker, T. Cooperation of protein machineries in mitochondrial protein sorting. *Biochim. Biophys. Acta - Mol. Cell Res.* (2015). doi:10.1016/j.bbamcr.2015.01.012
33. Höhr, A. I. C., Straub, S. P., Warscheid, B., Becker, T. & Wiedemann, N. Assembly of β -barrel proteins in the mitochondrial outer membrane. *Biochim. Biophys. Acta* (2014). doi:10.1016/j.bbamcr.2014.10.006
34. Schulz, C., Schendzielorz, A. & Rehling, P. Unlocking the presequence import pathway. *Trends Cell Biol.* (2014). doi:10.1016/j.tcb.2014.12.001
35. Ojala, T. *et al.* New mutation of mitochondrial DNAJC19 causing dilated and noncompaction cardiomyopathy, anemia, ataxia, and male genital anomalies. *Pediatr. Res.* **72**, 432–7 (2012).
36. Richter-Dennerlein, R. *et al.* DNAJC19, a mitochondrial cochaperone associated with cardiomyopathy, forms a complex with prohibitins to regulate cardiolipin remodeling. *Cell Metab.* **20**, 158–71 (2014).
37. Teixeira, P. F. & Glaser, E. Processing peptidases in mitochondria and chloroplasts. *Biochim. Biophys. Acta* **null**, (2012).
38. Vögtle, F.-N. *et al.* Mitochondrial protein turnover: role of the precursor intermediate peptidase Oct1 in protein stabilization. *Mol. Biol. Cell* **22**, 2135–43 (2011).
39. Luciano, P. & Géli, V. The mitochondrial processing peptidase: function and specificity. *Experientia* **52**, 1077–82 (1996).
40. Harbauer, A. B., Zahedi, R. P., Sickmann, A., Pfanner, N. & Meisinger, C. The protein import machinery of mitochondria—a regulatory hub in metabolism, stress, and disease. *Cell Metab.* **19**, 357–72 (2014).
41. Vögtle, F.-N. *et al.* Global analysis of the mitochondrial N-proteome identifies a processing peptidase critical for protein stability. *Cell* **139**, 428–39 (2009).
42. Naamati, A., Regev-Rudzki, N., Galperin, S., Lill, R. & Pines, O. Dual targeting of Nfs1 and discovery of its novel processing enzyme, Icp55. *J. Biol. Chem.* **284**, 30200–8 (2009).

43. Park, K., Botelho, S. C., Hong, J., Österberg, M. & Kim, H. Dissecting stop transfer versus conservative sorting pathways for mitochondrial inner membrane proteins in vivo. *J. Biol. Chem.* **288**, 1521–32 (2013).
44. Quirós, P. M., Langer, T. & López-Otín, C. New roles for mitochondrial proteases in health, ageing and disease. *Nat. Rev. Mol. Cell Biol.* **16**, 345–359 (2015).
45. Jin, S. M. *et al.* Mitochondrial membrane potential regulates PINK1 import and proteolytic destabilization by PARL. *J. Cell Biol.* **191**, 933–42 (2010).
46. Hill, R. B. & Pellegrini, L. The PARL family of mitochondrial rhomboid proteases. *Semin. Cell Dev. Biol.* **21**, 582–92 (2010).
47. Jobling, R. K. *et al.* PMPCA mutations cause abnormal mitochondrial protein processing in patients with non-progressive cerebellar ataxia. *Brain* awv057– (2015). doi:10.1093/brain/awv057
48. Punga, T. & Bühler, M. Long intronic GAA repeats causing Friedreich ataxia impede transcription elongation. *EMBO Mol. Med.* **2**, 120–9 (2010).
49. Hadzhieva, M., Kirches, E. & Mawrin, C. Review: iron metabolism and the role of iron in neurodegenerative disorders. *Neuropathol. Appl. Neurobiol.* **40**, 240–57 (2014).
50. Mancini, C. *et al.* Genome-wide expression profiling and functional characterization of SCA28 lymphoblastoid cell lines reveal impairment in cell growth and activation of apoptotic pathways. *BMC Med. Genomics* **6**, 22 (2013).
51. Stahl, A. *et al.* Isolation and identification of a novel mitochondrial metalloprotease (PreP) that degrades targeting presequences in plants. *J. Biol. Chem.* **277**, 41931–9 (2002).
52. Glaser, S. M. & Cumsky, M. G. A synthetic presequence reversibly inhibits protein import into yeast mitochondria. *J. Biol. Chem.* **265**, 8808–16 (1990).
53. Glasers, M. Localization of a Synthetic into Mitochondria ” Presequence That Blocks Protein Import Import rxn. *J. Biol. Chem.* **265**, 8817–8822 (1990).
54. Falkevall, A. *et al.* Degradation of the amyloid beta-protein by the novel mitochondrial peptidasome, PreP. *J. Biol. Chem.* **281**, 29096–104 (2006).
55. Goard, C. A. & Schimmer, a D. Mitochondrial matrix proteases as novel therapeutic targets in malignancy. *Oncogene* **33**, 2690–9 (2014).
56. Pierson, T. M. *et al.* Whole-exome sequencing identifies homozygous AFG3L2 mutations in a spastic ataxia-neuropathy syndrome linked to mitochondrial m-AAA proteases. *PLoS Genet.* **7**, e1002325 (2011).

57. Cagnoli, C. *et al.* Missense mutations in the AFG3L2 proteolytic domain account for ~1.5% of European autosomal dominant cerebellar ataxias. *Hum. Mutat.* **31**, 1117–24 (2010).
58. Kondadi, A. K. *et al.* Loss of the m-AAA protease subunit AFG₃L₂ causes mitochondrial transport defects and tau hyperphosphorylation. *EMBO J.* **33**, 1011–26 (2014).
59. Dupuis, L. Mitochondrial quality control in neurodegenerative diseases. *Biochimie* **100**, 177–83 (2014).
60. García-Nafria, J. *et al.* Structure of the catalytic domain of the human mitochondrial Lon protease: proposed relation of oligomer formation and activity. *Protein Sci.* **19**, 987–99 (2010).
61. Hoshino, A. *et al.* Oxidative post-translational modifications develop LONP1 dysfunction in pressure overload heart failure. *Circ. Heart Fail.* **7**, 500–9 (2014).
62. Fukuda, R. *et al.* HIF-1 regulates cytochrome oxidase subunits to optimize efficiency of respiration in hypoxic cells. *Cell* **129**, 111–22 (2007).
63. Bernstein, S. H. *et al.* The mitochondrial ATP-dependent Lon protease: a novel target in lymphoma death mediated by the synthetic triterpenoid CDDO and its derivatives. *Blood* **119**, 3321–9 (2012).
64. López-Otín, C. & Matrisian, L. M. Emerging roles of proteases in tumour suppression. *Nat. Rev. Cancer* **7**, 800–8 (2007).
65. Runkel, E. D., Baumeister, R. & Schulze, E. Mitochondrial stress: balancing friend and foe. *Exp. Gerontol.* **56**, 194–201 (2014).
66. Haynes, C. M. & Ron, D. The mitochondrial UPR - protecting organelle protein homeostasis. *J. Cell Sci.* **123**, 3849–55 (2010).
67. Jovaisaite, V., Mouchiroud, L. & Auwerx, J. The mitochondrial unfolded protein response, a conserved stress response pathway with implications in health and disease. *J. Exp. Biol.* **217**, 137–43 (2014).
68. Al-Furoukh, N. *et al.* ClpX stimulates the mitochondrial unfolded protein response (UPR(mt)) in mammalian cells. *Biochim. Biophys. Acta* **1853**, 2580–2591 (2015).
69. Bulteau, A.-L. & Bayot, A. Mitochondrial proteases and cancer. *Biochim. Biophys. Acta* **1807**, 595–601 (2011).
70. Mottis, A., Jovaisaite, V. & Auwerx, J. The mitochondrial unfolded protein response in mammalian physiology. *Mamm. Genome* (2014). doi:10.1007/s00335-014-9525-z

71. Rainbolt, T. K., Saunders, J. M. & Wiseman, R. L. YME1L degradation reduces mitochondrial proteolytic capacity during oxidative stress. *EMBO Rep.* **16**, 97–106 (2015).
72. Mishra, P., Carelli, V., Manfredi, G. & Chan, D. C. Proteolytic cleavage of Opa1 stimulates mitochondrial inner membrane fusion and couples fusion to oxidative phosphorylation. *Cell Metab.* **19**, 630–41 (2014).
73. Ashrafi, G. & Schwarz, T. L. The pathways of mitophagy for quality control and clearance of mitochondria. *Cell Death Differ.* **20**, 31–42 (2013).
74. Rosano, G. L. & Ceccarelli, E. A. Recombinant protein expression in *Escherichia coli*: advances and challenges. *Front. Microbiol.* **5**, 172 (2014).
75. Nettleship, J. E. *et al.* Transient expression in HEK 293 cells: an alternative to *E. coli* for the production of secreted and intracellular mammalian proteins. *Methods Mol. Biol.* **1258**, 209–22 (2015).
76. Osz-Papai, J. *et al.* Insect cells-baculovirus system for the production of difficult to express proteins. *Methods Mol. Biol.* **1258**, 181–205 (2015).
77. Looser, V. *et al.* Cultivation strategies to enhance productivity of *Pichia pastoris*: A review. *Biotechnol. Adv.* (2015). doi:10.1016/j.biotechadv.2015.05.008
78. Ferrer-Miralles, N., Saccardo, P., Corchero, J. L., Xu, Z. & García-Fruitós, E. General introduction: recombinant protein production and purification of insoluble proteins. *Methods Mol. Biol.* **1258**, 1–24 (2015).
79. Chow, K. M. *et al.* Mammalian pitrilysin: substrate specificity and mitochondrial targeting. *Biochemistry* **48**, 2868–77 (2009).
80. Zhang, J.-H. *et al.* Application of Titration-Based Screening for the Rapid Pilot Testing of High-Throughput Assays. *J. Biomol. Screen.* **19**, 651–660 (2013).
81. Copeland, R. A. *Kinetics of single-substrate enzyme reactions.* **7**, (2000).
82. Copeland, R. A. *Experimental measures of enzyme activity.* **7**, (2000).
83. Copeland, R. A. *Reversible inhibitors.* **7**, (2000).
84. Copeland, R. A. Mechanistic considerations in high-throughput screening. *Anal. Biochem.* **320**, 1–12 (2003).
85. Points, K. E. Y. L. REVERSIBLE MODES OF INHIBITOR INTERACTIONS WITH ENZYMES. (1997).

86. Hackney, D. D. & Jiang, W. Assays for kinesin microtubule-stimulated ATPase activity. *Methods Mol. Biol.* **164**, 65–71 (2001).
87. Harris, J. L. *et al.* Rapid and general profiling of protease specificity by using combinatorial fluorogenic substrate libraries. *Proc. Natl. Acad. Sci. U. S. A.* **97**, 7754–9 (2000).
88. Baruch, A., Jeffery, D. A. & Bogoy, M. Enzyme activity – it’s all about image. *Trends Cell Biol.* **14**, 29–35 (2004).
89. Yan, Z.-H. *et al.* Development of intramolecularly quenched fluorescent peptides as substrates of angiotensin-converting enzyme 2. *Anal. Biochem.* **312**, 141–147 (2003).
90. Liu, Y. *et al.* Use of a fluorescence plate reader for measuring kinetic parameters with inner filter effect correction. *Anal. Biochem.* **267**, 331–5 (1999).
91. Dabir, D. V *et al.* A small molecule inhibitor of redox-regulated protein translocation into mitochondria. *Dev. Cell* **25**, 81–92 (2013).
92. Zhao, B., Summers, F. A. & Mason, R. P. Photooxidation of Amplex Red to resorufin: implications of exposing the Amplex Red assay to light. *Free Radic. Biol. Med.* **53**, 1080–7 (2012).
93. Sanman, L. E. & Bogoy, M. Activity-based profiling of proteases. *Annu. Rev. Biochem.* **83**, 249–73 (2014).
94. Willems, L. I., Overkleeft, H. S. & van Kasteren, S. I. Current developments in activity-based protein profiling. *Bioconjug. Chem.* **25**, 1181–91 (2014).
95. Wolf, E. V *et al.* A new class of rhomboid protease inhibitors discovered by activity-based fluorescence polarization. *PLoS One* **8**, e72307 (2013).
96. Wolf, E. V, Zeissler, A. & Verhelst, S. H. L. Inhibitor fingerprinting of rhomboid proteases by activity-based protein profiling reveals inhibitor selectivity and rhomboid autoprocessing. *ACS Chem. Biol.* (2015). doi:10.1021/acscchembio.5b00514
97. Fishovitz, J. *et al.* Active-site-directed chemical tools for profiling mitochondrial Lon protease. *ACS Chem. Biol.* **6**, 781–8 (2011).
98. Wassermann, A. M., Lounkine, E., Davies, J. W., Glick, M. & Camargo, L. M. The opportunities of mining historical and collective data in drug discovery. *Drug Discov. Today* **20**, 422–34 (2015).
99. Bajorath, J. Large-scale SAR analysis. *Drug Discov. Today. Technol.* **10**, e419–26 (2013).

100. Patching, S. G. Surface plasmon resonance spectroscopy for characterisation of membrane protein–ligand interactions and its potential for drug discovery. *Biochim. Biophys. Acta - Biomembr.* **1838**, 43–55 (2014).
101. O’Neill, M. A. A. & Gaisford, S. Application and use of isothermal calorimetry in pharmaceutical development. *Int. J. Pharm.* **417**, 83–93 (2011).
102. Marciano, D. P., Dharmarajan, V. & Griffin, P. R. Methods in Molecular Biolog. *Curr. Opin. Struct. Biol.* **28C**, 105–111 (2014).
103. Arrowsmith, C. H. *et al.* The promise and peril of chemical probes. *Nat. Chem. Biol.* **11**, 536–541 (2015).
104. Iannetti, E. F. *et al.* Toward high-content screening of mitochondrial morphology and membrane potential in living cells. *Int. J. Biochem. Cell Biol.* **63**, 66–70 (2015).
105. Makmura, L. *et al.* Development of a sensitive assay to detect reversibly oxidized protein cysteine sulfhydryl groups. *Antioxid. Redox Signal.* **3**, 1105–18 (2001).
106. Meyer, A. J. & Dick, T. P. Fluorescent protein-based redox probes. *Antioxid. Redox Signal.* **13**, 621–50 (2010).
107. Wojtala, A. *et al.* *Methods to monitor ROS production by fluorescence microscopy and fluorometry.* *Methods Enzymol.* **542**, (Elsevier Inc., 2014).
108. Woolley, J. F., Stanicka, J. & Cotter, T. G. Recent advances in reactive oxygen species measurement in biological systems. *Trends Biochem. Sci.* **38**, 556–65 (2013).
109. Perry, S. W., Norman, J. P., Barbieri, J., Brown, E. B. & Gelbard, H. a. Mitochondrial membrane potential probes and the proton gradient: A practical usage guide. *Biotechniques* **50**, 98–115 (2011).
110. Cannon, M. B. & James Remington, S. Redox-sensitive green fluorescent protein: probes for dynamic intracellular redox responses. A review. *Methods Mol. Biol.* **476**, 50–64 (2009).
111. Billis, P., Will, Y. & Nadanaciva, S. High-Content Imaging Assays for Identifying Compounds that Generate Superoxide and Impair Mitochondrial Membrane Potential in Adherent Eukaryotic Cells. *Curr. Protoc. Toxicol.* **59**, 25.1.1–25.1.14 (2014).
112. Auld, D. S., Thorne, N., Nguyen, D.-T. T. & Inglese, J. A specific mechanism for nonspecific activation in reporter-gene assays. *ACS Chem. Biol.* **3**, 463–70 (2008).
113. Montague, C. R., Fitzmaurice, A., Hover, B. M., Salazar, N. A. & Fey, J. P. Screen for small molecules increasing the mitochondrial membrane potential. *J. Biomol. Screen.* **19**, 387–98 (2014).

114. Hasson, S. A. *et al.* Substrate specificity of the TIM22 mitochondrial import pathway revealed with small molecule inhibitor of protein translocation. *Proc. Natl. Acad. Sci. U. S. A.* **107**, 9578–83 (2010).
115. Voos, W., Martin, H., Krimmer, T. & Pfanner, N. Mechanisms of protein translocation into mitochondria. *Biochim. Biophys. Acta - Rev. Biomembr.* **1422**, 235–254 (1999).
116. Miyata, N. *et al.* Pharmacologic rescue of an enzyme-trafficking defect in primary hyperoxaluria 1. *Proc. Natl. Acad. Sci. U. S. A.* **111**, 14406–11 (2014).
117. Madoux, F. *et al.* Development of a phenotypic high-content assay to identify pharmacoperone drugs for the treatment of primary hyperoxaluria type 1 by high-throughput screening. *Assay Drug Dev. Technol.* **13**, 16–24 (2015).
118. Downward, J. Targeting RAS signalling pathways in cancer therapy. *Nat. Rev. Cancer* **3**, 11–22 (2003).
119. Dekker, F. J. *et al.* Small-molecule inhibition of APT1 affects Ras localization and signaling. *Nat. Chem. Biol.* **6**, 449–56 (2010).
120. Sudarshan, S. *et al.* Fumarate hydratase deficiency in renal cancer induces glycolytic addiction and hypoxia-inducible transcription factor 1alpha stabilization by glucose-dependent generation of reactive oxygen species. *Mol. Cell. Biol.* **29**, 4080–90 (2009).
121. Tomlinson, I. P. M. *et al.* Germline mutations in FH predispose to dominantly inherited uterine fibroids, skin leiomyomata and papillary renal cell cancer. *Nat. Genet.* **30**, 406–10 (2002).
122. Launonen, V. *et al.* Inherited susceptibility to uterine leiomyomas and renal cell cancer. *Proc. Natl. Acad. Sci. U. S. A.* **98**, 3387–92 (2001).
123. Yogev, O., Naamati, A. & Pines, O. Fumarase: a paradigm of dual targeting and dual localized functions. *FEBS J.* **278**, 4230–42 (2011).
124. Yogev, O. *et al.* Fumarase: a mitochondrial metabolic enzyme and a cytosolic/nuclear component of the DNA damage response. *PLoS Biol.* **8**, e1000328 (2010).
125. Steele, S. L., Prykhozhiy, S. V & Berman, J. N. Zebrafish as a model system for mitochondrial biology and diseases. *Transl. Res.* **163**, 79–98 (2014).
126. Guerrero, C., Tagwerker, C., Kaiser, P. & Huang, L. An integrated mass spectrometry-based proteomic approach: quantitative analysis of tandem affinity-purified in vivo cross-linked protein complexes (QTAX) to decipher the 26 S proteasome-interacting network. *Mol. Cell. Proteomics* **5**, 366–78 (2006).

127. Figeys, D., McBroom, L. D. & Moran, M. F. Mass spectrometry for the study of protein-protein interactions. *Methods* **24**, 230–9 (2001).
128. Ong, S.-E. *et al.* Identifying the proteins to which small-molecule probes and drugs bind in cells. *Proc. Natl. Acad. Sci. U. S. A.* **106**, 4617–22 (2009).
129. Lomenick, B., Olsen, R. W. & Huang, J. Identification of direct protein targets of small molecules. *ACS Chem. Biol.* **6**, 34–46 (2011).
130. Chan, J. N. Y. *et al.* Target identification by chromatographic co-elution: monitoring of drug-protein interactions without immobilization or chemical derivatization. *Mol. Cell. Proteomics* **11**, M111.016642 (2012).
131. Martinez Molina, D. *et al.* Monitoring drug target engagement in cells and tissues using the cellular thermal shift assay. *Science* **341**, 84–7 (2013).
132. Jafari, R. *et al.* The cellular thermal shift assay for evaluating drug target interactions in cells. *Nat. Protoc.* **9**, 2100–2122 (2014).
133. Fauster, A. *et al.* A cellular screen identifies ponatinib and pazopanib as inhibitors of necroptosis. *Cell Death Dis.* **6**, e1767 (2015).
134. Tan, B. X. *et al.* Assessing the Efficacy of Mdm2/Mdm4-Inhibiting Stapled Peptides Using Cellular Thermal Shift Assays. *Sci. Rep.* **5**, 12116 (2015).
135. Giaever, G. *et al.* Genomic profiling of drug sensitivities via induced haploinsufficiency. *Nat. Genet.* **21**, 278–83 (1999).
136. Feng, Y., Mitchison, T. J., Bender, A., Young, D. W. & Tallarico, J. A. Multi-parameter phenotypic profiling: using cellular effects to characterize small-molecule compounds. *Nat. Rev. Drug Discov.* **8**, 567–78 (2009).
137. Parsons, A. B. *et al.* Integration of chemical-genetic and genetic interaction data links bioactive compounds to cellular target pathways. *Nat. Biotechnol.* **22**, 62–9 (2004).
138. Ho, C. H. *et al.* Combining functional genomics and chemical biology to identify targets of bioactive compounds. *Curr. Opin. Chem. Biol.* **15**, 66–78 (2011).
139. Weiss, W. A., Taylor, S. S. & Shokat, K. M. Recognizing and exploiting differences between RNAi and small-molecule inhibitors. *Nat. Chem. Biol.* **3**, 739–744 (2007).
140. Sato, S. *et al.* Marine natural product aurilide activates the OPA1-mediated apoptosis by binding to prohibitin. *Chem. Biol.* **18**, 131–9 (2011).
141. Castoreno, A. B. *et al.* Small molecules discovered in a pathway screen target the Rho pathway in cytokinesis. *Nat. Chem. Biol.* **6**, 457–463 (2010).

142. Lamb, J. *et al.* The Connectivity Map: using gene-expression signatures to connect small molecules, genes, and disease. *Science* **313**, 1929–35 (2006).
143. Lo, Y.-C. *et al.* Large-Scale Chemical Similarity Networks for Target Profiling of Compounds Identified in Cell-Based Chemical Screens. *PLoS Comput. Biol.* **11**, e1004153 (2015).
144. Koutsoukas, A. *et al.* From in silico target prediction to multi-target drug design: current databases, methods and applications. *J. Proteomics* **74**, 2554–74 (2011).
145. Braga, R. C. *et al.* Virtual screening strategies in medicinal chemistry: the state of the art and current challenges. *Curr. Top. Med. Chem.* **14**, 1899–912 (2014).
146. Ekins, S., Mestres, J. & Testa, B. In silico pharmacology for drug discovery: methods for virtual ligand screening and profiling. *Br. J. Pharmacol.* **152**, 9–20 (2007).
147. Lavecchia, A. Machine-learning approaches in drug discovery: methods and applications. *Drug Discov. Today* **20**, 318–331 (2015).
148. Chacinska, A. & Rehling, P. Moving proteins from the cytosol into mitochondria. *Biochem. Soc. Trans.* **32**, 774–6 (2004).

Chapter 2: Discovery and characterization of small molecule modulators of mitochondrial presequence-degrading protease

Introduction

An organelle found within eukaryotic cells, the mitochondrion is involved in cell signaling, control of cell cycle, cell death, homeostasis, metabolism, and energy production¹(Figure 1-1). A handful of proteins involved in these processes reside in the mitochondrion. Although some proteins are synthesized inside the organelle, most mitochondrial proteins are synthesized by ribosomes in the cytosol as preproteins². These preproteins carry mitochondrial targeting signal(s) (MTS) that are recognized by receptors on the surface of the outer membrane of the mitochondrion². Most of the time, the MTS is located on the N-terminus of the preprotein. Membrane proteins often carry internal targeting sequence that allows them to be inserted into the membrane³. Most targeting sequences are about 20 to 60 amino acids in length. When the MTS is recognized by outermembrane translocases, the import of mitochondrial-targeted proteins is initiated by passing through the pore of the Translocase of Outer Membrane (TOM). Depending on the final destination of the protein, it can interact with different translocation systems. The Translocase of the Inner Membrane (TIM) 23 recognizes matrix-targeted proteins and facilitates insertion of these proteins to the matrix (Figure 1-2). The TIM23 complex also recognizes a subset of proteins that are targeted to the inner membrane (IM), typically those with a single transmembrane (TM) domain⁴. These IM-targeted proteins are inserted in the membrane by the TIM23 complex through the recognition of the stop-transfer

signal^{3,5}. Alternatively, IM-targeted proteins with multiple TM domains are inserted through TIM22 import pathway⁶. Upon successful localization, the MTS are typically cleaved by one or multiple proteases in the respective mitochondrial compartments^{7,8} (Figure 1-2). The Matrix Processing Peptidase (MPP) cleaves the MTS of matrix-targeted preproteins, whereas the Matrix Intermediate Processing Peptidase (MIP) mediates an additional cleavage for a small number of preproteins^{8,9}. For proteins that are translocated by the TIM23 complex but reside in the inner membrane or intermembrane space, the Inner Membrane Peptidase (IMP) cleaves the precursor after an initial cleavage by MPP^{8,10}. The cleaved presequence is further degraded by metalloendopeptidase 1 (MP1) or also known as the presequence protease (PreP)^{7,10-12}, which is the subject of this study.

PreP was first identified in the mitochondrial matrix and chloroplast stroma of *Arabidopsis thaliana*¹². This metalloprotease has been characterized as a member of pitrilysin family, and M16 subfamily of proteases with the inverted zinc-binding domain HXXEH^{7,11,13}. Further studies show that this ATP-independent protein degrades small targeting peptides⁷. The crystal structure of AtPreP suggests that this protease has a proteolytic chamber of 10,000 Å³ that is spacious enough to accommodate peptide substrates such as a cleaved MTS, but not larger proteins, such as the preprotein¹⁴. A model for its proteolytic mechanism has since been proposed. The MTS is first cleaved by a processing protease such as MPP, leaving the MTS as a small peptide. The binding peptide within the proteolytic chamber triggers a conformational change that brings the two halves of the enzyme closer together, adapting a closed conformation. The protein returns to its open conformation upon proteolysis to release the cleaved products¹⁴. Additional studies suggest that PreP might be redox-regulated. It was found that when the protein is oxidized, it loses the capability to degrade small peptides^{11,15}.

Human PreP has been further identified as the functional analogue of human Insulin Degrading Enzyme (IDE)¹⁶. IDE has been implicated in Alzheimer's disease (AD) due to its ability to degrade amyloid-beta peptide (A β), which is believed to be one of the leading causes of AD¹⁷⁻¹⁹. A collection of studies has implicated the involvement of mitochondria in AD. A β accumulates in the neurons of transgenic mice as well as AD patients²⁰. Inside the mitochondrion, A β has been shown to interact with both IM and matrix proteins. In the IM, A β can interact with cytochrome oxidase (COX) and cyclophilin D (CypD), inhibiting their activity²¹. Additionally, A β can also bind to A β binding protein alcohol dehydrogenase (ABAD) in the matrix²¹. The interaction of A β with IM and matrix proteins leads to elevated reactive oxygen species (ROS), which is detrimental as it causes oxidative stress and cell toxicity^{21,22}. Amyloid Protein Precursor (APP), the precursor of A β , has been shown to be arrested in the TOM complex in AD patients²³. Importantly, hPreP can degrade A β *in vitro*, which directly links PreP and mitochondria to AD¹². While PreP's role aside from degrading MTS remains largely unknown, its ability to degrade A β warrants further investigation especially since mitochondrial dysfunction contributes to AD pathology. Decrease in proteolytic activity of PreP was found in mitochondria of AD patients and in transgenic AD mice²⁰. Interestingly, there is only a slight decrease of expression of hPreP in the temporal lobe of AD and non-AD individuals²⁰. Various PreP single-nucleotide polymorphisms have been mapped, however there has not been any clear genetic association linking PreP to AD²⁴. Most recent study showed overexpression of PreP in AD mouse model decreased A β level, improved synaptic mitochondrial function, decreased ROS level and reduced level of inflammatory cytokines²⁵.

To gain a better understanding of the role of mitochondria in diseases such as AD, better tools are needed to flexibly modulate mitochondrial activity in biological model systems. In this

study, we have identified modulators of PreP by a high throughput screening (HTS) approach (Figure 2-1 for project overview). HTS method is chosen because of its simplicity, reproducibility, and speed²⁶⁻²⁸. Small molecule inhibitors of PreP will be advantageous for mechanistic studies as well modeling studies in biological systems^{29,30}. Small molecule inhibitors can induce change instantly and specifically^{31,32}. Overall, small molecules that modulate activity of PreP will be insightful as they can provide a basis for developing therapeutic agents. Our hypothesis is that probes discovered through this study will be important for altering regulated proteolysis in vivo and understanding the role of PreP in mitochondrial function in general and in AD. Here we present the methodologies and initial results from our study.

Results

Development of a robust assay to measure activity of PreP

To discover novel modulators to study mitochondrial proteolysis, we developed an in vitro assay to measure activity of PreP (Figure 2-1). The enzyme assay is composed of recombinant His-tagged PreP and a fluorogenic peptide. We utilized an intra-molecularly quenched peptide (MCA-RRQFKVVTRSQ-JPT) derived from bioactive peptide, leumorphin⁷. The activity of the protease can be monitored overtime by measuring increase in fluorescence as a result of peptide cleavage. To purify recombinant PreP, PreP cDNA purchased from Open Biosystems was subcloned into pET28a expression vector, appending 6 repeats of His on the N-terminus (Figure 2-2). The MTS is removed in the expression construct to ensure that the protein folds properly. Upon successful confirmation of the cloned construct by sequencing, an auto induction method was utilized that gives robust expression of the recombinant protein, and further allows for purification of the protein with a Co²⁺-column (Figure 2-3)³³. The identity of the recombinant protein was confirmed by western blot using an anti His antibody (Figure 2-4). The activity of the protease was initially tested in a single tube assay. We titrated from 125-550 ng of PreP in a 50 µl reaction with initially 10-15 µM final peptide concentration. Cleavage of the peptide by recombinant PreP resulted in increased fluorescence count, which was monitored over time. Specifically, PreP degraded the peptide in a concentration dependent manner. Moreover, when PreP was chelated with 1,10 *o*-phenanthroline and EDTA (Figure 3-1A), the protein is no longer able to cleave peptide (Figure 3-1A). Other parameters were also tested to optimize the assay for HTS. Assay optimization included testing buffers like HEPES and phosphate, determining the right protein and substrate concentrations, and testing the effect of

metals, DMSO tolerance, automation, and measuring Z' of the assay (Figure 3-1A-G). PreP activity also was not altered when the protein was frozen and thawed (Data not shown). Furthermore, we found PreP is not inhibited by general protease inhibitors such as iodoacetamide (IAA) - an inhibitor of cysteine peptidases, phenylmethanesulfonylfluoride (PMSF) - inhibitor of serine proteases, soybean trypsin inhibitor (STI)- an inhibitor of trypsin. Chymostatin leupeptin, and pepstain protease inhibitors cocktail also did not significantly inhibit the proteolytic activity (Figure 3-2), suggesting that we would be able to find a novel inhibitor of PreP.

Prior to generating enough quantity of PreP to carry out HTS, we established that the assay is suitable for HTS. To this end, a statistical parameter was measured. Pre-pilot experiments gave a Z' -prime (Z') value of 0.7, indicating a good HTS assay quality. The Z' is a statistical measure of the ratio between signal and background in the assay where a $Z' > 0.5$ indicates a good quality assay³⁴. We also took into account that drugs in the library are delivered in DMSO vehicle, giving 2% final DMSO in the assay and tested if this inhibits proteolytic activity. Activity was not inhibited by 2% DMSO (Figure 3-1E). Another consideration in high-throughput adaptation is the way in which the reagents are dispensed or delivered. Initial validation experiments demonstrated that automated dispensing of both protein and peptide using the liquid handling system did not affect the activity of the protein (Figure 3-1F).

High-throughput screen for modulators of PreP

During HTS, the activity assay was integrated with a robotic screening platform where each step was automated and tightly coordinated to provide maximum reproducibility. Prior to extensive screening runs, we performed a pilot screen in which known small molecules inhibitors from the biomol library (comprised of 600 small molecules) were screened for both inhibitors

and activators of PreP. Fluorescence counts were measured prior to the start of the reaction, which is initiated by fluorogenic peptide addition, and 20-30 minutes after the peptide is added. We expect that inhibitor of PreP will give a fluorescent count that is comparable or even lower than the control wells (PreP chelated with 2 mM EDTA and 0.5 mM *o*-phenanthroline). On the other hand, an activator of PreP will enhance cleavage of substrate and gives a fluorescent count that is higher than vehicle (DMSO) treated control. The data obtained from the screen was analyzed using an algorithm courtesy of Dr. Samuel Hasson, allowing us to identify hits for potential inhibitors and activators. Additionally, the quality of pilot screen plates demonstrated a favorable Z' score of >0.5 . Due to the small size of molecules screened during the pilot round, we were able to measure fluorescence every 15 minutes (Fig 4-1A-C). Nonetheless, this was not the case of the rest of the libraries screened. The pilot screen gave a hit for a potential inhibitor, dichlorobenzamil (Figure 4-1C). We proceeded to purchase dichlorobenzamil from a chemical vendor; unfortunately, the inhibitory effect of dichlorobenzamil was not confirmed (Figure 4-2). This further stress the importance of confirming the hits obtained from the screen. Small molecules on a plate could get degraded or oxidized over time. Other variations such as lot number, purify differences, and many others could lead to irreproducible result.

Following successful pilot screen, we continued with our search to discover small molecule modulators of PreP from various libraries available at MSSR (Table I). Conversion of raw data to table format aided in data analysis (Fig 4-3). Furthermore, we analyzed the robustness of the assay during the screen by monitoring z' value of each plate. Plates with z' values less than 0.5 were repeated. For in depth data analysis, we sorted our hits according to its % survival, indicating the % activity remaining in the presence of small molecule (Figure 4-4). The % survival value was normalized to DMSO-treated PreP (100%) and chelators-treated PreP (0%).

We marked compounds that inhibited PreP by 70% (30% survival) as hits. Our first screen of 88,000 small molecules gave a hit rate of 0.48% (Table 2-1). 464 compounds that were marked as hits were then cherry-picked onto a clear plate for secondary screens. Our second round 40,000 molecules screen, carried out 2 years later, gave us a hit rate of 0.67% (Table 2-2).

Counter-screen eliminates hits that non-specific to PreP

To ensure that the hits are specific for PreP, two counter-screens were conducted. The first counter-screen was against human Insulin-degrading enzyme (IDE) and the second one was against yeast matrix processing peptidase (MPP).

Insulin-degrading enzyme (IDE) was selected for its similarities to PreP with respect to structure, catalysis, and substrate. IDE belongs in the M16A family of metalloproteases with HxxEH inverted zinc binding domain³⁵. The M16 family of proteins is comprised of two halves, about 50-55 kDa each. The two domains (N and C domains) are connected by a short loop in M16A proteins and an extended helical loop in M16C proteins¹⁶. IDE-N and IDE-C are connected by a 28 residues loop whereas a 65 residues extended helical hairpin connects PreP-N and PreP-C. For both proteins, The HxxEH motif is located in the N domain with where zinc ion is coordinated to two conserved histidines and glutamate residues. The N and C domains of both PreP and IDE form an enclosed catalytic chamber of 13,000 and 16,000 Å³, respectively^{35,36}. Structural studies have provided insight into substrate selectivity of both proteins. IDE and PreP are both able to degrade peptides up to 70 amino acids in length. Both proteins select their substrates based on size, shape and charge distribution. Additionally, both IDE and PreP are able to degrade amyloid-beta (A β) peptide^{7,13,18,37}. Furthermore, it has been shown that a second initiation site creates an IDE isoform that localizes to mitochondria¹⁹. Due to the high degree of

similarities between PreP and IDE, we believe that IDE would be a good candidate for counter-screen against PreP hits.

To perform a counter-screen using IDE, we cloned full-length human IDE into pET28a expression vector³⁷. The His₆-tagged IDE was expressed in *E. coli* and purified by affinity purification (Figure 4-5). Since IDE shares similar substrate preference as PreP, we hypothesize IDE will also be able to degrade the same leumorphin fluorescence peptide that we used for the screen. To this end, we tested IDE activity with leumorphin substrate. IDE is able to degrade leumorphin peptide, but IDE is less efficient than PreP. The cleavage assay with IDE gave a z' of 0.7, indicating that this assay is suitable for high-throughput screening. We also determined that the liquid handler, and freeze-thaw cycle do not affect activity of the protease (data not shown). Cherry-picked hits were then screened against IDE. None of the molecules that were marked as hits from the first round of screening inhibited activity of IDE to degrade leumorphin peptide (Figure 4-6). From the second round of screening with LS libraries, 8 molecules were found to inhibit both IDE and PreP (Table 2-1 and 2-2, appendix A and B).

During the IDE counterscreen, a parallel screen of 100,000 small molecules to identify modulators of MPP were ongoing and conducted by Colin Douglas. Similar to PreP and IDE, MPP is a M16 protein with HxxEH inverted zinc binding motif^{38,9}. MPP is comprised of α and β subunit, about 50 kDa each¹⁰. Unlike PreP and IDE, MPP lacks a linker region that connects the two halves³⁶. Hits from MPP screen were cross-referenced with hits from PreP screen. There were a few molecules that overlap and inhibit both MPP and PreP (Table 2-1 and 2-2, appendix A and B).

Hits belong in different chemical scaffold and display diverse characteristics

Following successful counter-screen, the hits' chemical structures were analyzed and organized into different groups based on their structures similarities. Table III and appendix C display hits from LS library screen with over 10 different scaffolds of small molecules that inhibited PreP activity. The compounds that exhibit the lowest % survival from each scaffold group were purchased in powder form.

Our initial characterization began with determining the drug concentration at which PreP activity is inhibited by 50% (IC₅₀ analysis). We also confirmed the inhibitory effects of the hits on PreP by measuring PreP's ability to degrade of presequence of subunit 9 of ATP synthase from *neurospora crassa* (su9-DHFR) and fluorescently-labeled amyloid-beta peptide (FAM-A β). General mitochondrial functions were also examined. From past small molecule screening projects, small molecules that non-specifically permeabilize mitochondrial membrane often present themselves as hits. To this end, an assay to monitor the intactness of mitochondrial membrane was developed. Additionally, because PreP ablation in cells does not affect respiration, compounds that uncouple mitochondria and impair respiration are likely false-positive hits.

To determine whether our hits uncouple mitochondria or impair respiration, we employed a battery of secondary assays. First was using clark-type oxygen electrode to measure rate of oxygen consumption in isolated mitochondria. By measuring the rate of oxygen consumption, we were able to determine whether compounds uncouple mitochondria or inhibit respiration. Compounds that behave like a known mitochondrial uncoupler would display an increased in the rate of oxygen consumption greater than that of basal respiration level (NADH) whereas

compounds that inhibit respiration would prevent oxygen from being consumed. This assay was also complemented by a fluorescence based assay in which a potentiometric dye, 3,3'-Dipropylthiadicarbocyanide Iodide (DISC₃(5)), was used to measure level of coupling in mitochondria. DISC₃(5) accumulates in hyperpolarized membrane and is translocated into the lipid bilayer where its fluorescence is quenched. As such, in polarized mitochondria, DISC₃(5) fluorescence, is low, however, when mitochondria is depolarized by uncoupler such as carbonyl cyanide m-chlorophenyl hydrazine (CCCP), DISC₃(5) fluorescence is high. Compounds that uncouple mitochondria will give high fluorescence measurement in DISC₃(5) assay. Nonetheless, the DISC₃(5) assay might not be suitable for compounds that absorb or emit at the same excitation and emission wavelength as the potentiometric dye. Additionally, compounds that react non-specifically with the dye could give a false positive or negative output. Furthermore, we utilized another potentiometric dye, MitoTracker Red CMXRos to visualize whether compounds uncouple mitochondria. This particular dye also allows us to monitor mitochondrial morphology by microscopy and determine if there is a change in mitochondrial morphology when cells are cultured in the presence of small molecules.

Following our assays to measure compound potency, membrane intactness, and respiration, we determined whether the small molecules inhibited protein import into mitochondria. Furthermore, structurally similar compounds were purchased to gain more insight into the mechanism of action of the inhibitors. SAR compounds will aid in determining the specific functional groups important for inhibition and further in improving the efficacy of the compound. The characterization of T057 is highlighted below and the detailed characterization of MitoBlock-60 is highlighted in chapter 3.

T057 is a tetrahydroisoquinoline derivative that displays unique characteristics

T057 is a 2-[3-(1H-pyrrol-1-yl)benzoyl]-1,2,3,4-tetrahydroisoquinoline-3-carboxamide identified from the Enamine library (Figure 5-1A). T057 IC₅₀ using leuorphan peptide as a substrate in the *in vitro* fluorescence activity was 3.8 μM. The inhibitory effect of T057 was also confirmed using fluorescently labeled Aβ peptide (Figure 5-1 B,C). T057 does not permeabilize mitochondria as most proteins remained in the mitochondrial (pellet) fraction compared to MitoBloCK-2, which is known to permeabilize mitochondrial membrane (Figure 5-2). Furthermore, T057 does not impair respiration or uncouple mitochondria. The rate of oxygen consumption in isolated yeast mitochondria treated with 100 μM T057 is comparable to NADH, which measures basal rate of oxygen consumption (Figure 5-3A). Using a potentiometric probe, we confirmed T057 does not behave like a mitochondrial uncoupler, CCCP (Figure 5-3B).

Because PreP is downstream of MPP, and it might play a role in protein translocation and maturation³⁹. We tested if inactivation of PreP by T057 affects translocation of nuclearly-encoded mitochondrial proteins. We tested a subset of precursors that localize to different mitochondrial compartments and utilize distinct translocation machineries for their imports: Tom40 (outer membrane – TOM complex), AAC (inner membrane – TIM22 pathway), DDP1 (intermembrane space – MIA pathway), su9-DHFR (matrix – TIM23 pathway). Interestingly, T057 inhibits import of all of precursors tested (Figure 5-4).

To confirm that T057 indeed bind to PreP, Drug-Affinity Responsive Target Stability (DARTS) assay was conducted. Recombinant PreP was incubated with T057 or vehicle control for 2 hours prior to addition of thermolysin to degrade PreP. Small molecules that bind to PreP would induce a conformational change, therefore protecting PreP from degradation by

thermolysin. This was found to be the case for T057. Increasing concentration of T057 protects PreP from degradation by thermolysin, but not IDE, a structurally similar protease, suggesting T057 binds specifically to PreP (Figure 5-5). To determine the mechanism of action of T057, we determined the kinetics parameters of T057 inhibition. Fluorescence activity assay was conducted in the presence of increasing concentration of leumorphin peptide where PreP was inhibited at T057's IC50 concentration, 4 μM . To convert fluorescence signal to peptide concentration, we generated a standard curve using trypsin (Figure 5-5A). We then determine the initial velocities of the DMSO-treated and T057-treated PreP for each peptide concentration by taking the slope of peptide cleaved over time within the linear range of the reaction. The initial velocities were then plotted against peptide concentrations to generate Michaelis-Menten plot (Figure 5-5B). The Michaelis-Menten analysis suggests that T057 does not behave like a competitive inhibitor since the reaction with T057 could not reach the same maximum velocity as DMSO (0.0084 $\mu\text{M}/\text{s}$ for DMSO and 0.0072 $\mu\text{M}/\text{s}$ for T057). To further determine the nature of T057 inhibition, a lineweaver-burk plot was generated. Both Michaelis-Menten and lineweaver-burk analyses agree that T057 is not a competitive inhibitor (V_{max} was 0.02 $\mu\text{M}/\text{s}$ for DMSO and 0.004 $\mu\text{M}/\text{s}$ for T057). Moreover, since K_m of the reaction changed in the presence of inhibitor, we ruled out that T057 is non-competitive inhibitor, which is characterized by no change in K_m . Therefore, T057 is an uncompetitive or a mixed inhibitor. Michaelis-Menten analysis showed K_m of the reaction increased in the presence of inhibitor (2.5 μM to 9.4 μM), but lineweaver-burk analysis showed the opposite where K_m decreased from 20 μM to 3.3 μM in the presence of inhibitor. Additional analyses are necessary to determine the exact nature of inhibition.

Structure-Activity Relationship (SAR) study was carried out to further dissect the functional groups important for inhibition, we purchased analogs of T057 and measured activity of PreP. Analog 592, which differs from T057 by the absence of carboxamide group and the replacement of pyrrole group to the para position, was able to attenuate PreP activity, albeit at a lower efficiency compared to T057. Analog 579 and 901 did not inhibit PreP at all. Analog 579 differs from T057 in the presence of 2,5 dimethyl pyrrole in the para position and analog 901 lacked the pyrrole group all together (Figure 5-6). Our SAR data suggest that the carboxamide group is dispensable for inhibition as 592, which lacks carboxamide group is still able to inhibit PreP. The pyrrole group seems to play an important role in inhibition, likely forming specific hydrophobic and hydrogen bonding interactions within a specific pocket of PreP. Addition of two methyl groups in 579 completely abolished its inhibition, suggesting that the size of the pyrrole group is also important for interaction and binding.

Having determined the specific mechanism of action of T057, we were interested in understanding the implication of inhibiting PreP in cultured cells. Treatment of cultured cells with T057 for 24 hours does not seem to affect cell viability as measured by MTT viability assay (Figure 5-8A). This observation was surprising since T057 inhibits import of mitochondrial proteins, which likely affects cell survival. Additionally, there was no significant change in mitochondrial morphology when HeLa cells expressing mitochondria-targeted dsRed were treated for 24 hours with T057 (Figure 5-8B).

Discussion

Utilizing an HTS platform with an *in vitro* assay, we sought out to discover small molecule modulators of PreP. The goal of our HTS campaign is to validate and utilize the small molecules discovered from the screen to tease out mechanisms and functions of PreP in mitochondria. With over 100,000 compounds screened, we discovered diverse sets of small molecules that attenuate activity of PreP. Our study stresses the importance of validating hits obtained from primary screen. In our case, dichlorobenzamil came up as a hit in the pilot screen, however, when we purchased a fresh powder of the chemical, we could not confirm the inhibition of PreP activity.

Characterization of hits from the first round of screening suggests that most PreP inhibitors do not permeabilize mitochondrial membrane, impair respiration and uncouple mitochondria. In addition, the screening hits display a wide range of characteristics. For instance, the hits from the second round of screening (LS library) represent over 10 different scaffolds that inhibit PreP to varying extents (Table III, Appendix C). The hits from the LS library represent the best built-in SAR studies. For instance, scaffold 2, 4, 9, and 10 have over 8 similarly structured compounds inhibiting PreP. SAR studies using these compounds can quickly determine which functional groups that are important for inhibition. Determining the mechanism of action of these molecules through kinetics and structural studies would be essential to further validate these compounds as probes.

,We characterized a few compounds extensively. Characterization of MitoBloCK-60 is highlighted in detail in chapter 3. T057 is a tetrahydroisoquinoline derivative found to inhibit PreP at relatively low concentration. With an IC_{50} of 3.8 μ M, SAR study would aid in improving the efficacy of the molecule. Our preliminary SAR study suggests that the pyrrole group is

important for inhibition while the carboxamide group is dispensable. The fact that T057 protected PreP from proteolysis by thermolysin suggests that the presence or binding of T057 changes conformation of PreP in solution. Additionally, our kinetics study suggests T057 is not a competitive inhibitor of PreP, hence it does not bind in the same binding pocket as the substrate. The conformational change induced by T057 binding could lead to an allosteric change that causes the substrate binding pocket to be inaccessible to substrate. Complementing our kinetics study with biophysical approach using isothermal titration calorimetry (ITC) would further confirm our hypothesis. A co-crystal of T057 bound to PreP would also provide insight into T057's mode of inhibition. A higher-throughput way of performing these assays would enhance probe validation greatly.

From the biology standpoint, T057 is particularly interesting as it does not permeabilize mitochondrial membrane, uncouple mitochondria, and impair respiration, but it inhibits import of proteins targeted to different mitochondrial compartments at high concentration. A better import study with an extensive drug titration will give us a better idea of the specificity of import defect. Nonetheless, it is really surprising that respiration does not seem to be impaired but import of all proteins is essentially blocked. In the literature, tetrahydroisoquinoline derivatives are studied as neurotoxins that could cause degradation of dopaminergic neuron in Parkinson's disease⁴⁰. Tetrahydroisoquinoline derivatives have also been shown to bind to cell receptors such transient receptor potential (TRP) channel and opioid channel^{41,42}. Since some of the hits in the LS library also block import of matrix and inner membrane protein, it would be interesting to see if these are indeed a consequence of inactivating PreP *in vivo*. If that is the case, how does mitochondria deal defect in protein import while maintaining respiration?

In the near future, our hits could be tested on model systems such as zebrafish or mice. Knockout of atPreP 1 and 2 has been shown to cause reduction in chlorophyll a and b, and decreased in respiration during development⁴³. Furthermore, PreP has also been shown to be involved in hedgehog signaling during mouse development⁴⁴. Zebrafish is an excellent model system to study development due to the ease of manipulation and a high degree of conservation between human and zebrafish genes⁴⁵. Zebrafish could be treated with small molecules to detect any developmental defects associated with PreP inactivation. Furthermore, there are numerous AD mice model that could be used to validate the role of PreP in AD. Small molecule attenuators of PreP could be injected to mice to see whether A β accumulates more when PreP is inactivated, and to investigate the functional and phenotypic consequences of PreP inactivation.

In addition to the hits that are specific to PreP, our screen also revealed several molecules that both inhibit MPP and PreP, but not IDE (Appendix A and B). The fact that these molecules did not affect activity of IDE suggests that they are not inhibitors of M16 family of proteases. These chemicals follow somewhat of a trend where a lot of them contain a quinone group or a sulfonyl group (Appendix B). A follow up study to characterize the hits that affect MPP and PreP could be interesting as these molecules could bind within a region that is conserved between MPP and PreP and could be used to mechanistically dissect the binding of mitochondria targeting sequences to these proteases. It could also be used to understand how non-cleavable sequences bind to MPP. Similarly, compounds to attenuate activity of all three proteases screened will be useful to highlight the conserved proteolysis within the M16 family of proteins. A lot of these compounds contain benzyl halide, quinone, and sulfonyl functional group (Appendix 2). Whether these functional groups specifically contribute to inhibition of M16 family of proteases require additional investigation.

In summary, we have discovered small molecules with great potentials for use as tools to understand the mechanisms of mitochondrial proteases. These small molecules would allow for rapid and specific manipulations of target proteins. Complemented with multifaceted approaches such as genetics and biochemistry, chemical biology could expand our understanding of cellular functions.

Materials and Methods

Cloning Human PreP/MP1 cDNA was purchased from OpenBiosystems (Accession: BC 005025). Mature PreP (amino acid 27-1036) was amplified using primers containing BamHI and XhoI restriction sites, digested, and ligated into pET28a expression vector (Novagen). PreP cloning was performed by Colin Douglas. Human IDE cDNA was purchased from OpenBiosystems (Accession: BC 096336). Full-length IDE was amplified using primers containing NotI and XhoI restriction sites, digested and ligated into pET28a expression vector (Novagen). IDE cloning was performed with Julia Mayer in fulfillment of the requirements for her degree of Bachelor of Science in Engineering. The sequences of all constructs were verified by sequencing (Agencourt).

Protein Expression and Purification pET28a-containing PreP plasmid was transformed into BL21 DE3 *E. coli* expression strain. PreP was expressed using auto-induction method. Starter culture streak from a single colony was grown at 37°C overnight in ZYP-0.8G (see media composition below) supplemented with 40 µg/mL kanamycin and 35 µg/mL chloramphenicol. The next day, cultures were diluted 2000 fold (500 µL) to 1 L of ZYP-5052 supplemented with 40 µg/mL kanamycin and 35 µg/mL chloramphenicol and grown at 30°C for 24 hours. Following 24 hours induction, Cells were harvested by centrifugation at 7,000 x g at 4°C for 10 minutes. Cell paste was resuspended in 0.9% NaCl for a quick wash. Following centrifugation, the bacterial pellet was resuspended in equilibration buffer. Cells were lysed using a high-pressure homogenizer, emulsiflex (Avestin). Cleared lysate, obtained by centrifugation at 10,000 x g at 4°C for 30 minutes, was applied to talon/cobalt metal affinity beads (Clontech) and rotated at

4°C for 2 hours . Beads were washed 3 times with wash buffer on a gravity-flow column. His₆-tagged recombinant PreP was eluted with elution buffer and 1 mL fractions were collected. Protein concentration was measured with BCA assay kit (Thermo Scientific). Most concentrated fractions were pooled together and purified protein was stored frozen at -80°C in 20% glycerol.

IDE construct was transformed into BL21-DE3 gold *E. coli* expression strain. Starter culture streak from a single colony was grown at 37°C overnight in 2YT medium supplemented with 40 µg/mL kanamycin and 15 µg/mL tetracycline. The next day, 20 mL overnight culture was transferred to 1 L flask containing 2YT medium supplemented with 40 µg/mL kanamycin and 15 µg/mL tetracycline. Cultures were grown to OD of 0.6 at 37°C. Protein expression was induced by addition of 1 mM Isopropyl-β-D-Thiogalactopyranoside (IPTG). Six hours post-induction, cells were harvested and washed as described above. Cell pellet after NaCl wash was resuspended in Ni²⁺ lysis buffer (solution composition below). Cells were lysed with 30 minutes incubation in lysis buffer containing 1 mg/mL lysozyme followed by sonication on ice. Cleared lysate, obtained by centrifugation at 10,000 x g at 4°C for 30 minutes, was applied to Ni²⁺ metal affinity beads (Thermo) and rotated at 4°C for 2 hours. Beads were washed 3 times with wash buffer on a gravity-flow column. His₆-tagged recombinant IDE was eluted with elution buffer and 1 mL fractions were collected. Protein concentration was measured with BCA assay kit (Thermo Scientific). Most concentrated fractions were pooled together and purified protein was stored frozen at -80°C in 20% glycerol.

Media and solutions composition described in protein expression and purification PreP

Expression media: ZY (1% tryptone, 0.5% yeast extract), ZYP-0.8G (ZY, 1 mM MgSO₄, 0.8% glucose, 25 mM (NH₄)₂SO₄, 50 mM KH₂PO₄, 50 mM Na₂HPO₄), ZYP-5052 (ZY, 1 mM MgSO₄,

0.8% glucose, 25 mM (NH₄)₂SO₄, 50 mM KH₂PO₄, 50 mM Na₂HPO₄, 0.5% glycerol, 0.05% glucose, 0.2% lactose), 2YT (1.6% tryptone, 1% yeast extract, 0.5% NaCl, 10 mM Tris-HCl pH 7.4). Solutions for PreP purification: Equilibration buffer (50 mM sodium phosphate pH 7.0, 300 mM NaCl), Wash buffer (50 mM sodium phosphate pH 7.0, 300 mM NaCl, 7.5 mM imidazole), Elution buffer (50 mM sodium phosphate pH 7.0, 300 mM NaCl, 150 mM imidazole). Solutions for IDE purification: Lysis buffer (50 mM NaH₂PO₄.H₂O, 300 mM NaCl, 10 mM imidazole; pH 8.0), Wash buffer (50 mM NaH₂PO₄.H₂O, 300 mM NaCl, 20 mM imidazole; pH 8.0), Elution buffer (50 mM NaH₂PO₄.H₂O, 300 mM NaCl, 250 mM imidazole; pH 8.0).

High-throughput Screen (HTS) The primary screen was performed using 22 nM of recombinant PreP in 10 mM HEPES pH 7.4, 50 mM NaCl, 0.01% BSA). A titertrek multidrop was used to dispense 35 μ L protein or protein chelated with 0.1 mM EDTA and 0.5 μ M *o*-phenanthroline to all wells of black 384-wells plate (GreinerBio one). 0.5 μ L of small molecules from the 1 mM stock library or vehicle control DMSO stock (10 μ M final concentration) was then pinned to each well using a biomek FX (Beckman Coulter). Plates were incubated at 30°C for one hour, followed by a fluorescence measurement prior to substrate addition. A titertrek multidrop was used to dispense 15 μ L of fluorogenic leumorphin peptide (MCA-RRQFKVVTRSQ-JPT. The final concentration of substrate was 15 μ M. The peptide solution was shielded from light throughout the experiment. Following 30 minutes incubation at 30°C, plates were read for an end-point measurement using an excitation and emission wavelength of 330 and 425 nm respectively. Screens were conducted using an automated plate scheduler to ensure consistency across the run. Assay quality and reproducibility of each each plate was

monitored using the statistical parameter, Z' ³⁴. All plates had Z' values greater than 0.5. Compounds that inhibited activity by 70% were marked as potential hits. 5 μ L hits were then cherry-picked from the original plate onto a 384-well low volume, v-bottom plates. Hits were then rescreened against PreP and counter-screened against Insulin-Degrading Enzyme (IDE). IDE counter-screen was conducted with the help of Julia Mayer. Hits from the rescreen and counter-screened were compared to hits from a parallel screen against Matrix Processing Peptidase (MPP). Small molecules that inhibited PreP but not MPP and IDE were grouped according to their chemical structure similarities. Commercially available compounds were purchased and assayed for IC_{50} analyses – the concentration of small molecule required to inhibit activity of the protein by 50%. For IC_{50} analysis, serial dilution of small molecule was added into assay plates containing protein as described above. For cleavage with amyloid-beta substrate, intramolecularly quenched $A\beta$ 1-42 (Abz-DAEFRHDSGYEVHHQKLVFFAEDVGSNKGAIIGLMVGGVVIA-EDDnp) was purchased from AnaSpec and dissolved in DMSO. 45 nM of recombinant PreP was used for cleavage assay with amyloid-beta peptide as the substrate.

Oxygen consumption and membrane potential measurements Oxygen consumption of isolated mitochondria were performed as described previously (cite). Briefly, ___ μ g of mitochondria isolated from yeast were incubated in respiration buffer with gentle stirring. Respiration was initiated with addition of 2 mM NADH. Small molecules were added once steady-state level was reached. As a control, mitochondria were uncoupled by addition of 20 μ M Carbonyl cyanide 4-(trifluoromethoxy) phenylhydrazone (CCCP). Slope indicates the rates of oxygen consumption. Membrane potential measurements of purified mitochondria were

performed with fluorescent 3,3'-Dipropylthiadicarbocyanine Iodide dye DiSC3(5). 1% DMSO, CCCP or small molecules were added to mitochondria in import buffer (. 0.2 μ M of dye in import buffer was added following 10 minutes small molecule incubation. 5 minutes later, fluorescence was measured at excitation and emission length of 620 nm and 670 nm respectively.

Mitochondria integrity assay 25 μ g of yeast isolated mitochondria were incubated in import buffer (0.6 M sorbitol, 2 mM KH_2PO_4 , 60 mM KCl, 50 mM HEPES-KOH, 5 mM MgCl_2 , 2.5 mM EDTA, 5 mM L-methionine, pH 7.1) the presence of varying concentration of small molecules at 25°C for 30 minutes. Mitochondria were then pelleted by centrifugation at 8,000 x g for 10 minutes at 4°C. Supernatant containing released proteins from mitochondria were TCA precipitated on ice for 30 minutes. Precipitated proteins were recovered by centrifugation at maximum speed for 15 minutes at 4°C. Both mitochondrial pellet and released proteins were resuspended in 5x-Laemmli sample buffer (0.25 M Tris-Cl pH 6.8, 10% SDS, 30% glycerol, 0.02% bromophenol blue) with 5% β -mercaptoethanol (β ME) and analyzed on SDS-PAGE. Resulting gel were stained with coomassie blue for 30 minutes or transferred to nitrocellulose membrane and blotted with key mitochondrial proteins.

In vitro activity assays for PreP. For amyloid-beta degradation, 0.5 μ M of PreP was incubated in DMSO or small molecule in screening buffer for 1 hour prior to addition of 10 μ M fluorescent-labeled amyloid beta, FAM- labeled amyloid beta (1-42) peptide (FAM-A β 1-42) (Anaspec). Reactions were stopped after 1 hour by adding 5x-Laemmli sample buffer. Samples were resolved on 16% Tris-Tricine gel. Gels were visualized using a BioRad imager to detect

FAM at 494 and 521 nm excitation and emission wavelength. For Su9-DHFR degradation, radiolabeled precursor was generated using TNT Quick coupled transcription translation kit (Promega). During translation, 200 nM PreP in screening buffer were incubated with small molecule for 1 hour. To cleave targeting sequence from Su9-DHFR, 4 μ M of MPP was incubated with 5 μ L of precursor for 30 minutes at 30 °C. PreP previously incubated with drug was then added to MPP-precursor mixture. Reactions were stopped at specified time points by adding Laemmli sample buffer. Samples were resolved on 16% Tris-Tricine gel. Gels were fixed, dried and exposed to film.

Cell culture. HeLa or HEK293T cells were grown in DMEM (life technologies), 10% Fetal Bovine Serum, 1% penicillin/streptomycin in humidified atmosphere with 5% CO₂.

Cell Toxicology Assay. Cells were seeded at 70% confluency in 48 wells plate and treated the next day with indicated small molecules concentrations for 24 or 48 hours. Cell viability was measured by MTT toxicology assay (Sigma). 3-(4,5-dimethylthiazol-2-yl)-2,5-diphenyltetrazolium bromide (MTT) solution was added for 4 hours. Formazan crystals formed were solubilized by MTT solubilization solution. Formazan absorbance was measured at 570 nm along with turbidity measurement at 630 nM. Cell viability was normalized to vehicle-treated control.

Mitochondria isolation from mammalian cells. Cultured cells were grown to confluency. One day prior to mitochondria isolation, cells were fed with fresh media. The next day, cells were harvested and homogenized in 20 mM HEPES pH 7.6, 220 mM mannitol, 70 mM sucrose, 2

mg/ml BSA, and 0.5 mM PMSF (if mitochondria were not to be used for import, cells were homogenized in the buffer above with addition of 10 mM N-ethylmaleimide (NEM) and 1 μ M MG132). Lysates were dounced with Teflon dounce or passed through 25 G needle to lyse cells. Homogenates were centrifuged at 770 x g at 4°C for 5 minutes. Post-nuclear supernatants were centrifuged at 10,000 x g for 10 minutes to obtain mitochondria pellets. Pellets were further washed with homogenization buffer without BSA. Protein concentrations were measured using BCA assay (Thermo Scientific).

Immunofluorescence. Cells were seeded on a 12-wells plate containing glass coverslips, and treated the next day with indicated small molecules or DMSO vehicle control. Cells were fixed in 3.7% formaldehyde for 15 minutes followed by 3 times PBS wash. For immunostaining, cells were permeabilized in ice-cold methanol for 10 minutes after fixation. Cells were blocked in 1% BSA for 30 minutes prior to incubation with primary antibody (in 1% BSA). Following PBS washes, cells were incubated with secondary antibodies conjugated Alexa Fluor dyes 350, 488, or 568 (Life Technologies). For MitoTracker Red staining, cells were incubated in 25 nM MitoTracker Red CMXRos (Life Technologies) for 30 minutes prior to fixation. Cells were visualized with Leica TCS SPE DMI 4000B inverted confocal microscope or Axiovert 200M Carl Zeiss inverted microscope. Cell quantification was performed on ImageJ software (NIH) where at least 100 cells were counted in 3 independent experiments.

Import of radiolabeled proteins into isolated yeast mitochondria. Mitochondria were purified from yeast grown in ethanol-glycerol media as described previously. ³⁵S-labeled precursors were synthesized using TNT Quick Coupled Transcription/Translation kits (Promega). 25 μ g

mitochondria were added to import buffer (0.6 M sorbitol, 2 mM KH_2PO_4 , 60 mM KCl, 50 mM HEPES-KOH, 5 mM MgCl_2 , 2.5 mM EDTA, 5 mM L-methionine, pH 7.1) supplemented with 2 mM NADH. Once equilibrated, small molecules or DMSO vehicle control were added and samples were incubated for 15 minutes at 25 °C. Import reactions were initiated by precursor addition. Reaction aliquots were withdrawn at specified time points. Import was stopped by adding cold import buffer or 50 $\mu\text{g}/\text{mL}$ trypsin. 250 $\mu\text{g}/\text{mL}$ soybean trypsin inhibitor was added following 15 minutes trypsin treatment. Mitochondria were isolated by centrifugation at 8,000 x g at 4°C for 10 minutes. Final mitochondria pellet were dissolved in 5x Laemlli sample buffer. Samples were resolved on SDS-PAGE. Gels were dried prior to exposure to film.

Import of radiolabeled proteins into isolated mammalian mitochondria. Mitochondria were isolated as described above. ^{35}S -labeled precursors were synthesized using TNT Quick Coupled Transcription/Translation kits (Promega). 10 or 20 μg mitochondria were added to import buffer (20 mM HEPES pH 7.6, 220 mM mannitol, 70 mM sucrose) supplemented with 1 mM ATP, 0.5 mM magnesium acetate, 5 mM NADH, and 20 mM sodium succinate. Once equilibrated, small molecules or DMSO vehicle control were added and samples were incubated for additional 15 minutes at 25°C. 10-20 μL precursors were then added to initiate import. Reaction aliquots were withdrawn at specified time points. Import was stopped by adding cold import buffer or 25 $\mu\text{g}/\text{mL}$ trypsin. Soybean trypsin inhibitor (50 $\mu\text{g}/\text{mL}$) was added following 15 minutes trypsin treatment. Mitochondria were isolated by centrifugation at 12,000 x g at 4°C for 5 minutes. Final mitochondria pellet were dissolved in 5x Laemlli sample buffer. Samples were resolved on SDS-PAGE. Gels were dried prior to exposure to film.

Drug Affinity Responsive Target Stability (DARTS). 1 μM (0.12 mg/mL) PreP was incubated with small molecules in screening buffer at 4°C. Following 2 hours incubation with drug, 5 $\mu\text{g/mL}$ of thermolysin was added to the samples. Proteolysis was stopped after 15 minutes by addition of 5 mM EDTA. Samples were resolved on SDS-PAGE. Gels were stained with coomassie blue or transferred onto nitrocellulose membrane and blotted with indicated antibodies. For in organello DARTS, 25 μg mitochondria isolated from HeLa cells were solubilized in 20 μL solubilization buffer (composition) for 15 minutes on ice. Soluble mitochondrial proteins were obtained by centrifugation at maximum speed for 5 mins at 4°C. Soluble extract was incubated with small molecules for 1 hour at 4°C prior to addition of 0.25 μg of thermolysin. Proteolysis was stopped at specified time points by addition of 5 mM EDTA. Samples were resolved on SDS-PAGE and transferred onto nitrocellulose membrane. Membrane was blotted with indicated mitochondrial proteins.

Kinetics Study. 22 nM of PreP was incubated with small molecules at their IC_{50} concentration (4 μM for T057) for 1 hour in screening buffer. 3, 4, 5, 7.5, 10, 15, 25, and 30 μM peptide substrate were then added to the samples. Fluorescence was monitored over the period of 2 hours on the FlexStation II plate reader with excitation and emission wavelength of 330 and 425 nm, respectively. To convert RFU to μM peptide, a trypsin standard curve was generated. Trypsin was incubated with the peptide range as indicated above. The final fluorescence counts obtained from trypsin reactions signify maximum cleavage and hence corresponds to the amount of peptide. Initial velocity was determined by measuring the rate of peptide cleaved over time within the linear range of the reaction. Michaelis-Menten plot and lineweaver-burk plot were generated and analyzed using graphpad Prism software.

In vitro fluorescence peptide cleavage assay with mop112. Same as PreP activity assay. 22 nM of recombinant mop112 was incubated with indicated small molecules for 1 hour prior to addition of 15 μ M fluorescent substrate.

Yeast cell survival assay. GA74 wildtype and GA74 Δ SNQ2 Δ PDR5 yeast strains were inoculated and grown in YPEG (1% yeast extract, 2% peptone, 3% glycerol, 3% ethanol) overnight at 30°C. The next day, cells were plated onto 96-wells plate at OD₆₀₀ of 0.02 in the presence of varying concentrations of small molecules. The cell density (OD₆₀₀) was measured after 48 hours incubation at 30°C.

Peptide export. Peptide export from mitochondria assay was performed as previously described (cite). Briefly, mitochondria peptides were synthesized *in organello* by incubating isolated mitochondria in translation buffer (0.6 M sorbitol, 150 mM KCl, 15 mM K₂HPO₄, 20 mM Tris-Cl pH 7.4, 12.7 mM MgSO₄, 0.3% BSA, 4 mM ATP, 0.5 mM GTP, 1.13 mg/ml α -ketoglutarate, 2.33 mg/ml pyruvate kinase, 0.1 mM of all amino acids and ³⁵S methionine for 20 minutes at 30°C. Drugs or DMSO were added during translation. Following translation, mitochondria were pelleted and washed with buffer containing cold methionine. Mitochondria were then resuspended in translation buffer containing drug or dms. To allow proteolysis of non-assembled polypeptides, samples were incubated at 37°C. Reaction aliquots were withdrawn at specified time points and immediately centrifuged at 13,200 x g at 4°C for 4 minutes. Supernatant containing degradation products released from mitochondria were mixed with scintillation fluid to measure radioactivity. Mitochondria were resuspended in Laemmli sample

buffer and mixed with scintillation fluid to measure radioactivity. The amount of peptide exported was measured as the amount of radioactivity in supernatant fraction over the total amount of radioactivity in supernatant and mitochondria fraction.

Miscellaneous. Mitochondrial proteins were analyzed by SDS-PAGE using a 12 or 15% polyacrylamide gel and a Tricine-based running buffer. Proteins were detected by immunoblotting using nitrocellulose membranes.

Figures and Tables

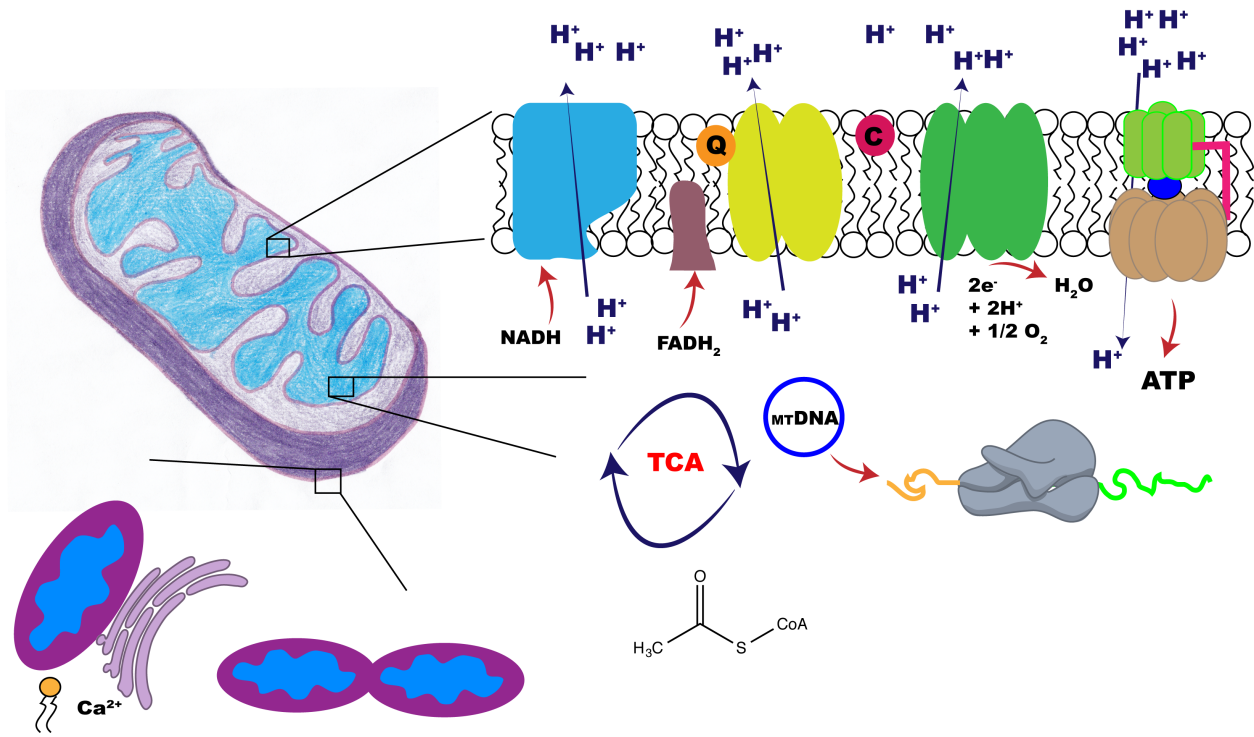


Figure 1-1. The mitochondrion is a site for various cellular processes. The mitochondrion is a double-membrane bound organelle. Various cellular processes occur inside the mitochondrion. In the inner membrane, the electron transport chain complexes transfer accepts electrons from reducing equivalent such as NADH and FADH₂ to create electrochemical gradient that can then be used by ATP synthase to produce ATP. In the matrix, mitochondria can transcribe and translate mtDNA that encodes for subunits of the respiratory chain complexes and tRNAs required for translation of these proteins. On the outer membrane, fusion proteins govern mitochondrial dynamics, which is influenced by the environment. Mitochondria are also in close contact with the ER to ensure proper calcium signaling and phospholipid transfer.

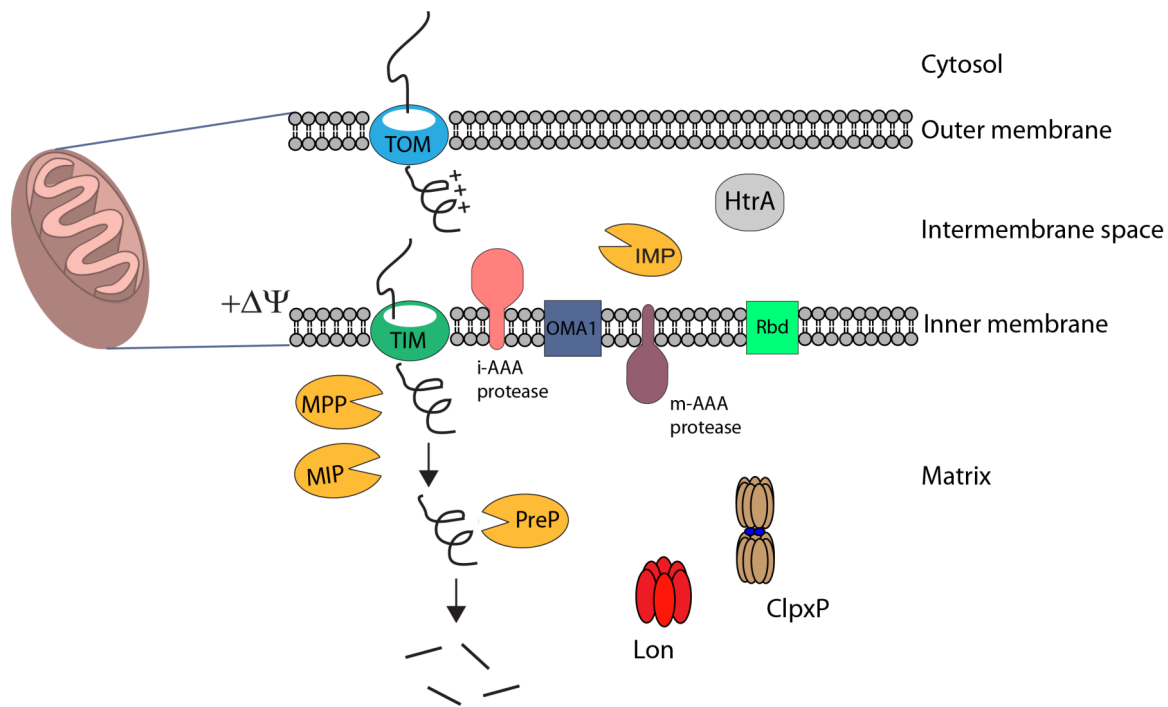


Figure 1-2. Import of matrix-targeted precursor to mitochondria. Mitochondrial proteins are synthesized in the cytosol as preproteins carrying N-terminal targeting signal that target them to mitochondria. The TOM complex recognizes the α -helical amphiphatic amino acids and drives translocation to mitochondria. For matrix proteins, preproteins are passed on to the TIM23 complex. Once preproteins get to the matrix, the targeting signal is cleaved by MPP. Additional cleavage by MIP might occur. For inner membrane proteins, IMP might perform additional processing. Once targeting sequences are removed, proteins can fold and function properly. PreP degrades the MPP and MIP-cleaved sequence to smaller peptides that are then exported to the cytosol by ABC transporter.

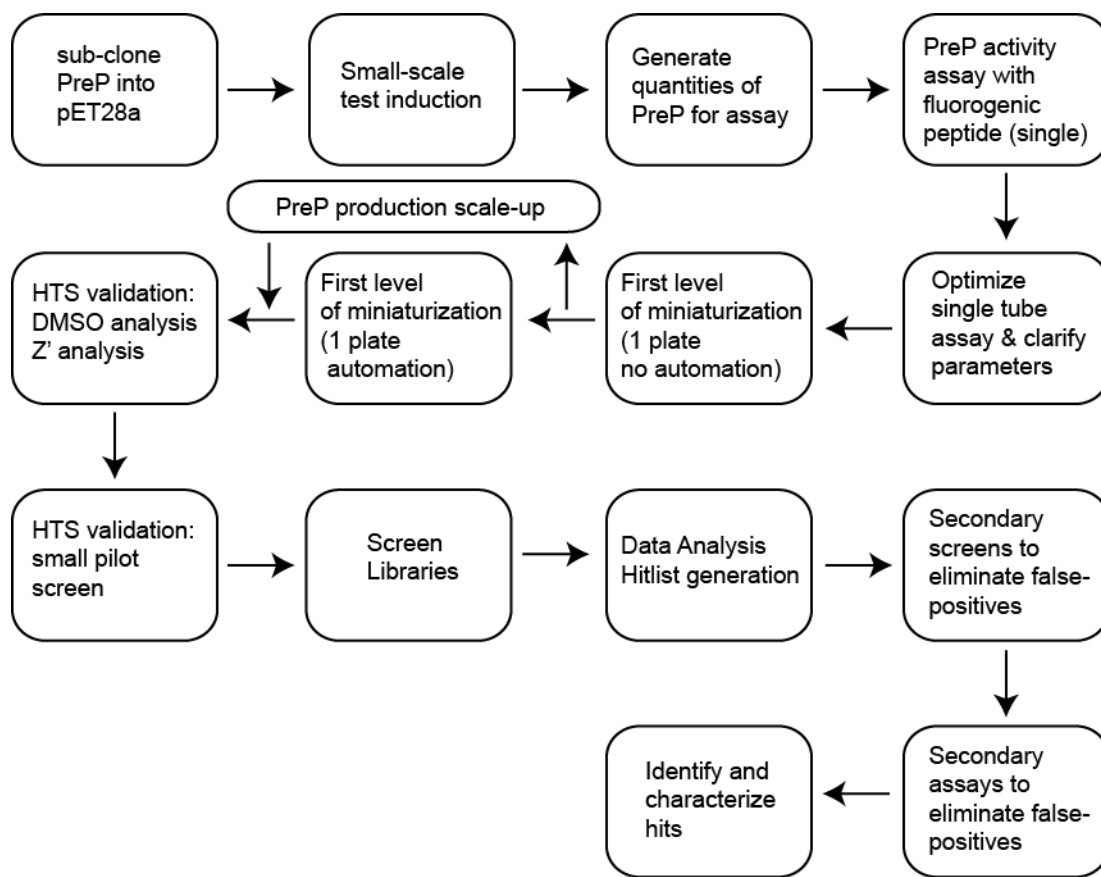


Figure 2-1. Workflow of PreP high-throughput screening project. PreP lacking the mitochondrial-targeting sequence was first subcloned into the pET28a expression vector. Upon successful cloning, the construct was tested for a small-scale expression. The activity of the purified protein was then tested in a single tube activity assay with fluorogenic peptide as the substrate. Once it was established that the protein was active, assay conditions and parameters were optimized. HTS validation included Z' prime, DMSO-tolerance, and automation analyses. A pilot screen followed. A large-scale screen using the libraries available at MSSR was then completed. Following extensive data analyses, hitlist generation, counterscreens and secondary assays were conducted to identify and characterize hits.

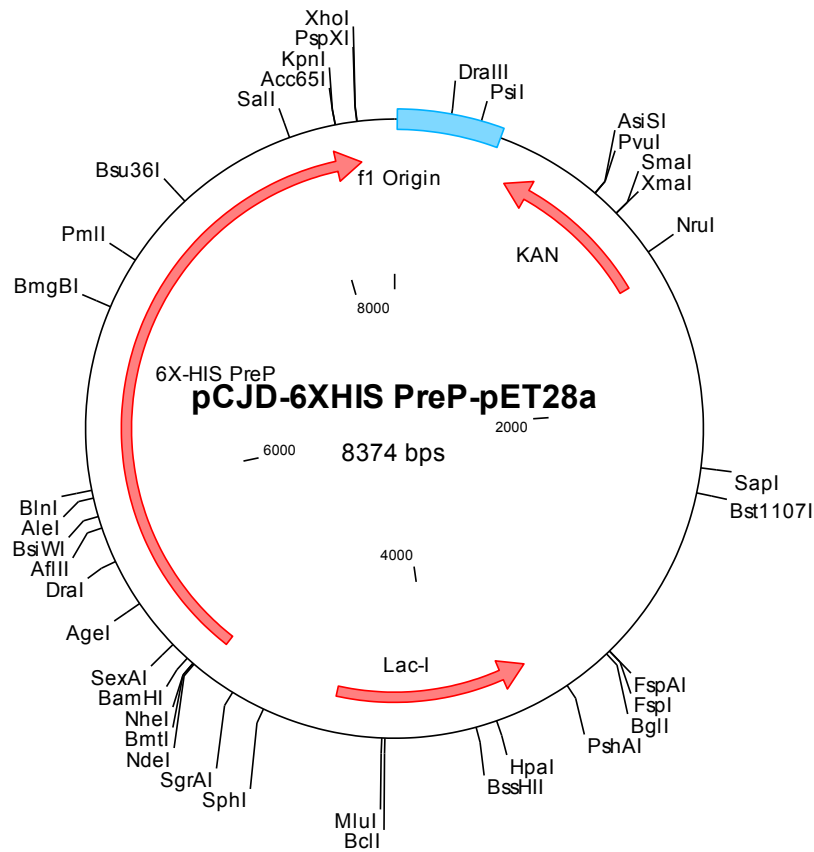


Figure 2-2. Plasmid map of PreP construct for HTS. PreP without the mitochondrial targeting sequence (MTS) was created by PCR of PreP cDNA purchased from Open Biosystems. The insert was digested with BamHI and XhoI and subsequently subcloned into pET28a expression vector. The sequence of the resulting clone was confirmed by sequencing.

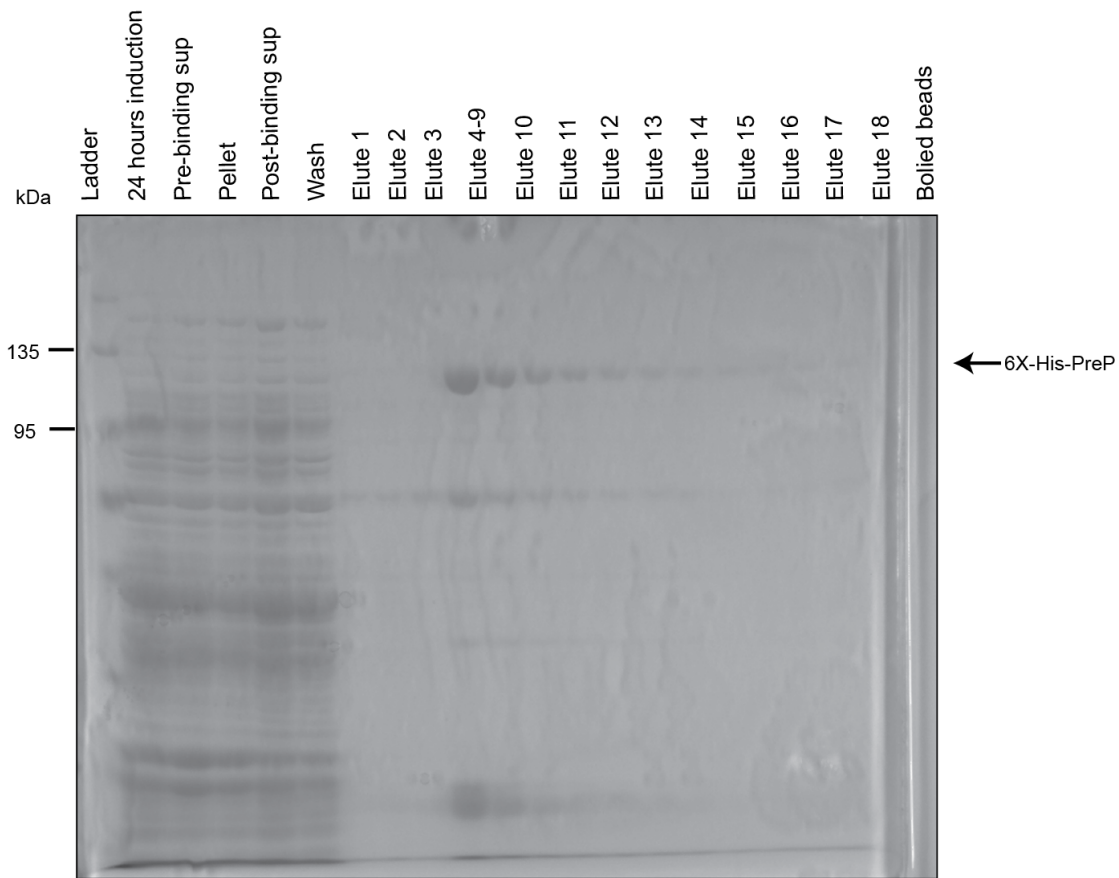


Figure 2-3. Robust expression and successful purification of recombinant 6X-His PreP. *E. coli* overexpression strain, BL21 DE3, was transformed with the construct pCJD-6xHIS PreP pET28a and expressed for 24 hrs using an auto-induction method (see methods). The lysate was collected and the His-tagged PreP was purified using Co^{2+} column. 1 ml fractions were collected and analyzed by SDS-PAGE. The Coomassie-stained gel above indicates that the 120 kDa PreP protein was successfully expressed and purified.

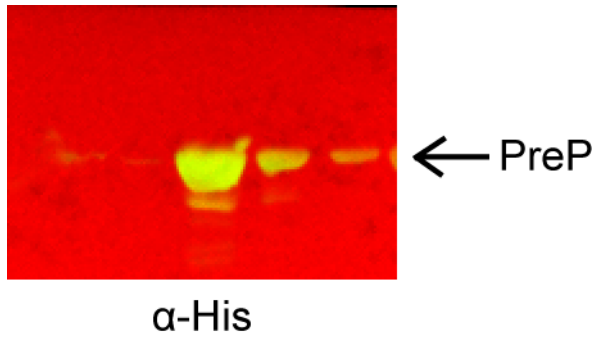
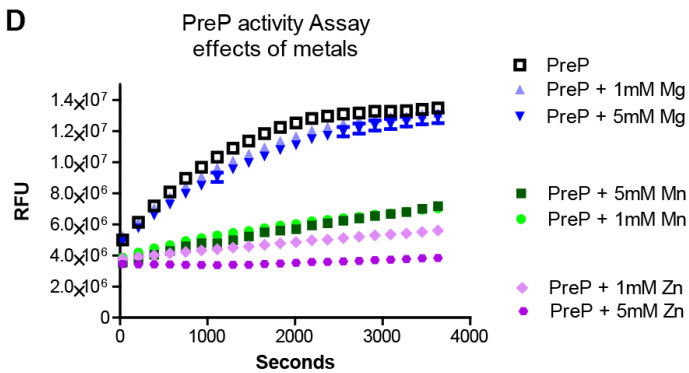
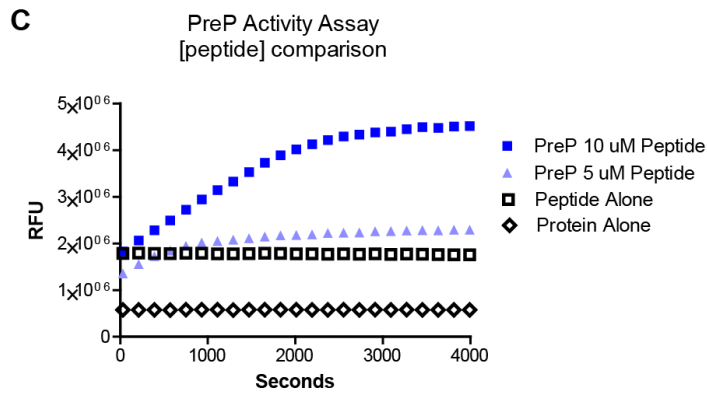
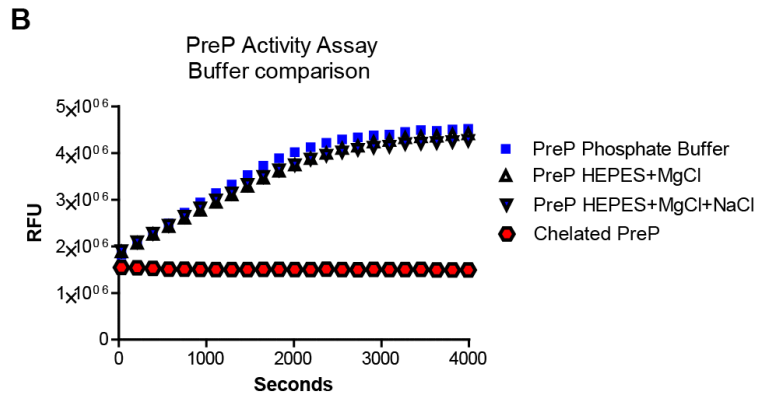
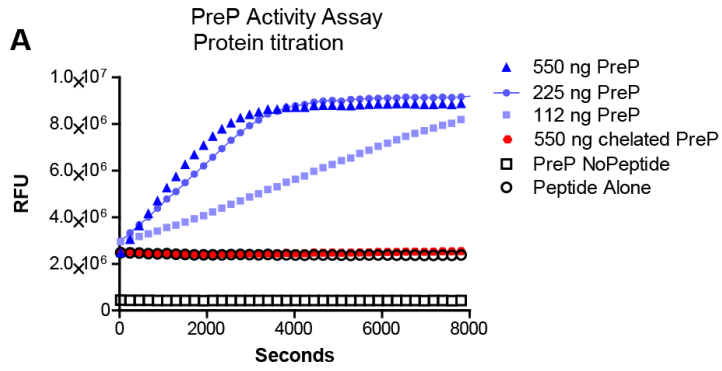


Figure 2-4 – Western blot confirmed successful PreP purification. 2 μ l of the purified PreP from elution fractions was loaded on a 7% polyacrylamide gel. Proteins were transferred to nitrocellulose membrane and blotted with an anti-His antibody. The identity of the expressed recombinant protein was confirmed by this Western blot.



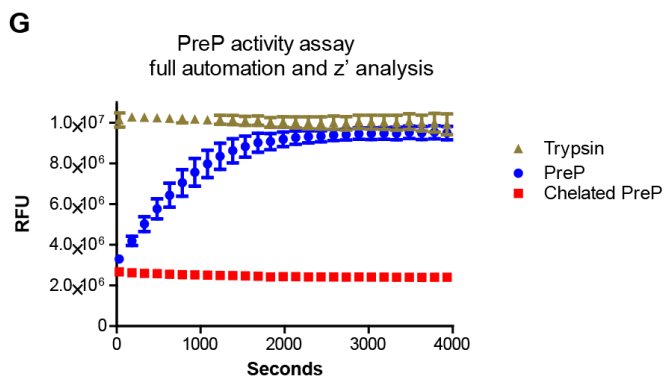
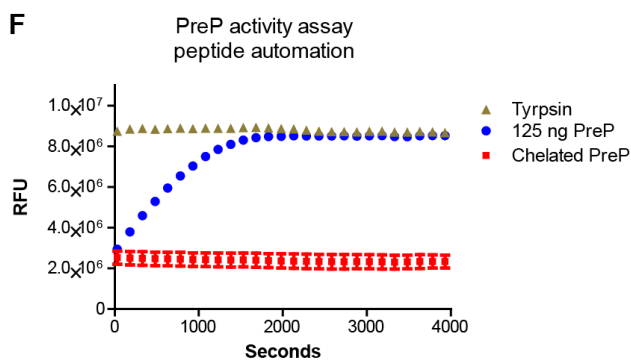
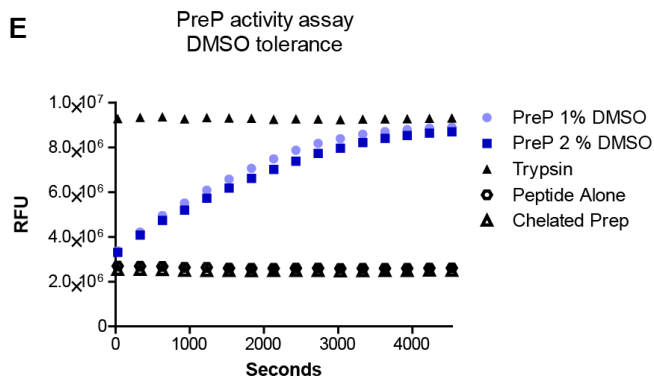


Figure 3-1. HTS Assay development and optimization (A) Recombinant PreP was incubated in assay buffer prior to addition of fluorogenic peptide. PreP cleavage of fluorogenic peptide follows Michaelis-Menten kinetics. Other assay conditions were tested to create a robust assay. These includes buffer composition (B), peptide concentration (C) metal level (D), DMSO tolerance (E), automation (F), and a Z' analysis (G).

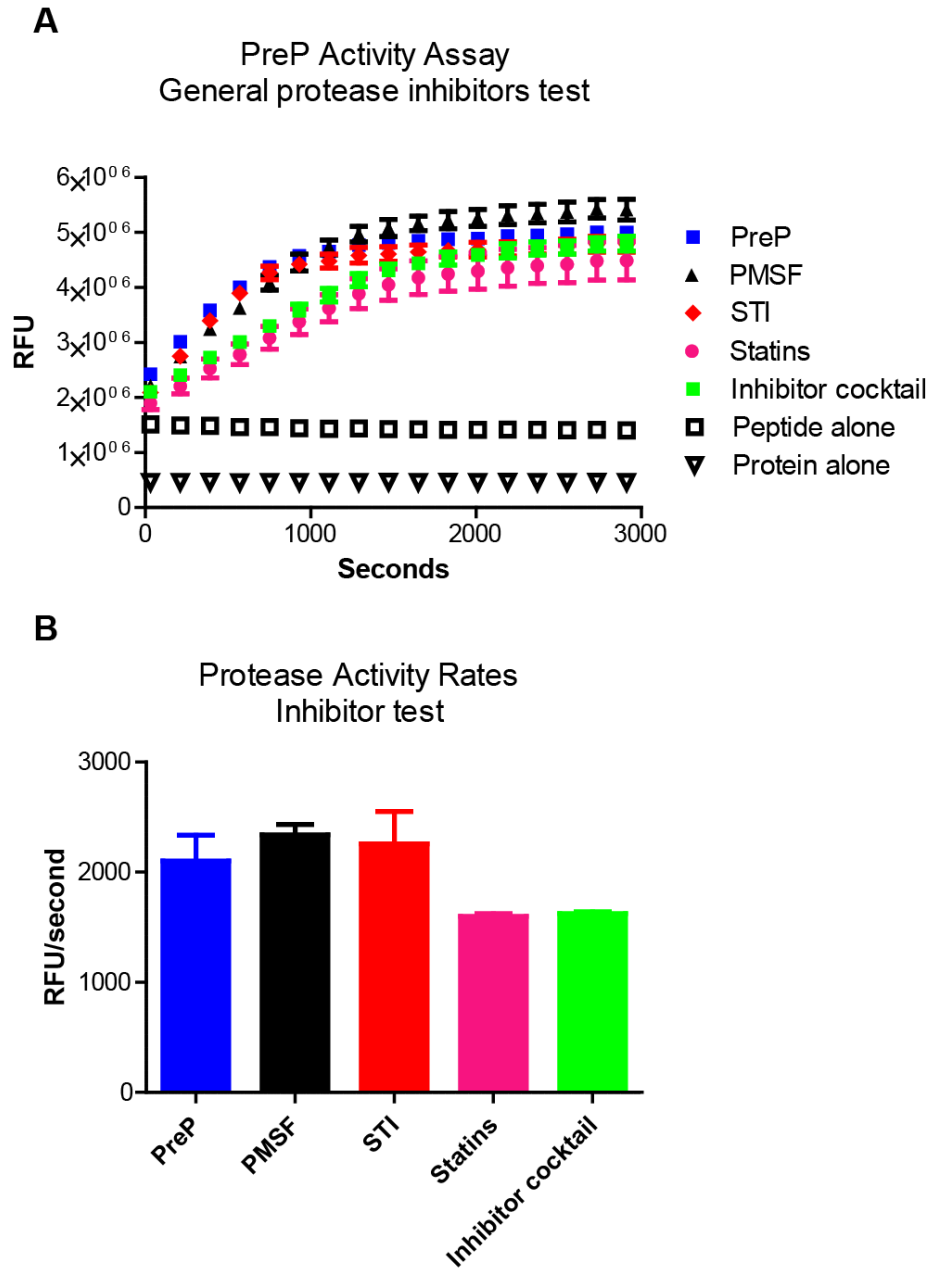


Figure 3-2. General protease inhibitors do not inhibit PreP activity. The PreP activity assay was carried out in the presence of commercially available protease inhibitors. PMSF, IAA, and STI do not alter PreP protease activity.

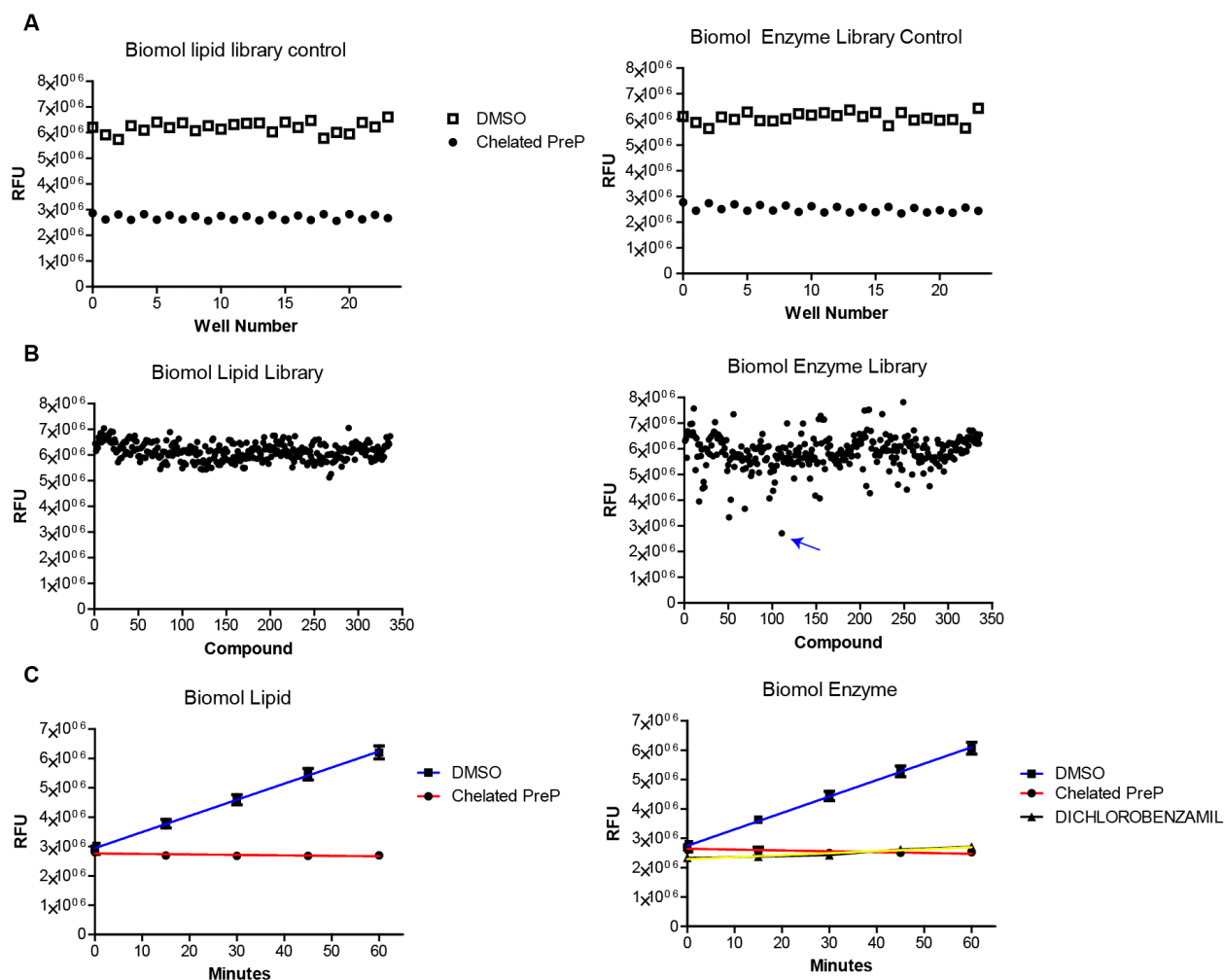


Figure 4-1. Pilot screen result. (A) Scatter plots of control wells from biomol lipid (left) and biomol enzyme (right) library. DMSO (vehicle) treated WT PreP gave an average reading of 6×10^6 RFU and DMSO treated chelated PreP control gave an average reading of 3×10^6 RFU (data not shown). (B) Scatter plots of the end point fluorescence reading (20 minutes after peptide addition) from each drug-treated well (C) Time plots of fluorescence measurement. No compound was identified as a hit from the Biomol Lipid library whereas 1 compound was marked as a hit from the Biomol enzyme library (arrow).

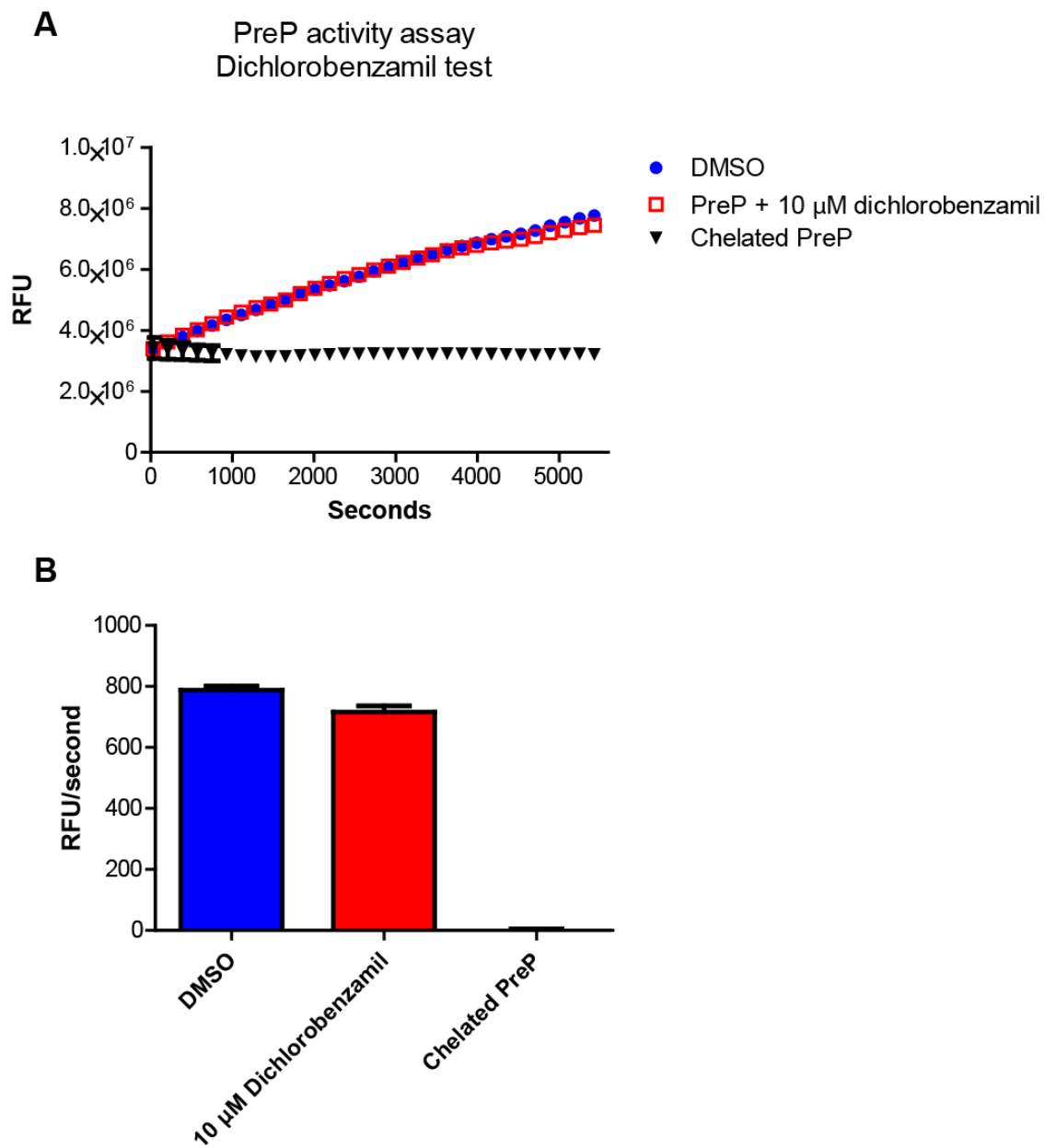


Figure 4-2. Dichlorobenzamil does not inhibit PreP (A) The activity assay was performed to measure the inhibitory effect of dichlorobenzamil purchased from chemical vendor (B) Rate of reactions remained similar between small molecule (dichlorobenzamil) and vehicle (DMSO)-treated PreP.

A	7464214	6992174	6992174	5562478	5344537	6948100	8771552	8917072	8962023	8656033	9185348	8520188	9298013	7327485	9037603	8820617	9107145	7418500	8453177	9455890	9244630	2761277	2583653	
B	9040534	8877395	8375592	8465448	8056115	8599199	8565977	8714702	8832313	7682046	3542823	7831775	8326449	6966231	7735144	9272186	8504188	9290606	6259819	9201838	8196029	6774551	2567371	2817886
C	7074842	7987108	7994441	7475986	6963278	7437195	8150752	6739185	7291567	8714662	9150229	7561604	9279288	8585419	8871218	8170348	7603639	8322704	7902855	6308127	8818470	8430837	2663457	2565951
D	8567991	8347211	8044210	7815399	8023413	7632785	7945938	8951896	8006358	6411375	8116113	8532862	8691304	8937017	9129709	9134389	8713498	8681055	8768070	4588743	7451308	8560632	2509817	2701118
E	6908999	7684172	7804075	8046025	6918801	7861078	8091106	8180732	7974789	8277321	8345933	8642897	8515955	9555976	9178183	8662936	9098625	6944109	8844346	8642605	8146256	8591977	2675573	2591570
F	8681696	8524455	7536721	8644360	8121910	8498517	7724400	8368926	6182781	8084989	8572205	9013212	8500141	7947080	8844417	6778417	6377295	8741342	8367389	12258662	8962157	8810195	2529045	2689988
G	6650628	7834870	4649805	7400620	6181917	8402510	7285973	6636568	8057400	7632581	7987860	8447934	8429955	7922419	7763990	8811722	8809674	8742956	8691205	8489309	9081469	8749206	2651622	2543823
H	8032784	8172039	5578865	7733006	8147021	7434942	7737414	8237204	6735245	3968573	8620514	8204206	8147836	7874958	7501899	7266698	8452630	6740777	8045609	8328750	7654409	2448084	2645802	
I	6784914	7257180	7042599	7074210	7227181	7125911	8520185	7554842	7899864	8259893	8806547	7144645	8314242	8523141	7676592	8533972	7700517	8659433	8555122	8075237	7632981	7537299	2515699	2424701
J	7923810	8018298	7380686	7904812	8269683	7294668	3727279	8786472	7999425	8535209	8568583	9018693	7894146	7694081	6263132	8392184	4004454	8343141	8140887	8339917	6156323	8214851	2372667	2580779
K	6358235	8024599	8379408	727635	8666885	8575187	8973237	7784777	7760281	7151310	8585209	8331798	8804279	8696866	8662862	8658324	9016623	8619659	8003174	8810093	8611990	8544898	2586208	2500606
L	7915110	8127367	7515360	5993806	8424442	8069417	8304492	8553362	7959174	7577266	8456805	8336885	8749684	8766095	8029758	8530766	8744150	8780797	1645227	7930091	8806154	8764443	2482866	2579416
M	6651763	7599451	8100799	7602280	7036081	8245718	8055123	7540036	7420853	7969384	2849206	8769716	5381958	7003074	8647755	8453377	6714193	60776314	7140220	8130568	6394145	7669104	2448688	2486801
N	8677992	8151699	7647347	7991898	6488805	7911989	7957996	8597638	8641819	7421946	8624968	7948475	7767317	8059089	8032587	7835904	6977382	8041870	8075083	7697382	7855390	2497086	2647760	
O	8600368	8023455	8481228	7590680	8644938	7661948	7002229	7488003	7783696	8786085	8744170	8664178	6962359	7548324	7003378	8801672	8742632	6561295	8978984	7651279	8830673	8213462	2628152	2506377
P	9216233	9192088	7813639	8249280	8346071	8832518	8516452	7944417	7773906	8791510	8700066	9132518	8647411	8647661	7703676	8652470	8728748	9350350	8936612	9330667	8430728	9311930	2527391	2659988

Control Analysis:

Positive Control Average 2552938
 Positive Control Standard Dev. 101112
 Negative Control Average 8124354
 Negative Control Standard Dev. 467413
 -10*SD from Neg. Control 3450223
 +10*SD from Neg. Control 12798484
 Z Score 0.69

Figure 4-3. Data processing sample. Fluorescence raw data of plate 92 from the UCLA library (Chembridge) was converted into a table format to aid in data analysis by VBA algorithm written by Dr. Samuel Hasson. Z' score indicates successful assay. Light green cells are DMSO-treated well. Yellow cells are for chelated-PreP wells. Red and dark green colored wells marked compounds whose measurements differ from controls by +/- 3 SD.

1	Well	Location	Well Type	Well Reading	Negative Control			Well		% Survival	
					Ave	Negative Control SD	+10*SD	-10*SD	Reading 0		% Survival 0
66	M11	92M11	Sample	2829206	8124354	467413	12798484	3450223	314648	98	5
67	B11	92B11	Sample	3542823	8124354	467413	12798484	3450223	324110	101	18
68	J07	92J07	Sample	3737279	8124354	467413	12798484	3450223	321414	100	21
69	H10	92H10	Sample	3968573	8124354	467413	12798484	3450223	338208	105	25
70	J17	92J17	Sample	4004454	8124354	467413	12798484	3450223	316493	99	28
71	D20	92D20	Sample	4588743	8124354	467413	12798484	3450223	314706	98	37
72	G03	92G03	Sample	4649805	8124354	467413	12798484	3450223	313579	98	38
73	H14	92H14	Sample	5338373	8124354	467413	12798484	3450223	319212	99	50
74	A05	92A05	Sample	5344537	8124354	467413	12798484	3450223	320219	100	50
75	M13	92M13	Sample	5381958	8124354	467413	12798484	3450223	319243	99	51
76	A04	92A04	Sample	5562478	8124354	467413	12798484	3450223	320161	100	54
77	H03	92H03	Sample	5578865	8124354	467413	12798484	3450223	334386	104	54
78	L04	92L04	Sample	5993806	8124354	467413	12798484	3450223	318698	99	62
79	M18	92M18	Sample	6076314	8124354	467413	12798484	3450223	323981	101	63
80	J21	92J21	Sample	6156323	8124354	467413	12798484	3450223	318555	99	65
81	G05	92G05	Sample	6181917	8124354	467413	12798484	3450223	322081	100	65

1	Well	Location	Well Type	Well Reading	Negative Control			Well		% Survival	
					Ave	Negative Control SD	+10*SD	-10*SD	Reading 0		% Survival 0
365	E17	92E17	Sample	9098625	8124354	467413	12798484	3450223	335769	105	117
366	A18	92A18	Sample	9107145	8124354	467413	12798484	3450223	320822	100	118
367	D15	92D15	Sample	9129709	8124354	467413	12798484	3450223	321736	100	118
368	P12	92P12	Sample	9132518	8124354	467413	12798484	3450223	325815	101	118
369	D16	92D16	Sample	9134389	8124354	467413	12798484	3450223	324545	101	118
370	C11	92C11	Sample	9150229	8124354	467413	12798484	3450223	323572	101	118
371	E15	92E15	Sample	9178183	8124354	467413	12798484	3450223	319839	100	119
372	A11	92A11	Sample	9185348	8124354	467413	12798484	3450223	318088	99	119
373	B20	92B20	Sample	9201838	8124354	467413	12798484	3450223	323310	101	119
374	A22	92A22	Sample	9244630	8124354	467413	12798484	3450223	317313	99	120
375	B16	92B16	Sample	9272186	8124354	467413	12798484	3450223	324529	101	121
376	C13	92C13	Sample	9279288	8124354	467413	12798484	3450223	323091	101	121
377	B18	92B18	Sample	9290606	8124354	467413	12798484	3450223	321532	100	121
378	A13	92A13	Sample	9298013	8124354	467413	12798484	3450223	319570	99	121
379	P22	92P22	Sample	9311930	8124354	467413	12798484	3450223	327107	102	121
380	P20	92P20	Sample	9330667	8124354	467413	12798484	3450223	319264	99	122
381	P18	92P18	Sample	9350350	8124354	467413	12798484	3450223	331834	103	122
382	A21	92A21	Sample	9455890	8124354	467413	12798484	3450223	320095	100	124
383	E14	92E14	Sample	9555976	8124354	467413	12798484	3450223	1647983	513	126
384	F20	92F20	Sample	12258662	8124354	467413	12798484	3450223	6271181	1952	174
385	J11	92J11	Sample	15625583	8124354	467413	12798484	3450223	11541791	3592	235

Figure 4-4. Data analyses to mark compounds that inhibited and enhanced PreP activity. Sample data analyses from plate 92 of the UCLA library. Data were sorted by well readings, well types and % survival. Red-colored cells mark compounds that decreased fluorescence reading by 70% (lower than 30% survival). Light green-colored cells mark compounds that increase fluorescence by 20% (120% and up % survival). Well reading 0 gives fluorescence values prior to peptide addition. % survival 0 normalizes well reading 0 value to that of DMSO vehicle. % survival 0 higher than 100% indicates small molecules that are intrinsically fluorescence.

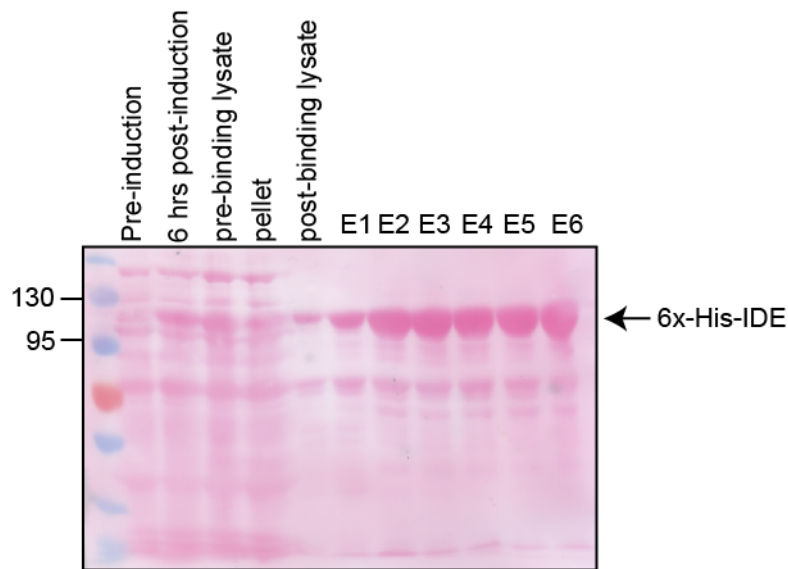


Figure 4-5. IDE expression and purification. *E. coli* overexpression strain, BL21 DE3, was transformed with the 6x-His-IDE construct. Expression was induced by addition of 1 mM IPTG. Six hours post-induction, lysate was collected and His-tagged IDE was purified using Ni²⁺ column. 1 ml fractions were collected and analyzed by SDS-PAGE. The ponceau-stained gel above indicates IDE was robustly expressed and purified.

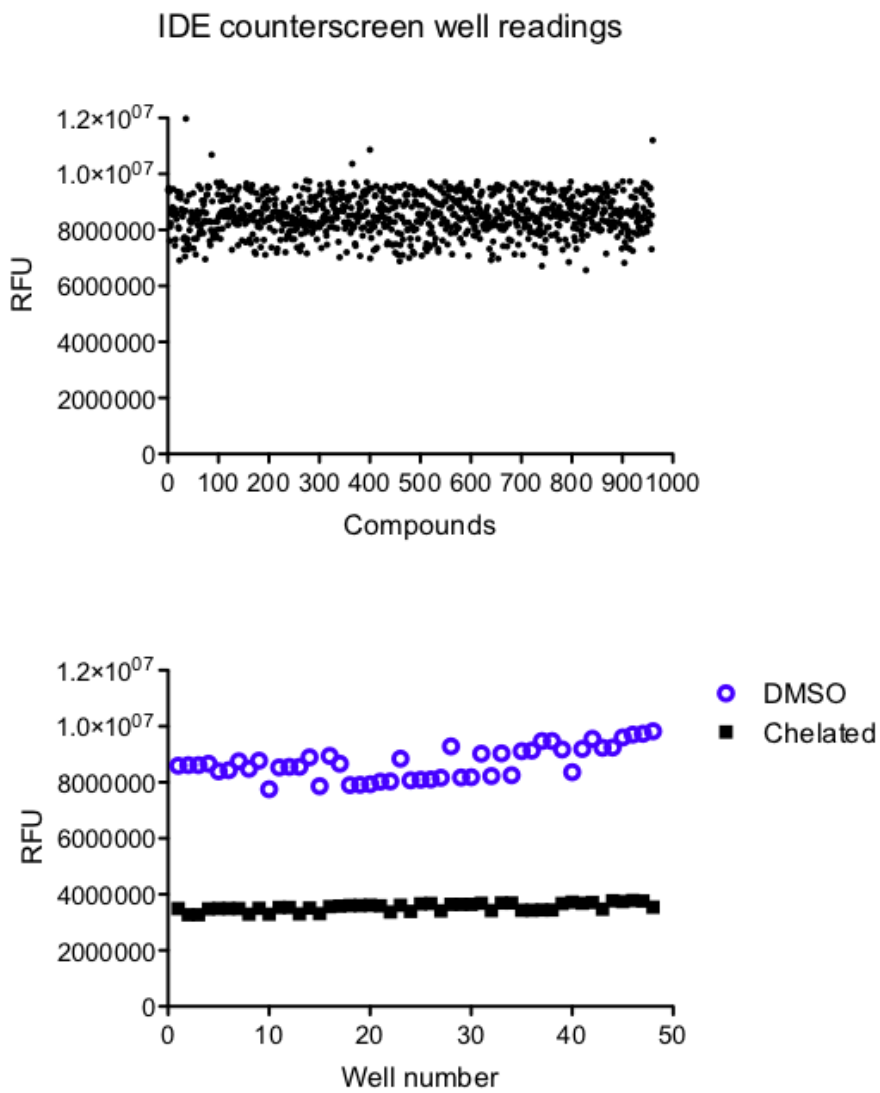


Figure 4-6. Representative data for IDE counterscreen. Cherry picked compounds were pinned on plates containing wildtype or chelated IDE. Leumorphin peptide was used for the counterscreen as described previously.

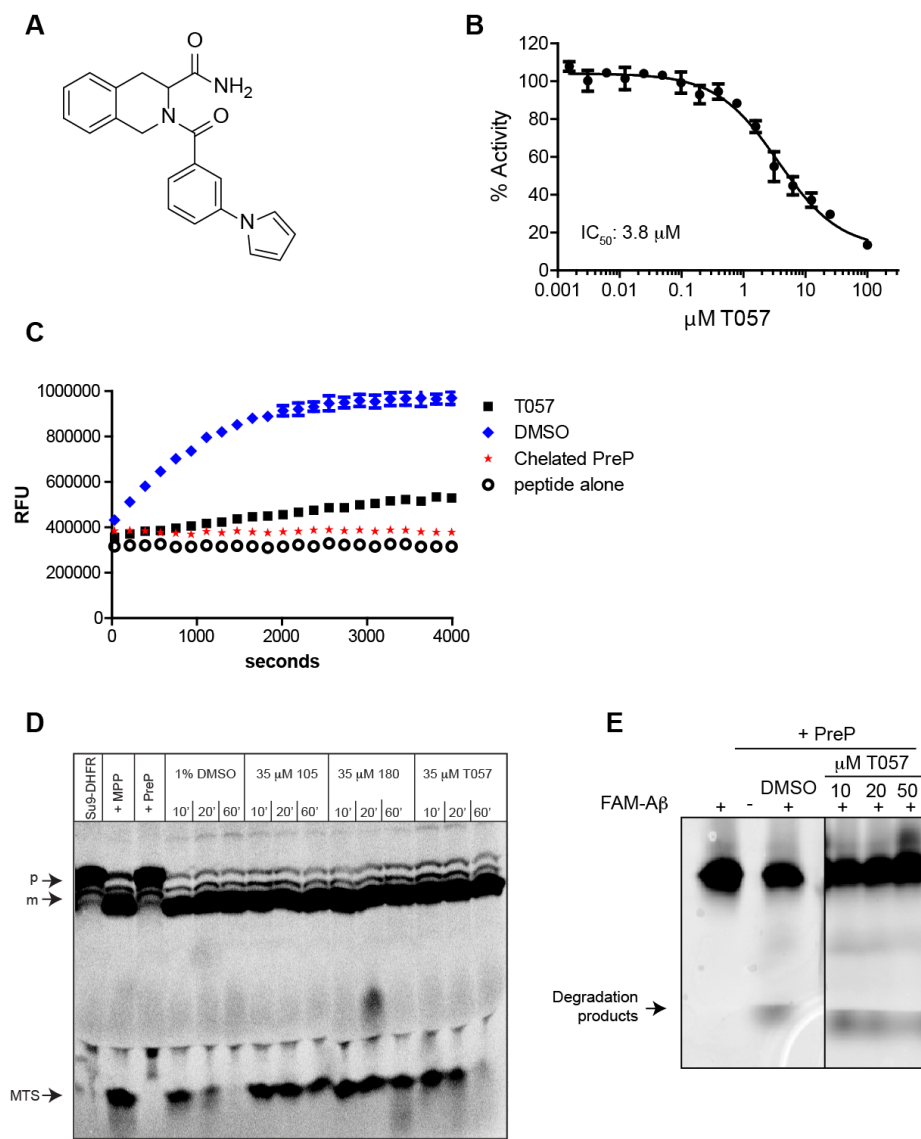


Figure 5-1. T057 attenuates activity of PreP *in vitro*. (A) T057 is a 2-[3-(1H-pyrrol-1-yl)benzoyl]-1,2,3,4-tetrahydroisoquinoline-3-carboxamidetetrahydroquinoline. (B) T057 has a relative IC_{50} of 3.8 μ M in the *in vitro* activity assay with leuromorphin peptide. (C) Presence of 10 μ M T057 prevents PreP to degrade fluorescently-labeled A β . (D) T057 stabilizes su9 derived from MPP-cleaved su9-DHFR (D) FAM-labeled A β was added to recombinant PreP that has been incubated with DMSO vehicle or increasing concentration of T057. Presence of degradation products decreased with increasing concentration of T057.

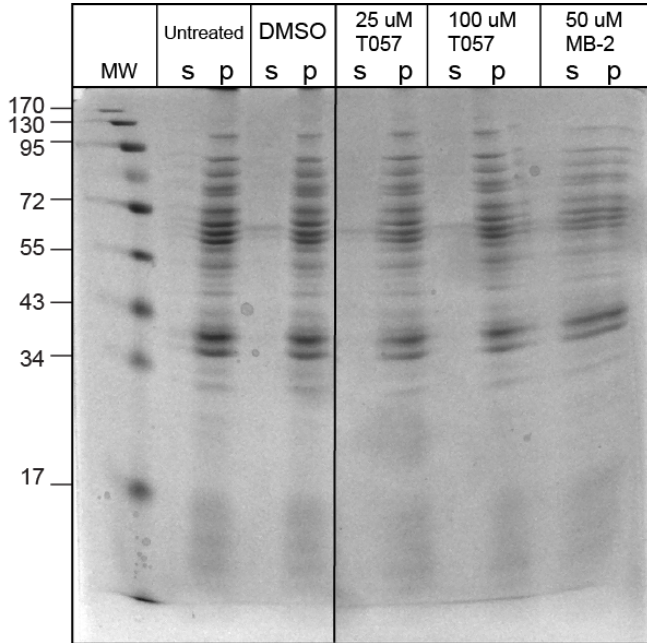


Figure 5-2. T057 does not permeabilize mitochondria. Isolated yeast mitochondria were incubated with T057 or DMSO and MitoBloCK-2 as controls for 30 minutes. Mitochondria were separated from released proteins by centrifugation. Supernatant were precipitated with 5% trichloroacetic acid (TCA). Supernatant and pellet fractions were loaded on SDS-PAGE. Gel was stained with coomassie blue to visualize proteins.

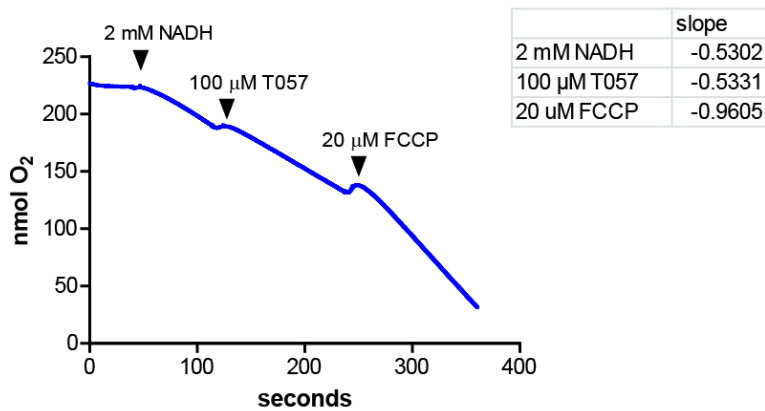
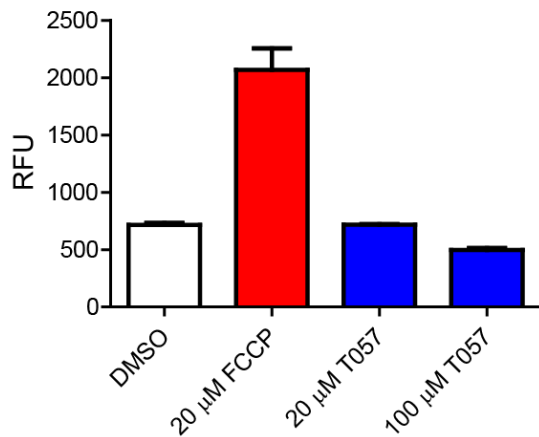
A**B**

Figure 5-3. T057 does not impair respiration and uncouple mitochondria. (A) Respiration in isolated mitochondria was measured using Clark-type oxygen electrode. Respiration was initiated by addition of NADH. Rate of oxygen consumption was measured by taking the the slope of oxygen consumed over time. CCCP was used as a positive control for mitochondrial uncoupler. (B) Mitochondria were incubated import buffer in the presence of T057 for 15 minutes prior to addition of DISC₃(5) dye. DMSO and FCCP were used as controls. DISC₃(5) fluorescence was measured 5 minutes after dye was added.

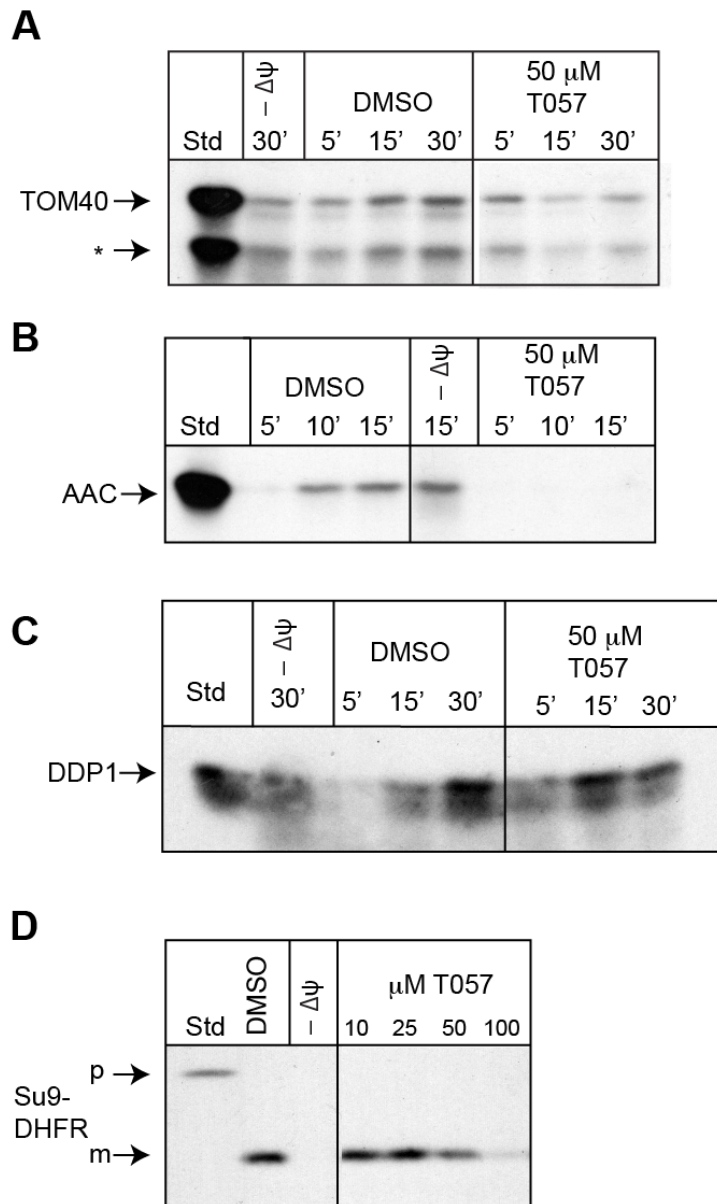


Figure 5-4. T057 inhibits import of mitochondrial proteins. Mitochondria purified from HeLa cells were incubated with DMSO, drug, or CCCP for 15 minutes prior. Import was initiated by adding (A) outer membrane-targeted precursor, TOM40 (B) Inner membrane-targeted precursor, AAC (C) intermembrane space-targeted precursor DDP1 (D) and matrix-targeted precursor, su9-DHFR. Reaction aliquots were withdrawn at specified time points. Import was stopped by addition of trypsin. Reactions were analyzed on SDS-PAGE and visualized by autoradiography.

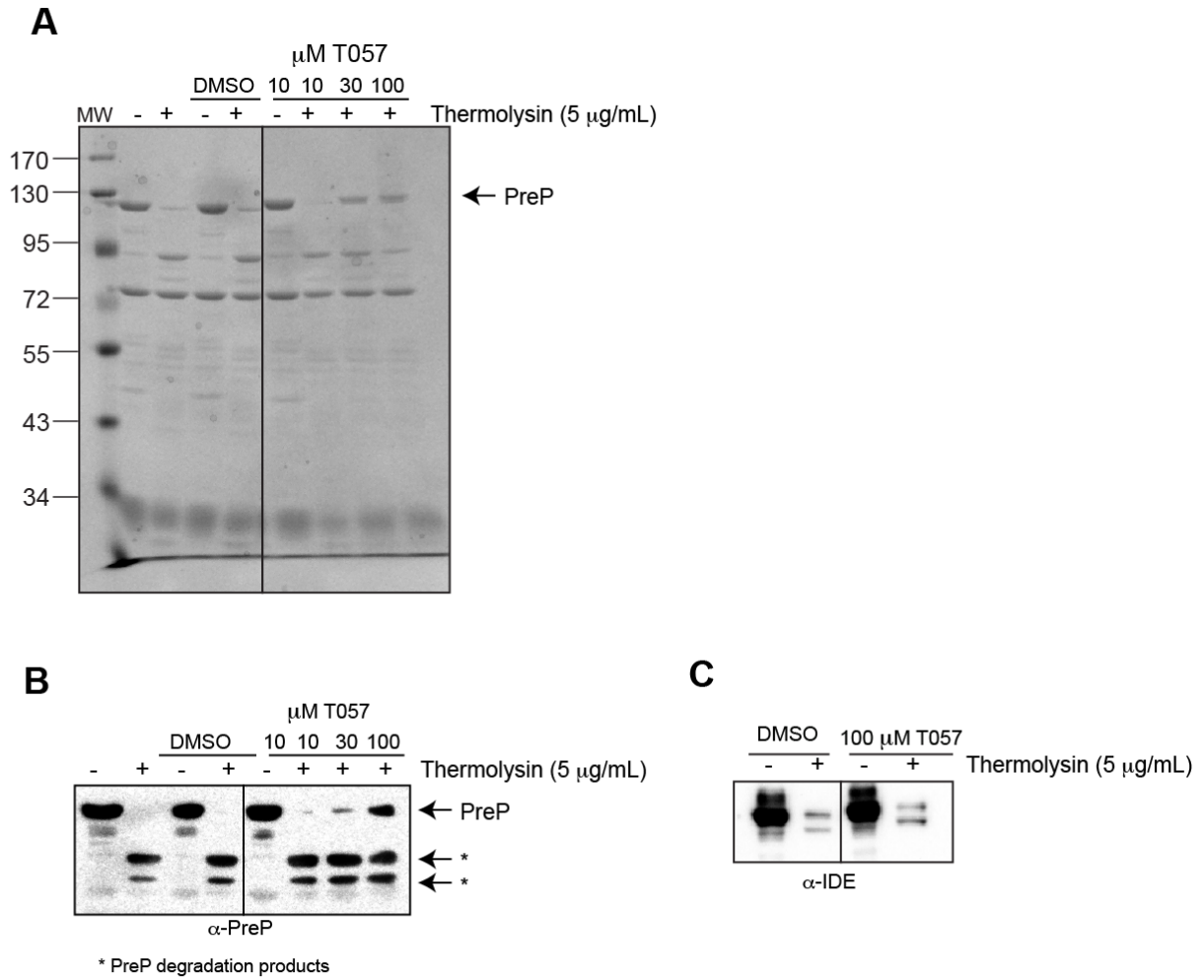


Figure 5-5. T057 protects PreP but not IDE from degradation by thermolysin. DARTS assay. Recombinant PreP was incubated in DMSO or T057 for 2 hours prior to addition of thermolysin for 15 minutes. Reactions were stopped by addition of EDTA and laemmli sample buffer. Samples were loaded on SDS-PAGE and stained with coomassie blue (A) or blotted with anti PreP (B) and IDE (C) antibodies.

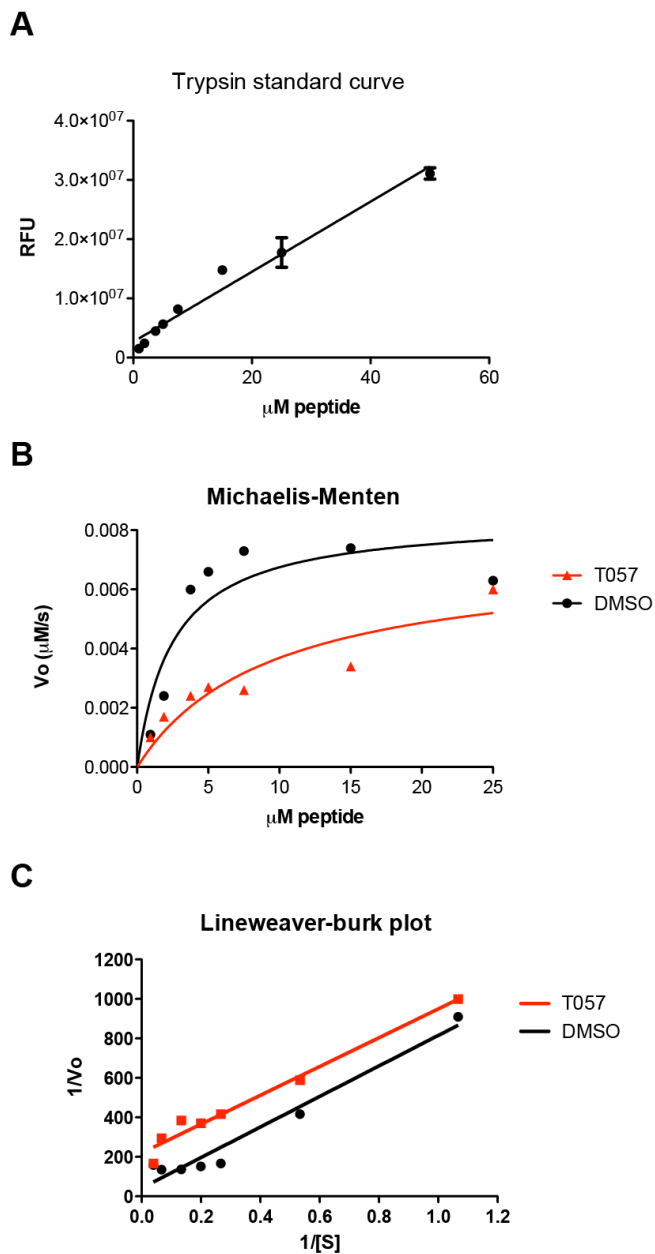


Figure 5-6. T057 is an uncompetitive or a mixed inhibitor. (A) Trypsin standard curve was generated to convert fluorescence to μM peptide. (B) Plot of initial velocity versus substrate concentration allowed for measurement of Michaelis-Menten kinetics parameters. (C) Double-reciprocal plot of Michaelis-Menten results in lineweaver-burk plot. The kinetic parameters of Michaelis-Menten and lineweaver-burk analyses did not complement each other, thus we can only conclude that T057 is not a competitive or noncompetitive inhibitor.

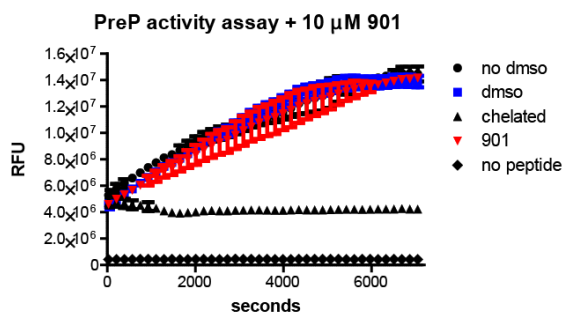
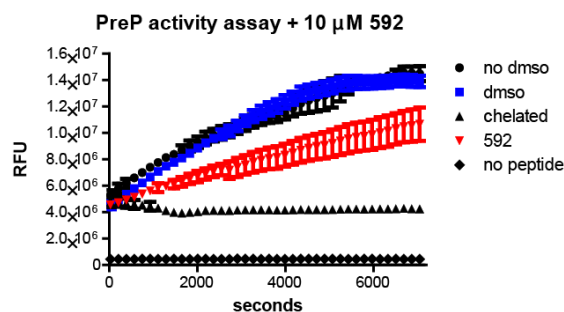
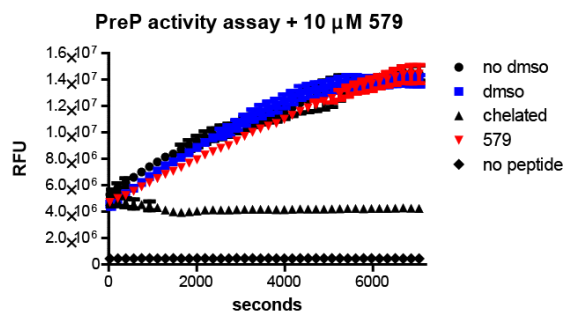
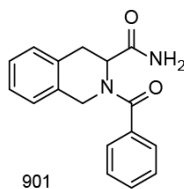
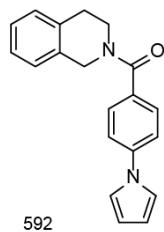
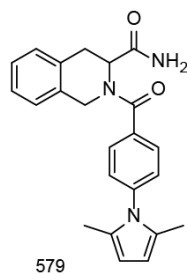
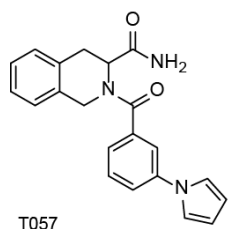


Figure 5-7. Structure-Activity Relationship (SAR) study of T057. *In vitro* fluorescence activity assay (leumorphin peptide) with T057 analogs. Analog 579 and 901 does not inhibit activity of PreP at 10 μ M whereas analog 572 inhibits PreP at lower concentration compared to that of T057.

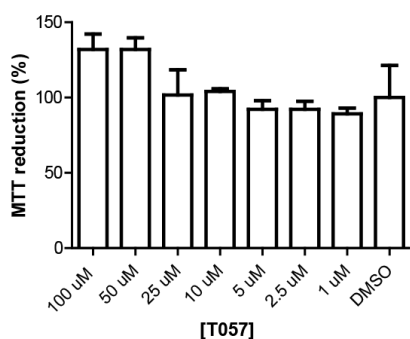
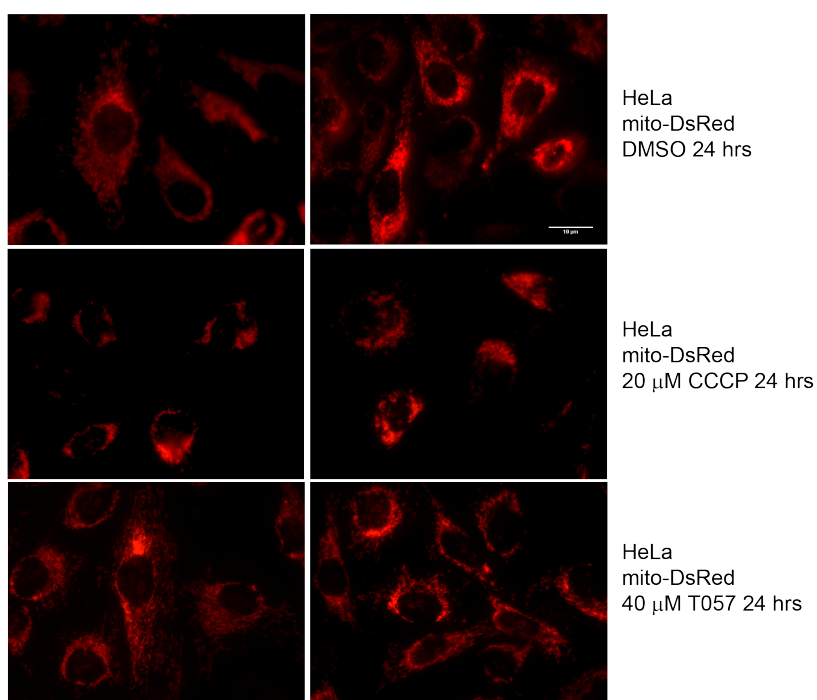
A**B**

Figure 5-8. T057 treatment in cultured cells does not affect viability and impair mitochondrial morphology. (A) HeLa cells were treated with varying concentration of T057 for 24 hours. Cell viability was measured as normalized % of MTT reduction where DMSO-treated cells were set as 100%. (B) HeLa cells expressing mitochondria-targeted dsRed were treated with small molecule or vehicle control for 24 hours. Mitochondria morphology visualized by microscopy on the texas red channel.

Table I. Chemical libraries screened at UCLA Molecular Screening Shared Resources (MSSR)

Library name	# of molecules	Description
Biomol	640	Known inhibitors, bioactive lipid
PW	1280	Preswick chemicals FDA-approved collection
UCLA	29760	Chembridge collection
TAR	8640	Asinex targeted set
DL	19840	Asinex diversity set
SS	2560	Asinex synergy set
ESI	1920	Asinex emerald set
MS	2240	Microsource collection
NIH	640	NIH collection
EAM	20480	Enamine collection
LS	40000	Life Chemicals screening set

Table 2-1. Summary of screened compounds (1st round of screening)

	Number of compounds	Inhibitors	Inhibitors hit rate (%)	Inhibitors confirmed in rescreening	Hits confirmed after IDE counterscreen	Hits confirmed after MPP data analysis
Chembridge	29,760	209	0.7	118 (56.5%)	0	2 (1.69%)
Asinex	19,840	134	0.68	67 (50%)	0	1 (1.49%)
Others (focused libraries)	38,400	121	0.32	48 (40%)	0	4 (8.3%)
Total	88,000	464	0.53	233 (48.1%)	233 (100%)	226 (97%)

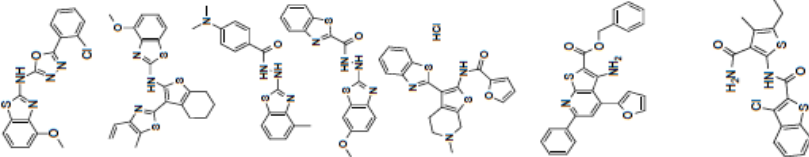
Table 2-2. Summary of screened compounds (2nd round of screening)

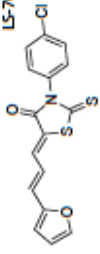
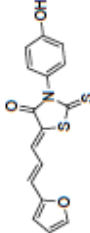
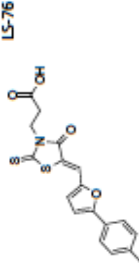
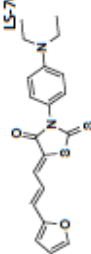
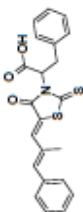
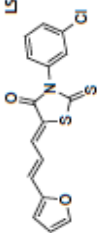
	Number of compounds	Inhibitors	Inhibitors hit rate (%)	Inhibitors confirmed in rescreening	Hits confirmed after IDE counterscreen	Hits confirmed after MPP data analysis
Life Chemicals	40,000	271	0.6775	131	8	13
Total	40,000	271	0.6775	141 (52%)	133 (94%)	120 (91%)

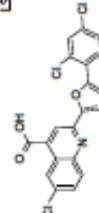
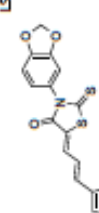
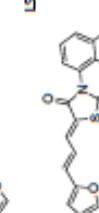
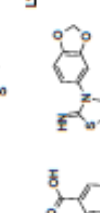
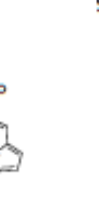
Table III. Summary of hits from LS library

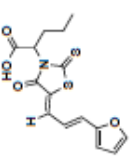
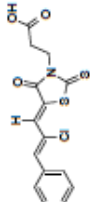
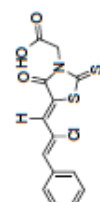
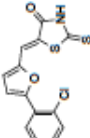
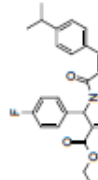
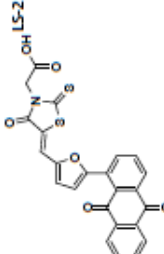
Source Plate	Well Number	% Survival	Vendor	Catalog #	Status	Dissolve easily in DMSO	IC50	Inhibits Ab degradation	Inhibits sup-cleavage	Permeabilize mito	Uncouple mito	AAC import	su9 import	Recruits Parkin	Mito morphology	IC50 in cultured cells
LS-15	E12	-2	Life Chemicals	F0646-1298	Ordered	Yes	0.84 μ M	Need to do titrate	No. Need to repeat	No	No	Inhibit at 100	Inhibit at 25	No	Aberrant mito	Cells dead at 100
LS-15	G15	18	Life Chemicals	F0642-1820												
LS-15	M09	13	Life Chemicals	F0646-2989												
LS-15	A12	25	Life Chemicals	F0646-1141												
LS-9	J18	6	Life Chemicals	F0526-1819												
LS-27	D04	30	LC	F1155-0256												
LS-10	O03	25	LC	F0526-2290												

Scaffold 1



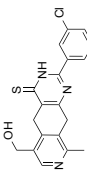
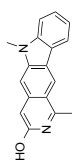
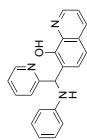
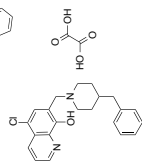
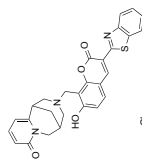
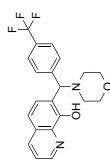
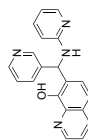
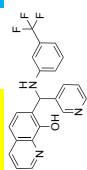
Source Plate	Well Number	% Survival	Vendor	Catalog #	Status	Dissolve easily in DMSO	IC50	Inhibits Ab degradation	inhibits su9-cleavage	Permeability to mito	Uncouple mito	AAC import	su9 import	Recruits Parkin	Mito morphology	IC50 in cultured cells	
Scaffold 2	L5-76	17	Life Chemicals	F3104-0041	Ordered	No											
		A15															
	L5-76	21	Life Chemicals	F3104-0028													
		I13															
	L5-76	22	Life Chemicals	F3210-0050													
		J20															
	L5-76	21	Life Chemicals	F3104-0034													
		M13															
L5-6	29	Life chemicals	F0393-0256														
	O17																
L5-103	G17	-1	LC	F3104-0040	Ordered	Yes	1.84 µM	Mild at 50	Yes at 50. Need to titrate	No	No	Inhibit at 25	Inhibit at 25	No	Appeared normal	n/a does not kill cells after 24 hrs	
																	

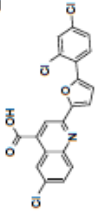
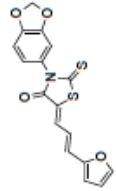
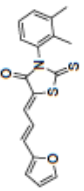
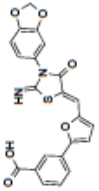
LS-103	H08	-2	LC	F3139-0021	Ordered No
					
	C17	12	LC	F3104-0036	
	O13	22	LC	F3104-0014	
	D21	26	LC	F0931-1394	
	E08	7	LC	F3217-0063	

LS-41		D18	20	LC	F1951-0297	Ordered	Yes	3.1 µM	No	Inhibit at 100	Inhibit at 100	No	appeared normal							
LS-41		F22	22	LC	F1951-0047															
LS-41		D22	11	LC	F1951-0046															
LS-8		D20		LC	F0494-0018															
LS-56		I04	29	LC	F2359-0282															
LS-2		B16	14	LC	F0165-0083															

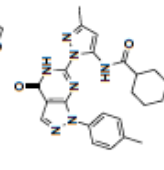
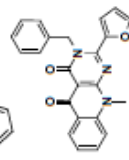
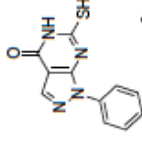
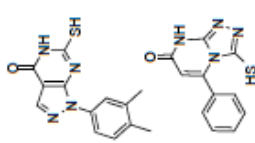
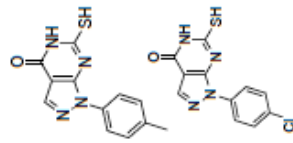
Source Plate	Well Number	% Survival	Vendor	Catalog #	Status	DMSO	Dissolve easily in	IC50	Inhibits Ab degradation	Inhibits su9-cleavage	Permeabilize mito	Uncouple mito	AAC import	su9 import	Recruits Parkin	Mito morphology
LS-23	J07	24	LC	F0842-0003												
LS-23	N07	19	LC	F0841-0010	Ordered	Yes	Yes	0.7 μM	Mild at 50	Yes at 50. Need to titrate	No	No	Mild inhibiti on at 25	Mild inhibiti on at 25		Appeared aberrant at 50
LS-22	D16	14	LC	F0815-0045	Ordered	No	No									
LS-23	M07	4	LC	F0821-0240												
LS-20	L17	7	LC	F0743-0024												
LS-5	G03	27	LC	F0318-0154												
LS-106	P14	23	LC	F3255-0021												
LS-32	A14	14	LC	F1603-0118												

Scaffold 3



LS-103	H08	-2	LC	F3159-0021	Ordered No
	C17	12	LC	F3104-0036	
	O15	22	LC	F3104-0014	
	D21	26	LC	F0931-1394	
	E08	7	LC	F3217-0063	

Scaffold 4



Source Plate	Well Number	% Survival	Vendor	Catalog #	Status	Dissolve easily in DMSO	IC50	Inhibits Ab degradation	inhibits sub-cleavage	Permeability to mito	Uncouple mito	AAC import	su9 import	Recruits Parkin	Mito morphology	IC50 in cultured cells
--------------	-------------	------------	--------	-----------	--------	-------------------------	------	-------------------------	-----------------------	----------------------	---------------	------------	------------	-----------------	-----------------	------------------------

LS-46 A07 15 LC F2135-0112 Ordered No

LS-46 C07 15 LC F2135-0113

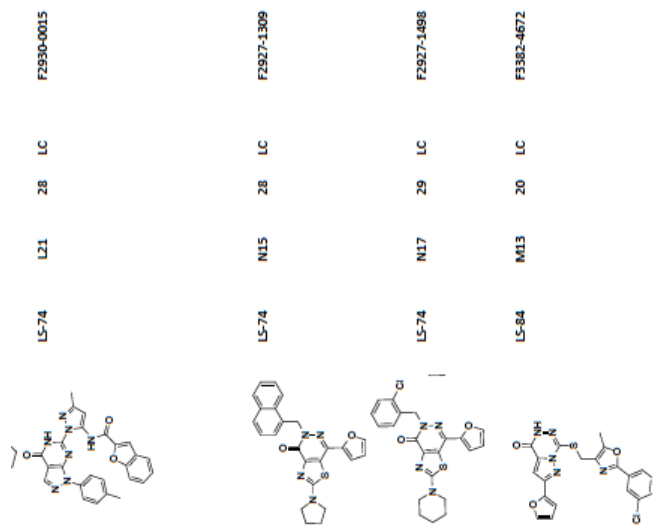
LS-46 E07 7 LC F2135-0116

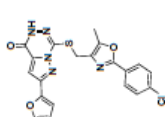
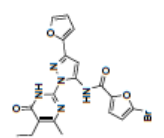
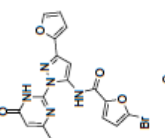
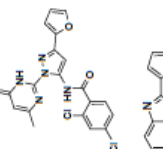
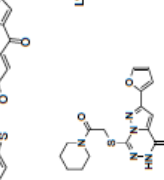
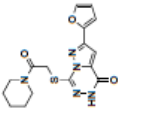
LS-46 G05 20 LC F2135-0064

LS-46 M05 25 LC F2135-0109

LS-78 D08 27 LC F3225-7014 Ordered No

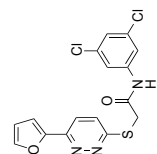
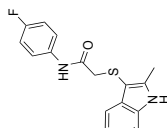
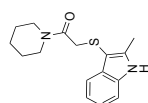
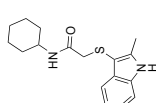
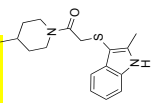
LS-74 D21 28 LC F2950-0005



LS-84	O13	25	LC	F3382-4673
				
LS-93	G19	26	LC	F5297-0925
				
LS-93	M17	24	LC	F5297-0125
				
LS-116	C22	27	LC	F5297-0061
				
LS-34	G08	7	LC	F1762-0033
				
LS-109	A15	20	LC	F3382-4832
				

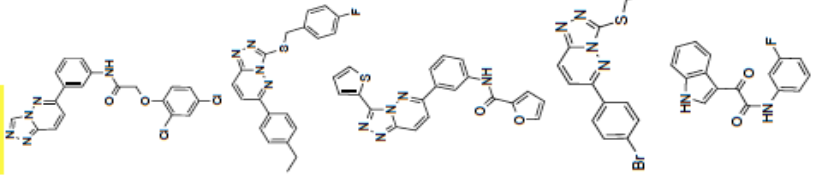
Source Plate	Well Number	% Survival	Vendor	Catalog #	Status	Dissolve easily in DMSO	IC50	Inhibits Ab degradation	inhibits sub9-cleavage	Permeabili ze mito	Uncouple mito	AAC import	su9 import	Recruits Parkin	Mito morphology	IC50 in cultured cells
LS-11	D19	8	LC	F0575-0005												
LS-11	L21	10	LC	F0575-0028												
LS-11	N17	19	LC	F0575-0002												
LS-11	P19	13	LC	F0575-0018												
LS-99	B12	20	LC	F2787-0046												

Scaffold 5



Source Plate	Well Number	Survival %	Vendor	Catalog #	Status	Dissolve easily in DMSO	IC50	Inhibits Ab degradation	Inhibits su3-cleavage	Permeability to mito	Uncouple mito	AAC import	su9 import	Recruits Parkin	Mito morphology	IC50 in cultured cells
LS-61	A22	14	LC	F2508-0111												
LS-61	C17	18	LC	F2506-0952												
LS-61	G22	29	LC	F2508-0504												
LS-61	I17	21	LC	F2506-1052												
LS-17	A05	13	LC	F0675-0131												

Scaffold 6



n/a does not
kill cells after
24 hrs

Appeared
aberrant

Inhibits
at 100
100
No

No

Yes at .50 need
to titrate

0.26 μ M Mild at 50

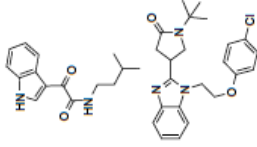
Ordered Yes

F0675-0061
F2143-0618

6 LC
15 LC

E03
L05

LS-17
LS-106

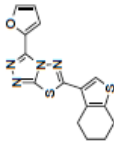


F1711-0154

17 LC

P04

LS-33



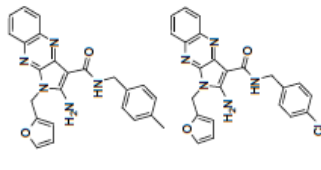
Ordered yes

F3225-2935

15 LC

K10

LS-78



appeared
normal

Mild
inhibition
at 100

No

0.97 μ M

F3225-3020

18 LC

M10

LS-78

2

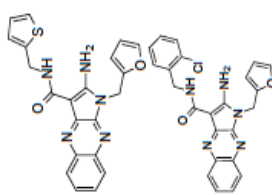
Ordered No

F3225-3345

18 LC

E04

LS-105



Mild
Mild at inhibition
100 at 100

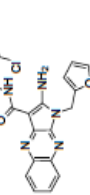
Ordered Yes

F3225-2984

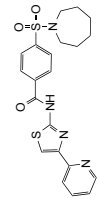
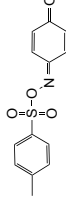
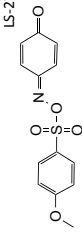
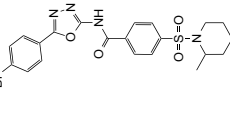
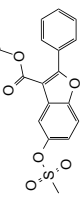
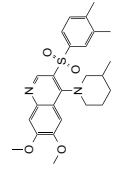
18 LC

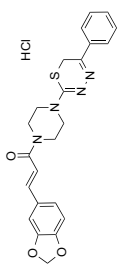
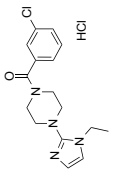
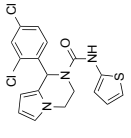
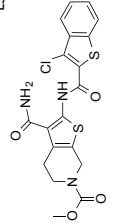
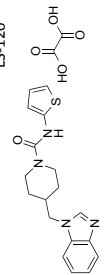
K21

LS-105



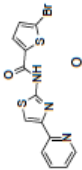
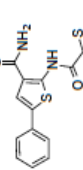
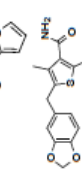
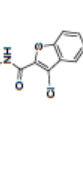
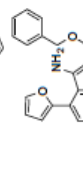
3.2 μ M

Scaffold 7	Source Plate		Well Number	% Survival	Vendor	Catalog #	Status	Dissolve easily in		IC50	Inhibits Ab degradation	inhibits su9 cleavage	Permeability to mito	Uncouple mito	AAC import	su9 import	Recruits Parkin	Mito morphology	IC50 in cultured cells	
	LS-19	F0700-0020						DMSO	IC50											
	LS-19	F0700-0020	C22	29	LC															
	LS-27	F1153-0155	F19	24	LC															
	LS-27	F1153-0158	H19	24	LC															
	LS-62	F2518-0516	N17	19	LC															
	LS-103	F3056-0614	P13	14	LC															
	LS-111	F3407-2253	J22	23	LC															

Source Plate	Well Number	% Survival	Vendor	Catalog #	Status	Dissolve easily in DMSO	IC50	Inhibits Ab degradation	inhibits su9-cleavage	Permeability ze mito	Uncouple mito	AAC import	su9 import	Recruits Parkin	Mito morphology	IC50 in cultured cells
LS-121	J08	19	LC	LS5792-0404												
																
LS-114	L8	26	LC	F5095-0200												
																
LS-97	B03	27	LC	F2707-0221												
																
LS-97	A18	2	LC	F2701-0384												
																
LS-120	G18	30	LC	F5755-0034												
																

Scaffold 9

Source Plate	Well Number	% Survival	Vendor	Catalog #	Status	Dissolve easily in DMSO	IC50	Inhibits Ab degradation	inhibits su9-cleavage	Permeability to mito	Uncouple mito	AAC import	su9 import	Recruits Parkin	Mito morphology	IC50 in cultured cells
LS-106	J13	27	LC	F3244-0399												
LS-106	L13	25	LC	F3244-0400												
LS-59	E20	19	LC	F2478-0037												
LS-59	18	19	LC	F2478-0013												
LS-28	B22	28	LC	F1256-0059												
LS-6	E11	12	LC	F0388-0063												
LS-7	A09	28	LC	F0440-0159												

LS-7	C06	20	LC	F0447-0273	
LS-28	K09	12	LC	F1174-2920	
LS-10	O03	25	LC	F0526-2290	
LS-27	D04	30	LC	F1155-0256	
LS-29	K18	30	LC	F1298-0997	

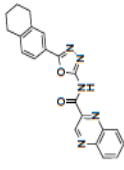
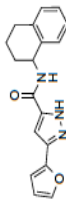
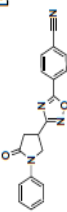
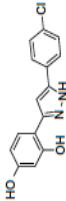
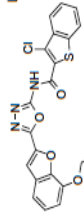
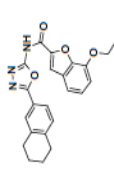
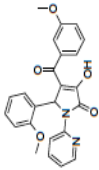
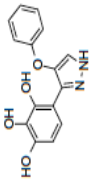
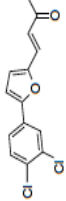
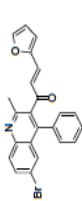
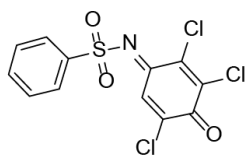
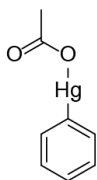
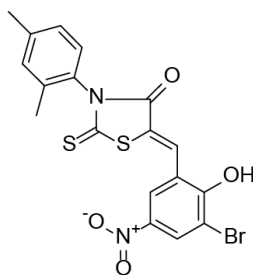
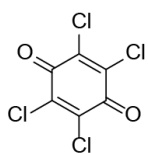
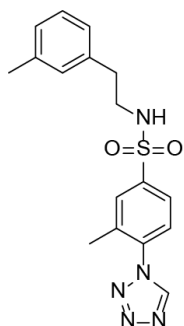
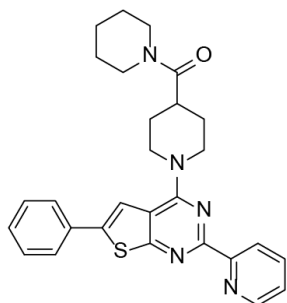
Source Plate		Well Number	% Survival	Vendor	Catalog #	Status	IC50	Inhibits Ab degradation	inhibits su9-cleavage	Permeability mito	Uncouple mito	AAC import	su9 import	Recruits Parkin	Mito morphology	IC50 in cultured cells	
Source Plate		Well Number	% Survival	Vendor	Catalog #	Status	IC50	Inhibits Ab degradation	inhibits su9-cleavage	Permeability mito	Uncouple mito	AAC import	su9 import	Recruits Parkin	Mito morphology	IC50 in cultured cells	
Scaffold 11	LS-121	M03	26	LC	F5773-2356												
																	
	LS-121	M12	17	LC	F5791-0267	Ordered	Yes	11.1 µM		No		No	100	No	Appeared normal		
																	
	LS-119	D08	17	LC	F5659-0019												
																	
	LS-80	M03	16	LC	F3228-0168												
																	
	LS-53	F06	30	LC	F2265-1006												
																	
LS-54	I07	18	LC	F2273-0238													
																	
LS-79	I13	30	LC	F3226-1087													
																	
Miscellaneous	LS-20	B13	7	LC	F0738-0126												
																	
LS-8	H22	23	LC	F0494-0117													
																	
LS-35	C04	16	LC	F1791-2001													
																	

Table 4. Yeast strains used in this study

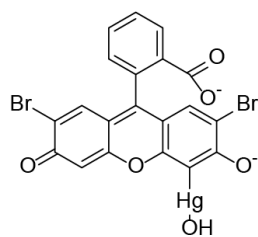
Strain	Genotype	Source
GA74-1A	<i>his3 leu2 ura3 trp1 ade8 ura 3</i>	Koehler et al, 1998
GA74 $\Delta pdr5\Delta snq2$	<i>his3 leu2 ura3 trp1 ade8 ura 3</i> <i>pdr5Δ0::HIS3 snq2Δ0::KANMX</i>	Miyata et al, 2015

Appedices – compounds repository

A Small molecules that inhibit MPP and PreP

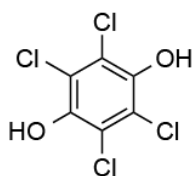
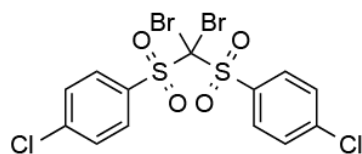
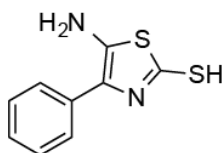


Na⁺ Na⁺

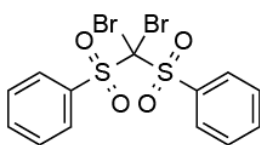
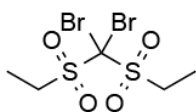
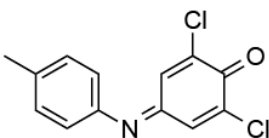
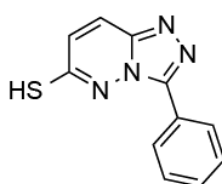
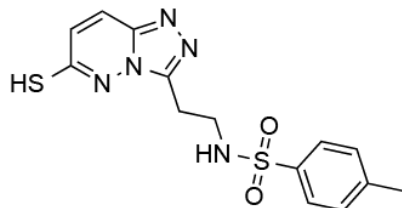


B Overlaps hits from LS library

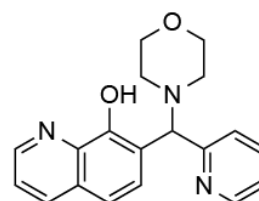
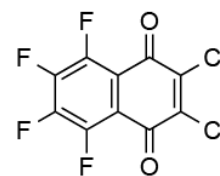
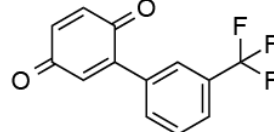
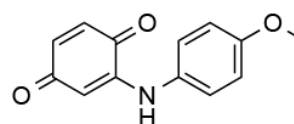
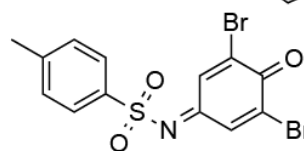
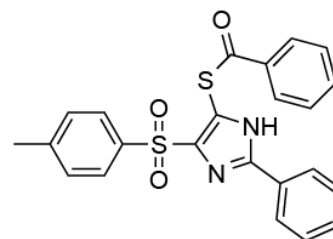
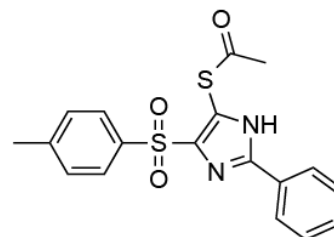
PreP and IDE



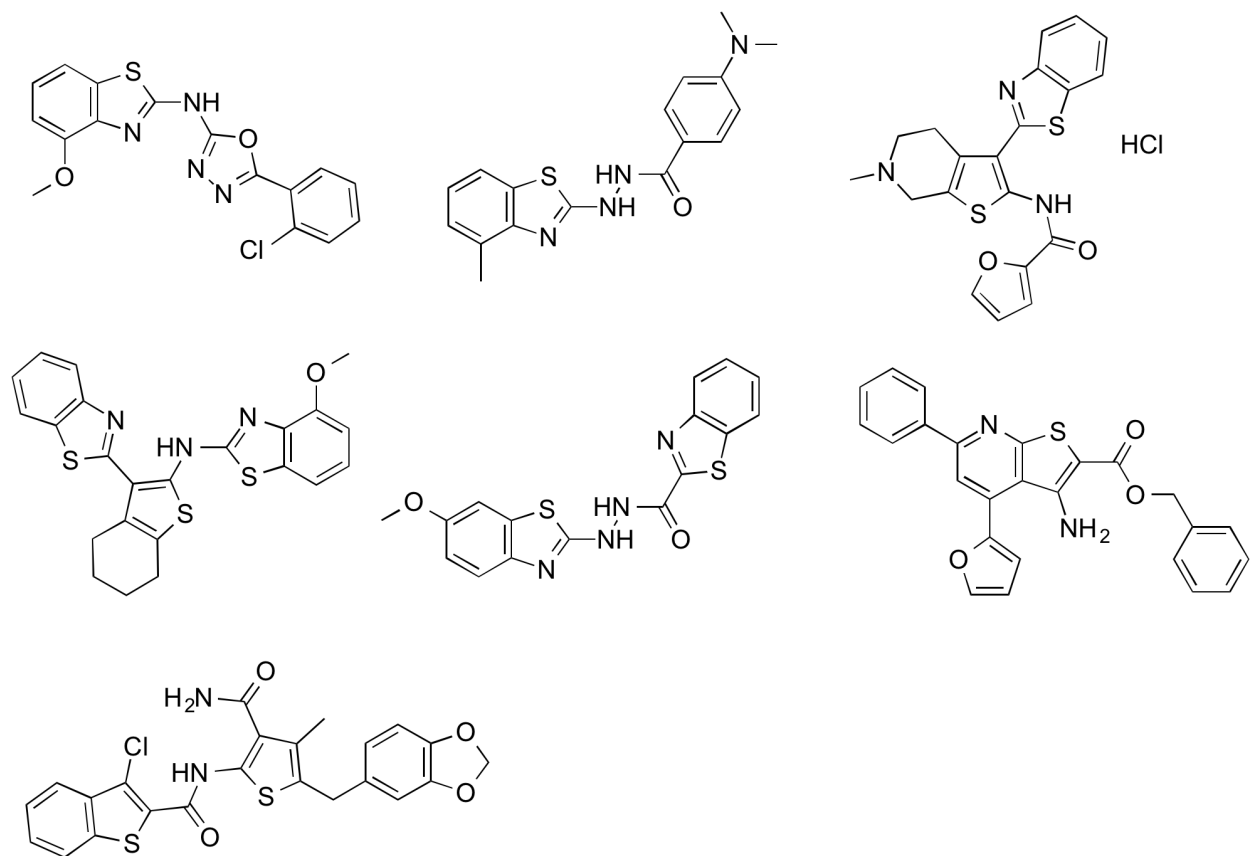
PreP, MPP and IDE



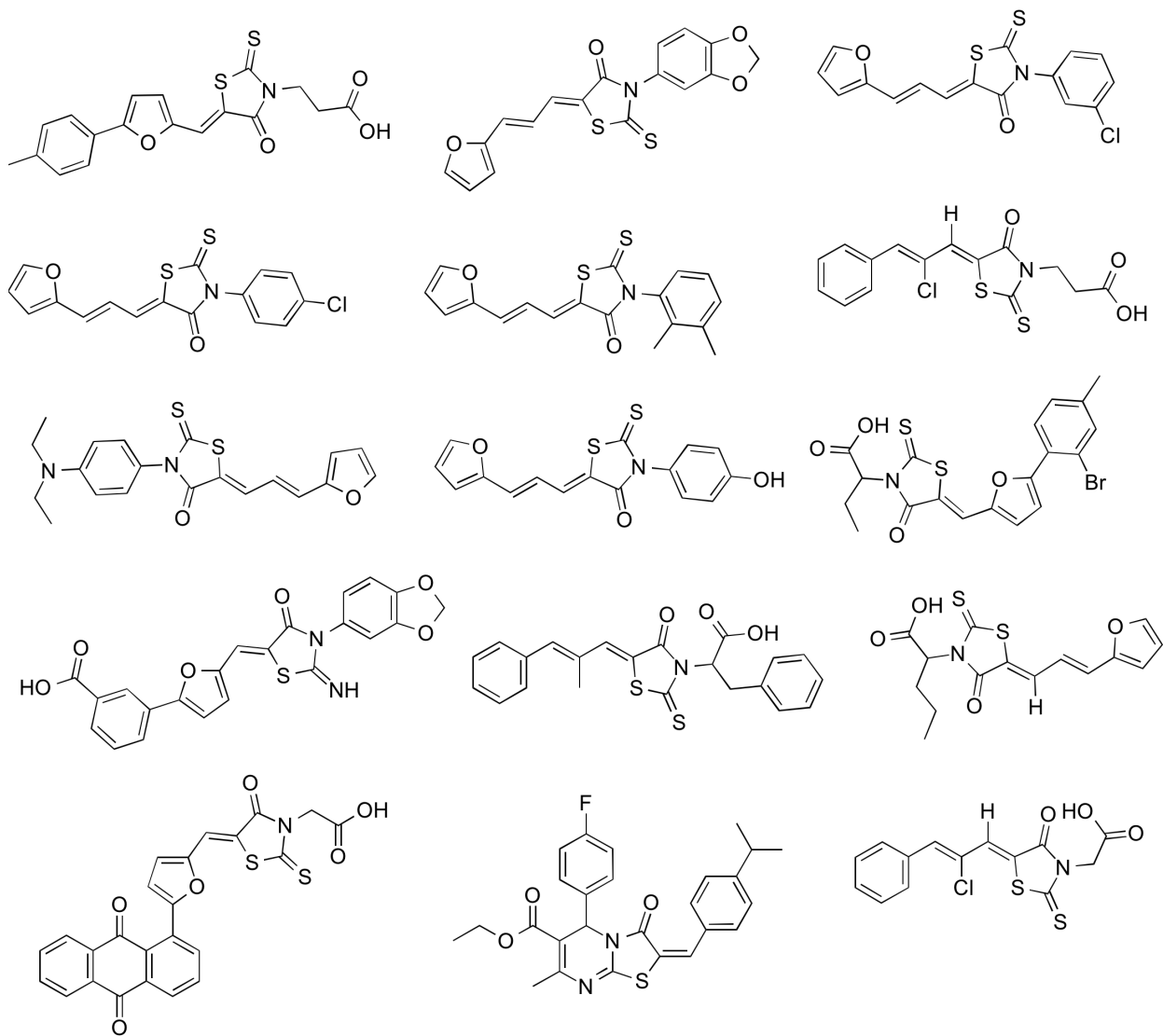
PreP and MPP



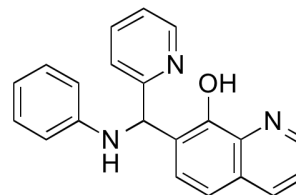
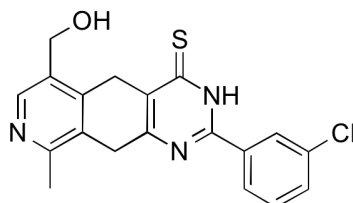
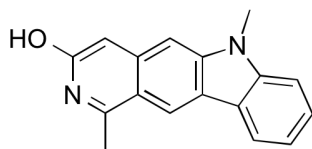
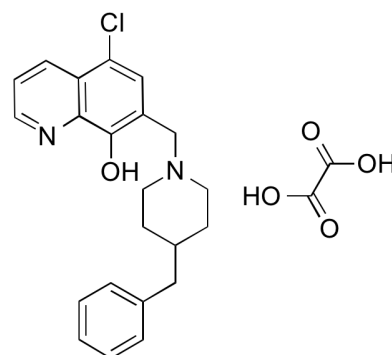
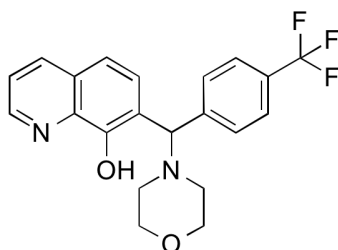
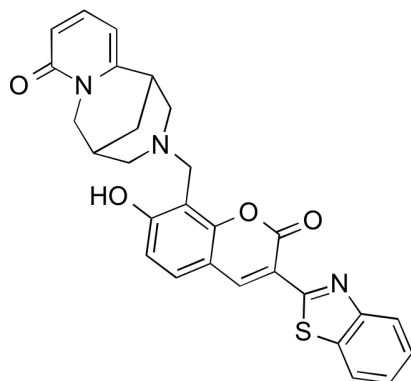
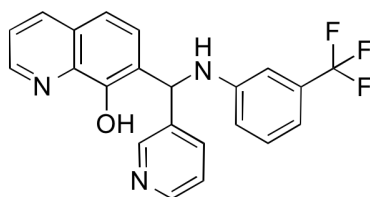
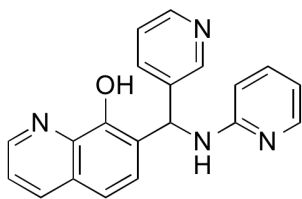
C Scaffold 1



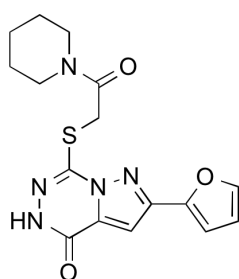
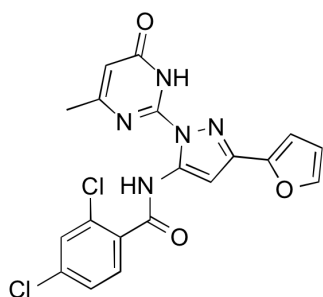
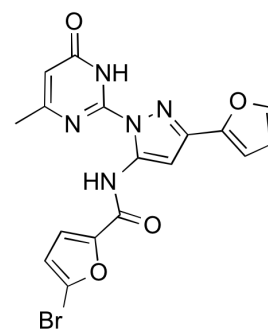
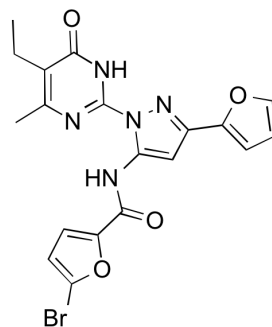
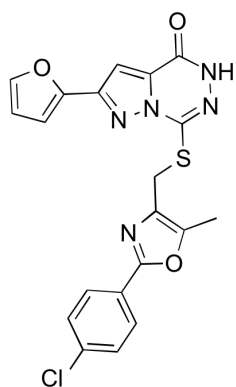
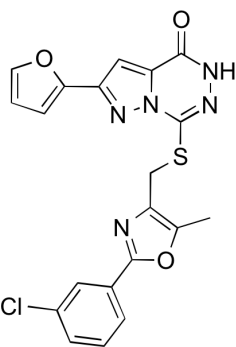
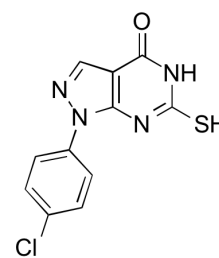
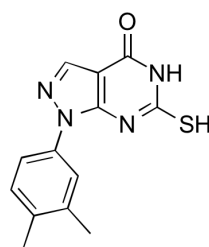
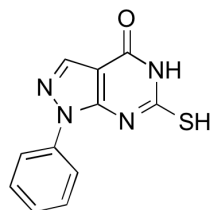
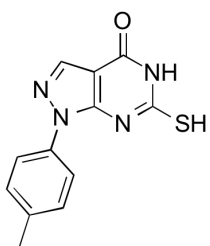
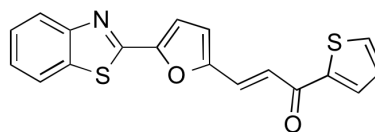
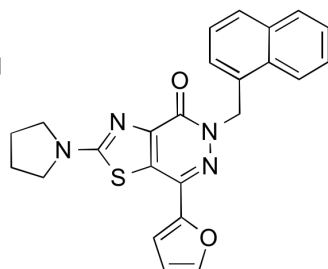
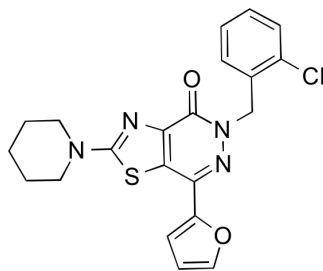
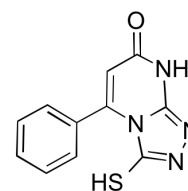
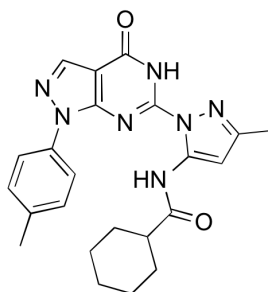
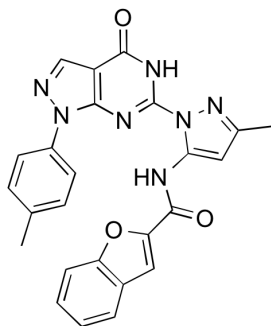
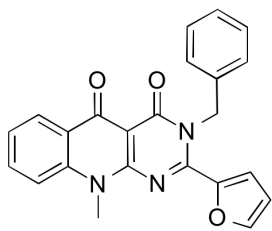
Scaffold 2



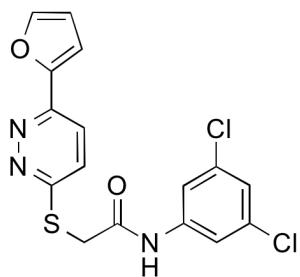
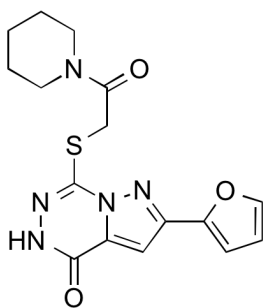
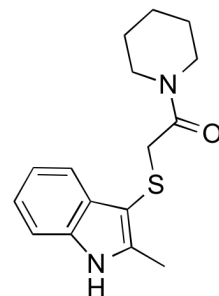
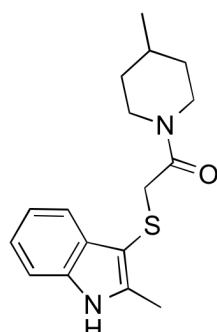
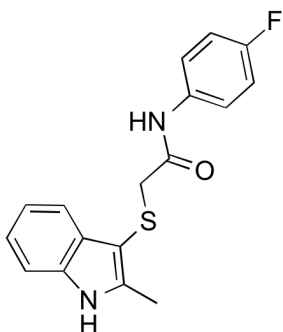
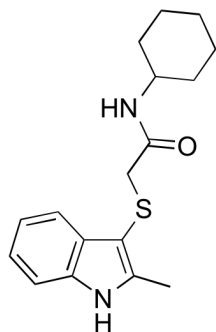
Scaffold 3



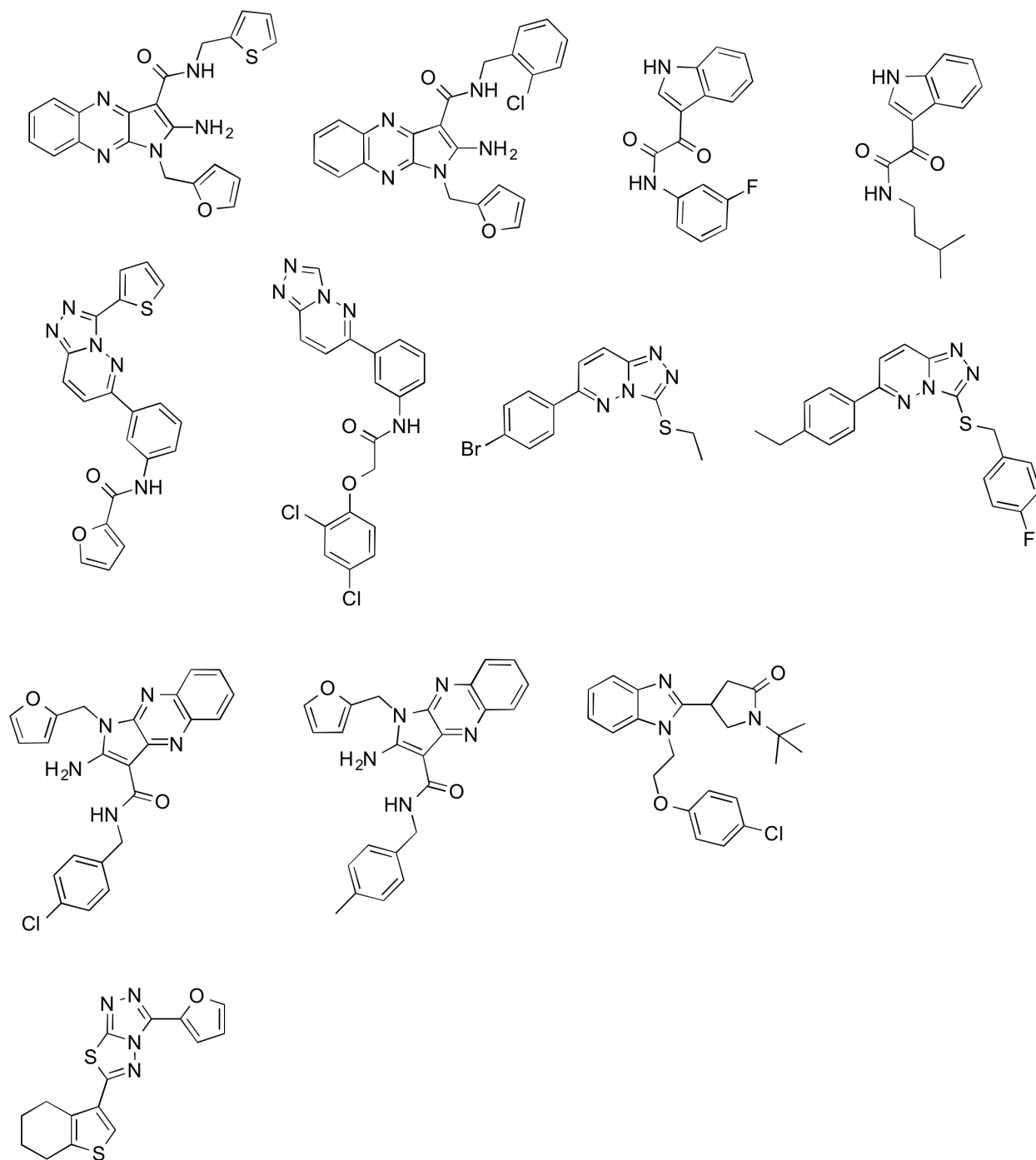
Scaffold 4



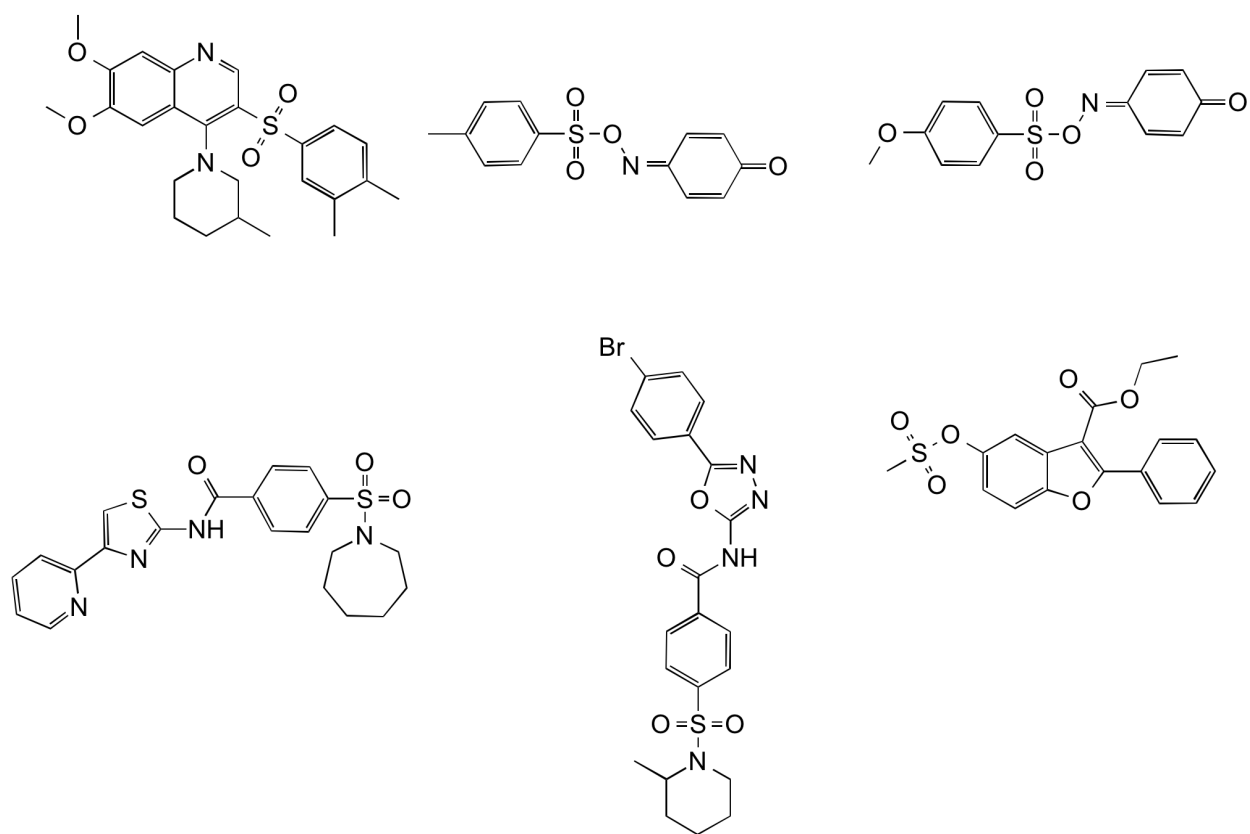
Scaffold 5



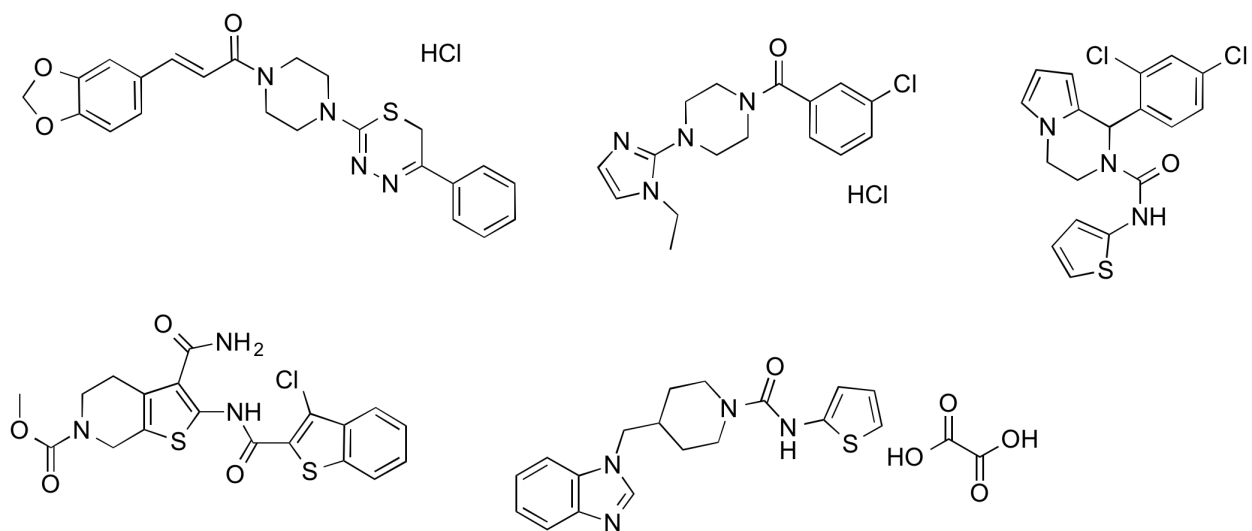
Scaffold 6



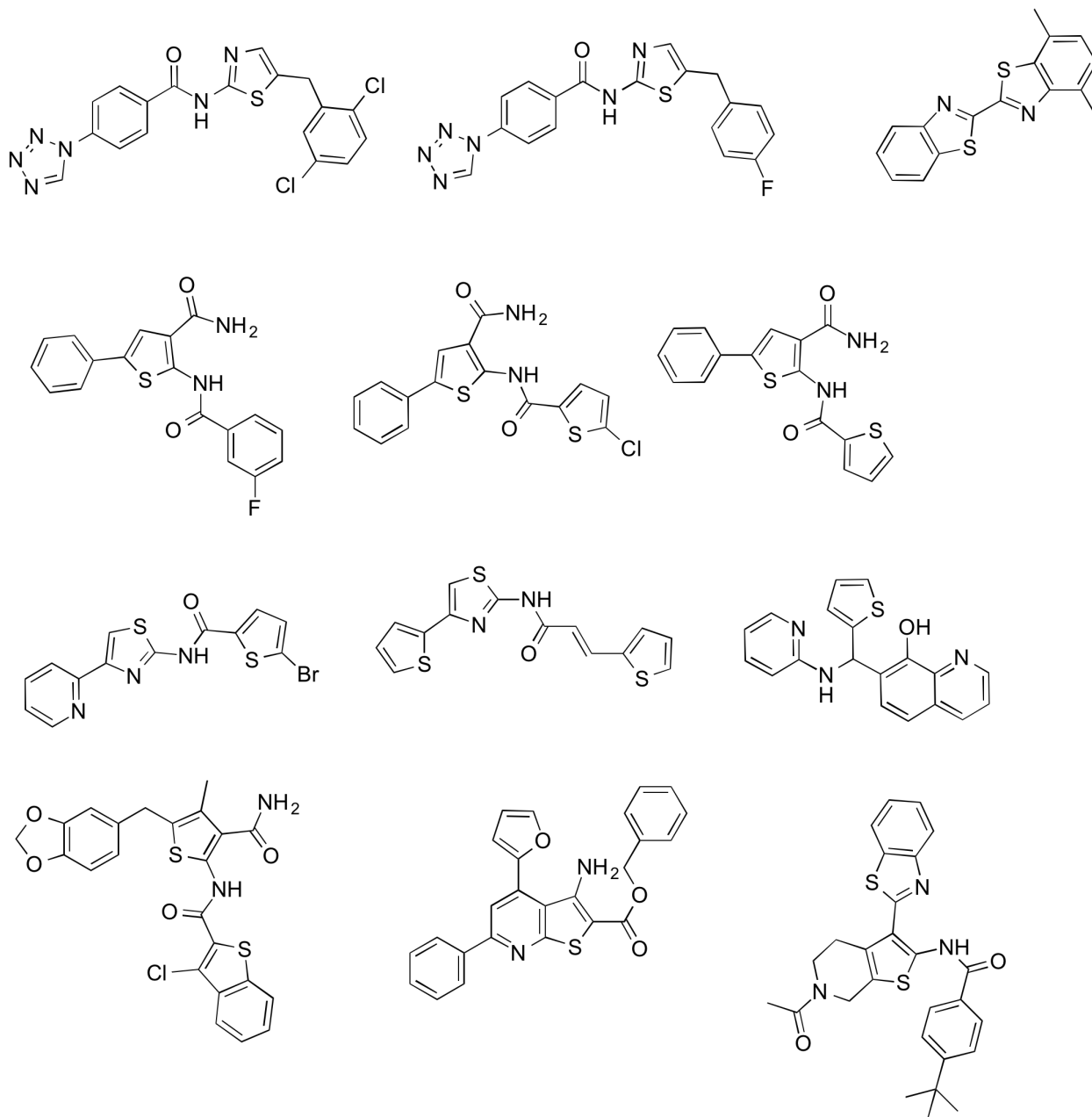
Scaffold 7



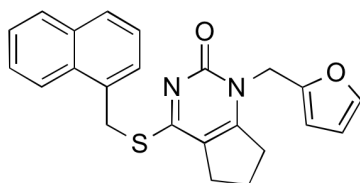
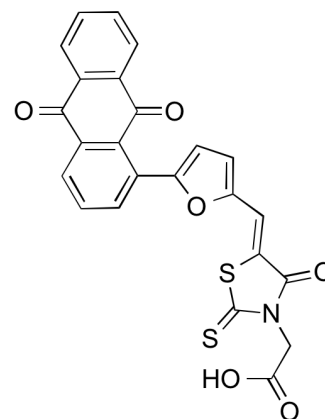
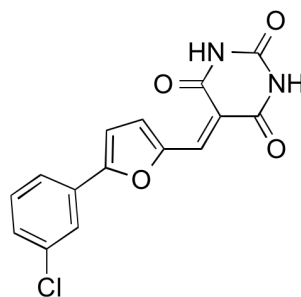
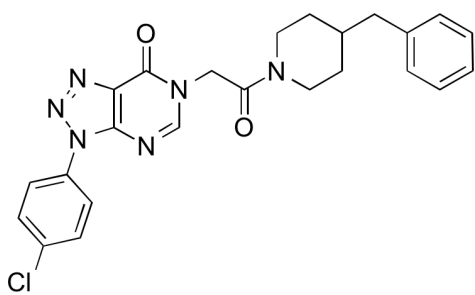
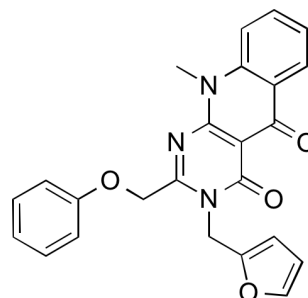
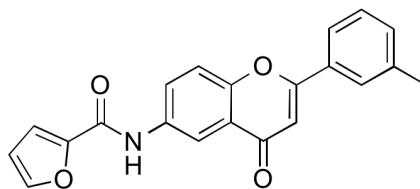
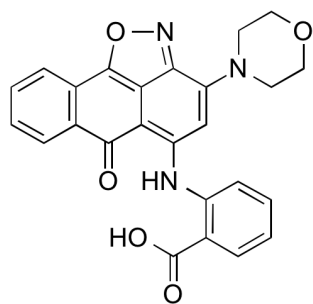
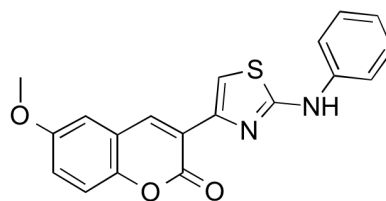
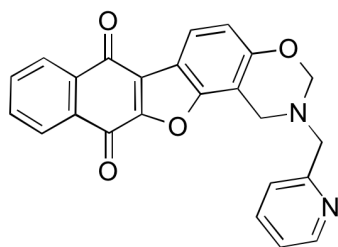
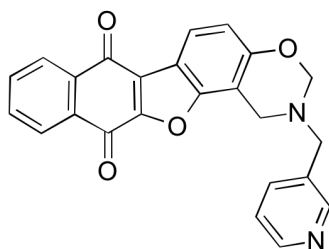
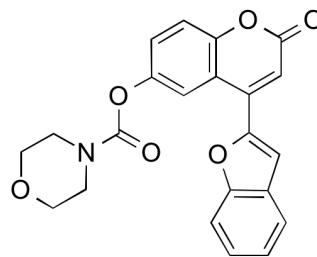
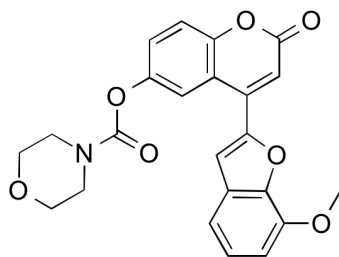
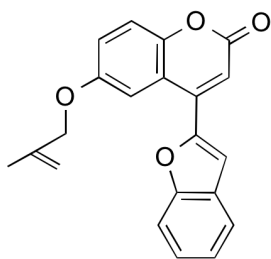
Scaffold 8



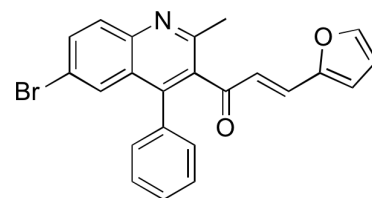
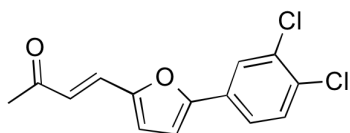
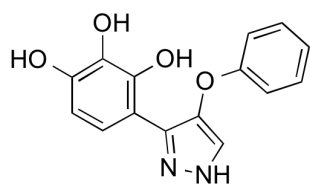
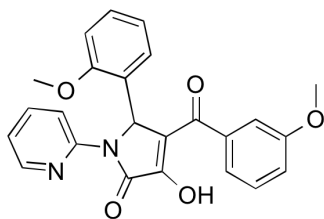
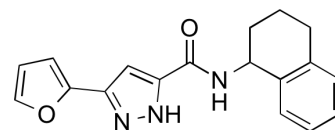
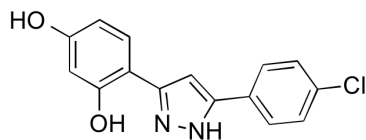
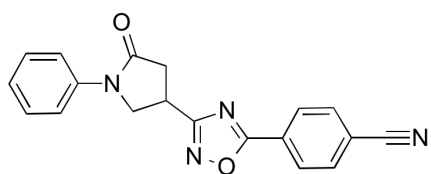
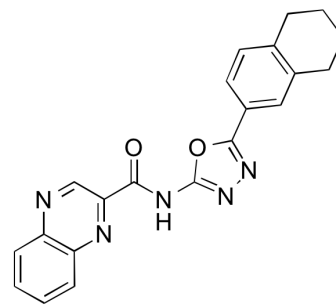
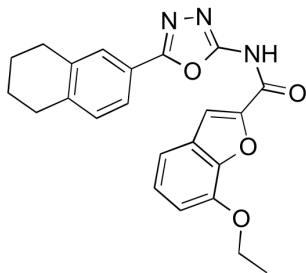
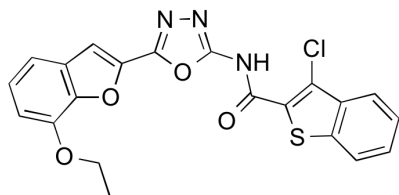
Scaffold 9



Scaffold 10



Scaffold 11



References

1. Scheibye-Knudsen, M., Fang, E. F., Croteau, D. L., Wilson, D. M. & Bohr, V. A. Protecting the mitochondrial powerhouse. *Trends Cell Biol.* (2014). doi:10.1016/j.tcb.2014.11.002
2. Neupert, W. *et al.* [17] Analysis of Mitochondrial Protein Import Pathway in *Saccharomyces cerevisiae* with Translocation Intermediates By. **8432**, 241–252 (1995).
3. Chacinska, A., Koehler, C. M., Milenkovic, D., Lithgow, T. & Pfanner, N. Importing mitochondrial proteins: machineries and mechanisms. *Cell* **138**, 628–44 (2009).
4. Neupert, W. Protein import into mitochondria. *Annu. Rev. Biochem.* **66**, 863–917 (1997).
5. Koehler, C. M. Protein translocation pathways of the mitochondrion. *FEBS Lett.* **476**, 27–31 (2000).
6. Park, K., Botelho, S. C., Hong, J., Österberg, M. & Kim, H. Dissecting stop transfer versus conservative sorting pathways for mitochondrial inner membrane proteins in vivo. *J. Biol. Chem.* **288**, 1521–32 (2013).
7. Chow, K. M. *et al.* Mammalian pitrilysin: substrate specificity and mitochondrial targeting. *Biochemistry* **48**, 2868–77 (2009).
8. Luciano, P. & Géli, V. The mitochondrial processing peptidase: function and specificity. *Experientia* **52**, 1077–82 (1996).
9. Mukhopadhyay, A., Yang, C., Wei, B. & Weiner, H. Precursor protein is readily degraded in mitochondrial matrix space if the leader is not processed by mitochondrial processing peptidase. *J. Biol. Chem.* **282**, 37266–75 (2007).
10. Teixeira, P. F. & Glaser, E. Processing peptidases in mitochondria and chloroplasts. *Biochim. Biophys. Acta* **null**, (2012).
11. Falkevall, A. *et al.* Degradation of the amyloid beta-protein by the novel mitochondrial peptidasome, PreP. *J. Biol. Chem.* **281**, 29096–104 (2006).
12. Moberg, P. *et al.* Characterization of a novel zinc metalloprotease involved in degrading targeting peptides in mitochondria and chloroplasts. *Plant J.* **36**, 616–628 (2003).
13. Mzhavia, N., Berman, Y. L., Qian, Y., Yan, L. & Devi, L. A. Cloning, expression, and characterization of human metalloprotease 1: a novel member of the pitrilysin family of metalloendoproteases. *DNA Cell Biol.* **18**, 369–80 (1999).

14. Johnson, K. a *et al.* The closed structure of presequence protease PreP forms a unique 10,000 Angstroms³ chamber for proteolysis. *EMBO J.* **25**, 1977–1986 (2006).
15. Teixeira, P. F. *et al.* In vitro oxidative inactivation of human presequence protease (hPreP). *Free Radic. Biol. Med.* **53**, 2188–95 (2012).
16. Malito, E., Hulse, R. E. & Tang, W.-J. Amyloid beta-degrading cryptidases: insulin degrading enzyme, presequence peptidase, and neprilysin. *Cell. Mol. Life Sci.* **65**, 2574–85 (2008).
17. Shen, Y., Joachimiak, A., Rosner, M. R. & Tang, W.-J. Structures of human insulin-degrading enzyme reveal a new substrate recognition mechanism. *Nature* **443**, 870–4 (2006).
18. V, C., K, V., M, R. & D, S. Purified recombinant insulin-degrading enzyme degrades amyloid β -protein but does not promote its oligomerization. (2000). at <<http://www.biochemj.org/bj/351/0509/bj3510509.htm>>
19. M, L. *et al.* Alternative translation initiation generates a novel isoform of insulin-degrading enzyme targeted to mitochondria. (2004). at <<http://www.biochemj.org/bj/383/0439/bj3830439.htm>>
20. Alikhani, N. *et al.* Decreased proteolytic activity of the mitochondrial amyloid- β degrading enzyme, PreP peptidasome, in Alzheimer's disease brain mitochondria. *J. Alzheimers. Dis.* **27**, 75–87 (2011).
21. Lustbader, J. W. *et al.* ABAD directly links Abeta to mitochondrial toxicity in Alzheimer's disease. *Science* **304**, 448–52 (2004).
22. Leuner, K. *et al.* Mitochondrion-derived reactive oxygen species lead to enhanced amyloid beta formation. *Antioxid. Redox Signal.* **16**, 1421–33 (2012).
23. Anandatheerthavarada, H. K. & Devi, L. Amyloid precursor protein and mitochondrial dysfunction in Alzheimer's disease. *Neuroscientist* **13**, 626–38 (2007).
24. Pinho, C. M. *et al.* Genetic and biochemical studies of SNPs of the mitochondrial A beta-degrading protease, hPreP. *Neurosci. Lett.* **469**, 204–8 (2010).
25. Fang, D. *et al.* Increased neuronal PreP activity reduces A β accumulation, attenuates neuroinflammation and improves mitochondrial and synaptic function in Alzheimer disease's mouse model. *Hum. Mol. Genet.* ddv241– (2015). doi:10.1093/hmg/ddv241
26. Hasson, S. A. & Inglese, J. Innovation in academic chemical screening: filling the gaps in chemical biology. *Curr. Opin. Chem. Biol.* **17**, 329–38 (2013).

27. Eggert, U. Ulrike Eggert: Big things from small molecules. *J. Cell Biol.* **194**, 352–353 (2011).
28. Calamini, B. *et al.* Small-molecule proteostasis regulators for protein conformational diseases. *Nat. Chem. Biol.* **8**, 185–196 (2011).
29. Madoux, F. *et al.* Development of a phenotypic high-content assay to identify pharmacoperone drugs for the treatment of primary hyperoxaluria type 1 by high-throughput screening. *Assay Drug Dev. Technol.* **13**, 16–24 (2015).
30. Inglese, J. Expanding the HTS paradigm. *Drug Discov. Today* **7**, S105–S106 (2002).
31. Schreiber, S. L. Small molecules: the missing link in the central dogma. *Nat. Chem. Biol.* **1**, 64–6 (2005).
32. Smith, R. A. J., Hartley, R. C. & Murphy, M. P. Mitochondria-targeted small molecule therapeutics and probes. *Antioxid. Redox Signal.* **15**, 3021–38 (2011).
33. Studier, F. W. Protein production by auto-induction in high density shaking cultures. *Protein Expr. Purif.* **41**, 207–34 (2005).
34. Zhang, J., Chung, T. & Oldenburg, K. A Simple Statistical Parameter for Use in Evaluation and Validation of High Throughput Screening Assays. *J. Biomol. Screen.* **4**, 67–73 (1999).
35. Im, H. *et al.* Structure of substrate-free human insulin-degrading enzyme (IDE) and biophysical analysis of ATP-induced conformational switch of IDE. *J. Biol. Chem.* **282**, 25453–63 (2007).
36. King, J. V *et al.* Molecular basis of substrate recognition and degradation by human presequence protease. *Structure* **22**, 996–1007 (2014).
37. Chesneau, V. & Rosner, M. R. Functional human insulin-degrading enzyme can be expressed in bacteria. *Protein Expr. Purif.* **19**, 91–8 (2000).
38. Hammen, P. K., Gorenstein, D. G. & Weiner, H. Structure of the signal sequences for two mitochondrial matrix proteins that are not proteolytically processed upon import. *Biochemistry* **33**, 8610–7 (1994).
39. Mossmann, D. *et al.* Amyloid- β Peptide Induces Mitochondrial Dysfunction by Inhibition of Preprotein Maturation. *Cell Metab.* (2014). doi:10.1016/j.cmet.2014.07.024
40. Kobayashi, H. *et al.* The mechanisms of oxidative DNA damage and apoptosis induced by norsalsolinol, an endogenous tetrahydroisoquinoline derivative associated with Parkinson's disease. *J. Neurochem.* **108**, 397–407 (2009).

41. Qiu, Q. *et al.* Synthesis of carbamide derivatives bearing tetrahydroisoquinoline moieties and biological evaluation as analgesia drugs in mice. *Arch. Pharm. (Weinheim)*. **348**, 347–52 (2015).
42. Gan, Z.-J. *et al.* Discovery, stereospecific characterization and peripheral modification of 1-(pyrrolidin-1-ylmethyl)-2-[(6-chloro-3-oxo-indan)-formyl]-1,2,3,4-tetrahydroisoquinolines as novel selective κ opioid receptor agonists. *Org. Biomol. Chem.* **13**, 5656–73 (2015).
43. Nilsson Cederholm, S., Bäckman, H. G., Pesaresi, P., Leister, D. & Glaser, E. Deletion of an organellar peptidosome PreP affects early development in *Arabidopsis thaliana*. *Plant Mol. Biol.* **71**, 497–508 (2009).
44. Town, L. *et al.* The metalloendopeptidase gene *Pitrm1* is regulated by hedgehog signaling in the developing mouse limb and is expressed in muscle progenitors. *Dev. Dyn.* **238**, 3175–84 (2009).
45. Steele, S. L., Prykhozhij, S. V & Berman, J. N. Zebrafish as a model system for mitochondrial biology and diseases. *Transl. Res.* **163**, 79–98 (2014).

Chapter 3: Small molecule modulator reveals the role of presequence-degrading protease in mitochondrial quality control pathways

Abstract

Growing evidence shows mitochondrial dysfunction plays a major role in neurodegenerative diseases. The major shortcoming in understanding the link of mitochondria to diseases is that dissecting the role of mitochondria in these diverse diseases is essentially insurmountable because very few tools are available that can rapidly modulate mitochondrial activity in biological systems such as yeast, worms, fish, mouse and cultured cells. Presequence protease (PreP) degrades mitochondrial targeting sequences, after cleavage by matrix processing peptidase (MPP), as well as other small bioactive peptides including amyloid-beta ($A\beta$) peptide. Here, we describe the discovery and characterization of MitoBloCK-60, a novel inhibitor of presequence protease (PreP). X-ray crystallography, light scattering, and mass spectrometry analyses reveal key bindings and specificity determinants of MB-60. Two MB-60 molecules bind hydrophobic pockets distal to the catalytic zinc ion and shift the equilibrium of PreP to the closed, inactive conformation. Using MB-60 as a functional probe, we showed PreP inactivation triggers mitophagy under stress. Our study revealed a previously uncharacterized involvement of PreP in mitochondrial stress and quality control pathway.

Introduction

Proper mitochondrial function contributes to cellular integrity and health. Assembly and biogenesis of mitochondria require coordinated protein import and proteolysis pathways. Aside from the 13 proteins encoded by mitochondrial DNA, over 1000 mitochondrial proteins are nuclearly-encoded and synthesized in the cytosol¹. These proteins typically carry mitochondrial-targeting sequences (MTS) at the N-terminus that are recognized by mitochondrial translocation machineries¹. During translocation, MTS are removed to ensure proper protein folding. Matrix processing peptidase (MPP) cleaves MTS on matrix-targeted proteins². Presequence protease (PreP) further degrades MTS in the matrix³. PreP is an ATP-independent, zinc-binding protease belonging to the M16 family of proteases, which includes MPP and insulin degrading enzyme (IDE)^{4,5}. These proteases degrade peptides based on size and charge distribution that allow them to enter their catalytic chambers. The degraded peptides are exported to the cytosol. Synthetic presequence has been shown to inhibit protein import to mitochondria, implicating the crucial role of PreP in ensuring mitochondrial homeostasis^{6,7}. Additionally, studies in yeast suggest PreP is necessary for survival under stress condition⁸. Studies on mitochondrial unfolded response (UPR^{mt}) also implicate the possible role of PreP in this pathway^{9,10}.

Several lines of evidence have implicated the role of PreP in Alzheimer's Disease (AD). PreP can degrade several amyloid-beta (A β) variants generated from amyloid-precursor protein (APP) processing by β and γ secretases¹¹. In addition, A β has been found in mitochondria of AD patients post mortem^{12,13}. APP and A β localization in mitochondria requires TOMM40 import channel¹⁴. In AD patients, the decline in activity of PreP has been reported and mitochondrial A β accumulation impairs respiration and increases the level of reactive oxygen species (ROS)^{15,16}.

However, APP traffics through the secretory system and typically found in the plasma membrane and extracellular matrix^{17,18}. Thus, the mechanism by which A β traffics to mitochondria requires additional support.

To characterize PreP activity *in vivo*, we conducted a small molecule screen to identify modulators of PreP. Here, we report characterization of a specific inhibitor, MitoBloCK-60. Structural studies revealed an unexpected binding mechanism wherein two molecules bind within the substrate recognition exosite of PreP. However, attempts to trap stabilized A β in mitochondria were not successful, even though several approaches were repeated as described in the literature^{16,17}. Instead, we propose that inactivation of PreP contributes to activation of mitochondrial stress pathways and induction of mitophagy via the Pink1-Parkin pathway.

Results

A chemical screen to identify inhibitors of PreP proteolytic activity

To identify small molecules that attenuate PreP, we developed an *in vitro* assay to monitor PreP proteolytic activity¹⁹. Recombinant PreP was purified and PreP activity was confirmed using an intra-molecularly quenched peptide, designed around a cleavage site of leumorphin, which mimics MTS. Proteolysis ability of PreP was monitored by increased in fluorescence of the MCA-RRQFKVVTRSQ-JPT peptide. The assay was validated for high-throughput screen (HTS) and miniaturized to 384 well format, and a chemical screen was conducted using an integrated robotic system. A total of 88,000 drug-like small molecules from diverse set of libraries were screened at 10 μ M for inhibition of PreP activity. Briefly, recombinant PreP and PreP chelated with EDTA and *o*-phenanthroline dispensed, followed by compound pinning into assay wells. DMSO vehicle was pinned into columns of wells containing PreP and chelated PreP as negative and positive controls, respectively. Incubation of the pinned compounds with PreP for 1 hr was followed by an initial fluorescence measurement. Compounds with autofluorescence were noted and eliminated. The reaction was initiated by addition of 15 μ M substrate. After 30 min, the reaction was in the linear kinetic range and a high signal-to-noise ratio was achieved. Fluorescence intensity was measured again, and reactions that were inhibited by more than 70% were picked as potential PreP inhibitors and selected for secondary analysis (**Supplementary Fig 1, Supplementary Table 1A, 1B**). In total, 233 primary candidates were identified (**Supplementary Table 2**). 250 plates were processed with a *Z'* greater than 0.6 across the screen, indicating that the screen was consistent and robust.

To eliminate false positives, two counter-screens were developed to test whether the small molecules specifically inhibited PreP. Similar fluorescent screens were established for additional M16 metalloproteases, insulin degrading enzyme (IDE) and the mitochondrial processing peptidase (MPP). Small molecules that selectively inhibited PreP were considered for additional characterization (~226 compounds) and designated as *mitochondrial protein import blockers* from the Carla Koehler lab (MitoBloCK) compounds based on their potential to inhibit PreP activity. Of the potential “lead” inhibitors, 12 were initially characterized and MitoBloCK-60 (MB-60) was chosen for additional analysis (**Fig. 1a**).

MB-60 inhibits PreP activity in vitro

MB-60 is 1-(diphenylmethyl)-4-(3-methyl-4-nitrobenzoyl)piperazine from the Chembridge library (**Fig. 1a**). Upon reordering, MB-60 showed the same PreP inhibitory activity as the original aliquot from the pinned library. The inhibitory concentration at which PreP degradation activity was reduced by 50% (IC₅₀) for MB-60 in the cleavage assay with the leumorphin substrate was 0.49 μM (**Fig. 1b**). A similar test was conducted with an intramolecularly quenched Aβ(1-42) peptide and the IC₅₀ was 0.21 μM (**Fig. 1c**). To identify specific properties of MB-60 that inhibit PreP activity, we purchased two small molecules with similar structures, designated MB-60.1 and Analog 2 (**Fig. 1a**). We tested these compounds in the in vitro activity assay with the leumorphin peptide (**Fig. 1d,e**). The IC₅₀ of MB-60.1 and Analog 2 with the peptide were 2.25 μM and 12.7 μM, respectively. The chemical library was also mined to identify additional compounds that shared a similar structure (**Supplementary Fig. 2**). Numerous piperazine compounds were identified, some with very similar structures, but

none of these inhibited PreP activity. Thus, the properties of MB-60 suggest that it may be a unique inhibitor of PreP.

To confirm that MB-60 inhibited PreP activity, we tested MB-60 in two additional formats. A construct in which the mitochondrial targeting sequence (MTS, residues 1-69) of *N. crassa* subunit 9 of the ATPase was fused to DHFR (Su9-DHFR) was used as a model substrate and a radiolabeled fusion protein was synthesized in an in vitro transcription-translation reaction²⁰. Su9-DHFR contains two MPP cleavage sites at 35 and 66; the construct is cleaved efficiently by recombinant MPP and generates an MTS that can be detected in a Tris-Tricine gel system (**Fig. 2a**). The addition of recombinant PreP subsequently degraded the cleaved MTS, establishing this as an assay to gauge PreP activity. In the presence of DMSO, PreP degraded the MTS, but the addition of MB-60 inhibited PreP activity and the MTS was stable (**Fig. 2a**). We also tested the inhibitory activity of the two purchased SAR compounds, MB-60.1 and Analog 2. However, the MTS was not readily detected on the gel, indicating that these compounds did not effectively inhibit PreP activity (**Fig. 2b**). In a second assay, we also tested PreP activity in the cleavage of fluorescent-labeled A β 1-42 peptide¹¹(**Fig. 2c**). In the presence of the vehicle (1% DMSO), PreP cleaved A β ; whereas, the addition of chelators (chel.) EDTA and *o*-phenathroline inhibited PreP proteolytic activity. Varying concentrations of MB-60 also effectively inhibited PreP activity. As a control for A β degradation, trypsin was included. Using a different gel system, the cleaved form of A β was detected and confirmed that MB-60 effectively blocked PreP activity (**Fig. 2d**). In sum, MB-60 seems to be a specific inhibitor of PreP activity, but analogs with similar structures were not effective inhibitors.

Two MB-60 molecules together bind a hydrophobic exosite of PreP

To understand the mechanism of inhibition of MB-60, we co-crystallized MB-60 with human PreP. The structure of MB-60-bound PreP at 2.3 Å resolution reveals an unexpected binding mechanism of MB-60 (**Fig. 3a**). In the presence of MB-60, PreP exists in a closed conformation that is nearly identical to structures of substrate-free and A β -bound PreP (RMSD=0.15 Å and 0.31 Å, respectively)⁵. The N- and C-terminal domains of PreP (PreP-N and PreP-C, respectively) come together to form an enclosed catalytic chamber (**Fig. 3a**). Within the catalytic chamber, two MB-60 molecules wrap around each other to make intimate interactions to bury 313 Å² and bind the hydrophobic pockets of PreP-N that is 20-30 Å away from the catalytic zinc ion (**Fig. 3a, 3b**). Two MB-60 molecules, MB-60-a (cyan) and MB-60-b (green), bind distinct pockets of PreP via various contacts. The contacts bury 808 Å² and 658 Å² surface between MB-60 and the catalytic chamber of PreP (**Fig. 3c, 3d**). For MB-60-a, two phenyl groups bind a hydrophobic pocket with close contacts with L60, F344, I432, M446, L447, and L467. The carbonyl group of MB-60-a forms hydrogen bonds with waters coordinated by the carbonyl group of M446 and hydroxyl group of Y383. The piperazine group of MB-60-a forms hydrogen bond with water coordinated with the side chain of Q435. The nitro group of MB-60-a forms a hydrogen bond with the main chain of G382 and a cation- π interaction with Y383. For MB-60-b, two phenyl groups interact with the hydrophobic pocket formed by I337, A343, F344, I451, and L464 while the nitro group of MB-60-b forms a salt bridge with K431. MB-60 occupies the exosite required for A β -PreP interaction, revealed by A β -bound PreP structure⁵. This explains how MB-60 prevents degradation of A β , by blocking the vital binding site A β to PreP

The MB-60-bound PreP structure provides the structural basis as to why the other analogs of MB-60 are not effective inhibitors. The close interactions of PreP with both phenyl groups of MB-60 show that the loss of one or both phenyl group(s) should profoundly affect the affinity of MitoBloCK-60.1 and other analogs to PreP (**Fig. 1a, 3b, 3c, Supplementary Fig. 2**). Similarly, as the nitro groups of both MB-60 play critical roles in binding within the catalytic chamber of PreP, the relocation of nitro group within the tolyl group of MB-60 (analog 2) (**Fig. 1a**) and the loss this nitro group (**Supplementary Fig. 2**) would reduce their affinity to PreP.

MB-60 allosterically induced PreP to the closed conformation to prevent substrate binding.

Peptide substrates cannot enter the catalytic chamber of PreP in its closed state and the transition between the open and closed conformation is required for the catalysis by PreP⁵. Using small angle X-ray scattering (SAXS) analysis, we have shown that ~20% of PreP exists in the open state while A β induces PreP to mostly closed conformation⁵. Thus, in addition to binding to the hydrophobic exosite and competing with the binding of substrates, MB-60 might also limit access for substrate binding in the catalytic chamber by inducing PreP to transition from an open to a close confirmation. To test this hypothesis, we performed the SAXS analysis of PreP in the absence and presence of MB-60 (**Fig. 3e, Supplementary Fig. 4**) The simulation of the scattering curve reveals that the degree of dip at q range from 0.1 \AA^{-1} to 0.15 \AA^{-1} is the key difference between the open and closed conformation of PreP (**Fig. 3e**). Indeed, MB-60 noticeably enhanced the degree of dip in the SAXS profile at this q range, suggesting that MB-60 shifts the equilibrium of PreP to the closed conformation in solution (**Fig 3e**). Consistent with this notion, we found that the presence of MB-60 reduced the Rg value and the percentage of PreP open state from 26% to 14% (**Supplementary Fig. 4**).

We further used deuterium exchange mass spectrometry (DXMS) to probe the molecular basis of the MB-60-induced conformational switch.

To do so, we obtained amide hydrogen/deuterium (H/D) exchange profiles of PreP alone and PreP in presence of MB-60 (**Supplementary Fig. 5**) and examined the differences between these two profiles (**Supplementary Fig. 6**). We found that most of the amide H/D exchanges were unchanged (**Fig. 4a**). Of a few regions that have noticeable reduction in H/D exchange, the peptides around MB-60 binding pockets are most prevalent, which include residues 349-364, 371-388, and 415-478 (**Fig. 4**). This supports the notion that MB-60 in solution binds the hydrophobic pockets revealed by our MB-60-bound PreP structure. We also found regions at the interface between PreP-N and PreP-C with reduced H/D exchange such as residues 201-213 from PreP-N and residues 703-720 from PreP-C (**Fig. 4**). Two additional regions at PreP-C that have significant reduced H/D exchange are residues 890-918 and residues 929-940, which are also nearby the interface between PreP-N and PreP-C. Our H/D exchange data suggest that the binding of MB-60 also enhances the interaction between PreP-N and PreP-C. Together with our SAXS study, our data strongly support the notion that MB-60 allosterically induces PreP into the closed conformation. Our co-crystal structure shows that MB-60 only binds PreP-N and should not bridge PreP-N and PreP-C together physically. Such allostery is likely mediated by the change in protein dynamics of the linker joining PreP-N and PreP-C, which is postulated to control the rigid body motion of PreP-N and PreP-C for the open-closed transition of PreP (**Fig. 3a**)⁵. Consistent with this hypothesis, we also observed reduced H/D exchange in residues 503-522, which is a part of the PreP linker region (**Fig. 4**).

MB-60 is not toxic to mitochondria or cells

Once the mechanism of PreP inhibition by MB-60 was understood, we utilized MB-60 to probe for functions of PreP in mitochondria and in cultured cells. Small molecules may have off-target effects in cells. Previously we have found that small molecules can dissipate the membrane potential ($\Delta\Psi$) and permeabilize membranes²¹⁻²³, making them unsuitable for in vivo studies. We therefore tested MB-60 in established assays (**Supplementary Fig. 7**). Isolated mitochondria were incubated in a 0.5-ml chamber of an oxygen electrode at 25°C, and respiration was initiated with NADH. The measured oxygen consumption rate was indicative of well-coupled mitochondria and the addition of MB-60 did not alter the oxygen consumption rate (**Supplementary Fig. 7a**). Only the addition of the protonophore CCCP resulted in a drastic increase in respiration, confirming uncoupling of mitochondria. The $\Delta\Psi$ of isolated mitochondria was also measured with a potentiometric dye, 3,3' - dipropylthiadicarbocyanine iodide (DISC3[5]), which is taken up by mitochondria and then released when the $\Delta\Psi$ is dissipated. The relative change of fluorescence between dye uptake and release is a relative measure of the $\Delta\Psi$; the dye that loads into coupled mitochondria (causing quenching and a decrease in fluorescence) is released when treated with the uncoupler CCCP. The fluorescence was not changed in the presence of either DMSO or 100 μ M MB-60 (**Supplementary Fig. 7b**).

To test the integrity of the mitochondrial membranes in the presence of MB-60, yeast mitochondria were incubated with MB-60 for 30 min at 25°C followed by centrifugation to pellet mitochondria. Released mitochondrial proteins were recovered in the supernatant fraction and analyzed by immunoblot analysis for key proteins and coomassie staining for the collective release of proteins (**Supplementary Fig. 7c,d**). Immunoblot analysis indicated that Mop112, Mia40, and AAC were not released from mitochondria in the presence of MB-60. Gel staining

indicated that a large pool of mitochondrial proteins was not released. Thus, treatment with MB-60 does not impair mitochondrial respiration or mitochondrial membrane integrity.

We examined whether MB-60 impaired protein import into isolated mitochondria from HeLa cells. MB-60 and vehicle (1% DMSO) were pre-incubated with mitochondria. Radiolabeled Su9-DHFR was then imported into mitochondria and aliquots were removed over time; the non-imported precursor was removed by trypsin treatment. The rate of import was identical in the presence of DMSO or 100 μ M DMSO (**Supplementary Fig. 8a**). MB-60 titrated over a concentration range of 10 to 100 μ M did not impair import of Su9-DHFR (**Supplementary Fig. 8b**). In addition, MB-60 did not impair the import of Hsp60, tom40, , and AAC, matrix, outer membrane, inner membrane space, and inner membrane resident proteins, into mitochondria (**Supplementary Fig. 8c**)

In addition, import of matrix-targeted protein was visualized in vivo using fluorescence microscopy (**Supplementary Fig. 9a**). Cells were transiently transfected with a construct that contained a fusion between Cox7 MTS and EGFP (MTS-EGFP). In the presence of 40 μ M MB-60 after 24 hr, MTS-EGFP was imported into mitochondria and the mitochondrial network looked similar to cells treated with DMSO. In contrast, cells incubated with 20 μ M CCCP had MTS-EGFP distributed in the cytosol and the mitochondrial network was collapsed. Moreover, the membrane potential was not perturbed when cells were treated with MB-60, because staining with MitoTracker was robust (**Supplementary Fig. 9b**). Again, CCCP-treated cells were negative for MitoTracker staining, confirming that the membrane potential was dissipated. Viability of cells was measured using a commercial MTT toxicology assay (**Supplementary Fig. 9c**); viability was not impaired, even at a concentration of 200 μ M MB-60. In summary, MB-60 seems to inhibit PreP activity in vitro, but MB-60 addition to mitochondria and cells did

not markedly abrogate mitochondrial function. The normal phenotype in cells treated with MB-60 aligns with studies in yeast in that the homolog *CYMI* can be deleted without compromising growth or mitochondrial functions²¹.

A β does not enter mitochondria in biochemical models

Numerous studies have cited a role for PreP in the degradation of A β and Alzheimer's disease. Specifically, a series of publications show that A β is imported into mitochondria^{12,24,25}. We repeated in vitro and in vivo import assays in which A β was added directly to mitochondria and cells or mutant APP was expressed in cultured cells^{12,25}, but we could not reproduce previously published results (**Fig. 5a**), including in vitro import assays. Specifically, when A β was added directly to cells, the peptide was taken into cells, but did not co-localize with mitochondria as previously published²⁵. Even the addition of MB-60 did not stabilize a potential Ab cohort in mitochondria. Whereas A β may localize to mitochondria in brains from Alzheimer's patients^{11,15,24}, our studies in model systems did not recapitulate this scenario and precluded us from effectively testing whether MB-60 addition to cells might stabilize A β .

PreP is redox regulated and functions in a mitochondrial stress pathway

Molecular modeling of human PreP based on the crystal structure at 2.1 Å resolution of Arabidopsis PreP showed that cysteine residues at position 90 and 527 can form a disulfide bond and mutagenesis studies suggested that human PreP might be redox regulated⁷. We therefore measured the midpoint potential (E_m) of PreP over a range of redox potentials by using monobromobimane (mBBBr) titration^{24,25}. Recombinant PreP was equilibrated in DTT/DTT_{ox} redox buffers to poise samples at redox potential (E_h) values ranging from -240 to -310 mV or in

GSH/GSSG redox buffers to poise samples at E_h values ranging from -230 to -80 mV and then incubated with mBBr to form a thiol-specific fluorescent covalent adduct. The titration results were independent of the equilibrium time and the anaerobic/aerobic state, indicating the likelihood of good redox equilibration between PreP and the ambient potential imposed by the redox buffers. The titration results were fit to a curve for a two-electron couple calculated from the Nernst equation. The E_m was calculated at -270 mV (**Fig. 5b**). We also tested the proteolytic activity of PreP at the different redox potentials using the leumorphin peptide. Activity versus E_h was plotted; PreP activity is close to the mBBr-calculated E_m , with a midpoint of -210 mV (**Fig 5c**). Given that the mitochondrial matrix has a redox potential of approximately -300 mV²⁶, PreP is predicted to normally be active, but oxidizing conditions could favor the formation of a disulfide bond and reversible inactivation of PreP. Previous studies have also shown PreP is inactive in the presence of oxidizing agents such as hydrogen peroxide and diamide^{26,27}. Thus, PreP activity may be modulated by mitochondrial stress.

PreP inactivation induces a mitochondrial stress pathway, resulting in Pink1 recruitment

Because PreP is redox regulated and is required for growth in yeast under stress⁸, we explored whether inhibition of PreP activity by MB-60 might induce a mitochondrial stress pathway²⁸. We focused on Pink1/Parkin activation because this mitochondrial stress pathway is typically activated in mammalian cells to induce mitophagy, and misfolded proteins activate Pink1 stabilization on the mitochondrial outer membrane and subsequent Parkin recruitment²⁸. Addition of MB-60 did not perturb the mitochondrial network, protein import, or the mitochondrial membrane potential (**Supplementary Fig. 9**).

Because inactivation of PreP and MPP in yeast impaired preprotein maturation and subsequently induced mitochondrial stress²⁴, we tested whether inhibition of PreP might be synergistic with a second mitochondrial stress inducer in mammalian cells; we incubated cells with CCCP (at 2.5 and 5 μ M) for 3 hrs and found that both concentrations do not abrogate the membrane potential and only result in minimal Parkin recruitment in a HeLa cell model with stable expression of EGFP-Parkin (**Fig. 6a, Supplementary Fig. 10,11**). MB-60 (10, 40, and 100 μ M) was added to cells for 3 hours followed by the addition of 5 μ M CCCP for 3 hours. Mitochondria were subsequently isolated and the status of mitophagy markers was investigated by immunoblot analysis (**Fig. 6b**). Pink1 accumulated in the presence of 10 μ M MB-60 (Fig. 6b, lane 6) but was not detected in the presence of 40 and 100 μ M MB-60 (Fig 6b, lane 7,8) because mitochondria were being degraded via mitophagy. Ubiquitinated Parkin was recruited to mitochondria and MFN1 and TOMM20, sensitive markers for degradation via mitophagy, were degraded in the presence of MB-60 and CCCP (Fig. 6b, lanes 5-8). Finally, the autophagy pathway was also induced because the LC3 pool that was recruited to mitochondria shifted to the lipidated form (LC3-II) (Fig. 6b, lanes 5-7), which was subsequently degraded in the presence of 100 μ M MB-60 (Fig. 6b, lane 8). As controls, DMSO addition did not induce mitophagy and mitochondrial turnover (Fig. 6b, lane 1), but 1 μ M valinomycin induced mitophagy, whereas the addition of proteasome inhibitor MG132 inhibited protein turnover of outer membrane proteins and stabilized a form of Pink1 that was cleaved by MPP and PARL^{28,29}. MB-60 accelerates Pink1 stabilization and Parkin recruitment to mitochondria during stress (**Fig. 6c**). PreP inhibition by MB-60 also stabilized Pink1 in HeLa cells, which lack Parkin (**Supplementary Fig. 12a**)

To confirm that Pink1 arrested on the outer membrane, the required location to recruit Parkin and activate mitophagy, we treated isolated mitochondria with increasing concentrations of Proteinase K. (**Fig. 6d**). In the presence of 1 $\mu\text{g/ml}$ Proteinase K, Pink1 was not degraded; however, 10 $\mu\text{g/ml}$ protease subsequently degraded Pink1, similar to outer membrane protein MFN1, whereas inner membrane and matrix protein, YME1L and mortalin, were not degraded by Proteinase K. Thus, inactivation of PreP with MB-60 induces a specific mitochondrial stress pathway that involved Pink1/Parkin activation.

To validate the role of PreP in the mitochondrial stress pathway, we complemented the chemical biology approach and confirmed our findings using genetic perturbations. Knockdown of PreP with RNAi does not alter mitochondrial morphology, which correlates with the small molecule result (**Supplementary Fig.13a**). Moreover, RNAi sensitizes the cells to stress and MB-60 as the level of PINK1 increased in RNAi-treated cells compared to wild-type cells (**Supplementary Fig.13b**). We also generated PreP knockout cells using CRISPR technology. PreP $-/-$ cells are sensitive to stress, as indicated by Pink1 accumulation in PreP knockout compared to wildtype cells. (**Supplementary Fig. 13c**). Moreover, overexpression of PreP in PreP $-/-$ cells rescues cell sensitivity to stress as shown by decreased in Pink1 level (**Supplementary Fig. 13d**) (compare lane 2 and 6). We also observed that in the absence of PreP, MB-60 does not induce Pink1 recruitment, further confirming that PreP is indeed the target of MB-60 (lane 3). Together, our genetic approach complemented our small molecule findings in where PreP plays a role in activating a mitochondrial stress response under stress, specifically by stabilizing Pink1 in mitochondria.

Discussion

Perturbations in mitochondrial homeostasis have been linked to diseases, specifically neurodegenerative disease. The mitochondrion is equipped with proteases that together serve as a quality control system to maintain homeostasis. The major shortcoming in understanding the link of mitochondria to diseases is that very few tools are available that can rapidly modulate mitochondrial activity in biological systems such as yeast, worms, fish, mouse and cultured cells. In this study, we described the characterization of MitoBloCK-60, a novel small molecule inhibitor of PreP. Our chemical biology approach provided us with a tool to probe mitochondrial proteolysis pathways rapidly and selectively, allowing for mechanistic and phenotypic questions about PreP to be answered. We described a unique binding mechanism in which two small molecules bind within the catalytic chamber of the protease. Our observations suggest that PreP is redox-regulated and while PreP inactivation does not impair general mitochondrial functions such as respiration and protein import, compromised PreP catalytic activity in the presence of stress is sufficient to trigger a mitochondrial stress response, specifically mitophagy via the PINK1-Parkin dependent pathway.

Our effort to understand the mechanism of action of MitoBloCK-60 by x-ray crystallography led to an unexpected discovery in which we observed two molecules of MB-60 wrap around each other within the substrate recognition pocket of PreP. To our knowledge, this is the first report of such distinct binding between a small molecule and a target protein. Binding of MB-60 within hydrophobic exosite is particularly unique as this exosite is weakly conserved, suggesting a very specific binding³⁰. The interactions observed in the crystal structure of MB-60 bound PreP also explained why some of the analogs we pursued were not as effective at

inhibiting PreP activity. The phenyl, nitro, and carboxy groups of MB-60 form critical interactions with the protease. Additionally, our data explained how MB-60 renders PreP inactive – by shifting the equilibrium of PreP in solution to mostly closed confirmation, where substrate accessibility to catalytic chamber is limited. Finally, our structural analyses will provide basis from which improvement on the compounds can be achieved. Compounds may then be synthesized to have improved solubility, absorption, distribution, metabolism, excretion, and toxicity (ADMET) characteristics.

Our study demonstrated that PreP is redox-regulated. Under normal condition of matrix reducing environment, PreP is active and able to degrade its substrates. However, under oxidizing condition, PreP activity is compromised. We postulate that under mitochondrial stress such as the presence of misfolded proteins or high ROS level, inactivation of PreP triggers downstream pathway to maintain mitochondrial homeostasis. Specifically, we found inactivating PreP using MB-60 accelerates PINK1 stabilization in the mitochondrial outer membrane, which results in Parkin recruitment to mitochondria and ultimately, in selective removal of damaged mitochondria (**Supplementary Figure 14**). The crucial role of PreP in mitochondrial quality control pathway is corroborated by studies in yeast where knockout of PreP homolog CYM1/mop112p results in growth defect in non-fermentable carbon source under stress⁸. Furthermore, results obtained through the chemical biology approach have been confirmed and complemented by genetic approach. PreP knockdown sensitizes cells to MB-60 and stress, further confirming that PreP is indeed the target of MB-60. Complete ablation of PreP results in higher basal level of PINK1 in cells and increased sensitivity of cells to stress as shown by rapid stabilization and increased in Pink1 level. The role of PreP in inducing mitophagy under stress

was further confirmed when overexpression of PreP in PreP $-/-$ cells reduces cell's sensitivity to stress.

The identification and characterization of MB-60 is timely as there is a growing evidence implicating PreP in AD^{11,15}. MB-60 is a validated probe with the potential to provide insight between the link of PreP, mitochondria and AD, providing A β can be found in mitochondria. Many secretory proteins contain within them two targeting motifs, for ER and mitochondria. Alternative targeting of secretory proteins to mitochondria have been observed when ER import is compromised³¹. APP in particular, is alternatively translocated to mitochondria where ER import is blocked. As such, this could be one way in which APP or A β is found in mitochondria³¹.

Accumulation of A β in mitochondria has been shown to increase ROS production and reduce electron transport chain activity^{16,25}. Reduced PreP activity, has been observed in AD patients even though the protein level remains the same compared to healthy controls¹⁵. Overexpression of A β in yeast is shown to negatively affect PreP activity leading to accumulation of mitochondrial targeting peptides, which then increases ROS level in mitochondria²⁴. It is interesting to note that MB-60 and A β occupy the same binding pocket within PreP. Thus inhibition of PreP activity by MB-60 could be beneficial dually; in one instance it could prevent A β binding to PreP; and on the other hand inactivation of PreP would be the tipping point for activation of mitochondrial stress response. As such, MB-60 could be used in mouse model of AD to see if complete ablation of PreP activity could trigger a protective stress pathway.

Most recently, PreP has been shown to degrade islet amyloid polypeptide (IAPP/Amylin)³². Huan et al showed IAPP localized to mitochondria and induced caspase 3

cleavage in beta cells. Knockdown of PreP with siRNA increased IAPP-induced apoptosis as measured by caspase 3 cleavage whereas overexpression of PreP protects cells³². Since PreP is involved in mitophagy, it is plausible that PreP ablation could prime cells for apoptosis upon insult such as IAPP. Alternatively, this could be a way for cells to deal with stress if they are that are not able to undergo mitophagy. Further studies are required to fully understand if PreP plays a role in apoptosis.

Our most recent findings suggest that PreP inactivation by MB-60 induces transcription of mitochondrial proteostasis gene such as mtHSP70, HSP60, LON, CLPP, and DNAJA3 (Data not shown). Taken together, our data show that PreP is a part of the mitochondrial quality control system. We propose a model wherein PreP is a redox-regulated protease whose function serves as a signal to maintain mitochondrial homeostasis (**Supplementary Figure S14**). Under oxidizing condition, compromised PreP activity signals for induction of mitochondrial proteostasis gene. However, when mitochondria are no longer able to cope with stress, mitophagy is activated. Interestingly, LON, a matrix protease that degrades damaged and misfolded proteins is also found to be redox-regulated, with a midpoint potential of -227 mV³³, very close to PreP's midpoint potential of -210 mV. Although the redox study was performed on bacterial LON, it would be interesting to study if human LON is also redox-regulated. Nonetheless, similarly to PreP, activity of human LON is also inhibited by hydrogen peroxide³⁴. Inhibition and knockdown of LON in lymphoma cells leads to apoptosis³⁵. Whether redox regulation of matrix proteases is a common theme requires further investigation. Nonetheless, these studies highlight the complex mechanisms of mitochondrial homeostasis where on one hand, proteases function as a quality control system to degrade peptides that might harm mitochondria, and on the other, they can serve as stress signals and trigger downstream quality control pathways.

Here we demonstrate that our chemical biology approach has successfully identified MB-60 as a novel inhibitor of PreP. By using MB-60, we revealed a novel role of PreP in mitochondrial quality control pathways. Studies are underway to determine genes that are co-regulated in response to inactivation of PreP (collaboration with Wiseman group). Defining these networks of genes will provide insight into the mechanisms of mitochondrial homeostasis and elucidate the physiological relevance of these pathways. Additionally, overexpressing various mutants of PreP such as catalytically inactive mutant, hinge mutant, and MB-60 binding mutants could aid in understanding the specific mechanisms by which PreP is involved in activation stress pathways. Most recent study by the Youle group revealed additional players in mitophagy. Xenophagy receptors NDP52 and optineurin are recruited to mitochondria independent of Parkin and bind to phosphorylated ubiquitin³⁶. These receptors then recruit LC3 and the other autophagosome machineries. Our study MB-60 is synergistic with CCCP recruit Pink1 is recruited to mitochondria of HeLa cells, a cell type that does not have Parkin. It would be worthwhile to investigate whether PreP inactivation can also induce mitophagy by recruiting NDP52 and optineurin.

Furthermore, MitoBloCK-60 could be used in global proteomics studies to reveal peptides that accumulate when PreP is compromised and when mitochondria are under duress. These peptides could serve as a marker for mitochondrial dysfunction.

SAXS and native PAGE analyses reveal PreP exist as a dimer. The biological relevance of PreP dimer remains unknown and warrants further investigation. Native gel analysis of PreP showed higher molecular weight ranging from 200-400 kDa, which could represent PreP dimer and a tetramer. It could also signify that PreP interaction with other proteins. Proteomics studies have suggested that PreP is phosphorylated^{37,38}. Finally, from our most recent collaboration, we

found that a patient with a homozygous knockout of PreP suffers from cyclic vomiting syndrome, hence implicating PreP in this particular type of episodic vomiting. In collaboration with Tang group and his colleagues at University of Chicago, MB-60 could be used, as a tool to inhibit PreP in animal model and determine if the phenotype associated with PreP inactivation will mimic that of cyclic vomiting syndrome. Specifically, we will monitor gastrointestinal functions in animal models. Mitochondria have been implicated in the pathogenesis of diseases such as AD and Parkinson's disease. Modulating stress response through understanding mechanisms of PreP could be an approach to treat these diseases.

Materials and Methods

Cloning Human PreP/MP1 cDNA was purchased from OpenBiosystems (Accession: BC 005025). Mature PreP (amino acid 27-1036) was amplified using primers containing BamHI and XhoI restriction sites, digested, and ligated into pET28a expression vector (Novagen). PreP cloning was performed by Colin Douglas. Human IDE cDNA was purchased from OpenBiosystems (Accession: BC 096336). Full-length IDE was amplified using primers containing NotI and XhoI restriction sites, digested and ligated into pET28a expression vector (Novagen). IDE cloning was performed with Julia Mayer in fulfillment of the requirements for her degree of Bachelor of Science in Engineering. The sequences of all constructs were verified by sequencing (Agencourt).

Protein Expression and Purification pET28a-containing PreP plasmid was transformed into BL21 DE3 *E. coli* expression strain. PreP was expressed using auto-induction method. Starter culture streak from a single colony was grown at 37°C overnight in ZYP-0.8G (see media composition below) supplemented with 40 µg/mL kanamycin and 35 µg/mL chloramphenicol. The next day, cultures were diluted 2000 fold (500 µL) to 1 L of ZYP-5052 supplemented with 40 µg/mL kanamycin and 35 µg/mL chloramphenicol and grown at 30°C for 24 hours. Following 24 hours induction, Cells were harvested by centrifugation at 7,000 x g at 4°C for 10 minutes. Cell paste was resuspended in 0.9% NaCl for a quick wash. Following centrifugation, the bacterial pellet was resuspended in equilibration buffer. Cells were lysed using a high-pressure homogenizer, emulsiflex (Avestin). Cleared lysate, obtained by centrifugation at 10,000 x g at 4°C for 30 minutes, was applied to talon/cobalt metal affinity beads (Clontech) and rotated at

4°C for 2 hours . Beads were washed 3 times with wash buffer on a gravity-flow column. His₆-tagged recombinant PreP was eluted with elution buffer and 1 mL fractions were collected. Protein concentration was measured with BCA assay kit (Thermo Scientific). Most concentrated fractions were pooled together and purified protein was stored frozen at -80°C in 20% glycerol.

IDE construct was transformed into BL21-DE3 gold *E. coli* expression strain. Starter culture streak from a single colony was grown at 37°C overnight in 2YT medium supplemented with 40 µg/mL kanamycin and 15 µg/mL tetracycline. The next day, 20 mL overnight culture was transferred to 1 L flask containing 2YT medium supplemented with 40 µg/mL kanamycin and 15 µg/mL tetracycline. Cultures were grown to OD of 0.6 at 37°C. Protein expression was induced by addition of 1 mM Isopropyl-β-D-Thiogalactopyranoside (IPTG). Six hours post-induction, cells were harvested and washed as described above. Cell pellet after NaCl wash was resuspended in Ni²⁺ lysis buffer (solution composition below). Cells were lysed with 30 minutes incubation in lysis buffer containing 1 mg/mL lysozyme followed by sonication on ice. Cleared lysate, obtained by centrifugation at 10,000 x g at 4°C for 30 minutes, was applied to Ni²⁺ metal affinity beads (Thermo) and rotated at 4°C for 2 hours. Beads were washed 3 times with wash buffer on a gravity-flow column. His₆-tagged recombinant IDE was eluted with elution buffer and 1 mL fractions were collected. Protein concentration was measured with BCA assay kit (Thermo Scientific). Most concentrated fractions were pooled together and purified protein was stored frozen at -80°C in 20% glycerol. Plasmid containing alpha and beta subunits of matrix processing-peptidase³⁹ was transformed into BL21 DE3 gold expression strain. Protein was expressed using the auto-induction method and purified using Ni²⁺ metal affinity beads as described above.

Media and solutions composition described in protein expression and purification PreP

Expression media: ZY (1% tryptone, 0.5% yeast extract), ZYP-0.8G (ZY, 1 mM MgSO₄, 0.8% glucose, 25 mM (NH₄)₂SO₄, 50 mM KH₂PO₄, 50 mM Na₂HPO₄), ZYP-5052 (ZY, 1 mM MgSO₄, 0.8% glucose, 25 mM (NH₄)₂SO₄, 50 mM KH₂PO₄, 50 mM Na₂HPO₄, 0.5% glycerol, 0.05% glucose, 0.2% lactose), 2YT (1.6% tryptone, 1% yeast extract, 0.5% NaCl, 10 mM Tris-HCl pH 7.4). Solutions for PreP purification: Equilibration buffer (50 mM sodium phosphate pH 7.0, 300 mM NaCl), Wash buffer (50 mM sodium phosphate pH 7.0, 300 mM NaCl, 7.5 mM imidazole), Elution buffer (50 mM sodium phosphate pH 7.0, 300 mM NaCl, 150 mM imidazole). Solutions for IDE purification: Lysis buffer (50 mM NaH₂PO₄.H₂O, 300 mM NaCl, 10 mM imidazole; pH 8.0), Wash buffer (50 mM NaH₂PO₄.H₂O, 300 mM NaCl, 20 mM imidazole; pH 8.0), Elution buffer (50 mM NaH₂PO₄.H₂O, 300 mM NaCl, 250 mM imidazole; pH 8.0).

High-throughput Screen (HTS) The primary screen was performed using 22 nM of recombinant PreP in 10 mM HEPES pH 7.4, 50 mM NaCl, 0.01% BSA). A titertrek multidrop was used to dispense 35 µL protein or protein chelated with 0.1 mM EDTA and 0.5 µM *o*-phenanthroline to all wells of black 384-wells plate (GreinerBio one). 0.5 µL of small molecules from the 1 mM stock library or vehicle control DMSO stock (10 µM final concentration) was then pinned to each well using a biomek FX (Beckman Coulter). Plates were incubated at 30°C for one hour, followed by a fluorescence measurement prior to substrate addition. A titertrek multidrop was used to dispense 15 µL of fluorogenic leuomorphin peptide (MCA-RRQFKVVTRSQ-JPT). The final concentration of substrate was 15 µM. The peptide solution was shielded from light throughout the experiment. Following 30 minutes incubation at 30°C, plates were read for an end-point measurement using an excitation and emission wavelength of

330 and 425 nm respectively. Screens were conducted using an automated plate scheduler to ensure consistency across the run. Assay quality and reproducibility of each each plate was monitored using the statistical parameter, Z prime (Z')⁴⁰. All plates had Z' values greater than 0.5. Compounds that inhibited activity by 70% were marked as potential hits. 5 μ L hits were then cherry-picked from the original plate onto a 384-well low volume, v-bottom plates. Hits were then rescreened against PreP and counter-screened against Insulin-Degrading Enzyme (IDE). IDE counter-screen was conducted with the help of Julia Mayer. Hits from the rescreen and counter-screened were compared to hits from a parallel screen against Matrix Processing Peptidase (MPP). Small molecules that inhibited PreP but not MPP and IDE were grouped according to their chemical structure similarities. Commercially available compounds were purchased and assayed for IC₅₀ analyses – the concentration of small molecule required to inhibit activity of the protein by 50%. For IC₅₀ analysis, serial dilution of small molecule was added into assay plates containing protein as described above. For cleavage with amyloid-beta substrate, intramolecularly quenched A β 1-42 (Abz-DAEFRHDSGYEVHHQKLVFFAEDVGSNKGAIIGLMVGGVVIA-EDDnp) was purchased from AnaSpec and dissolved in DMSO. 45 nM of recombinant PreP was used for cleavage assay with amyloid-beta peptide as the substrate.

Oxygen consumption and membrane potential measurements Mitochondria were purified from yeast cells grown on YPEG as described in previous study²². Oxygen consumption measurements with isolated mitochondria were performed using an oxygen electrode (Hansatec) as described previously²¹. Membrane potential measurements of purified mitochondria were performed with fluorescent 3,3'-dipropylthiadicarbocyanine iodide dye [DiSC₃(5)]. 1% DMSO,,

carbonyl cyanide 4-(trifluoromethoxy) phenylhydrazone (FCCP), or MB-60 was added to mitochondria in import buffer (0.6 M sorbitol, 2 mM KH_2PO_4 , 60 mM KCl, 50 mM HEPES-KOH, 5 mM MgCl_2 , 2.5 mM EDTA, 5 mM L-methionine, pH 7.1) for 10 min. Subsequently 0.2 μM DiSC₃(5) in import buffer was added and incubated for 5 min, and fluorescence was measured at excitation and emission length of 620 nm and 670 nm, respectively.

Mitochondria integrity assay 25 μg of yeast isolated mitochondria were incubated in import buffer (0.6 M sorbitol, 2 mM KH_2PO_4 , 60 mM KCl, 50 mM HEPES-KOH, 5 mM MgCl_2 , 2.5 mM EDTA, 5 mM L-methionine, pH 7.1) and varying concentration of small molecules at 25°C for 30 minutes. Mitochondria were then pelleted by centrifugation at 8,000 x g for 10 minutes at 4°C. Supernatant containing released proteins from mitochondria were TCA precipitated on ice for 30 minutes. Precipitated proteins were recovered by centrifugation at maximum speed for 15 minutes at 4°C. Both mitochondrial pellet and released proteins were resuspended in 5x-Laemmli sample buffer (0.25 M Tris-Cl pH 6.8, 10% SDS, 30% glycerol, 0.02% bromophenol blue) with 5% β -mercaptoethanol (β ME) and analyzed on SDS-PAGE. Resulting gel were stained with coomassie blue for 30 minutes or transferred to nitrocellulose membrane and blotted with key mitochondrial proteins.

In vitro activity assays for PreP. For amyloid-beta degradation, 0.5 μM of PreP was incubated in DMSO or small molecule in screening buffer for 1 hour prior to addition of 10 μM fluorescent-labeled amyloid beta, FAM- labeled amyloid beta (1-42) peptide (FAM-A β 1-42) (Anaspec). Reactions were stopped after 1 hour by adding 5x-Laemmli sample buffer. Samples were resolved on 16% Tris-Tricine gel. Gels were visualized using a BioRad imager to detect

FAM at 494 and 521 nm excitation and emission wavelength. For Su9-DHFR degradation, radiolabeled precursor was generated using the TNT Quick coupled transcription translation kit (Promega). During translation, 200 nM PreP in screening buffer was preincubated with small molecule for 1 hour. To cleave targeting sequence from Su9-DHFR, 4 μ M of MPP was incubated with 5 μ L of precursor for 30 minutes at 30 °C. PreP previously incubated with drug was then added to the MPP-precursor mixture. Reactions were stopped at specified time points by adding Laemmli sample buffer. Samples were resolved on 16% Tris-Tricine gel. Gels were fixed, dried and exposed to film.

Ab peptide assays with mitochondria. 0.5 μ M FAM- A β (1-42) peptide was added to media of HeLa cells grown on coverslips. 24 hrs post-treatment, 25 nM Mitotracker was added to the media. After 30 min incubation, cells were washed with PBS and fixed in 3.7% formaldehyde in PBS for 15 min. Cells were then permeabilized in ice-cold methanol for 10 min prior to blocking and immunostaining with antibodies against mortalin. FAM-A β was visualized on the GFP filter.

Midpoint potential measurement. To measure the midpoint potential, recombinant PreP was incubated in 10 mM Hepes pH 7.0 buffer containing defined reduced and oxidized DTT or glutathione to establish ambient redox potential values as previously described⁴¹. Samples were incubated for 3 hours followed by incubation with monobromoamide (mBBR) in the dark for 30 minutes. Samples were precipitated with trichloroacetic acid (TCA) and resuspended in 0.1 M Tris pH 8.0 and 0.1% SDS. mBBR fluorescence was measured on Quant Master QM-4 spectrofluorometer from Photon Technology International (Lawrenceville, NJ), with an

excitation and emission wavelength of 380 nm and 475 nm respectively. To measure activity of PreP, PreP was incubated in redox buffers as described above for 1 hour prior to addition of leumorphin fluorogenic peptide as described above.

Cell culture. HeLa and HeLa cells stably expressing EGFP-Parkin were cultured in DMEM with pyruvate (Life Technologies) supplemented with 10% FBS (v/v) and 1% penicillin/streptomycin in humidified atmosphere with 5% CO₂. For small molecules treatment, cells were seeded at 70% confluency and treated the next day. HCT116 cells were cultured in McCoy's 5A media (HyClone) supplemented with 10% FBS (v/v) and 1% penicillin/streptomycin.

Cell viability measurement. Cells were seeded at 50% confluency, incubated for 24 hrs, then treated with the DMSO or the indicated MB-60 concentrations. After 24 hrs, cell viability was measured by the 3-(4,5-dimethylthiazol-2-yl)-2,5-diphenyltetrazolium bromide (MTT) toxicology assay (Sigma), according to the manufacturer's protocol.

Small molecule treatment and mitochondria isolation. HeLa cells, HeLa stably overexpressing EGFP-Parkin, or HCT116 cells were seeded at 70% confluency. After 24 hrs, cells were pre-treated with the indicated small molecule for 3 hrs, followed by CCCP addition. Cells were harvested at the indicated time points. For mitochondria isolation, cells were harvested and homogenized in 20 mM HEPES pH 7.6, 220 mM mannitol, 70 mM sucrose, 2 mg/ml BSA, 10 mM NEM and 0.5 mM PMSF and 1 μ M MG132. Cells were passed through a 25-gauge needle using a 1 mL syringe to lyse the cells. Homogenates were centrifuged at 770 \times g at 4°C for 5 min. To isolate mitochondria, post-nuclear supernatants were centrifuged at 10,000 \times

g at 4°C for 10 min. Pellets were washed with homogenization buffer lacking BSA. Protein concentrations were measured using BCA assay (Thermo Scientific). Samples were resolved on SDS-PAGE and transferred to polyvinyl difluoride (PVDF) membrane (EMD Millipore) for western blot analysis.

Mitochondria isolation from mammalian cells for protein import. Cultured cells were grown to confluency. One day prior to mitochondria isolation, cells were fed with fresh media. The next day, cells were harvested and homogenized in 20 mM HEPES pH 7.6, 220 mM mannitol, 70 mM sucrose, 2 mg/ml BSA, and 0.5 mM PMSF. Lysates were dounced with Teflon dounce. Homogenates were centrifuged at 770 x g at 4°C for 5 minutes. Post-nuclear supernatants were centrifuged at 10,000 x g for 10 minutes to obtain mitochondria pellets. Pellets were further washed with homogenization buffer without BSA. Protein concentrations were measured using BCA assay (Thermo Scientific).

Import of radiolabeled proteins into isolated mammalian mitochondria. Mitochondria were isolated as described above. ³⁵S-labeled precursors were synthesized using the TNT Quick Coupled Transcription/Translation kits (Promega). 10 or 20 µg mitochondria were added to import buffer (20 mM HEPES pH 7.6, 220 mM mannitol, 70 mM sucrose) supplemented with 1 mM ATP, 0.5 mM magnesium acetate, 5 mM NADH, and 20 mM sodium succinate. Small molecules or DMSO vehicle control were added and samples were incubated for 15 minutes at 25°C. 10-20 µL precursor was added to initiate import. Reaction aliquots were withdrawn at specified time points. Import was stopped by adding cold import buffer or 25 µg/mL trypsin. Soybean trypsin inhibitor (50 µg/mL) was added following 15 minutes trypsin treatment.

Mitochondria were pelleted by centrifugation at 12,000 x *g* at 4°C for 5 minutes. Final mitochondria pellet were dissolved in 5x Laemmli sample buffer. Samples were resolved on SDS-PAGE. Gels were dried prior to exposure to film for autoradiography.

Immunofluorescence. Cells were seeded on a 12-wells plate containing glass coverslips and treated the next day with indicated small molecules or DMSO vehicle control. Cells were fixed in 3.7% formaldehyde for 15 minutes followed by 3 times PBS wash. For immunostaining, cells were permeabilized in ice-cold methanol for 10 minutes after fixation. Cells were blocked in 1% BSA for 30 minutes prior to incubation with primary antibody (in 1% BSA). Following PBS washes, cells were incubated with secondary antibodies conjugated Alexa Fluor dyes 350, 488, or 568 (Life Technologies). For MitoTracker Red staining, cells were incubated in 25 nM MitoTracker Red CMXRos (Life Technologies) for 30 minutes prior to fixation. Cells were visualized on Leica TCS SPE DMI 4000B inverted confocal microscope or Axiovert 200M Carl Zeiss inverted microscope. Cell quantification was performed with ImageJ software (NIH) where at least 100 cells were counted in 3 independent experiments.

siRNA knockdown. The PreP siRNA construct was purchased from Qiagen (Cat # S100108647). On Day 1, HeLa cells were seeded at 50% confluency in 10 cm dish. On day 2, cells were transfected with 50 nM siRNA using lipofectamine 2000 according to manufacturer's protocol. 24 hours post-transfection, transfected cells were split and seeded to 6 cm dishes. The next day, cells were treated DMSO, CCCP or small molecule per the experiment.

Generation of PreP knockout cells. PreP knockout HCT116 colon cancer cells were generated using the CRISPR/Cas9 system as described previously⁴². Briefly, guide RNAs targeting different regions of PreP were designed and cloned into PX330-U6-Chimeric_BB-CBh-hSpCas9 (Addgene). Cells were seeded and transfected the next day using BioT transfection reagent (bioland) according to manufacturer's instructions. 2 days post-transfection, puromycin was added for additional 2 days to select for transfected cells. Fresh media without puromycin were then added and cells were grown until they reach confluency. To isolate single colonies, cells were serially diluted and seeded at 0.5 and 1 cells/well onto multiple 96 wells plates. Each single colony was screened for deletions of PreP by PCR and sequencing as well as by western blotting analysis.

Antibodies. The following antibodies were used in this study: PINK 494 (Novus Biologicals), Tom20 (sc-11415), Tim 17 (sc-13293), Parkin (sc-32282) (Santa Cruz Biotechnology, Inc.), LC3 (Cell Signaling), Mfn1 (kind gift from Dr. Richard Youle), Mortalin (NeuroMab).

Miscellaneous. Mitochondrial proteins were analyzed by SDS-PAGE using a 12 or 15% polyacrylamide gel and a Tricine-based running buffer. Proteins were detected by immunoblotting using nitrocellulose membranes or PVDF membranes.

For structural analyses:

Expression and Purification of hPreP. Wild type hPreP and E107Q were expressed and purified as described⁴³. Briefly, *E. coli* Rosetta (DE3) containing plasmid for the expression of hPreP were grown at 25 °C with 300 μM IPTG induction for 20 hours. Proteins were then

purified over Ni-NTA affinity, Source Q anion exchange, and Superdex 200 size exclusion columns and flash-frozen in liquid nitrogen and stored at -80 °C.

Protein Crystallization, data collection, and structure determination. hPreP E107Q was modified by reductive lysine methylation prior to Superdex 200 chromatography. 5-7 mg/ml lysine-methylated hPreP-E107Q in buffer containing 20 mM HEPES pH 7.5, 250 mM NaCl, 2 mM DTT, and 200 μ M MB60 was combined with mother liquor containing 15.0% (w/v) PEG 8,000, 15 mM TCEP, 80 mM sodium cacodylate pH 6.7, 160 mM calcium acetate, and 20% (v/v) glycerol in a 1:1 (v/v) ratio for the crystallization of hPreP-MB60 complex by hanging-drop vapor diffusion at 18°C. Crystals grew for one week prior to data collection. Crystals were cryoprotected in mother liquor containing 30% (v/v) glycerol, then flash-frozen in liquid nitrogen. Diffraction data were collected at beamline 19ID at Argonne National Laboratory and processed using HKL3000⁴⁴. The structure of hPreP in complex with MB-60 was determined by molecular replacement using Phaser and hPreP structure (4L3T) as the search model. The model building including the addition of missing 317-323 residues in chain A were performed using COOT⁴⁵ and refinement was done using PHENIX⁴⁶. The final 2.27Å resolution model (pdb=4RPU) has $R_{\text{work}}=18.6\%$ and $R_{\text{free}}= 20.6\%$. Data collection and structure refinement statistics are listed in Table S3. Due to the shorter time of crystallization, only cysteine 112 was modified with the dimethylarsenic moiety while cysteine 556 was not. Cysteine 556 is in the close proximity with cysteine 119 to form a disulfide bond. The absence of disulfide bond between these residues might be due to the presence of reducing agent during the purification and/or crystallization.

SAXS Data Collection and Analysis. SAXS data were collected at Argonne National Laboratory's Advanced Photon Source, beamline 12ID-B, at 23 °C using 1.1 mg/ml protein and an incident X-ray wavelength of 0.886 Å, and protein concentration of 0.5 mg/ml. For MB-60-binding experiments, hPreP was preincubated with 200 µM MB-60 on ice prior to SAXS data collection. The data was reduced and analyzed using ATSAS. PRIMUS⁴⁷ and GNOM⁴⁸ were used to determine the R_g value in reciprocal and real space, respectively. D_{max} and $P(r)$ distribution were calculated by GNOM. Theoretical scattering curves for different models were generated and fit to the experimental data using CRY SOL⁴⁹. OLIGOMER⁵⁰ was used to determine the percent composition by parsimonious conformational states that best fit the observed data. Data collection and scattering derived parameters are listed in Table S4⁵¹.

Deuterium exchange mass spectrometry (DXMS). Prior to performing comparative H/D exchange experiments, enzymatic and quench conditions that produced an optimal fragmentation pattern of hPreP were established as previously described⁵². Briefly, 3 µl 4.7 mg/ml hPreP in buffer containing 20 mM Tris-HCl (pH 7.5), and 50 mM NaCl was diluted with 9 µl of buffer A (8.3 mM Tris-HCl (pH 7.5), 50 mM NaCl in H₂O) at 0°C, and then mixed with 18 µl of ice cold quench buffers containing 0.8% formic acid, 16.6% glycerol and various concentrations of GuHCl (0.08, 0.8 and 1.6 M). The quenched samples were then subjected to DXMS apparatus for proteolysis and LC/MS analysis. The use of 0.8 M GuHCl resulted in the best sequence coverage of hPreP. For DXMS analysis, 13 µM hPreP in the presence or absence of 130 µM MB-60 in 8.3 mM Tris-HCl pH7.2, 50mM NaCl, and 2.1%DMSO in H₂O was incubated at room temperature for 30 minutes prior to chill to 0°C for deuteration studies. Functional hydrogen-deuterium exchange reactions were initiated by adding 3 µl sample into 9 µl of buffer A in D₂O

($pD_{\text{READ}}=7.2$) and incubated at 0°C for 10, 100, 1,000, and 10,000, 100,000 sec and at room temperature for 100000 sec (representing 1,000,000 sec at 0°C based on 10-fold enhanced rate at room temperature⁵³). The exchange reaction was terminated by adding 18 ml of ice-cold 0.8% formic acid, 0.8M GuHCl, 16.6% glycerol for a final pH of 2.5. Quenched samples were then immediately frozen on dry ice and stored at -80°C prior to LC/MS analysis. Un-deuterated and equilibrium-deuterated control samples are also prepared as previously described⁵⁴. The frozen samples were later loaded onto a cryogenic autosampler⁵⁵, thawed at 4°C , and then passed over an immobilized pepsin column (16 μl bed volume) for 30-40 sec digestion. Proteolytic fragments were collected on a trap column and separated using Michrom C18 reverse phase analytical column (Michrom MAGIC C18 AQ 0.2 x 50mm, 3mm) with an acetonitrile linear gradient (6.4%-38.4% over 30min). The effluent was directed into an OrbiTrap Elite Mass Spectrometer (ThermoFisher Scientific, San Jose, CA). Instruments settings were optimized to minimize the back-exchange⁵⁶. The data was acquired in either MS1 profile mode or data-dependent MS/MS mode. Peptide identification was done by the aid of Proteome Discoverer software (ThermoFisher). The centroids of the mass envelopes of deuterated peptides were calculated with DXMS Explorer (Sierra Analytics Inc, Modesto, CA) and then converted to corresponding deuterium incorporation with corrections for back-exchange⁵⁷.

Figures and Tables

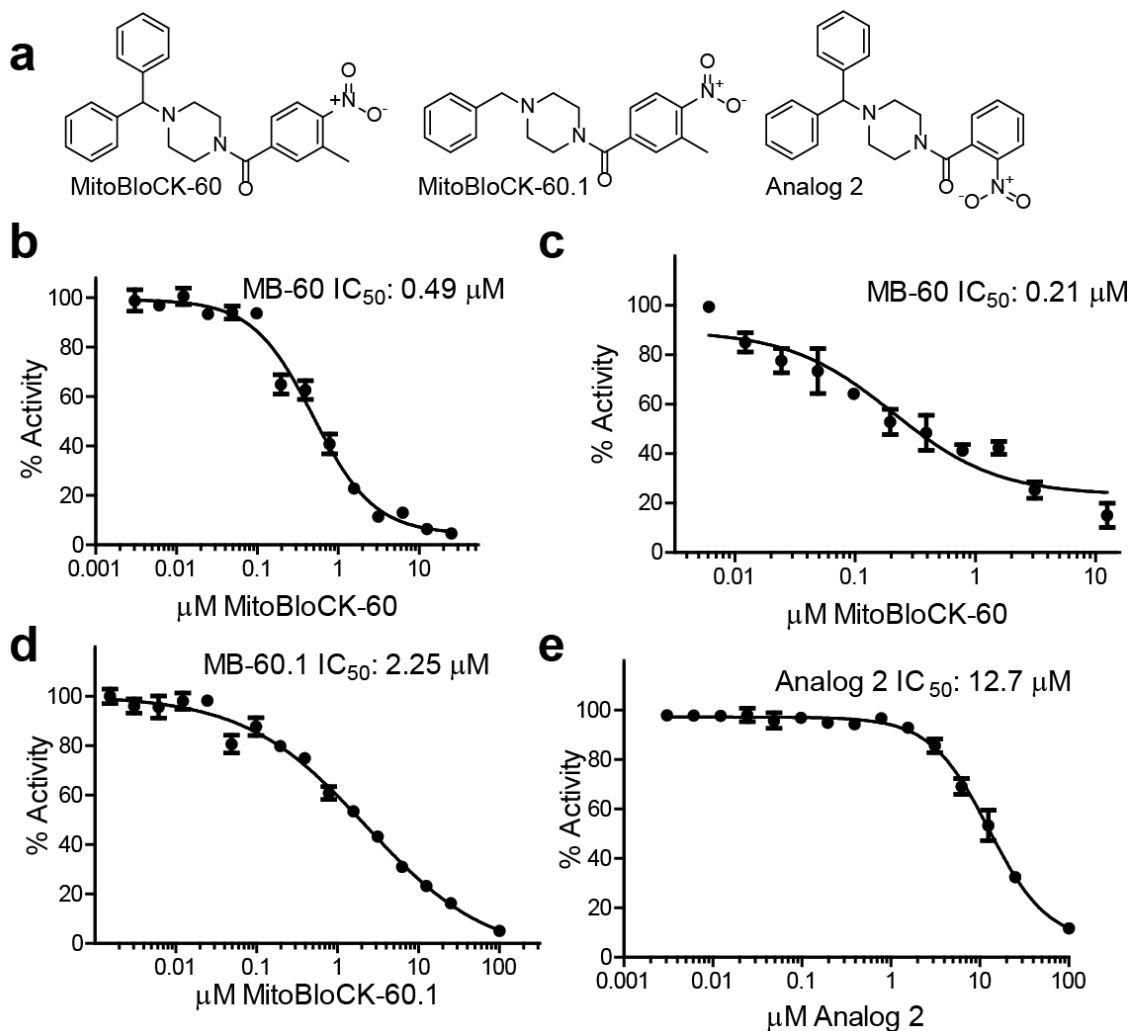


Figure 1. MitoBloCK-60 inhibits PreP activity. (a) Structure of MitoBloCK-60 and two analogs, MitoBloCK-60.1 and analog 2. IC₅₀ of (b) MB-60 using leumorphin peptide as substrate is 0.49 μM (c) using intra-molecularly quenched Aβ peptide is 0.21 μM. IC₅₀ of MB-60.1 (d) and Analog 2 (e) using leumorphin peptide as substrate are 2.25 μM respectively.

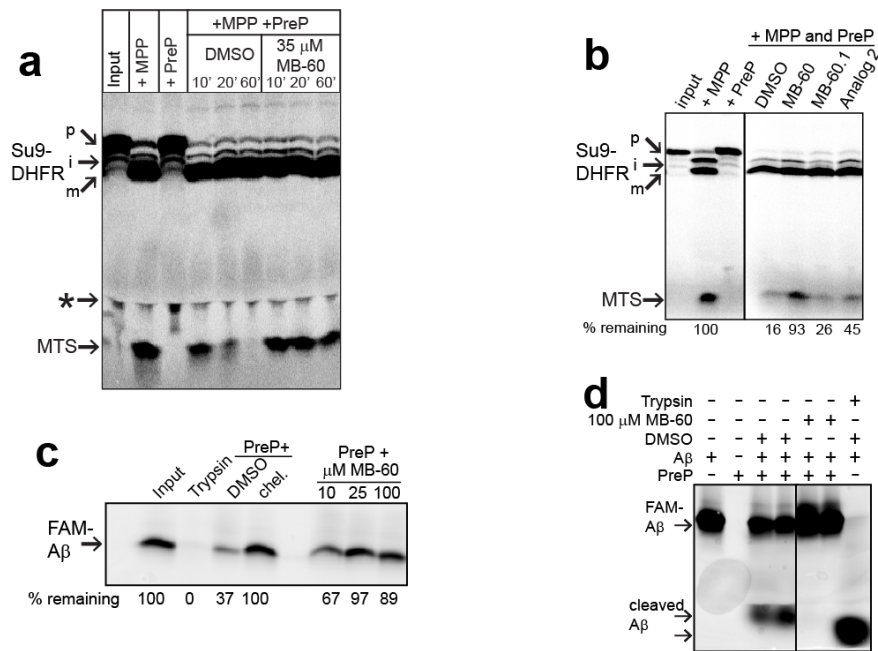


Figure 2. MB-60 inhibits PreP activity *in vitro*. (a) Radiolabeled Su9-DHFR was synthesized in an *in vitro* transcription-translation reaction and incubated with 4 μ M MPP and 200 nM PreP in the presence of 35 μ M MB-60 or vehicle (1% DMSO) for 60 mins. Products were separated on a 16% Tris-Tricine gel and detected by autoradiography. p, precursor; i, intermediate; m, mature; MTS, mitochondrial targeting sequence; * marks nonspecific product. (b) As in ‘a’, with 35 μ M MB-60, 100 μ M MB-60.1, and Analog 2. The amount of MTS that was resistant to degradation was quantified using ImageJ software; 100% was set as the amount of MTS generated by MPP cleavage. (c) FAM-A β 1-42 was incubated with PreP in the presence of DMSO, chelators (EDTA and o-phenanthroline, chel.), and MB-60 for 60 mins. The undigested peptide was separated on a 16% Tris-Tricine gel and the FAM fluorophore was detected by BioRad FX imager. As a control, trypsin was added directly to A β . The amount of peptide that was not degraded was set as 100%. (d) As in ‘c’, a gel system was used in which cleaved A β was detected.

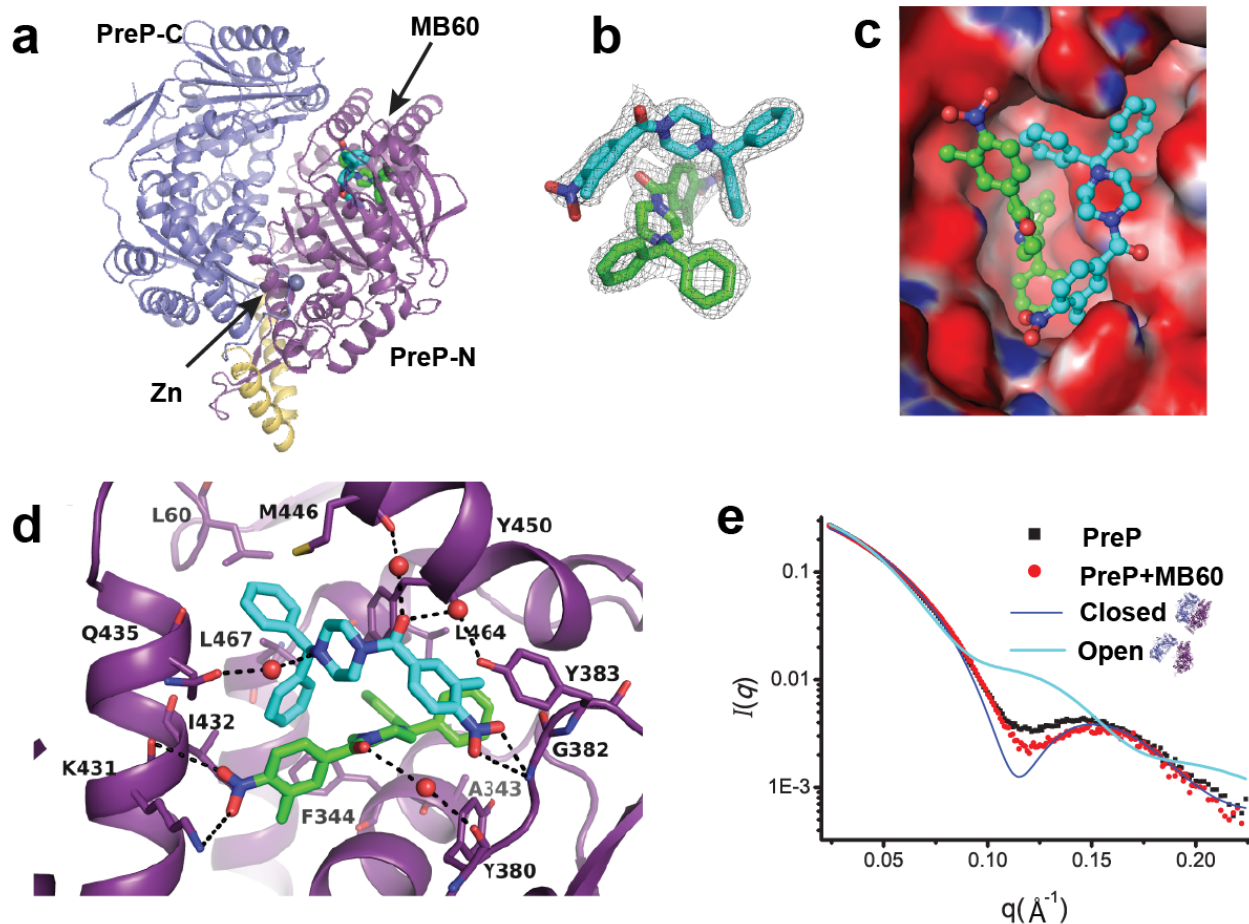


Figure 3. Structural analysis of MB-60-bound human PreP. (a) Overall structure of MB-60-bound PreP. PreP is depicted in a ribbon representation. The carbons of two MB-60 molecules are colored in cyan and green while N and O atoms are in blue and red, respectively. The catalytic zinc ion is in grey. (b) 2mFo-DFc omit map of MB-60 to depict the close contact between two MB-60 molecules at the hydrophobic exosite. The map was contoured to 1σ . (c) The close fit of MB-60 within the PreP exosite. The electrostatic surface was calculated using APBS2.1. (d) Detailed interactions of two MB-60 with PreP side chains. (e) SAXS scattering profile of PreP in the presence or absence of MB-60 (dotted lines). Theoretical scattering profiles of open and close PreP (solid lines) were modeled and calculated by CRY SOL.

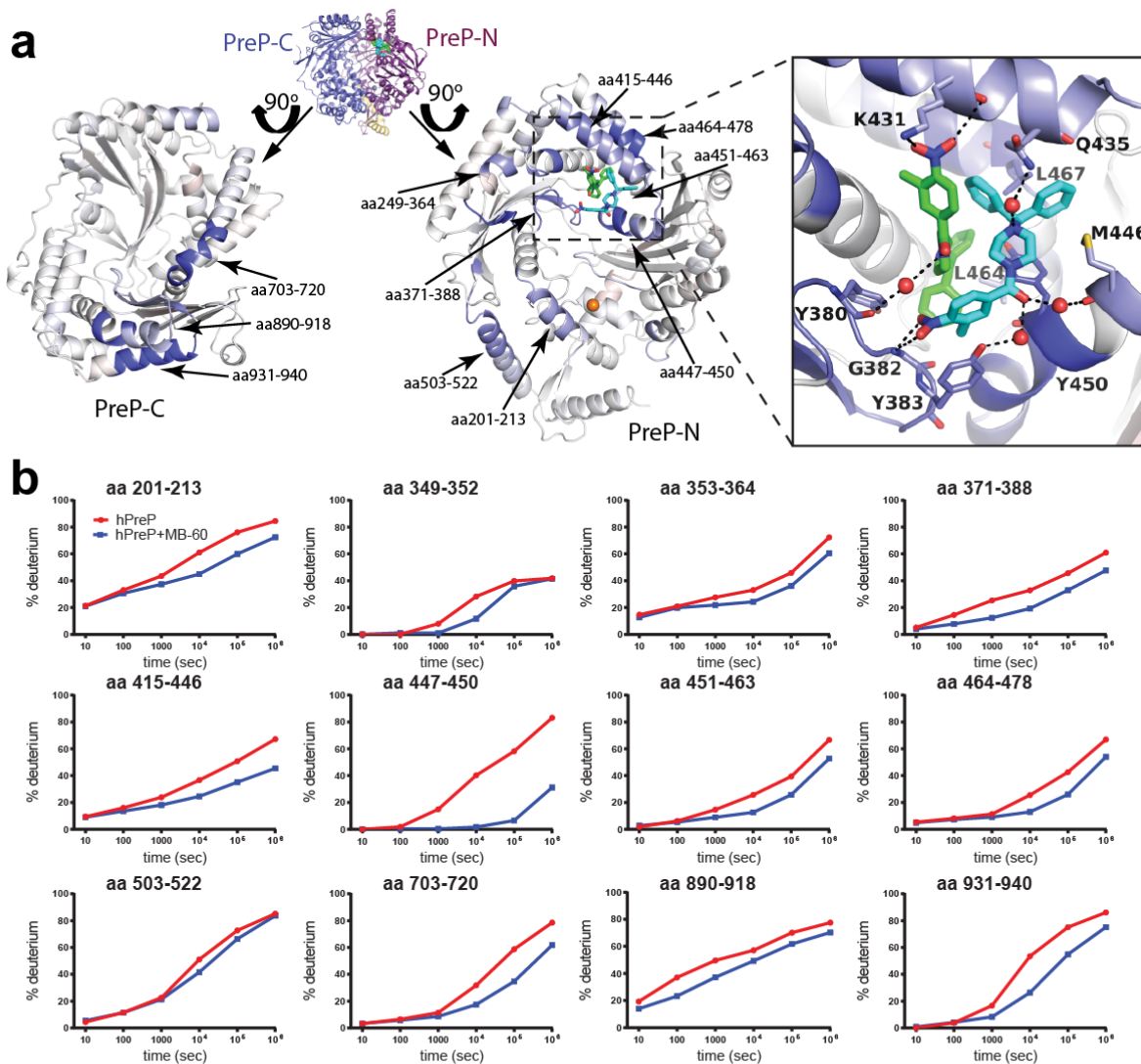


Figure 4. HDX-MS confirms MB-60 binding sites within PreP and explains the mechanism by which MB-60 enhances the interaction between PreP-N and PreP-C. (a) Differential HDX between PreP in the absence and presence of MB-60 mapped on the MB-60 bound PreP crystal structure (4RPU) from. Differences in the average HDX are represented as percent change and colored with blue being slower exchange with MB-60 while with red being faster. (b) Corresponding deuterium buildup curves for the regions that undergo the most significant change are shown.

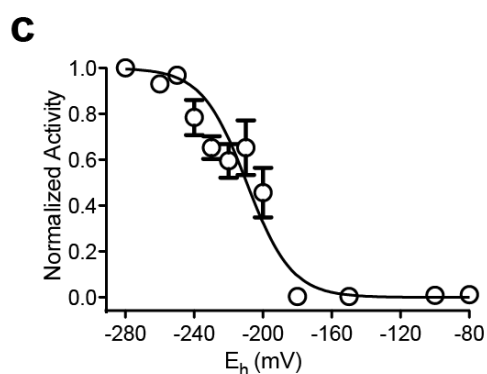
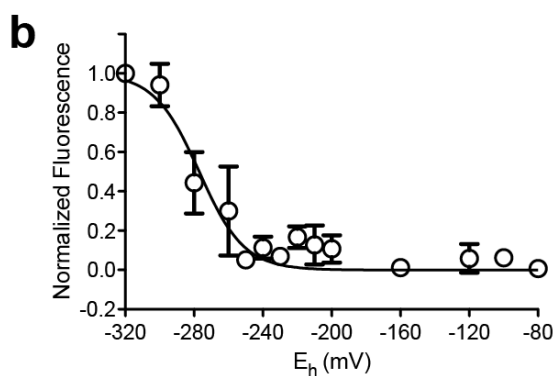
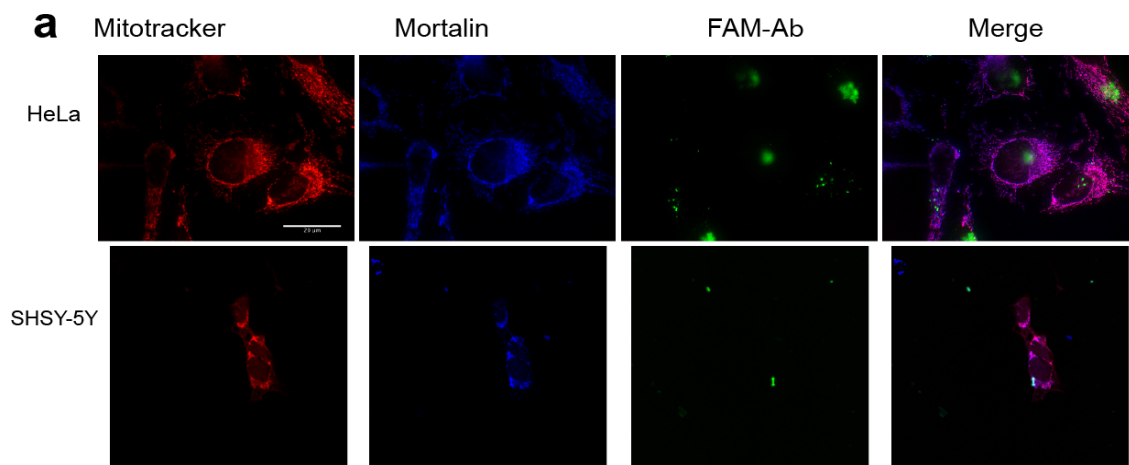


Figure 5. PreP activity is redox-regulated with midpoint potentials of -277 and -210 mV.

(a) HeLa cells (top panel) and SHSY-5Y cells (bottom panel) were incubated with fluorescent A β 1-42 (FAM-A β) for 24 hours and subcellular localization was monitored by microscopy. An antibody against mortalin marked mitochondria and the membrane potential was verified by MitoTracker staining (Scale bar = 20 μ m). (b) Redox titration of PreP was performed in a DTT or glutathione redox buffer. Equilibration was achieved at 3 hrs in pH 7.0 under anaerobic conditions. Data in all titrations were fit to the Nernst equation for a two-electron carrier. The

redox titration of PreP was performed with mBBr. The best fit to the mBBr fluorescence magnitude versus E_h value was obtained with an E_m of -277 mV ($n = 3$). (c) As in 'b', the activity of equilibrated PreP at different redox potentials was measured based on the cleavage of the fluorescent leumorphin peptide. The best fit to the activity versus E_h value was obtained with an E_m of -210 mV ($n = 3$).

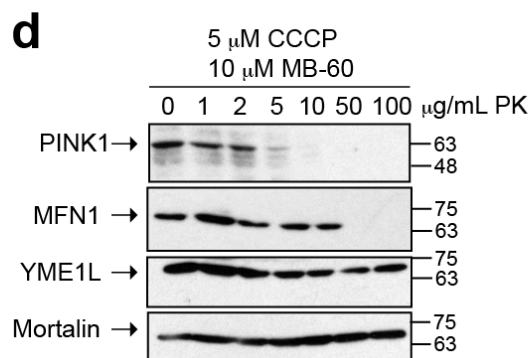
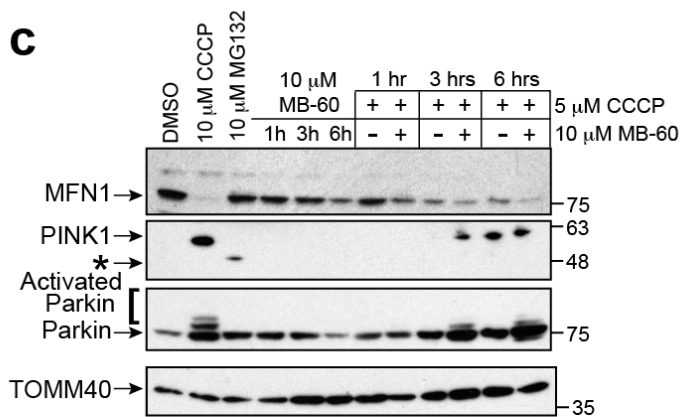
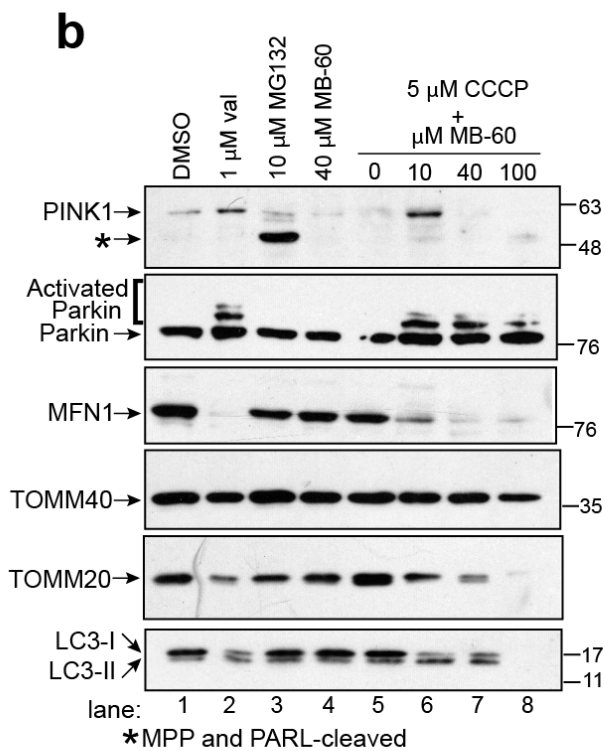
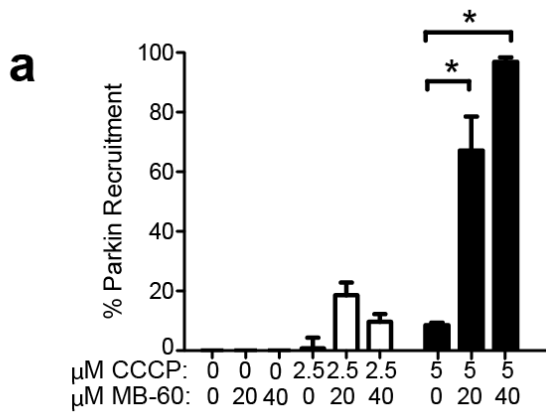


Figure 6. MB-60 is synergistic with CCCP to induce mitophagy. (a) HeLa cells expressing constitutive EGFP-Parkin were treated with combinations of 20 and 40 μ M MB-60 for three hours and then 2.5 and 5 μ M CCCP for additional 3 hours. EGFP-Parkin recruitment was monitored by fluorescence microscopy. Mitochondria were marked by TOMM20 and the membrane potential was monitored by MitoTracker staining. Parkin recruitment to mitochondria was quantitated in a pool of 100 cells in three separate experiments. Representative images are shown in **Supplementary Fig. 10** and **11**. (b) As in 'a', HeLa cells expressing constitutive EGFP-Parkin were treated with MB-60 for 3 hours then 5 μ M CCCP for additional 3 hours. Mitochondria were subsequently isolated and blotted with antibodies against MFN1, Parkin, PINK 1, TOMM40, TOMM20, LC3, and TIMM17. As a control to induce mitophagy, 1 mM valinomycin was added; as a control to show accumulation of cleaved, short form of PINK1 (marked with an asterisk, cleaved by MPP and PARL), 10 μ M MG132 was added. (b) As in 'a', but cells were incubated with 10 μ M MB-60 and 5 μ M CCCP, and mitochondria were isolated and subsequently treated with proteinase K (PK).

Supplementary Table 1A Small molecule screening data

Category	Parameter	Description
Assay	Type of assay	In vitro fluorescence-based activity assay.
	Target	Human Presequence-degrading Protease (PreP).
	Primary measurement	Detection of fluorescence at emission and excitation wavelength of 330 nm and 425 nm.
	Key reagents	Recombinant PreP, leuomorphin peptide substrate (JPT peptide technologies).
	Assay protocol	(see table S1B)
Library	Library size	88,000
	Library composition	Drug-like small molecules, FDA-approved small molecules, targeted libraries.
	Source	ChemBridge, Asinex, various vendors
Screen	Format	384-wells plates
	Concentration(s) tested	10 μ M compound, 1% DMSO
	Plate controls	DMSO
	Reagent/ compound dispensing system	Titertrek Multidrop
	Detection instrument and software	FlexStation II and SoftMax Pro
	Assay validation/QC	Z' > 0.5. Multidrop and plate reader calibration
	Correction factors	
	Normalization	
	Additional comments	Screening was conducted at UCLA Molecular Shared Screening Resource (MSSR)
Post-HTS analysis	Hit criteria	70% inhibition
	Hit rate	0.50%
	Additional assay(s)	Rescreen and counterscreen with IDE and MPP
	Confirmation of hit purity and structure	Provided by vendors
	Additional comments	Commercial small libraries were used; additional aliquots of compounds were purchased from the vendor to verify that the specific compound consistently inhibited PreP activity.

Supplementary Table 1B HTS Assay Protocol

Parameter	Value	Description
Dispense controls	35 μ L	Recombinant chelated PreP
Dispense protein	35 μ L	Recombinant wild-type PreP
Library compounds	0.5 μ L	Pin compounds from 10 mM stock plates
Assay readout at time 0	330 and 425 nM	Excitation and emission
Incubation time	1 hour	30°C
Dispense peptide	15 μ L	50 μ M stock peptide
Incubation time	30 minutes	30°C
Assay endpoint readout	330 and 425 nM	Excitation and emission

Notes

22 nM of controls dispensed to columns 23 and 24 of 384-wells black plate with clear bottom

22 nM of wild-type protein to columns 1-22

Pintool transfer

Flexstation II, SoftMax Pro software

Plates lidded until peptide dispense

8-tip dispense reagent to all wells

Plates lidded until endpoint reading

FlexStation II. 5 seconds mixing before measurement

Supplementary Table 2. Summary of screened compounds

	Number of compounds	Inhibitors	Inhibitors hit rate (%)	Inhibitors confirmed in rescreening	Hits confirmed after IDE countersreen	Hits confirmed after MPP data analysis
Chembrige	29,760	209	0.7	118 (56.5%)	0	2 (1.69%)
Asinex	19,840	134	0.68	67 (50%)	0	1 (1.49%)
Others (focused libraries)	38,400	121	0.32	48 (40%)	0	4 (8.3%)
Total	88,000	464	0.53	233 (48.1%)	233 (100%)	226 (97%)

Supplementary Table 3 Data collection and structure refinement statistics

hPreP with MB-60	
Data Collection	
Beamline	APS-19ID
Wavelength (Å)	0.9792
Space group	C2
Cell dimension(Å)	
a	245.6
b	85.5
c	158.2
α	90
β	127.5
γ	90
Resolution (Å)	44.85-2.27
R _{meas} (%) ^a	18.6 (80.1) ^e
R _{p.i.m} (%) ^b	3.8 (31.4) ^e
CC _{1/2} ^c	(0.793) ^e
CC* ^d	(0.941) ^e
I/sigma	19.4 (2.3) ^e
Redundancy ^f	9.7 (42.8) ^e
Completeness (%)	99.9 (98.0) ^e
Unique reflections	119317
Refinement	
R _{work} ^g	0.176
R _{free} ^h	0.208
No. atoms	
Protein	15879
Water	884
B-factors	
Protein	36.1
Substrate	33.5
Water	40.5
r.m.s. deviations	
Bond lengths (Å)	0.006
Bond angles (°)	0.972
Ramachandran plot (%)	
Favorable region	92.6
Allowed region	7.4
Generously allowed region	0

Disallowed region	0
PDE code	4RPU

$$^a R_{\text{meas}} = \sum_{hkl} [n/(n-1)]^{1/2} \sum_i |I_{hkl,i} - \langle I_{hkl} \rangle| / \sum_{hkl} \langle I_{hkl} \rangle$$

$$^b R_{\text{p.i.m.}} = \sum_{hkl} [1/(n-1)]^{1/2} \sum_i |I_{hkl,i} - \langle I_{hkl} \rangle| / \sum_{hkl} \langle I_{hkl} \rangle$$

^cCC_{1/2} – Pearson correlation coefficient between random half-datasets -

$$\rho_{x,y} = \text{cov}[(x,y)] / (\sigma_x \sigma_y)$$

$$^d \text{CC}^* = [2\text{CC}_{1/2} / (1 + \text{CC}_{1/2})]^{1/2}$$

$$^f N_{\text{obs}} / N_{\text{unique}}$$

$$^g R_{\text{work}} = \sum_{hkl} ||F_{\text{obs}}| - k |F_{\text{calc}}|| / \sum_{hkl} |F_{\text{obs}}|$$

^h **R_{free}**, calculated the same as for **R_{work}** but on the 5% data excluded from the refinement calculation.

^e the outer resolution shell. Values in parentheses indicate the highest resolution shell

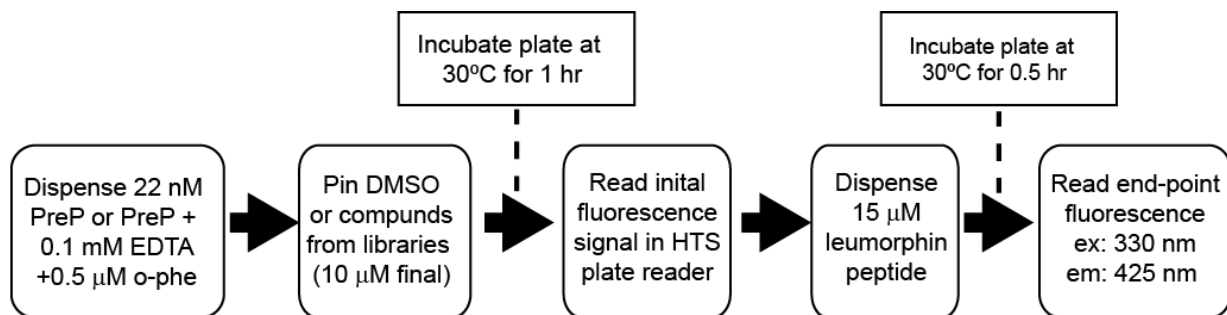
Supplementary Table 4 SAXS data collection and scattering-derived parameters

	hPreP	hPreP+MB-60
Data-collection parameters		
Instrument	12ID-B (APS)	12ID-B (APS)
Wavelength (Å)	0.886	0.886
q range (Å ⁻¹)	0.025-0.220	0.025-0.220
Exposure time (s)	2	2
Number of frames collected	30	30
Concentrations (mg/ml)	1.1	1.1
Temperature (°C)	23	23
Structural parameters		
I(0) [from P(r)]	(3.23±0.03)E-01	(2.73±0.03)E-01
Rg (Å) [from P(r)]	33.6±0.3	33.5±0.3
I(0) (from Guinier)	(3.40±0.08)E-01	(2.84±0.08)E-01
Rg (Å) (from Guinier)	34.8±1.0	34.3±1.1
Dmax ^a (Å)	115±5	115±5
Software employed		
Primary data reduction	Matlab & Igor Pro	Matlab & Igor Pro
Data processing	ATSAS	ATSAS
Oligmeric component fitting	Oligomer	Oligomer
Three-dimensional graphics representations	PyMOL	PyMOL

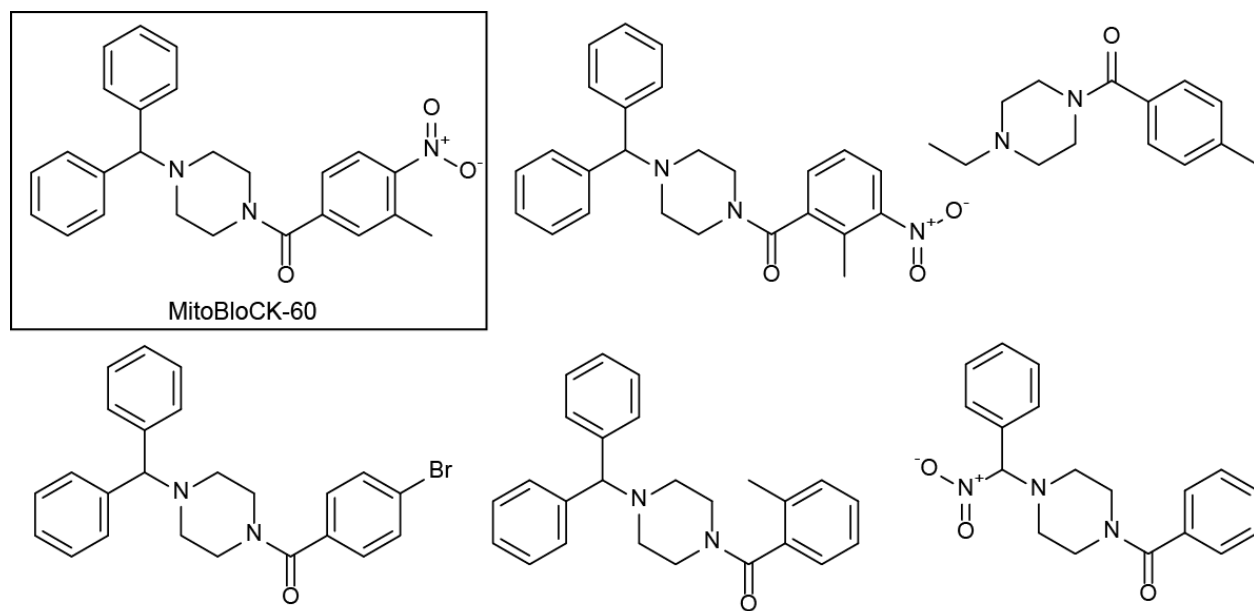
^aDmax is a model parameter in the P(r) calculation, the error is an estimate based on the results of P(r) calculations using a range of Dmax values.

Supplementary Table 5. Yeast strains used in this study

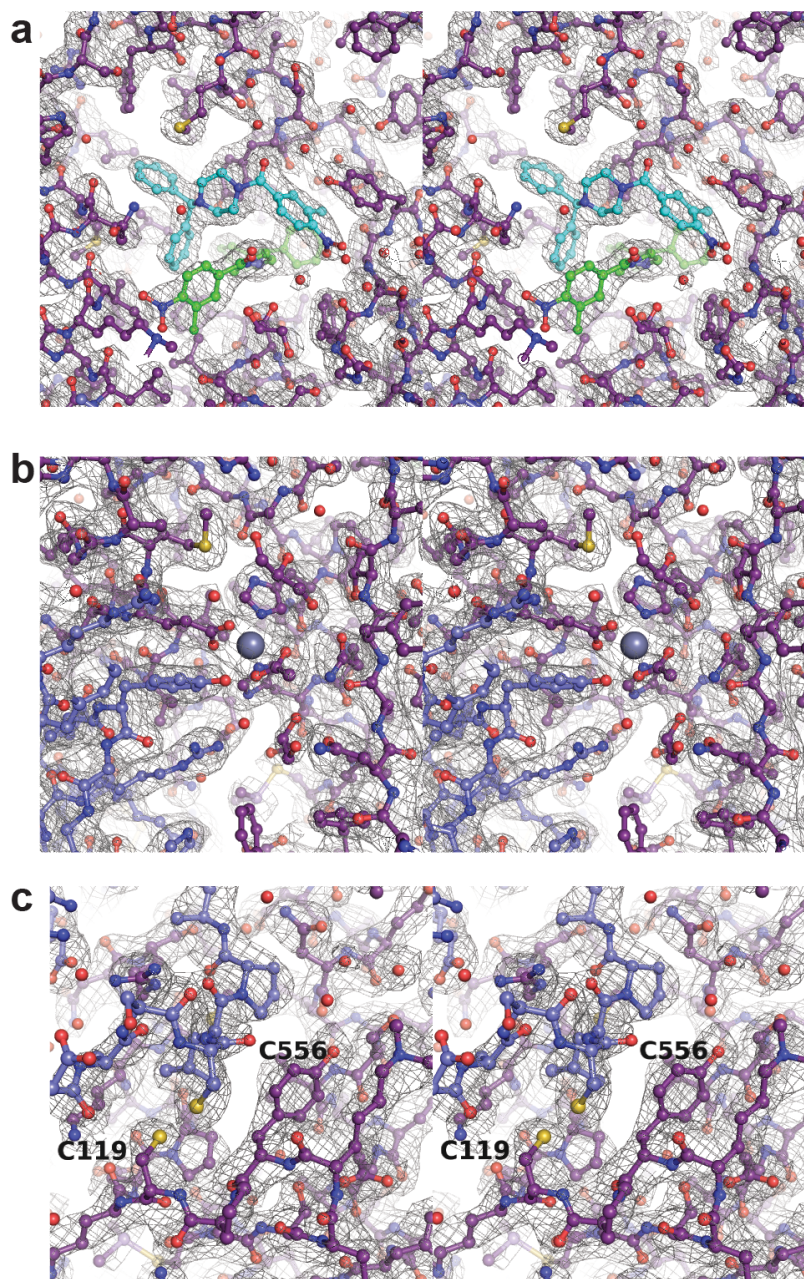
Strain	Genotype	Source
GA74-1A	<i>his3 leu2 ura3 trp1 ade8 ura 3</i>	Koehler et al, 1998
GA74 $\Delta pdr5\Delta snq2$	<i>his3 leu2 ura3 trp1 ade8 ura 3</i> <i>pdr5Δ0::HIS3 snq2Δ0::KANMX</i>	Miyata et al, 2015



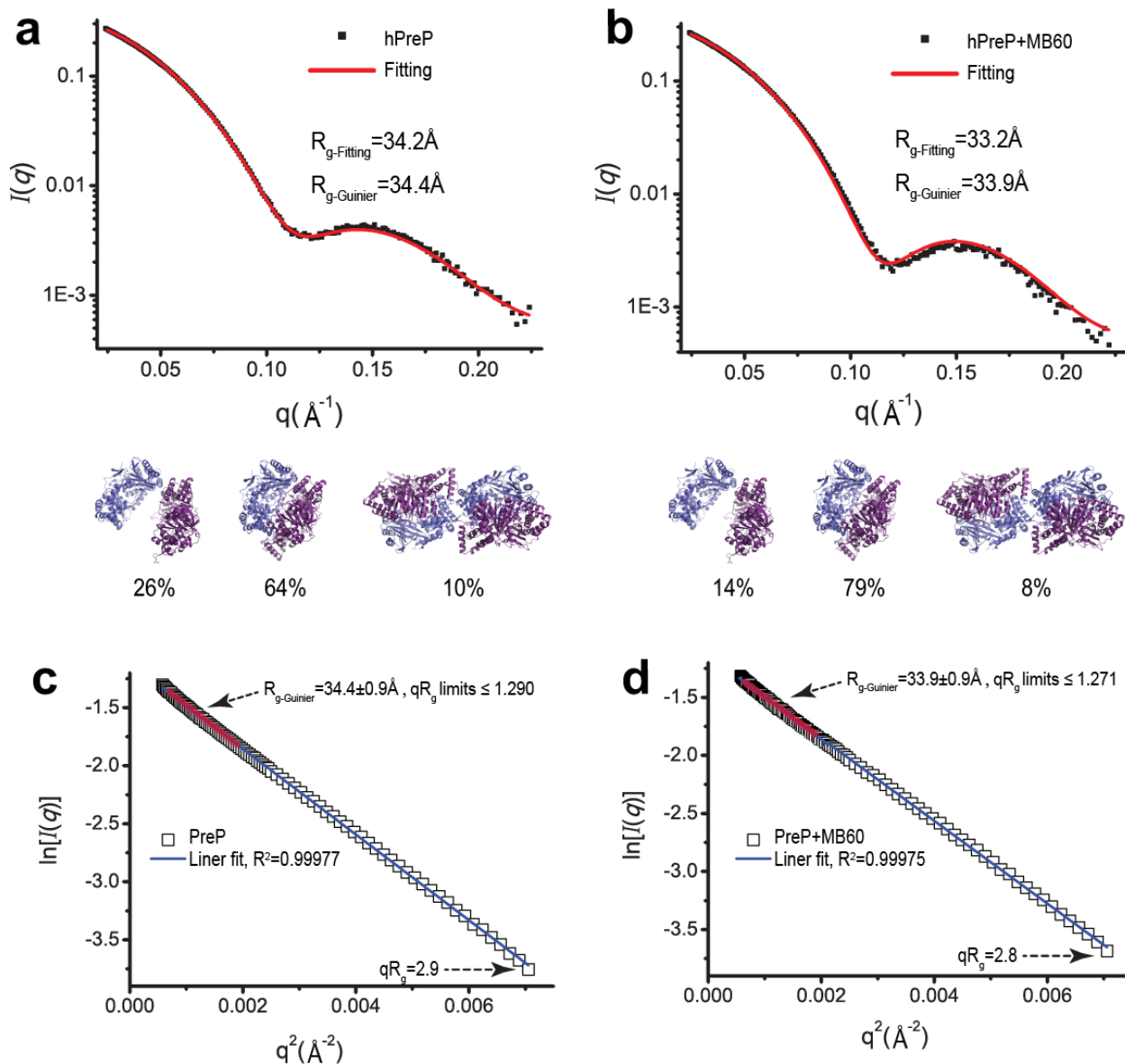
Supplementary Figure 1. Schematic of PreP high-throughput screen. Flowchart describing steps in small molecule screen to identify inhibitors of PreP.



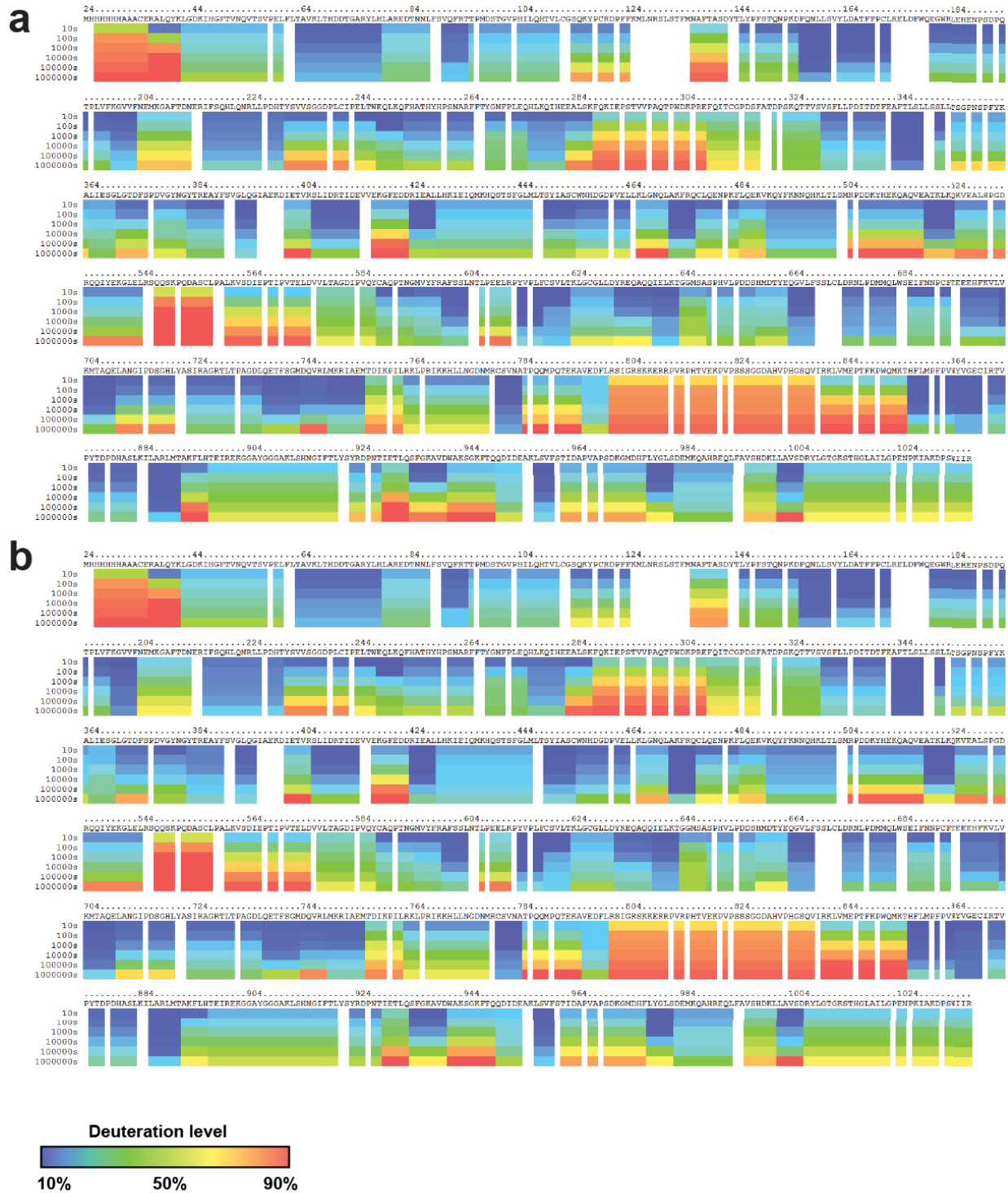
Supplementary Figure 2. Additional compounds in the chemical library that did not inhibit PreP. Data mining from the chemical screen revealed additional piperazine compounds that did not inhibit PreP activity.



Supplementary Figure 3. Representative regions of hPreP in complex with MB-60 in a stereoview. (a) MB-60 binding site within hPreP. (b) Zinc binding site of hPreP. (c) Regions around cysteines 119 and 556. These two cysteines have been postulated to form the disulfide bond. 2mFo-DFc map (grey mesh) was contoured to 1σ . Wall-eye stereo view was prepared with PyMOL.



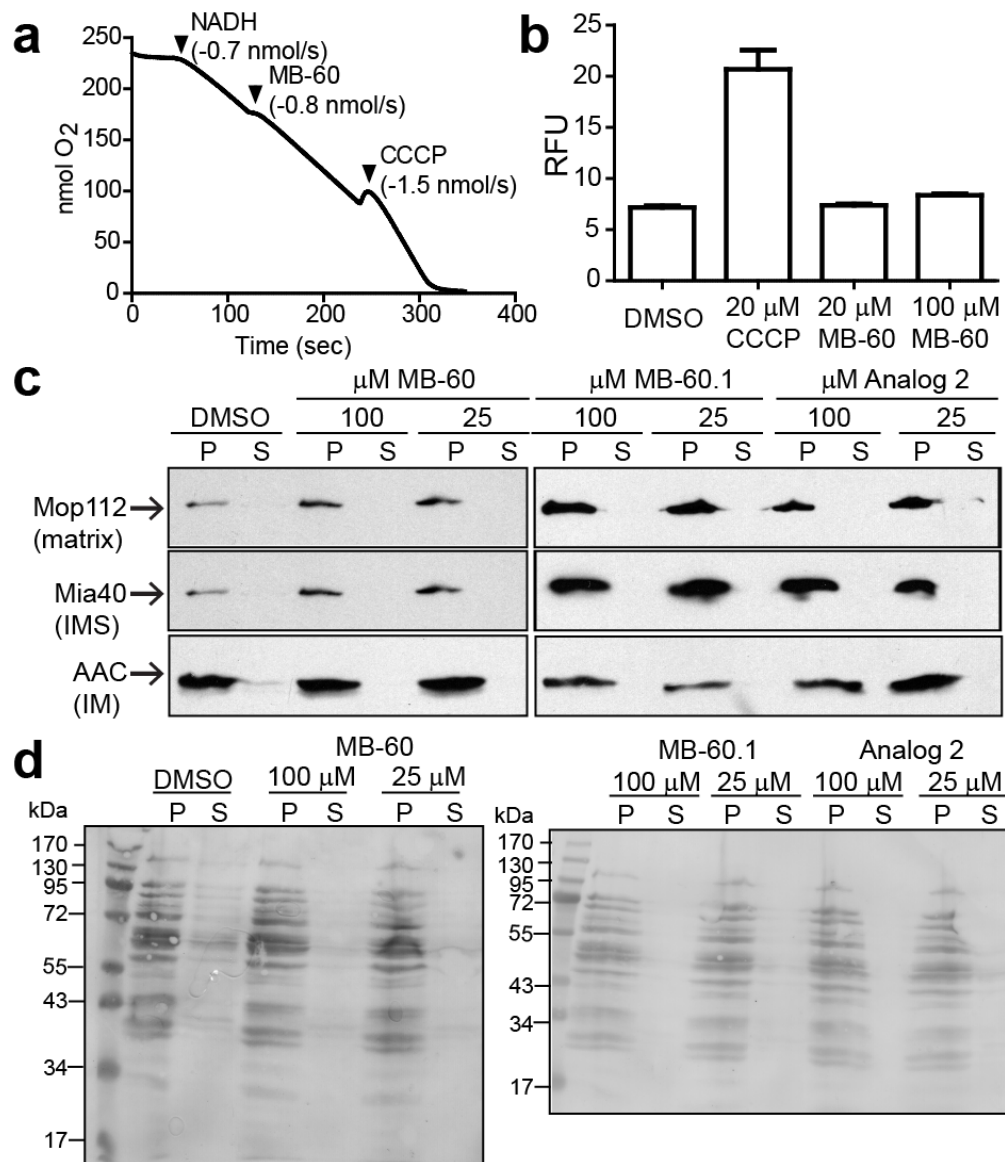
Supplementary Figure 4. SAXS data analysis of hPreP in the presence and absence of MB-60. Oligomer fittings of PreP SAXS data in the absence (a) or presence (b) of MB-60. The fitting is performed by OLIGOMER. Guinier plots of SAXS data of PreP in the absence (c) or presence (d) of MB-60.



Supplementary Figure 5. Summary of hydrogen/deuterium exchange rates of hPreP in the absence (a) and presence (b) of MB-60. Deuteration levels of representative peptide fragments at various time points (from top to bottom: 10, 100, 1,000, 10,000, and 100,000 s at 0°C and 100,000 at room temperature (representing 1000,000 s at 0°C) are shown as a pseudo color scale. The percentages of deuteration levels of each peptide fragment at various time points are shown as a heat map color-coded from blue (<10%) to red (>90%), as indicated at the bottom right of the figure.



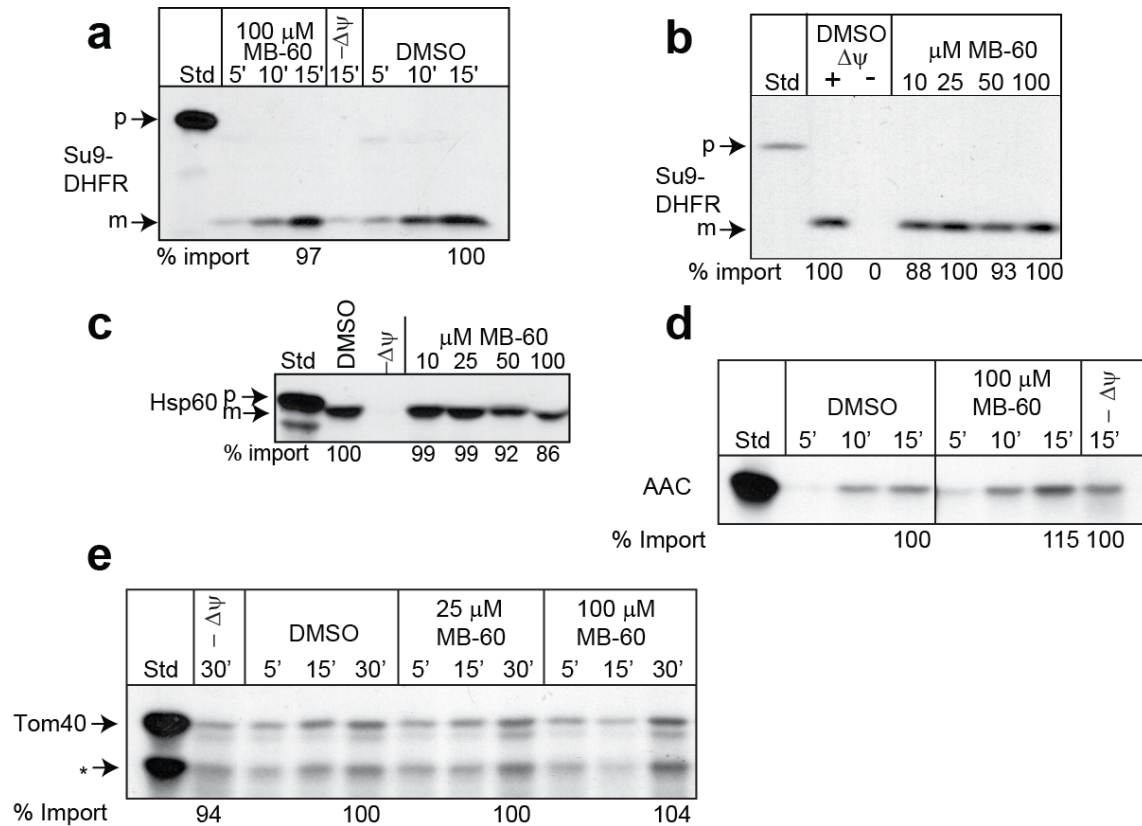
Supplementary Figure 6. Comparison of hydrogen/deuterium exchange rates of hPreP induced by MB-60 binding. Differences in deuteration levels in the presence and absence of MB-60 at various time points (from top to bottom: 10, 100, 1,000, 10,000, 100,000, and 1,000,000 s) are shown in a color-coded bar ranging from blue (-50%) to red (+50%), as indicated at the bottom right of the figure.



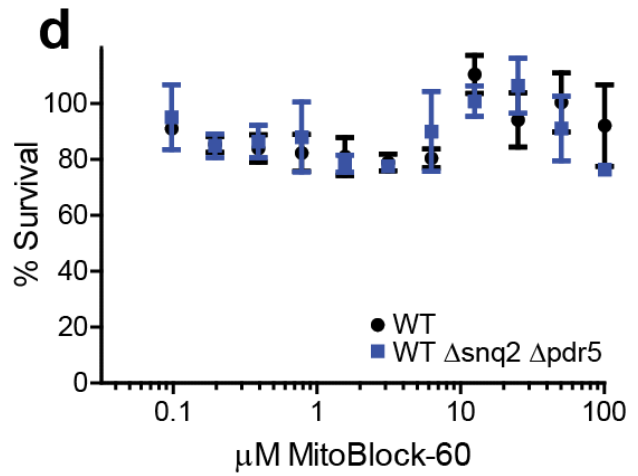
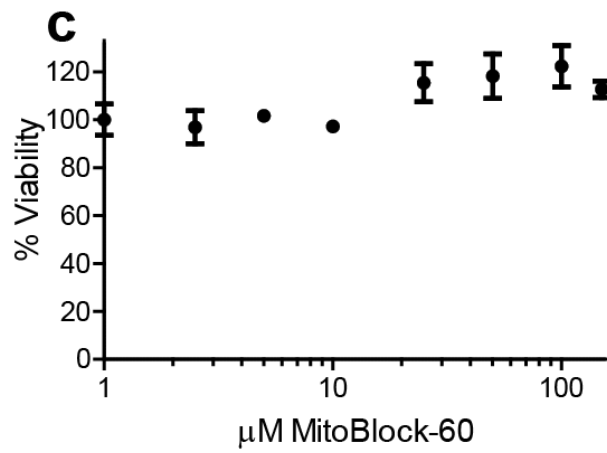
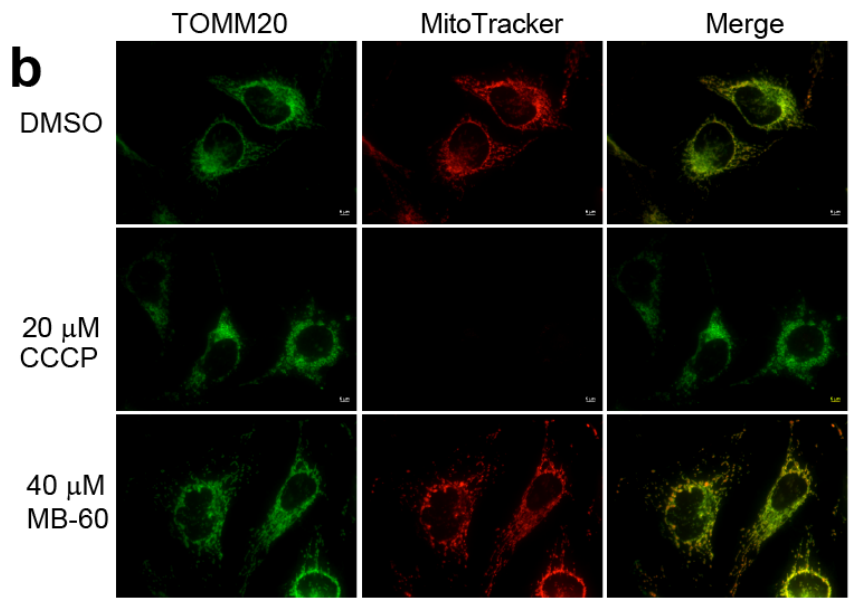
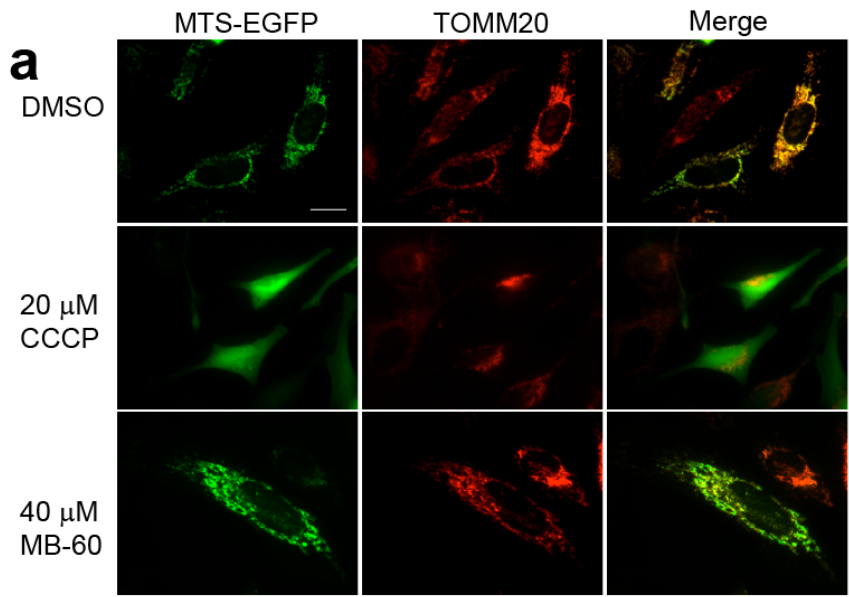
Supplementary Figure 7. MB-60 does not impair general mitochondrial function. (a)

Respiration measurements were performed with an oxygen electrode using isolated mitochondria and MB-60. Respiration was initiated with the addition of 2 mM NADH. 100 μM MB-60 was added once steady-state respiration was achieved, followed by the addition of 20 μM CCCP to uncouple the electron transport chain. Slopes were calculated in the linear range (-0.7 nmol/s for NADH, -0.8 nmol/s for MB-60, and -1.5 nmol/s for CCCP). (b) Membrane potential (Dy)

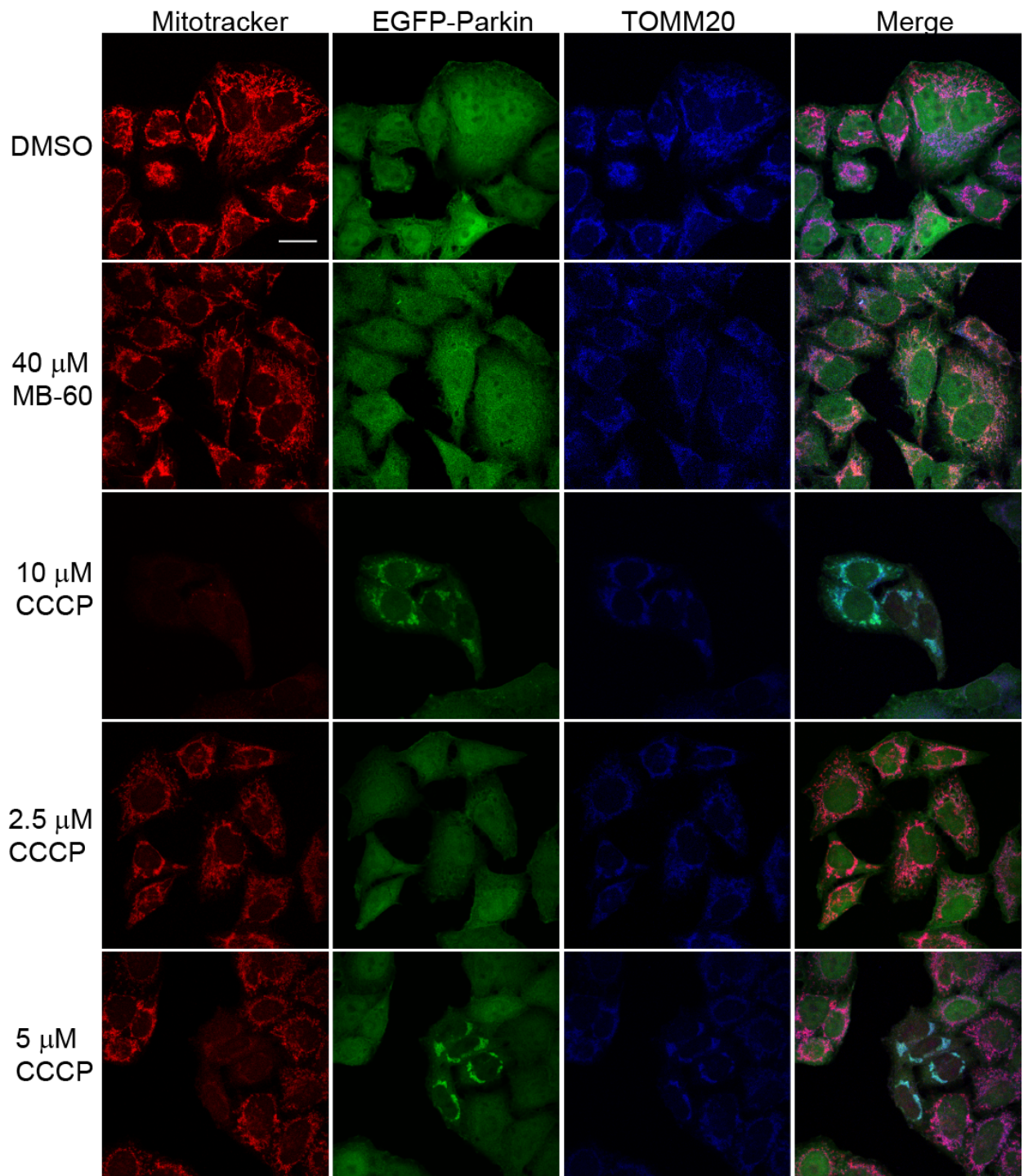
measurements on purified mitochondria were performed with the fluorescent dye DISC[3] using a fluorimeter. Coupled mitochondria sequestered and quenched the dye. 1% DMSO was added to determine the effect on the dye. Collapse of the Dy was initiated by 20 μ M CCCP. MB-60 was added at 20 and 100 μ M. (c) 25 and 100 μ M MB-60 were added to isolated yeast mitochondria in import buffer for 30 min at 25°C. Released proteins (S) were separated from mitochondria (P) by centrifugation at 8,000 x g for 5 min. Immunoblot analysis was performed to determine fractionation for Mop112 (matrix marker), Mia40 (intermembrane space marker), and AAC (inner membrane marker). As a control, treatment with the vehicle (1% DMSO) was included. (d) As in 'c', but integrity was investigated with Coomassie staining.

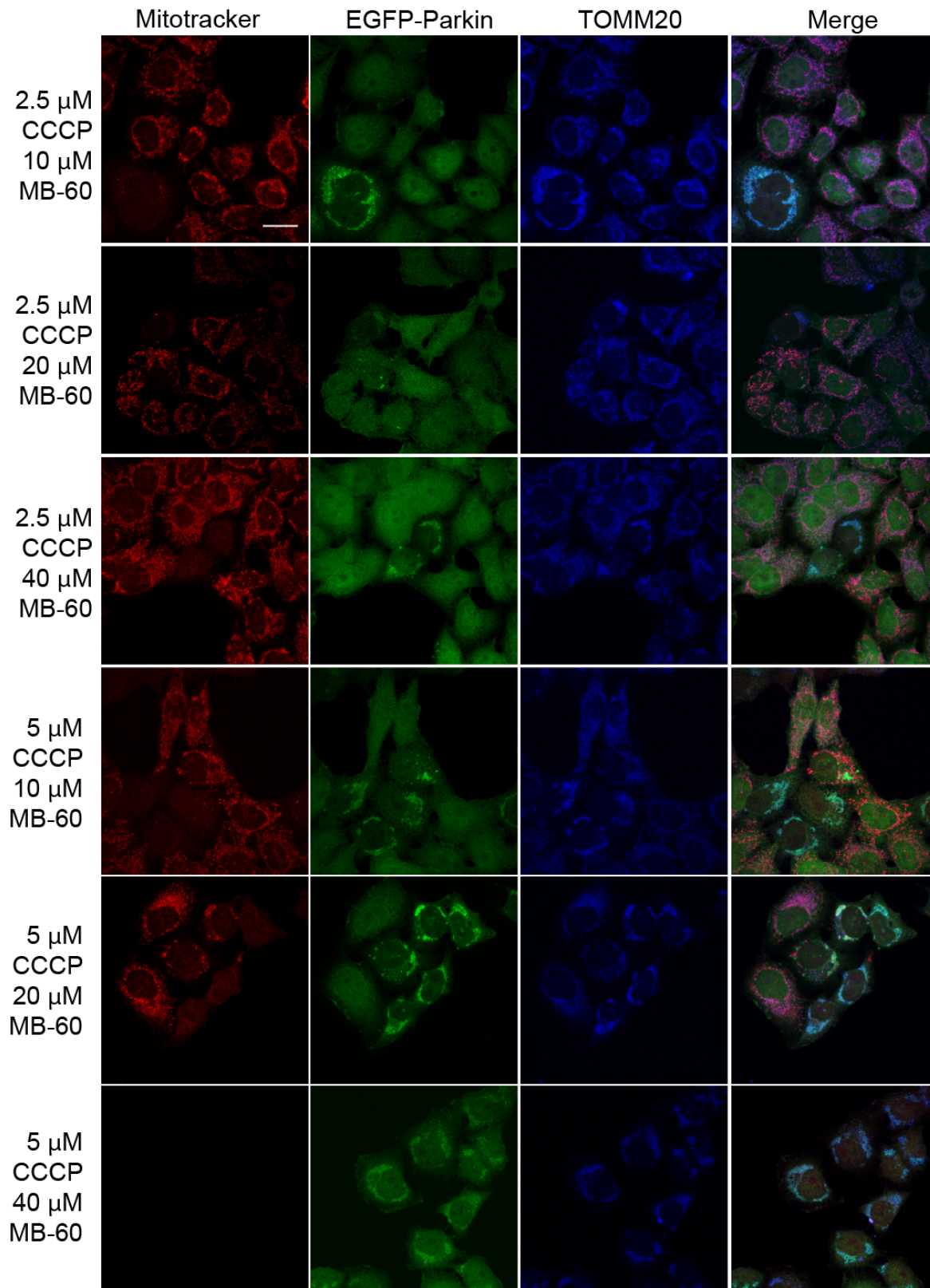


Supplementary Figure 8. MB-60 does not impair import of precursors into isolated mitochondria. (a) Mitochondria were pre-incubated with vehicle (1% DMSO) or 100 μ M MB-60 for 15 min. Radiolabeled Su9-DHFR was imported into isolated mammalian mitochondria and aliquots were removed at the indicated times, followed by protease treatment to remove non-imported precursor. (b) As in 'a', but MB-60 was tested over a concentration range. (c) As in 'a', but Hsp60 was imported in the presence of MB-60. Import reactions were quantitated using Image J software; 100% was set as the amount of precursor imported into WT mitochondria at the endpoint in the time course. p, precursor form; m, mature. (d,e) As in 'a' but AAC and Tom40 was imported respectively.



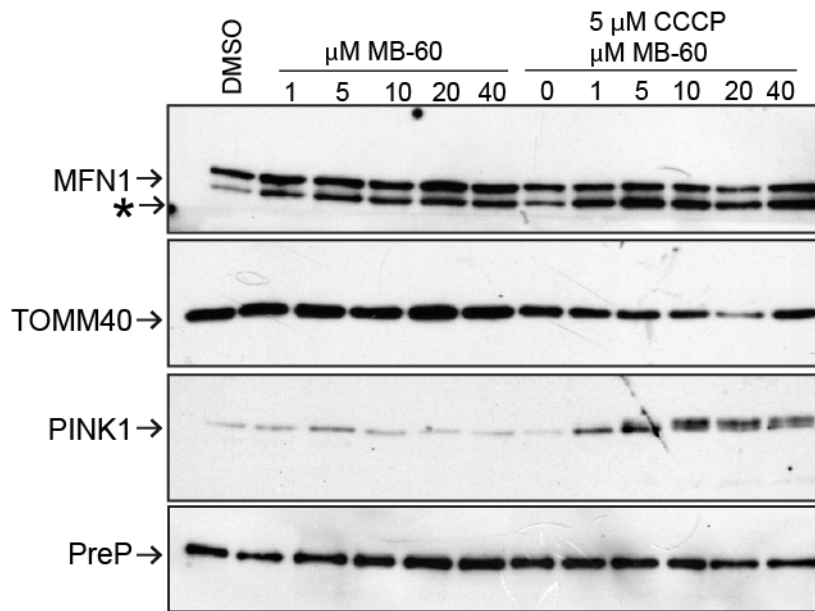
Supplementary Figure 9. MB-60 is not toxic to mammalian and yeast cells. (a) MTS-EGFP (EGFP targeted to the mitochondrial matrix) was transiently expressed in HeLa cells that were treated with 1% DMSO, 20 μ M CCCP, or 40 μ M MB-60. 24 hours post-transfection, cells were fixed and stained with anti-TOMM20 antibody and images were taken. (b) As in 'a', after 24 h post-transfection, cells were stained with the Dy-dependent dye MitoTracker, fixed, and incubated with anti-TOMM20 antibody. (c) Viability of HeLa cells grown in the presence of MB-60 was measured using an MTT assay and plotted over a concentration range of 1-200 μ M MB-60. (d) Yeast strains (WT and one lacking multidrug resistance pumps, *WT Δ pdv5 Δ snq2*) were grown in rich dextrose media, and the minimum inhibitory concentration required to inhibit the growth of yeast 50% of the yeast (MIC_{50}) in the presence of MB-60 was determined



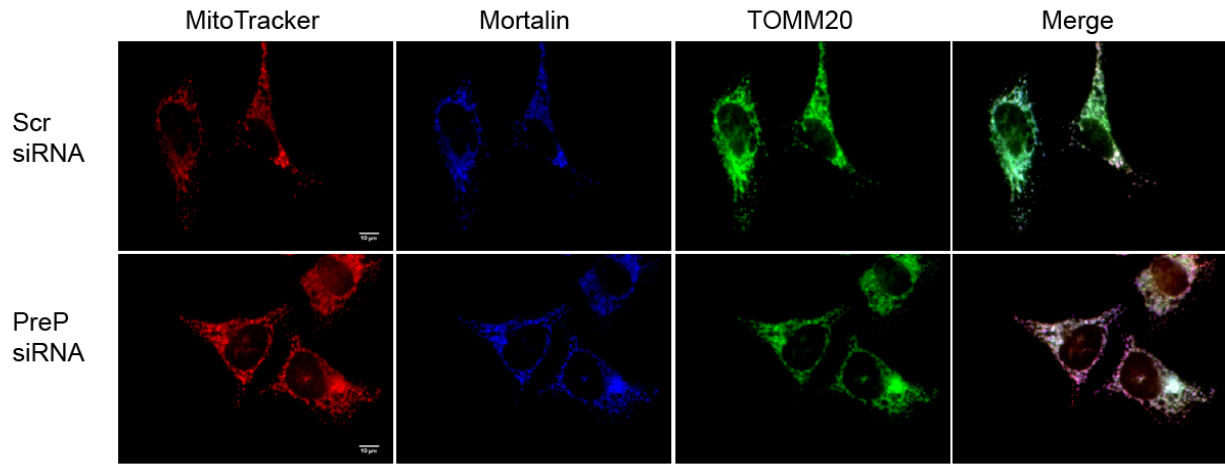
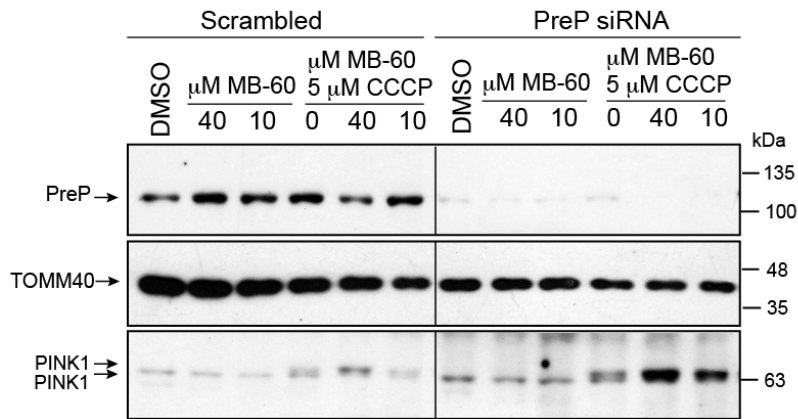
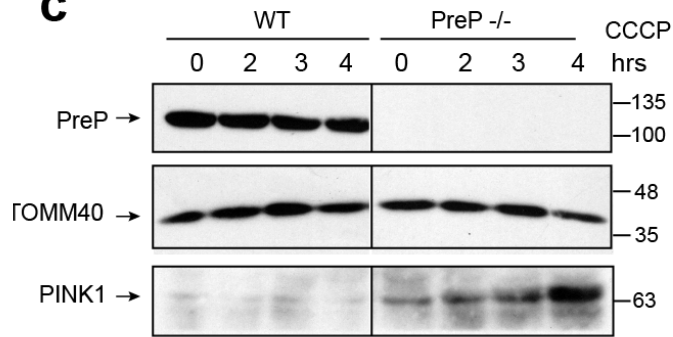
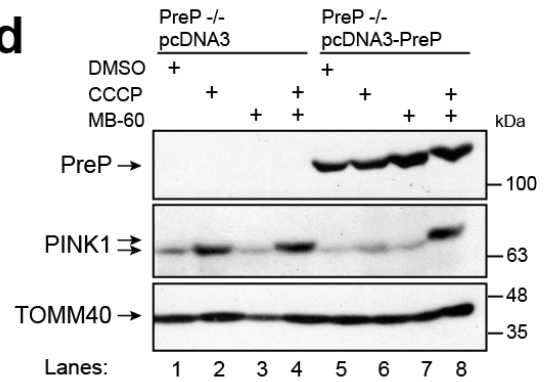


Supplementary Figure 10, 11. Examples of images that were quantitated for Fig. 6C.

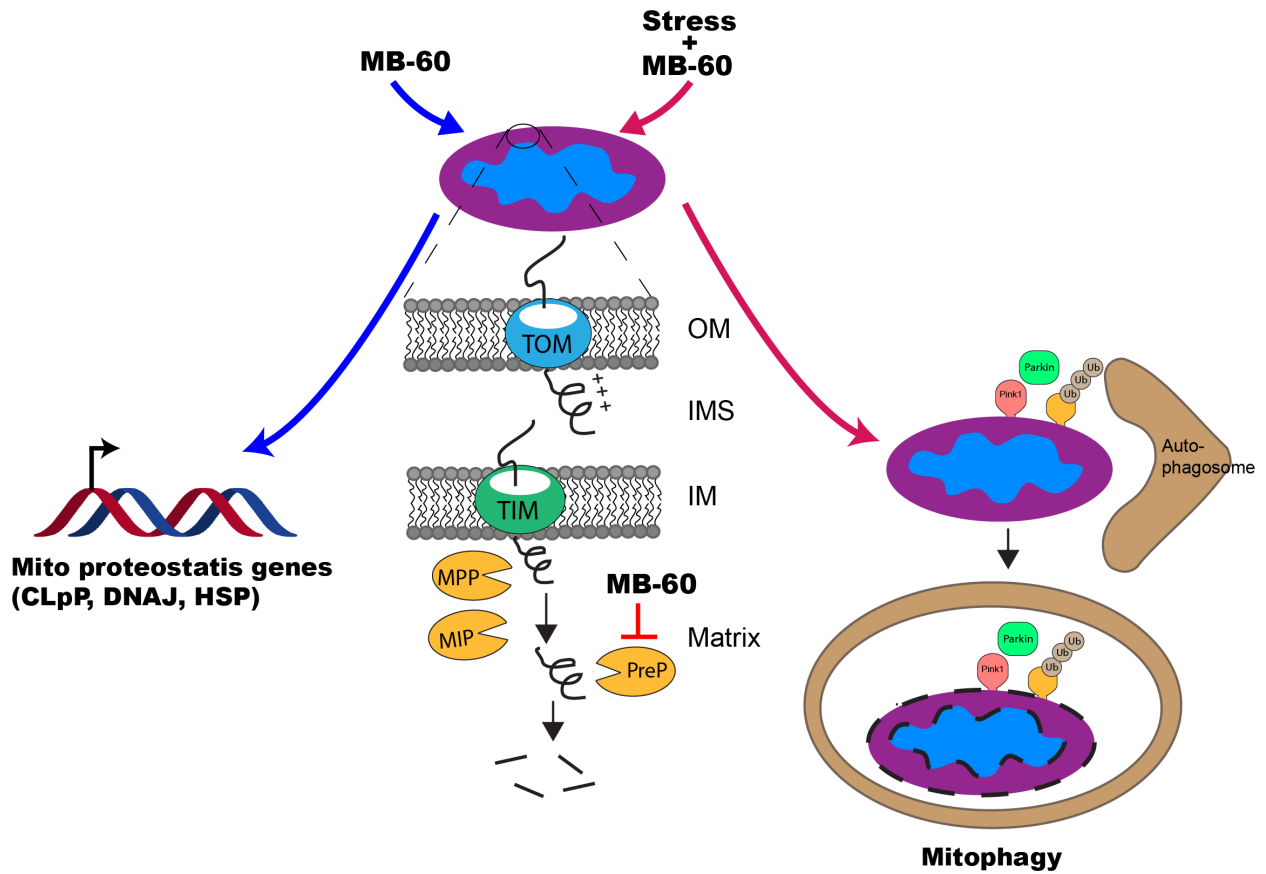
HeLa cells expressing constitutive EGFP-Parkin were treated with combinations of 20 and 40 μM MB-60 for three hours and then 2.5 and 5 μM CCCP for additional 3 hours. EGFP-Parkin recruitment was monitored by fluorescence microscopy. The mitochondria were marked by TOMM20 and the membrane potential was monitored by MitoTracker staining. Parkin recruitment to mitochondria was quantitated in a pool of 100 cells in three independent experiments (scale bar = 20 μm).



Supplementary Figure 12. MB-60 accelerates Pink1 recruitment in a dose-dependent manner. HeLa cells were pre-treated with varying dose of MB-60 for 3 hours prior. 5 μM CCCP then added for an additional 3 hours. Mitochondria were subsequently isolated and blotted for various mitochondrial protein markers.

a**b****c****d**

Supplementary Figure 13. Validation of PreP's role in mitochondrial stress pathway using knockdown and knockout approaches. (a) HeLa cells were transfected with 50 nM PreP siRNA. 24 hours post-transfection, cells were split and grown on coverslips. 48 hours post-transfection, cells were stained with MitoTracker red, fixed and immunostained with anti-mortalin and anti-TOMM20 to visualize mitochondria. (scale bar = 10 μ m). (b) As in 'a' but 48 hours post-transfection, cells were treated with 10 and 40 μ M MB-60 for 3 hours and then 5 μ M CCCP for additional 3 hours. Mitochondria were subsequently isolated, analyzed on 8% SDS-PAGE, transferred onto PVDF membrane and blotted against indicated antibodies. (c) Wildtype HCT116 and HCT116 PreP knockout cells were treated with 10 μ M CCCP as indicated. Cells were harvested and lysed in RIPA buffer. 100 μ g of lysate were loaded on 8% SDS-PAGE. Samples were transferred onto PVDF membrane and blotted with indicated proteins. (d) As in 'c' but HCT116 PreP^{-/-} cells were transfected with either empty vector (pCDNA3) or vector containing full-length PreP-3xflag (pDNA3-PreP) for 48 hours prior to small molecule treatment.



Supplementary Figure 14. MB-60 reveals the role of PreP in mitochondrial stress pathways. Inactivation of PreP by MB-60 activates UPR^{mt} by increasing transcription of mitochondrial proteostasis genes such as ClpP, DNAJ, and HSP. Under stress, PreP inactivation activates mitophagy, specifically through Pink1 stabilization and Parkin recruitment to mitochondria, ultimately resulting in removal of damaged mitochondria by the autophagosome.

References

1. Chacinska, A., Koehler, C. M., Milenkovic, D., Lithgow, T. & Pfanner, N. Importing mitochondrial proteins: machineries and mechanisms. *Cell* **138**, 628–44 (2009).
2. Luciano, P. & Géli, V. The mitochondrial processing peptidase: function and specificity. *Experientia* **52**, 1077–82 (1996).
3. Kmiec, B. & Glaser, E. A novel mitochondrial and chloroplast peptidasome, PreP. *Physiol. Plant.* (2011). doi:10.1111/j.1399-3054.2011.01531.x
4. Malito, E., Hulse, R. E. & Tang, W.-J. Amyloid beta-degrading cryptidases: insulin degrading enzyme, presequence peptidase, and neprilysin. *Cell. Mol. Life Sci.* **65**, 2574–85 (2008).
5. King, J. V *et al.* Molecular basis of substrate recognition and degradation by human presequence protease. *Structure* **22**, 996–1007 (2014).
6. Glasers, M. & Cumsky, G. A Synthetic Presequence Reversibly into Yeast Mitochondria ” Inhibits Protein Import. *Biochemistry* **265**, 8808–8816 (1990).
7. Glaser, S. M. & Cumsky, M. G. A synthetic presequence reversibly inhibits protein import into yeast mitochondria. *J. Biol. Chem.* **265**, 8808–16 (1990).
8. Kambacheld, M., Augustin, S., Tatsuta, T., Müller, S. & Langer, T. Role of the novel metallopeptidase Mop112 and saccharolysin for the complete degradation of proteins residing in different subcompartments of mitochondria. *J. Biol. Chem.* **280**, 20132–9 (2005).
9. Pellegrino, M. W., Nargund, A. M. & Haynes, C. M. Signaling the mitochondrial unfolded protein response. *Biochim. Biophys. Acta* **1833**, 410–6 (2013).
10. Haynes, C. M. & Ron, D. The mitochondrial UPR - protecting organelle protein homeostasis. *J. Cell Sci.* **123**, 3849–55 (2010).
11. Falkevall, A. *et al.* Degradation of the amyloid beta-protein by the novel mitochondrial peptidasome, PreP. *J. Biol. Chem.* **281**, 29096–104 (2006).
12. Manczak, M. *et al.* Mitochondria are a direct site of A beta accumulation in Alzheimer’s disease neurons: implications for free radical generation and oxidative damage in disease progression. *Hum. Mol. Genet.* **15**, 1437–49 (2006).
13. Pinho, C. M., Teixeira, P. F. & Glaser, E. Mitochondrial import and degradation of amyloid- β peptide. *Biochim. Biophys. Acta* (2014). doi:10.1016/j.bbabi.2014.02.007

14. Anandatheerthavarada, H. K. & Devi, L. Amyloid precursor protein and mitochondrial dysfunction in Alzheimer's disease. *Neuroscientist* **13**, 626–38 (2007).
15. Alikhani, N. *et al.* Decreased proteolytic activity of the mitochondrial amyloid- β degrading enzyme, PreP peptidasome, in Alzheimer's disease brain mitochondria. *J. Alzheimers. Dis.* **27**, 75–87 (2011).
16. Lustbader, J. W. *et al.* ABAD directly links Abeta to mitochondrial toxicity in Alzheimer's disease. *Science* **304**, 448–52 (2004).
17. Brunholz, S. *et al.* Axonal transport of APP and the spatial regulation of APP cleavage and function in neuronal cells. *Exp. Brain Res.* 1–12 (2011). doi:10.1007/s00221-011-2870-1
18. Reddy, P. H. Amyloid precursor protein-mediated free radicals and oxidative damage: implications for the development and progression of Alzheimer's disease. *J. Neurochem.* **96**, 1–13 (2006).
19. Chow, K. M. *et al.* Mammalian pitrilysin: substrate specificity and mitochondrial targeting. *Biochemistry* **48**, 2868–77 (2009).
20. Neupert, W. *et al.* [17] Analysis of Mitochondrial Protein Import Pathway in *Saccharomyces cerevisiae* with Translocation Intermediates By. **8432**, 241–252 (1995).
21. Dabir, D. V *et al.* A small molecule inhibitor of redox-regulated protein translocation into mitochondria. *Dev. Cell* **25**, 81–92 (2013).
22. Hasson, S. A. *et al.* Substrate specificity of the TIM22 mitochondrial import pathway revealed with small molecule inhibitor of protein translocation. *Proc. Natl. Acad. Sci. U. S. A.* **107**, 9578–83 (2010).
23. Miyata, N. *et al.* Pharmacologic rescue of an enzyme-trafficking defect in primary hyperoxaluria 1. *Proc. Natl. Acad. Sci. U. S. A.* **111**, 14406–11 (2014).
24. Mossmann, D. *et al.* Amyloid- β Peptide Induces Mitochondrial Dysfunction by Inhibition of Preprotein Maturation. *Cell Metab.* (2014). doi:10.1016/j.cmet.2014.07.024
25. Hansson Petersen, C. A. *et al.* The amyloid beta-peptide is imported into mitochondria via the TOM import machinery and localized to mitochondrial cristae. *Proc. Natl. Acad. Sci. U. S. A.* **105**, 13145–50 (2008).
26. Teixeira, P. F. *et al.* In vitro oxidative inactivation of human presequence protease (hPreP). *Free Radic. Biol. Med.* **53**, 2188–95 (2012).

27. Chen, J., Teixeira, P. F., Glaser, E. & Levine, R. L. Mechanism of oxidative inactivation of human presequence protease (hPreP) by hydrogen peroxide. *Free Radic. Biol. Med.* (2014). doi:10.1016/j.freeradbiomed.2014.08.016
28. Jin, S. M. *et al.* Mitochondrial membrane potential regulates PINK1 import and proteolytic destabilization by PARL. *J. Cell Biol.* **191**, 933–42 (2010).
29. Greene, A. W. *et al.* Mitochondrial processing peptidase regulates PINK1 processing, import and Parkin recruitment. *EMBO Rep.* **13**, 378–85 (2012).
30. King, J. V *et al.* Molecular basis of substrate recognition and degradation by human presequence protease. *Structure* **22**, 996–1007 (2014).
31. Pfeiffer, N. V *et al.* Structural features within the nascent chain regulate alternative targeting of secretory proteins to mitochondria. *EMBO J.* **32**, 1036–51 (2013).
32. Guan, H. *et al.* The Mitochondrial Peptidase Pitrilysin Degrades Islet Amyloid Polypeptide in Beta-Cells. *PLoS One* **10**, e0133263 (2015).
33. Nishii, W. *et al.* A redox switch shapes the Lon protease exit pore to facultatively regulate proteolysis. *Nat. Chem. Biol.* **11**, 46–51 (2015).
34. Hoshino, A. *et al.* Oxidative post-translational modifications develop LONP1 dysfunction in pressure overload heart failure. *Circ. Heart Fail.* **7**, 500–9 (2014).
35. Bernstein, S. H. *et al.* The mitochondrial ATP-dependent Lon protease: a novel target in lymphoma death mediated by the synthetic triterpenoid CDDO and its derivatives. *Blood* **119**, 3321–9 (2012).
36. Lazarou, M. *et al.* The ubiquitin kinase PINK1 recruits autophagy receptors to induce mitophagy. *Nature* (2015). doi:10.1038/nature14893
37. Lee, J. *et al.* Mitochondrial phosphoproteome revealed by an improved IMAC method and MS/MS/MS. *Mol. Cell. Proteomics* **6**, 669–76 (2007).
38. Bian, Y. *et al.* An enzyme assisted RP-RPLC approach for in-depth analysis of human liver phosphoproteome. *J. Proteomics* **96**, 253–62 (2014).
39. Geli, V. Functional reconstitution in *Escherichia coli* of the yeast mitochondrial matrix peptidase from its two inactive subunits. *Proc. Natl. Acad. Sci.* **90**, 6247–6251 (1993).
40. Zhang, J., Chung, T. & Oldenburg, K. A Simple Statistical Parameter for Use in Evaluation and Validation of High Throughput Screening Assays. *J. Biomol. Screen.* **4**, 67–73 (1999).

41. Tienson, H. L. *et al.* Reconstitution of the mia40-erv1 oxidative folding pathway for the small tim proteins. *Mol. Biol. Cell* **20**, 3481–90 (2009).
42. Ran, F. A. *et al.* Genome engineering using the CRISPR-Cas9 system. *Nat. Protoc.* **8**, 2281–308 (2013).
43. King, J. V *et al.* Molecular basis of substrate recognition and degradation by human presequence protease. *Structure* **22**, 996–1007 (2014).
44. Minor, W., Cymborowski, M., Otwinowski, Z. & Chruszcz, M. HKL-3000: the integration of data reduction and structure solution--from diffraction images to an initial model in minutes. *Acta Crystallogr D Biol Crystallogr* **62**, 859–866 (2006).
45. Emsley, P. & Cowtan, K. Coot: model-building tools for molecular graphics. *Acta Crystallogr D Biol Crystallogr* **60**, 2126–2132 (2004).
46. Adams, P. D. *et al.* The Phenix software for automated determination of macromolecular structures. *Methods* **55**, 94–106 (2011).
47. Konarev, P. V, Volkov, V. V, Sokolova, A. V, Koch, M. H. J. & Svergun, D. I. PRIMUS: a Windows PC-based system for small-angle scattering data analysis. *J Appl Crystallogr* **36**, 1277–1282 (2003).
48. Svergun, D. I. Determination of the Regularization Parameter in Indirect-Transform Methods Using Perceptual Criteria. *J Appl Crystallogr* **25**, 495–503 (1992).
49. Svergun, D., Barberato, C. & Koch, M. H. J. CRY SOL-a program to evaluate X-ray solution scattering of biological macromolecules from atomic coordinates. *J Appl Crystallogr* **28**, 768–773 (1995).
50. Petoukhov, M. V *et al.* New developments in the ATSAS program package for small-angle scattering data analysis. *J Appl Crystallogr* **45**, 342–350 (2012).
51. Jacques, D. A., Guss, J. M., Svergun, D. I. & Trewhella, J. Publication guidelines for structural modelling of small-angle scattering data from biomolecules in solution. *Acta Crystallogr D Biol Crystallogr* **68**, 620–626 (2012).
52. Marsh, J. J. *et al.* Structural insights into fibrinogen dynamics using amide hydrogen/deuterium exchange mass spectrometry. *Biochemistry* **52**, 5491–5502 (2013).
53. Coales, S. J. *et al.* Expansion of time window for mass spectrometric measurement of amide hydrogen/deuterium exchange reactions. *Rapid Commun Mass Spectrom* **24**, 3585–3592 (2010).
54. Tsalkova, T. *et al.* Isoform-specific antagonists of exchange proteins directly activated by cAMP. *Proc Natl Acad Sci U S A* **109**, 18613–18618 (2012).

55. Woods Jr., V. L. & Hamuro, Y. High resolution, high-throughput amide deuterium exchange-mass spectrometry (DXMS) determination of protein binding site structure and dynamics: utility in pharmaceutical design. *J Cell Biochem Suppl* **Suppl 37**, 89–98 (2001).
56. Walters, B. T., Ricciuti, A., Mayne, L. & Englander, S. W. Minimizing back exchange in the hydrogen exchange-mass spectrometry experiment. *J Am Soc Mass Spectrom* **23**, 2132–2139 (2012).
57. Zhang, Z. & Smith, D. L. Determination of amide hydrogen exchange by mass spectrometry: a new tool for protein structure elucidation. *Protein Sci* **2**, 522–531 (1993).